VOL. 676 NO. 2 AUGUST 5, 1994
THIS ISSUE COMPLETES VOL. 676

JOURNAL OF CHROMATOGRAPHY A

INCLUDING ELECTROPHORESIS AND OTHER SEPARATION METHODS

ELSEVIER

JOURNAL OF CHROMATOGRAPHY A

INCLUDING ELECTROPHORESIS AND OTHER SEPARATION METHODS

Scope. The *Journal of Chromatography A* publishes papers on all aspects of **chromatography, electrophoresis** and related methods. Contributions consist mainly of research papers dealing with chromatographic theory, instrumental developments and their applications. In the *Symposium volumes*, which are under separate editorship, proceedings of symposia on chromatography, electrophoresis and related methods are published. *Journal of Chromatography B: Biomedical Applications* —This journal, which is under separate editorship, deals with the following aspects: developments in and applications of chromatographic and electrophoretic techniques related to clinical diagnosis or alterations during medical treatment; screening and profiling of body fluids or tissues related to the analysis of active substances and to metabolic disorders; drug level monitoring and pharmacokinetic studies; clinical toxicology; forensic medicine; veterinary medicine; occupational medicine; results from basic medical research with direct consequences in clinical practice.

Submission of Papers. The preferred medium of submission is on disk with accompanying manuscript (see *Electronic manuscripts* in the Instructions to Authors, which can be obtained from the publisher, Elsevier Science B.V., P.O. Box 330, 1000 AH Amsterdam, Netherlands). Manuscripts (in English; *four* copies are required) should be submitted to: Editorial Office of *Journal of Chromatography A*, P.O. Box 681, 1000 AR Amsterdam, Netherlands, Telefax (+31-20) 5862 304, or to: The Editor of *Journal of Chromatography B: Biomedical Applications*, P.O. Box 681, 1000 AR Amsterdam, Netherlands. Review articles are invited or proposed in writing to the Editors who welcome suggestions for subjects. An outline of the proposed review should first be forwarded to the Editors for preliminary discussion prior to preparation. Submission of an article is understood to imply that the article is original and unpublished and is not being considered for publication elsewhere. For copyright regulations, see below.

Publication information. *Journal of Chromatography A* (ISSN 0021-9673): for 1994 Vols. 652–682 are scheduled for publication. *Journal of Chromatography B: Biomedical Applications* (ISSN 0378-4347): for 1994 Vols. 652–662 are scheduled for publication. Subscription prices for *Journal of Chromatography A*, *Journal of Chromatography B: Biomedical Applications* or a combined subscription are available upon request from the publisher. Subscriptions are accepted on a prepaid basis only and are entered on a calendar year basis. Issues are sent by surface mail except to the following countries where air delivery via SAL is ensured: Argentina, Australia, Brazil, Canada, China, Hong Kong, India, Israel, Japan, Malaysia, Mexico, New Zealand, Pakistan, Singapore, South Africa, South Korea, Taiwan, Thailand, USA. For all other countries airmail rates are available upon request. Claims for missing issues must be made within six months of our publication (mailing) date. Please address all your requests regarding orders and subscription queries to: Elsevier Science B.V., Journal Department, P.O. Box 211, 1000 AE Amsterdam, Netherlands. Tel.: (+31-20) 5803 642; Fax: (+31-20) 5803 598. Customers in the USA and Canada wishing information on this and other Elsevier journals, please contact Journal Information Center, Elsevier Science Inc., 655 Avenue of the Americas, New York, NY 10010, USA, Tel. (+1-212) 633 3750, Telefax (+1-212) 633 3764.

Abstracts/Contents Lists published in Analytical Abstracts, Biochemical Abstracts, Biological Abstracts, Chemical Abstracts, Chemical Titles, Chromatography Abstracts, Current Awareness in Biological Sciences (CABS), Current Contents/Life Sciences, Current Contents/Physical, Chemical & Earth Sciences, Deep-Sea Research/Part B: Oceanographic Literature Review, Excerpta Medica, Index Medicus, Mass Spectrometry Bulletin, PASCAL-CNRS, Referativnyi Zhurnal, Research Alert and Science Citation Index.

US Mailing Notice. *Journal of Chromatography A* (ISSN 0021-9673) is published weekly (total 52 issues) by Elsevier Science B.V., (Sara Burgerhartstraat 25, P.O. Box 211, 1000 AE Amsterdam, Netherlands). Annual subscription price in the USA US$ 4994.00 (US$ price valid in North, Central and South America only) including air speed delivery. Second class postage paid at Jamaica, NY 11431. **USA POSTMASTERS**: Send address changes to *Journal of Chromatography A*, Publications Expediting, Inc., 200 Meacham Avenue, Elmont, NY 11003. Airfreight and mailing in the USA by Publications Expediting.

See inside back cover for Publication Schedule, Information for Authors and information on Advertisements.

0021-9673/94/$07.00

Printed in the Netherlands

VOL. 676, NO. 2 JOURNAL OF CHROMATOGRAPHY A AUGUST 5, 1994

CONTENTS

(Abstracts/Contents Lists published in Analytical Abstracts, Biochemical Abstracts, Biological Abstracts, Chemical Abstracts, Chemical Titles, Chromatography Abstracts, Current Awareness in Biological Sciences (CABS), Current Contents/Life Sciences, Current Contents/Physical, Chemical & Earth Sciences, Deep-Sea Research/Part B: Oceanographic Literature Review, Excerpta Medica, Index Medicus, Mass Spectrometry Bulletin, PASCAL-CNRS, Referativnyi Zhurnal, Research Alert and Science Citation Index)

REGULAR PAPERS

Column Liquid Chromatography

Fast Flow Fractionation

(Continued overleaf)

Contents (continued)

ELSEVIER

Journal of Chromatography A, 676 (1994) 249–266

JOURNAL OF CHROMATOGRAPHY A

Silica-based metal chelate affinity sorbents II[☆]. Adsorption and elution behaviour of proteins on iminodiacetic acid affinity sorbents prepared via different immobilization techniques

F. Birger Anspach

GBF-National Research Centre for Biotechnology, Biochemical Engineering, Mascheroder Weg 1, D-38124 Braunschweig, Germany

First received 12 October 1993; revised manuscript received 14 March 1994

Abstract

The chromatographic characteristics of some model proteins on silica-based metal chelates run under various experimental conditions are described. The retention of proteins on silica-based iminodiacetic acid (IDA) was compared among the different immobilization methods employed and to chelates bound on soft gels, such as chelating Sepharose and epibromohydrin-activated Sepharose. All Cu(II)-loaded chelators displayed adsorption of proteins in the presence of 0.5–1 *M* NaCl at pH 7–8; however, elution in the pH and imidazole gradient varied with the immobilization chemistry. The chemical structure in the neighbourhood of the metal chelate was of influence on the development of a negative charge with increasing pH. Thus, a negative charge evolves at lower pH with alkyl- than epoxy-immobilized IDA:Cu(II). Glycidoxypropyltrimethoxysilane-immobilized IDA displayed almost identical chromatographic characteristics compared to chelating Sepharose FF. Basic proteins displayed higher retention on butyl-immobilized IDA compared to other chelates; interactions with positively charged amino acid residues seem to be superimposed on the interaction with histidyl residues. Proteins were least retained on 1,1′-carbonyldiimidazole-immobilized IDA:Cu(II); however, the selectivity for human and bovine serum albumins against other proteins employed was highest. The results obtained indicated that chelating interaction with some proteins depend on the spacer length. Thus, less flexible histidyl residues at protein surfaces might not be recognized from chelates immobilized by short spacers.

1. Introduction

Immobilised metal chelators are employed for the reversible immobilization of metal ions, thereby forming metal chelates. However, not the immobilised metal ion alone is responsible for the interaction of a protein with the resulting affinity sorbent. The results from the present investigations rather confirmed that the interaction of the protein with the entire metal chelate is responsible for interaction. The term metal chelate interaction chromatography (MCIC), as proposed by El Rassi and Horváth [1], is therefore preferred against other expressions and abbreviations used.

Many publications on MCIC appeared in the

[☆]For Part I, see ref. 7.

0021-9673/94/$07.00
SSDI 0021-9673(94)00333-5

Table 1
Properties of proteins employed in this study

Protein	Nucleophilic amino acids	His at surface	p*I*	M_r
RNase A (bovine pancreas)	4 His, 0 Trp, 8 Cys as S–S [37]	2 [6]	9.4	13 700
Cyt c (horse heart)	2 His, 1 Trp, 2 Cys [38]	1 [10]	10.6	12 300
Lysozyme (chicken egg white)	1 His, 6 Trp, 9 Cys (8 as S–S) [39]	1 [40]	11.0	14 400
HSA	16 His, 1 Trp, 35 Cys (34 as S–S) [41]	2–3 [15]	4.6	69 000
BSA	16 His, 2 Trp, 35 Cys (34 as S–S) [42]	2–3 [15]	4.8	66 700
DSA	15 His [6]	1 [15]		
OVA (chicken egg)	7 His, 3 Trp, 6 Cys [43]	1 [1]	4.7	45 000

last years concerning the interaction of mostly commercial immobilised metal chelates with proteins [2–4]. Mostly iminodiacetic acid (IDA) is employed as chelator because it combines tight binding of transition metal ions with high accessibility of the resulting metal chelate for amino acid residues at protein surfaces [5]. Today it is widely accepted that the basis for interaction of proteins with IDA chelates is the interaction of nucleophilic groups of amino acids, especially the imidazole group of histidine. It remains questionable, whether other nucleophilic amino acids, such as tryptophan or cysteine, participate in binding [6].

In Part I of this investigation, the covalent immobilization of IDA leading to distinct structures of the chelator is described. The chelates, as obtained through the different methods, displayed a deviate selectivity for amino acids when compared to each other [7].

The impact of the chemical neighbourhood of chelates on the chelate structure was also demonstrated by Chaberek and Martell [8], who developed metal chelates on the basis of carboxymethylated amines with different structure (for chelation of metal ions). Their results clearly demonstrated that small structural changes in the neighbourhood of the chelating group alters the titration curve of metal chelates; titration curves allow directly the calculation of the stability constant of chelates. Among other reasons, the stability constant depended on the ring size of the polydentate complex formed with the central metal ion and on hydroxyalkyl groups located in close proximity to the chelator [9]. These results are very important in view of metal chelates introduced in Part I but also of commercial metal chelate sorbents. Their exact chemical structure is mostly unknown to the user.

In order to gain a more systematic approach, more insight on the interactions of proteins with metal chelates is necessary, such as demonstrated by Porath and co-workers [10,11], using proteins or peptides, respectively. The influence of buffer compositions was demonstrated by El Rassi and Horváth [1] and Porath and Olin [12]. Those results are summarised in the following which should be seen in connection with results from this investigation:

(i) At least one histidyl residue at the protein surface is required for adsorption on immobilised IDA:Cu(II); interactions with cysteine and tryptophan are discussed, but need to be confirmed [6,10].

(ii) At least two histidyl residues are essential for adsorption on immobilised IDA:Ni(II) [4].

(iii) Two histidyl residues in vicinity are needed for adsorption on IDA:Zn(II) or IDA:Co(II), either sequential or conformational [13].

(iv) Ionic interactions can be modulated by buffers of different ionic strength [1].

(v) Adsorption and elution are affected by pH; pH-gradient elution is a common elution technique [14].

(vi) High-affinity metal ion binding sites of proteins may scavenge the metal ion from the immobilised metal chelator without binding [4,15].

Proteins employed in this study were chosen on the basis of their reported behaviour in MCIC; their properties are compiled in Table 1. Serum albumins employed and ovalbumin (OVA) exhibit a net negative charge at most of

the pH values chosen in this study. All other proteins remain positively charged. According to literature, they display a different number of accessible histidyl residues at the protein surface, some at least one, ribonuclease (RNase) A two, also bovine (BSA) and human serum albumin (HSA) at least two [15,16]. It was anticipated that the different properties of these proteins would allow a comparison of their binding properties onto these chelates under various chromatographic conditions. Besides influences of the spacer length, leading to different accessibility of protein surface-located histidine residues, the chemical neighbourhood of the chelate significantly influenced the adsorption of proteins. The appearance of a negative charge at Cu(II) chelates with increasing pH could be linked to the immobilization method employed. From the results of this study more selective adsorption and elution conditions can be predicted for some chromatographic protocols.

The Cu(II)-loaded 1,1′-carbonyldiimidazole (CDI)-immobilised IDA is a specific metal chelate chromatographic sorbent for the purification of some serum albumins.

2. Experimental

2.1. Chemicals and chromatographic materials

Imidazole, BSA, HSA, dog serum albumin (DSA) (all fraction V), OVA grade V from chicken egg and horse heart cytochrome *c* (Cyt c) were obtained from Sigma, Munich, Germany. Lysozyme from chicken egg white and RNase A from bovine pancreas were obtained from Serva, Heidelberg, Germany. All other chemicals were purchased from E. Merck, Darmstadt, Germany or Riedel-de Haen, Seelze, Germany. Analytical grade was used in all cases. Chelating Sepharose FF (CS) was purchased from Pharmacia, Freiburg, Germany.

2.2. Chromatographic sorbents

Silica-based chelators were prepared as described in Part I [7]. Briefly, GLYMO-IDA is a condensation product of 3-glycidoxypropyltrimethoxysilane (GLYMO) and iminodiacetic acid (IDA). Propyl-IDA and butyl-IDA are synthesised by reaction of 4-aminobutyl- and 3-aminopropyltriethoxysilane with bromoacetic acid, respectively. All α,ω-silano-chelators were bound to non-activated silica. CDI::IDA and Epi::IDA were prepared by reaction of IDA with CDI-activated diol-silica and epibromohydrin-activated Sepharose 4B, respectively. Metal chelates are abbreviated as IDA:M() with M being the metal ion, embracing the oxidation state in parentheses.

2.3. Instruments

The liquid chromatographic system for all chromatographic experiments was the Pharmacia 500 system assembled for zonal and frontal chromatography, respectively.

2.4. Chromatographic conditions

Sepharose 4B-based chelating gels and CS were packed in water. Silica-based chelating gels were dry-packed. All experiments were carried out with 5 mm I.D. columns with bed heights between 20 and 30 mm. Buffers, including water and metal ion solutions, were filtered through disposable filters (0.45 μm) before usage.

2.5. Zonal chromatography

Chromatographic tests were performed using standard fast protein liquid chromatography (FPLC) equipment, operating automatically. The columns were washed first with 30 m*M* EDTA + 0.5 *M* NaCl, pH 6, in order to remove metal ions or contaminants, then water, then 15 m*M* metal ion dissolved in 50 m*M* acetate buffer, pH 5, and finally with 50 m*M* acetate buffer, pH 5, in order to elute those metal ions which are adsorbed due to ionic interactions. The columns were equilibrated with 20–25 column volumes of the starting buffer. All experiments were conducted at 298 K at a flow-rate of 0.5 ml/min, unless stated otherwise.

2.6. Chromatography of proteins

Proteins were dissolved in buffer A at concentrations of 0.3 g/l for albumins and RNase A and 0.1 g/l for lysozyme and Cyt c. A 200-μl volume was applied on a column. Proteins were monitored at 280 nm.

2.7. Elution with salt gradient

Buffer A was a 25 m*M* phosphate buffer, adjusted to pH 5, 6, 7 or 8; buffer B comprised 1 *M* NaCl in addition. Gradients were formed by increasing buffer B concentration from 0 to 50% in 10 min, then to 100% B in 3 min, holding this concentration for 2 min. Then the column was reequilibrated with buffer A. Some investigations were performed in 50 m*M* acetate buffer, pH 5.0 and 50 m*M* Tris · HCl, pH 8.0 as buffer A, respectively. Gradient times were the same as for phosphate-buffered systems.

2.8. Elution with pH gradient

Buffer A was 25 m*M* phosphate + 0.5 *M* NaCl, adjusted to pH 8; buffer B was 100 m*M* phosphate + 0.5 m*M* NaCl, adjusted to pH 2.8. Elution was achieved by increasing the concentration of buffer B in 15 min to 100%, holding for 6 min.

2.9. Elution with 100 mM imidazole gradient

Buffer A was 25 m*M* phosphate + 0.5 *M* NaCl, adjusted to pH 6 or pH 7; buffer B comprised 100 m*M* imidazole in addition. Some experiments were also performed with 0.15 *M* NaCl. For the CDI::IDA chelate only 25 m*M* imidazole was used in buffer B. Gradients were formed by increasing buffer B from 0 to 50% in 20 min, then to 100% in 5 min, holding for 2 min. Then the column was reequilibrated with buffer A.

2.10. Frontal chromatography

Frontal chromatography was performed with automated adsorption, elution and equilibration of up to 7 columns and 5 protein concentrations in one set of experiments. Each run was terminated by the integrator after reaching the plateau region of the frontal breakthrough.

2.11. Adsorption of lysozyme and BSA on Cu(II)- and Fe(III)-loaded chelators

Before the first and after each run the metal chelate columns were washed with 30 m*M* EDTA + 0.5 m*M* NaCl to remove metal ion, adsorbed proteins and contaminants. Then columns were loaded with either Fe(III) or Cu(II) using 15 m*M* $Fe_2(SO_3)_2$ or $CuCl_2$ dissolved in water. For adsorption of lysozyme onto Fe(III)-loaded sorbents, 50 m*M* acetate + 0.5 *M* NaCl, pH 5 was used; for adsorption of BSA the buffer contained only 0.1 *M* NaCl. In case of Cu(II) chelates, 25 m*M* phosphate + 0.5 *M* NaCl, pH 7 was chosen during adsorption. Lysozyme concentrations between 0.04 and 2 g/l were applied. BSA concentrations ranged from 0.3 to 2.5 g/l.

2.12. Contour plots of proteins

Contour plots of the protein surface were achieved using the program BRAGI, developed at the GBF by Schomburg and Reichelt [17]. The program allows a close investigation of the accessibility of amino acids at protein surfaces using X-ray structural analysis data for calculation.

3. Results

3.1. Adsorption at low ionic strength

It is characteristic for IDA metal chelates that the chemical composition changes slightly with pH. Hence, a negative charge develops through deprotonation with increasing pH, as demonstrated in Fig. 1. The titration of metal chelates in solution revealed that the p*K*, corresponding to the development of a negative charge, depends both on the metal ion and the structure of the chelator [8]. Therefore, this p*K* is an important criterion for comparison of IDA

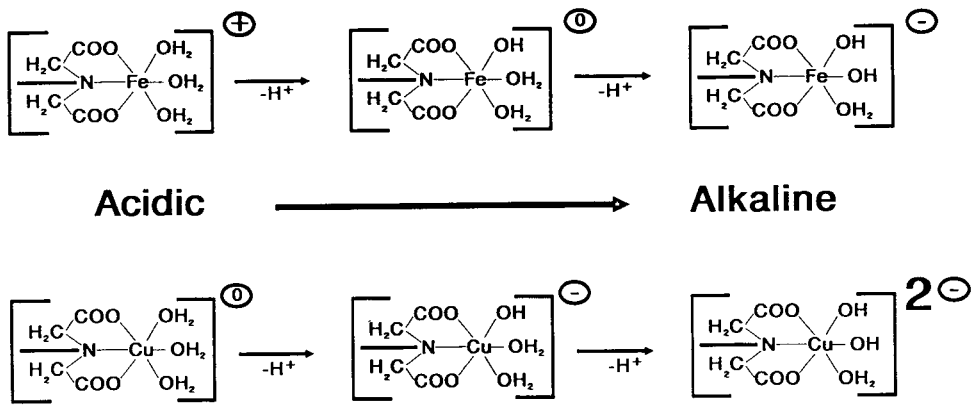

Fig. 1. Appearance of positive or negative charge at Fe(III) chelates and negative charges at Cu(II) chelates depending on pH. Whereas Cu(II) chelates presenting zero charge exhibit truly chelating interactions, charged chelates demonstrate ionic interactions during the adsorption step in addition.

chelators employed in this study. Ionic interactions with proteins, originating from a negative charge, are usually suppressed by the addition of 0.5–1 *M* NaCl. In order to compare the influence of the immobilization chemistry of metal chelates employed in this study on the retention of model proteins, both low and high NaCl concentration were employed.

IDA carries a negative charge at each carboxyl group and a positive charge at the nitrogen with one exception; CDI-immobilised IDA does not accommodate a positive charge due to the amidic character of the nitrogen. As a consequence, model proteins bearing a net negative charge at elevated pH values, such as albumins and OVA, were expelled from IDA at low ionic strength and eluted in the void volume. Proteins with net positive charge adsorbed at low and eluted at elevated NaCl concentration, similar to the retention on a cation exchanger.

The different IDA:Cu(II) chelates demonstrated a distinct adsorption behaviour at pH 8 and low ionic strength, depending on the immobilization method employed. Whereas all proteins adsorbed on chelates bound through an epoxy group, butyl-IDA:Cu(II) and CDI::IDA:Cu(II) did not retain serum albumins and OVA at low salt concentration. It appeared that the chemical neighbourhood of IDA, as obtained through the different immobilization methods [7], affected the p*K* corresponding to the development of a negative charge on IDA:Cu(II) chelates. A negative charge at copper chelates is discussed by other groups as well [11,18].

3.2. Elution with increasing salt gradient

Chromatographic results from silica-based GLYMO-IDA, butyl-IDA and CDI::IDA at pH 7 are illustrated in Figs. 2, 3, and 4, respectively. On all naked IDA sorbents albumins and OVA were expelled due to their net negative charge. The chromatographic behaviour of the basic proteins Cyt c, RNase A, and lysozyme corresponded on all the chelators employed to their retention on a cation exchanger.

Metal ion

When Ca(II) or La(III) were coordinated with IDA, proteins demonstrated nearly identical retention times as observed with naked IDA. Although adsorption of Ca(II) onto IDA sorbents was confirmed by atomic absorption spectroscopic measurements, the resulting IDA:Ca(II) chelate is weak, as were IDA chelates with other alkaline-earth metals, too. Consequently, these chelates demonstrated mainly the properties of naked IDA.

Results from Fe(III)-loaded GLYMO-IDA and butyl-IDA are indicative for a mixed interaction mechanism. IDA:Fe(III) behaved similar to naked IDA at pH 7. However, retention times

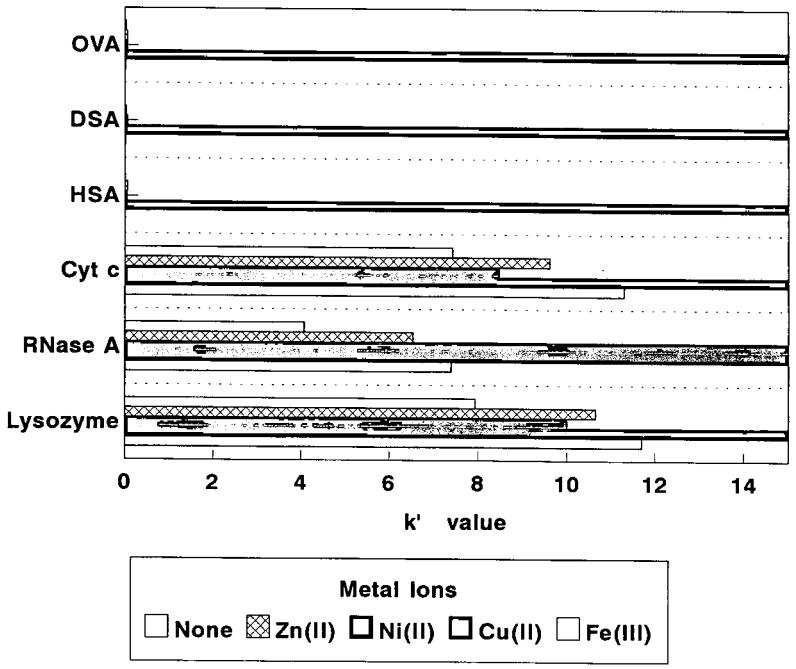

Fig. 2. Elution of proteins with increasing ionic strength on Polygosil 500 GLYMO-IDA charged with and without metal ions. Column, 30 × 5 mm I.D.; flow-rate, 0.5 ml/min; temperature, 298 K; buffer, 25 m*M* phosphate, pH 7.0; linear gradient in 10 min from 0 to 0.5 *M* NaCl, then in 3 min to 1.0 *M* NaCl. None of the proteins eluted on the GLYMO-IDA:Cu(II), parts of RNase A did not elute on the Ni(II)-loaded chelate, too.

of lysozyme and Cyt c were slightly increased, but not as high as with IDA:Cu(II). Serum albumins did not bind at pH 7 or 8, but at pH 6 and 5. Therefore, a positive charge on Fe(III)-chelates is questionable, as could be assumed from the complexation reaction of Fe(III) and IDA in water (Fig. 1). However, the model proteins and experimental conditions employed in this study do not allow a statement to be drawn on the actual interaction mechanism. Using other model proteins and chromatographic conditions, Sulkowski [19] was able to demonstrate more clearly the mixed interaction mechanism of IDA:Fe(III) and proteins.

On IDA:Zn(II) and IDA:Ni(II), basic proteins were retained more strongly than on naked IDA and alkaline-earth metal chelates, indicating the presence of chelating interactions. On GLYMO-IDA:Zn(II), Cyt c and lysozyme displayed slightly higher interaction than on the Ni(II) chelate. RNase A demonstrated higher interaction with chelated Ni(II) than Zn(II). In case of Ni(II)-loaded CS and GLYMO-IDA, RNase A did not elute in the salt gradient (data of CS not shown). It is important to mention that RNase A did not adsorb on GLYMO-IDA:Ni(II) at high salt concentration. Ni(II)-loaded Epi::IDA and GLYMO-IDA always exhibited broad and flat elution peaks of RNase A, indicating kinetic effects during desorption. It appeared that desorption of this protein from the latter chelates was not complete at elevated NaCl concentration and that parts of the total protein mass was adsorbed strongly.

The strongest chelating interactions were observed with all Cu(II)-loaded chelators. Proteins were not eluted in the salt gradient at pH 7 on GLYMO-IDA:Cu(II). DSA was eluted from butyl-IDA:Cu(II) with low mass recovery and BSA, HSA and RNase A did not elute on CDI::IDA:Cu(II). This is consistent with data obtained from the retention of amino acids [7] and results published by El Rassi and Horváth [1] and other groups [20,21]. Thus, all proteins

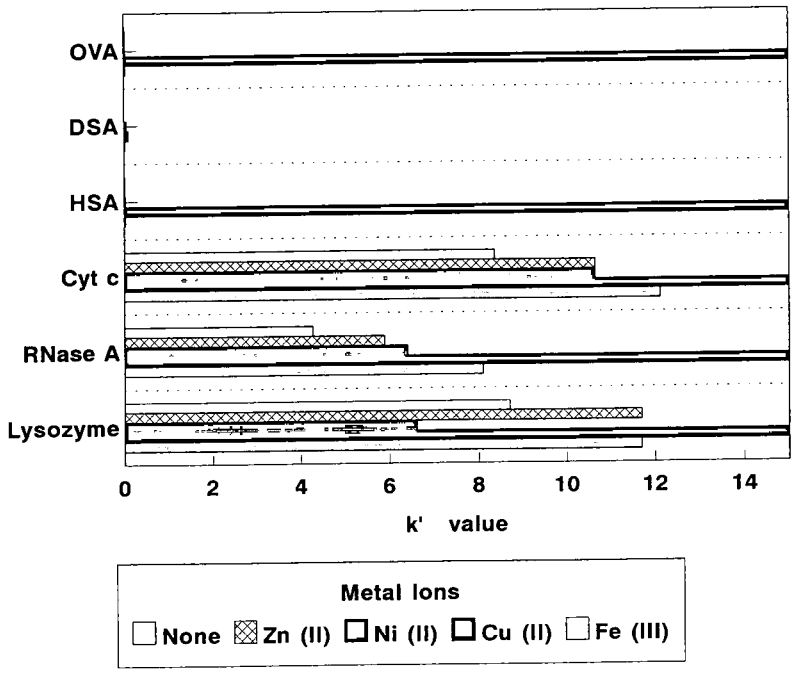

Fig. 3. Elution of proteins with increasing ionic strength on Polygosil 500 butyl-IDA charged with and without metal ions. Chromatographic conditions as in Fig. 2. Only DSA eluted on the Cu(II)-loaded chelate. Ionic interactions are more apparent than with the GLYMO-IDA chelator.

bear at least one accessible histidyl residue which is recognised by all Cu(II)-loaded chelators employed. The high-affinity binding site in BSA and HSA at the N-terminus, involving His 3 [22], does not take part in binding of these proteins onto chelates [15]. Therefore, binding must be ascribed to other histidyl residues present in BSA, HSA and DSA.

Immobilization chemistry

CDI::IDA behaved the most different compared to other chelates. If other metal ions than Cu(II) were loaded onto CDI::IDA, all proteins eluted at low salt content (Fig. 4); Fe(III) was not investigated.

BSA, HSA and RNase A did not elute from Cu(II)-loaded CDI::IDA. If 1 *M* NaCl was applied in the equilibration buffer all serum albumins adsorbed at pH 7 and 8. This indicates chelating interactions of CDI::IDA:Cu(II) with proteins. On the contrary, Cyt c and lysozyme eluted in the salt gradient. These results led to the conclusion that the interactions are ionic rather than chelating. At pH 6, serum albumins were not eluted without exception, but basic proteins less retained than at pH 7. At pH 8 the opposite was true; serum albumins were expelled at low ionic strength. The latter result corresponds well to results from GLYMO-IDA and butyl-IDA.

Non-specific ionic interactions

Considering non-specific ionic interactions, most silica-based sorbents displayed only slightly increased retention of basic proteins compared to Sepharose-based sorbents, except propyl-IDA. Compared with other silica-based affinity sorbents prepared in previous studies [23,24], the impact of these ionic interactions was tolerable; irreversible adsorption of proteins never occurred. However, in comparison to butyl-IDA and other silica-based chelators, on propyl-IDA non-specific interactions were most expressed. Native Sepharose 4B displayed also weak non-

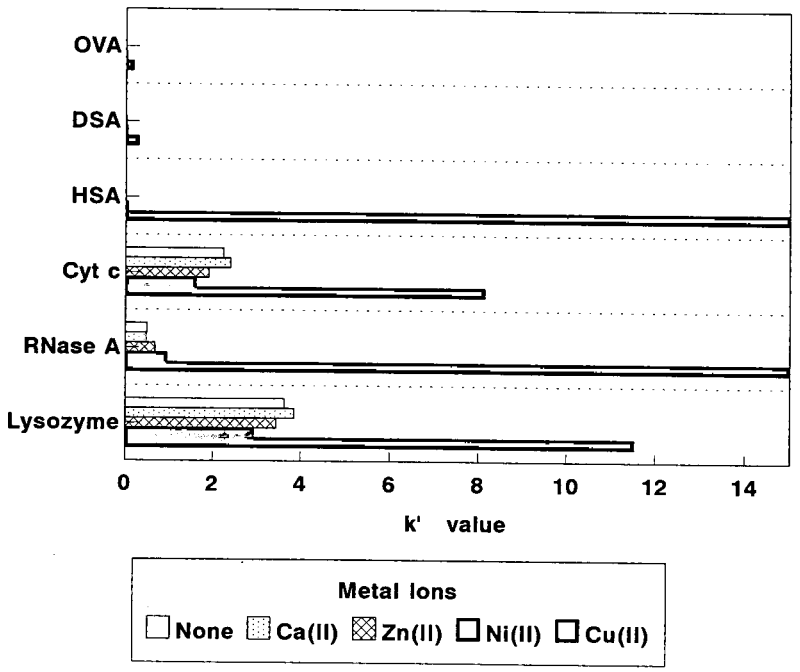

Fig. 4. Elution of proteins with increasing ionic strength on Polygosil 500 CDI::IDA charged with and without metal ions. Chromatographic conditions as in Fig. 2. RNase A and HSA did not elute on the Cu(II)-loaded chelate.

specific interactions with basic proteins. However, with both Sepharose- and silica-based chelators the majority of ionic interactions originated from the carboxyl group of IDA or metal chelates exhibiting a net negative charge, but neither from hydroxyl groups located at the silica surface nor the Sepharose matrix.

pH effects

The development of a negative charge at metal chelates does not occur in a narrow pH range but changes gradually in a range of approximately two pH units [8]. With all Cu(II)-loaded IDA sorbents the change of the interaction mechanism was most apparent, leading to non-binding of proteins at elevated pH. Comparing the adsorption behaviour of negatively charged serum albumins and OVA in Table 2, the development of a negative charge occurs at rather low pH (pH 5–7) on propyl-IDA and butyl-IDA but at elevated pH ($\geq$ pH 8) on epoxy-immobilised IDA. The exact pH cannot be provided at which the negative charge becomes effective; yet, the charge density on the metal chelate affinity sorbent increases with increasing pH. The present results indicated kinetic effects at the transition pH. Kinetic effects either led to partial breakthrough of negatively charged proteins or to apparent low protein recoveries in the salt gradient.

Histidyl residues coordinate to IDA chelates in their unprotonated form only [18]. Therefore, at pH 6 proteins were less retained on IDA:Ni(II) than at pH 7 or 8. At pH 6, all proteins, including RNase A, eluted in the salt gradient; thus interactions were mainly ionic. On IDA:Cu(II), proteins demonstrated significant changes in the elution behaviour at pH 5 only (Table 2). However, at this pH only basic proteins eluted at high salt concentration.

Buffer salt

Exchange of phosphate against acetate, pH 5 or Tris · HCl, pH 8, provided no benefits. Using acetate resulted in nearly identical retention of proteins as observed with phosphate buffers. Tris

Table 2
Retention behaviour of proteins on Cu(II)-loaded chelators

Sorbent	HSA				OVA				DSA				Cyt C				RNase A				Lysozyme			
	8	7	6	5	8	7	6	5	8	7	6	5	8	7	6	5	8	7	6	5	8	7	6	5
CS	○	○	○	○	○	○	○	○	○	○	○	○	○	○	○	+	○	○	○	○	○	○	○	+
Epi::IDA	/	○	○	/	/	○	○	/	/	○	○	/	/	○	○	/	/	○	○	/	/	○	○	/
GLYMO-IDA	○	○	○	○	–	○	○	○	–	○	○	○	○	○	+	+	○	○	○	+	○	○	○	+
CDI::IDA	□	○	○	○	□	–	▲	▲	□	–	○	○	+	+	+	+	○	○	▲	▲	○	+	▲	▲
Propyl-IDA	–	○	○	○	–	–	□	○	–	–	□	○	○	○	○	○	○	○	○	○	○	○	○	○
Butyl-IDA	–	○	○	○	–	○	○	○	–	□	○	○	○	○	○	+	○	○	○	+	○	○	○	+

Chromatographic conditions: 25 m*M* phosphate; linear gradient in 10 min from 0 to 0.5 *M* NaCl, in 3 min to 1 *M* NaCl, pH as indicated below proteins. Symbols: – = not retained; + = retained and eluted; ○ = not eluted; □ = low mass recovery; ▲ = broad peak; / = no data

caused a higher displacement of metal ions than phosphate. However, chromatographic properties did not change significantly. The displacement of Cu(II) by Tris is due to the complexation of this metal ion by Tris, resulting in a competition of IDA and Tris for it. This phenomenon was most apparent at low salt concentration.

In another study [25] the displacement of concanavalin A by Tris from Cu(II)-loaded IDA was observed over a long period of time. Concanavalin A is considered to bind very strongly onto this chelate [26]. However, in the presence of Tris displacement of the metal ion took place and consequently a decrease in capacity was evident over a long time scale.

3.3. Adsorption at high ionic strength

At high ionic strength ionic interactions on metal chelates are suppressed; thus, specific interactions with proteins are the dominating force under these conditions.

Spacer length

Considering Ni(II)-loaded IDA, complete adsorption of RNase A was evident on both CS and GLYMO-IDA in the presence of 0.5 or 1 *M* NaCl and pH 7 (data not shown). On Ni(II)-loaded Epi::IDA, butyl- and propyl-IDA, RNase A was not adsorbed. RNase A exposes 2 histidyl residues at the protein surface. It is discussed in literature that at least 2 accessible histidyl residues are required for adsorption on IDA:Ni(II) chelates [5]. The result mentioned above indicate that one of the two histidyl residues might only be reached by a long spacer, as provided by CS and GLYMO-IDA.

Propyl-IDA:Cu(II) did not display chelating interactions with OVA and DSA in contrast to epoxy-bound chelates (data not shown). Butyl-IDA displayed kinetic effects during adsorption of DSA and OVA, resulting in the breakthrough of minor amounts of these proteins (see also results at low salt concentrations). These results can be explained by the short spacers of these metal chelate sorbents. Short spacers restrict the flexibility of immobilised chelates. Consequently, the imidazole group of a histidyl residue cannot be reached if not exposed at the protein surface. It is plausible that also protein surface-located histidyl residues differ in their degree of flexibility, depending on the environment. Therefore, histidyl residues demonstrating low flexibility may only be attached to chelates immobilised through longer spacers, such as GLYMO or bisoxirane.

Elution with decreasing salt gradient

All proteins adsorbed on Cu(II)-loaded GLYMO-IDA, CDI::IDA, and butyl-IDA at pH 8 and 1 *M* NaCl (see also Fig. 6 for comparison).

It was of interest whether serum albumins would be expelled and consequently eluted at this pH and low salt concentration after being adsorbed at high salt content. In practice, elution at low ionic strength seemed to be an extremely slow process on the time scale of the experiment (25–30 column volumes in 10 min). Only on butyl-IDA:Cu(II) elution was apparent without doubt; also partial breakthrough of DSA and OVA took place. On CDI::IDA:Cu(II) elution did in fact not occur. On GLYMO-IDA, OVA eluted in a broad peak; the elution of serum albumins was uncertain. Likely, once the chelate–protein complex is formed at 1 *M* NaCl, desorption depends mainly on the dissociation rate at low ionic strength, which appears to be slow. Desorption seems not to be enhanced by repulsion of both negatively charged serum albumins or OVA and chelates at low ionic strength.

Elution with imidazole gradient

Imidazole is a competitive substrate, displacing adsorbed proteins at pH 7 or 8 through formation of a chelate–imidazole complex. Such elution conditions are important for sensitive proteins which may lose biological activity at low pH. In practice, best reproduction of chromatographic conditions is obtained by adding 1 m*M* imidazole in the equilibration buffer [6], thereby forming the chelate–imidazole complex before adsorption of proteins. However, some proteins, such as Cyt c, were found not to adsorb under this condition [10]. Imidazole was therefore not used in the equilibration buffer, in order to avoid misinterpretation of results. Thus, imidazole elution from this study cannot be compared directly with data from other groups.

Best binding conditions were found at pH 7 for Cu(II)- and Ni(II)-loaded IDA (Fig. 5). Below pH 6, basic proteins did not adsorb even

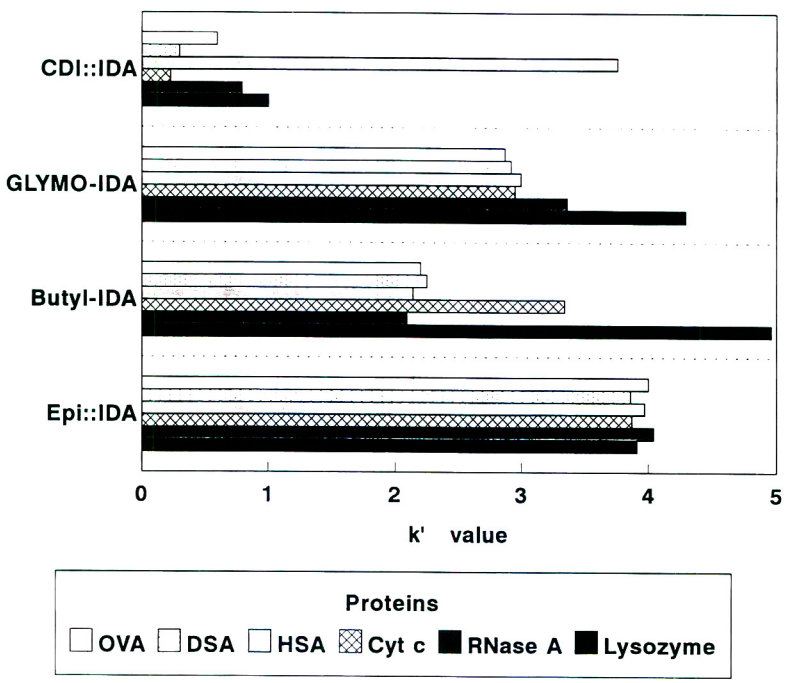

Fig. 5. Elution of proteins with imidazole gradient on Cu(II)-loaded chelators with different immobilization chemistry and spacer length. Column, 30 × 5 mm I.D.; flow-rate, 0.5 ml/min; temperature, 298 K; buffer, 25 m*M* phosphate + 0.5 *M* NaCl, pH 7; gradient in 20 min to 50 m*M* imidazole, then in 5 min to 100 m*M* imidazole; for the CDI::IDA chelate concentrations of imidazole of 12.5 and 25 m*M* were realised, respectively.

on Cu(II)-loaded butyl-IDA or epoxy-immobilised IDA. These results confirmed that interactions at pH 6 and low ionic strength were mainly ionic with these chelates. Consistently, BSA, HSA and RNase A eluted at higher retention times (≈30%) from Ni(II)-loaded than from Cu(II)-loaded CS and GLYMO-IDA. This seems to be contrary to the chromatography of human serum transferrin from Ni(II)- and Cu(II)-loaded CS which was eluted later from the latter chelate [13]. Perhaps the absence of imidazole in the adsorption buffer effects protein elution. However, an explanation for this behaviour has not been found yet.

In the presence of 0.15 *M* NaCl, silica-based IDA:Cu(II) and IDA:Ni(II) demonstrated nonspecific ionic interactions in addition, especially with Cyt c and lysozyme (data not shown). Nonspecific ionic interactions were most apparent with propyl-IDA. Presumably, the close proximity of hydroxyl groups at the silica surface resulted in ionic interactions with positively charged proteins. In the presence of 0.5 *M* NaCl, as represented in Fig. 5, all proteins eluted between 10 and 20 m*M* imidazole at very close retention times for individual chelating gels, except on CDI::IDA. Discrimination of surface properties of different proteins did not take place on GLYMO-IDA and Epi::IDA. This is a major disadvantage of this particular elution method.

Protein interactions with the CDI::IDA chelate were rather weak. Therefore, a shallower imidazole gradient was applied for this chelate. Most proteins were recovered from the column at approximately 2–3 m*M* imidazole (Fig. 5). The interaction with HSA was stronger; elution took place between 5 and 7 m*M* imidazole.

The interaction of basic proteins with epoxy- and butyl-immobilised IDA seems to be different, because the elution order of proteins changed (Fig. 5). Elution order is Cyt c < RNase A < lysozyme on GLYMO-IDA:Cu(II) whereas RNase A < Cyt c < lysozyme was found on the butyl-IDA:Cu(II) at pH 7. Retention of amino acids indicated lower selectivity for histidines but higher selectivity for lysine with butyl-IDA:Ni(II) compared to other chelates [7]. In view of these results, the interaction of RNase A seems to occur mainly with histidyl residues while Cyt c and lysozyme interact with basic amino acid residues, such as lysine and/or arginine, in addition. Both proteins are rich in the latter amino acids.

Elution with pH gradient on Cu(II)-loaded chelators

By decreasing the pH, histidyl residues are protonated, consequently leading to elution of adsorbed proteins. This represents a common elution protocol [16,27,28]. In a first set of experiments, a steep pH gradient was chosen. As a result, eluted proteins displayed similar retention times. With a shallower pH gradient better discrimination of proteins was achieved (Fig. 6).

CDI::IDA allows the separation of some proteins in the pH gradient. The peak of OVA was relatively broad compared to other proteins and the mass recovery of DSA relatively low. Perhaps DSA does not completely elute under these chromatographic conditions.

On epoxy-immobilised chelates, serum albumins and OVA were most strongly retained. Results varied with variation of the spacer length. On GLYMO-IDA and CS, HSA did not elute even on a prolonged time scale. Andersson *et al.* [15] observed the same chromatographic behaviour of HSA on CS:Cu(II) under these conditions. On the contrary, on Epi::IDA all proteins eluted at low pH.

Obviously, a shallow pH gradient is necessary to discriminate between surface properties of different proteins. These results are in concordance with results published by Nakagawa *et al.* [14], who applied very shallow pH gradients over a period of 80 min for the isolation of various peptides.

3.4. Bleeding of Cu(II)

Bleeding of Cu(II) was apparent with all immobilised metal chelates at elevated imidazole concentration or low pH. It was most evident with butyl-IDA and propyl-IDA, increasing in that order. With propyl-IDA the first 2 mm of

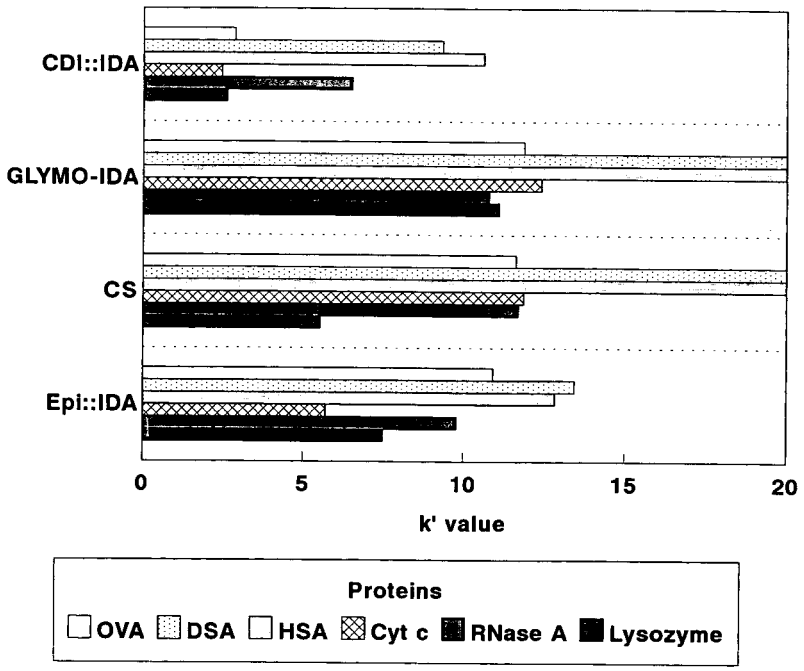

Fig. 6. Elution of proteins with decreasing pH on Cu(II)-loaded chelators with different immobilization chemistry and spacer length. Buffer, 25 m*M* phosphate + 0.5 *M* NaCl, pH 8; linear gradient in 15 min to pH 2.8 and holding at this pH for 10 min. Other chromatographic conditions as in Fig. 5

the column bed were virtually uncharged after running 8 times the pH gradient.

3.5. Capacity of affinity sorbents

IDA:Fe(III) chelates

During adsorption of lysozyme in the frontal chromatographic mode significant amounts of Cu(II) were displaced from propyl-IDA:Cu(II) at pH 7. Thus, determination of the protein capacity was not possible. Loading propyl-IDA with Fe(III) provided reproducible chromatographic conditions. Apparently, bleeding of Fe(III) from this chelate did not occur at pH 5. For the sake of comparison, also the other chelators were charged with Fe(III) and analyzed at this pH. Protein capacities and apparent dissociation constants (K_d) are displayed in Table 3. Comparing the capacities of the chelators for these proteins represent more or

Table 3
Adsorption of lysozyme and BSA on Fe(III) chelates

	Capacity (mmol/l)		Capacity (g/l)		Apparent K_d (*M*)	
	Lys	BSA	Lys	BSA	Lys	BSA
GLYMO-IDA	1.35	0.37	19.4	25.2	$7.9 \cdot 10^{-5}$	$3 \cdot 10^{-6}$
Propyl-IDA	1.53	0.59	22	40	$5.6 \cdot 10^{-5}$	$6.6 \cdot 10^{-6}$
CDI::IDA	0.09	0.05	1.3	3.6	$1.9 \cdot 10^{-4}$	$1.1 \cdot 10^{-5}$
CS	1.39	1.1	20	75	$8.3 \cdot 10^{-5}$	$2.9 \cdot 10^{-6}$

less a mirror of the Cu(II) capacities on these chelators, as described in Part I [7]. The CDI-immobilised chelate yielded the lowest capacity, as a consequence of the lower ligand densities. Except for CDI::IDA:Fe(III), dissociation constants of different metal chelates to a particular protein were close. CDI::IDA:Fe(III) displayed higher dissociation constants for lysozyme and BSA, indicating lower interactions with the chelate.

The capacity for lysozyme was lower than for BSA with all chelates. At first, this seems to be inconsistent with results obtained from other porous affinity sorbents. The capacities for larger proteins is usually lower than for smaller proteins due to pore size restrictions. However, the reason for the low capacity for lysozyme in this study is the higher NaCl concentration employed (0.5 *M* NaCl for lysozyme, 0.1 *M* was required for adsorption of BSA). The dependence on salt concentration is unusual for metal chelate interactions and indicative for ionic interactions [19]. Probably, the iron chelate exhibits a negative charge at pH 5. Therefore, ionic interactions may play a key role in the adsorption of proteins at IDA:Fe(III). Hence, the dissociation constant is an apparent thermodynamic value, the interaction is taking place at least partial via several charged groups at the protein surface.

IDA:Cu(II) chelates

Cu(II)-loaded butyl-IDA and GLYMO-IDA were stable during the application of proteins. Double reciprocal plots of experimental data revealed that the chelators displayed Langmuir-type adsorption behaviour, characterised by a linear relationship of transformed adsorbate concentration in solution and the stationary phase. Both lysozyme and BSA displayed lower interaction with Cu(II)-loaded butyl-IDA than GLYMO-IDA (Table 4) at pH 7. Furthermore, protein capacities were lower with butyl-IDA.

Both metal chelate sorbents demonstrated a lower capacity for BSA than for lysozyme. Thus, the copper chelate demonstrates rather chelating interaction. BSA requires more space in the porous system due to its size; therefore, the accessibility of the affinity ligands is lower [29,30].

The stability of the covalent linkage of GLYMO-IDA is high. In 10 consecutive runs no apparent loss in protein capacity took place (Fig. 7). Data fluctuations in Fig. 7 demonstrate the error in the determination of the breakthrough time, as calculated automatically by the integrator. The results confirm that the capacity of this copper chelate is nearly independent of the salt concentration, as typical for metal chelate interactions.

In contrast, the propyl-IDA sorbent demonstrated a loss of capacity with time. In zonal chromatography, such a decline in capacity is usually not evident because only parts of the total capacity of chromatographic sorbents are utilised. Of course, the loss in protein capacity restricts the life time of the propyl-IDA sorbent.

4. Discussion

It is apparent that chelators bound through an epoxy group onto silica, such as the glycidoxy group in GLYMO, displayed the most comparable results with CS. With CS, IDA is also bound

Table 4
Adsorption of lysozyme and BSA on Cu(II) chelates

	Capacity (mmol/l)		Capacity (g/l)		Apparent K_d (*M*)	
	Lys	BSA	Lys	BSA	Lys	BSA
Butyl-IDA	1.67	0.176	24	12	$1.6 \cdot 10^{-5}$	$3 \cdot 10^{-6}$
GLYMO-IDA	3.06	0.346	44	23.5	$5.9 \cdot 10^{-6}$	$1.7 \cdot 10^{-6}$

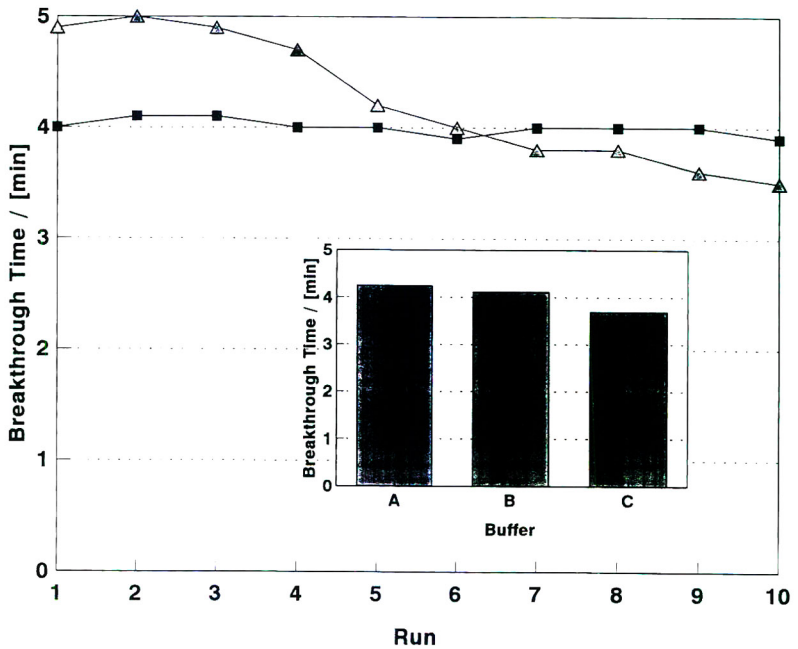

Fig. 7. Capacity and hydrolytic stability of Cu(II)-loaded silica-based sorbents during frontal chromatography of lysozyme. Column 25 × 4 mm I.D.; flow-rate, 0.5 ml/min; temperature, 298 K; buffer, 25 m*M* phosphate + 0.5 *M* NaCl, pH 7.0, lysozyme concentration 1 g/l. The capacity of Polygosil 500 butyl-IDA (▲) decreases from run to run, whereas the capacity of the GLYMO-IDA chelator (■) is almost constant. Inset: dependence of capacity on salt concentration on the GLYMO-IDA chelate; (A) no NaCl, (B) 0.5 *M* NaCl, (C) 1.2 *M* NaCl in phosphate buffer, pH 7.0.

through an epoxy group [6,28]. The adsorption and elution behaviour of GLYMO-IDA chelates was almost identical to CS under the chosen chromatographic conditions. This is in concordance with results obtained from the chromatography of amino acids [7]. Furthermore, Cu(II)- and Fe(III)-loaded GLYMO-IDA demonstrated high capacity for lysozyme and BSA. The capacity is similar to silica-based ion exchangers. Therefore, GLYMO-IDA is recommended in case published chromatographic protocols shall be applied for a silica-based metal chelate sorbent.

4.1. Spacer length

It is a general observation in affinity chromatography that long spacers lead to improved flexibility of affinity ligands [31,32]. Likely, this is true also for metal chelate affinity sorbents. Likely, also the mobility of amino acid residues located at the protein surface is of influence for binding.

Considering X-ray structural analysis data of OVA [33], most of the histidyl residues are not accessible. The adsorption of OVA onto IDA:Cu(II) occurs through His 44, which is situated in a hydrophobic environment at the protein surface. Due to the short spacer of propyl-IDA this histidyl residue may not be reached; therefore, no adsorption of OVA is observed on this chelate. Butyl- or GLYMO-spacers may facilitate the correct orientation of IDA in the encounter with this histidyl residue. In the experiment, OVA was indeed retained on both Cu(II)-loaded chelators. However, with the butyl-IDA partial breakthrough of OVA occurred. This indicates that steric restrictions at close encounter of protein and ligand take place. With GLYMO-IDA:Cu(II), no breakthrough of OVA took place.

Although GLYMO-IDA is immobilised through an epoxy group onto silica, it appears

that the spacer between the silica matrix and the chelator is somewhat shorter than with CS. This led to two exceptions of the compatibility of silica-based and commercial chelator with the proteins employed. HSA and BSA were adsorbed only on Ni(II)-loaded CS. Thus, the binding histidyl residues of these proteins (at least two [15]) are available only for interaction with the long spacer of CS:Ni(II) but not with GLYMO-IDA.

With RNase A, X-ray structural data revealed that the two histidyl residues with highest probability for interaction are located at different positions on the surface of the protein. RNase A displays a kidney-like shape [34]. While His 105 is highly accessible at the protein surface, His 119 is located in the active site at a less accessible position. This might be an explanation that RNase A adsorbed on CS:Ni(II) only.

Chelates bound via long spacers are able to penetrate more deeply into cavities or metal binding sites of proteins. After binding onto a histidyl residue they might be able to interact with amino acid residues located close to the chelate, in addition. Consequently, chelate–protein complexes might be formed which are more stable at low pH than a typical metal chelate. Although BSA and HSA display a change in protein conformation at pH 4, consequently leading to exposition of more histidyl residues, it seems to be unlikely that they would be uncharged at pH 4. The former interpretation would explain the apparent irreversible binding of HSA and BSA, as observed during pH gradient elution with Cu(II)-loaded GLYMO-IDA and CS. Such behaviour was found with HSA [15] and human serum transferrin [13], as well. With chelates immobilised by short spacers such strong interactions are unlikely, since only single amino acid residues at exposed positions can interact.

4.2. Flexibility of the chromatographic matrix

Comparing results from affinity sorbents based on either inorganic and polymeric chromatographic matrices is a complex task. Besides differences of the chemical composition also structural deviations of the matrices exist. Silica gel is a very rigid matrix which does not allow any structural changes of the surface [35]. In contrast, polymer gels consist of polymer chains, demonstrating a certain degree of mobility [32]. This often leads to compression of a column bed. However, it also allows some flexibility of those polymer chains which are not cross-linked [36].

Differences in the adsorption behaviour on different types of matrices will be more pronounced in case the active site is located in a cavity of the protein. It might be reached by a sufficiently long spacer, as noticed with OVA. In other cases an extremely long spacer or a flexible matrix is required to either extend to the bottom of a cavity or to adapt to a certain extent to the shape of a protein. This might have been required for His 119 of RNase A, which is located at the bottom of the kidney-like structure of this protein.

4.3. Adsorption and elution

Although differences between the metal chelate sorbents were most apparent employing an increasing salt gradient, in practice this elution method plays a minor role. Also, elution at low pH is not always possible, as was experienced with HSA. An imidazole gradient leads to smallest peak volumes compared to other elution models. In case imidazole is absent in the equilibration buffer, as was done in this study, retention times of different proteins were nearly identical, *i.e.* no discrimination of surface properties of proteins took place. Therefore, this method is not recommended in situations where adsorbed proteins shall be separated during elution.

It can be assumed that initially the formation of the metal chelate–protein complex is controlled by ionic interaction. Therefore, interaction of both negatively charged proteins and chelates is possible only at elevated salt content. After formation of the metal chelate–protein complex elution at low ionic strength is controlled mainly by the reverse reaction rate, which appeared to be slow. After dissociation, low ionic strength prevents renewed binding of pro-

teins; however, low ionic strength seemed not to promote the desorption process. Probably, adsorption of serum albumins on GLYMO-IDA and CDI::IDA-Cu(II) chelates is caused by an extremely slow reverse reaction rate which on the other hand indicates that the stabilities of each chelate–protein complex are high.

4.4. Recommendations

Beside chelating interactions, ionic interactions play a key role in MCIC. Primarily, this seems to be a negative property of these group-specific affinity sorbents, thus should be suppressed by addition of salt. However, with a given separation problem, comprising negatively charged contaminants, low salt concentration and high pH may expel negatively charged proteins from a negatively charged chelate which otherwise would have a chance to bind. This is particularly true for butyl-IDA:Cu(II). In case of Ni(II)- or Zn(II)-loaded chelators protein interaction increases at low salt concentration.

The spacer length should be seen as a variable by manufacturers of chelating chromatographic supports. No doubt, highest flexibility of an affinity ligand is achieved with a long spacer; however, high flexibility is not always needed. For those separation problems where the product of interest exposes a histidyl residue at the protein surface but the contaminant's histidyl residue is not as accessible and cannot be reached, a higher selectivity should be possible with a short spacer.

The immobilization chemistry of a commercial chelating gel is usually not known to the user. The present investigation revealed that chromatographic protocols might not be interchangeable without changing chromatographic conditions. This implies that the exact chemical structure of the chelate and the linkage of commercial chelating sorbents should be made available to the user, in order to avoid inconveniences.

5. Conclusions

All the silica-based metal chelate sorbents employed in this study displayed chelating interactions with histidyl residues at protein surfaces. The propyl-IDA however displayed highest non-specific interactions and lowest stability. Thus, it will be disregarded in future applications.

The protein capacities of Cu(II)-loaded GLYMO-IDA and butyl-IDA were comparable to silica-based ion exchangers. The capacity of CDI::IDA:Cu(II) was lowest but can be improved. All three metal chelators displayed low non-specific interactions and good stability of the chemical linkage.

GLYMO-IDA:Cu(II) displayed almost identical chromatographic characteristics compared to commercial CS.

The selectivity of metal chelate affinity sorbents is changed by alteration of the spacer length and/or binding chemistry. Hence, the butyl-IDA chelator and CDI::IDA chelator demonstrated the most different elution behaviour compared to epoxy-immobilised metal chelate sorbents. It seems that butyl-IDA:Cu(II) recognises also lysine and/or arginine residues. CDI::IDA:Cu(II) displayed tight interactions only with serum albumins; thus, the selectivity for these proteins was highest compared to other chelates employed.

The current state of investigation revealed that further optimization in view of pH, ionic strength and composition of the adsorption buffer might be advantageous. Coming investigations will demonstrate whether these new metal chelators represent attractive alternatives for the isolation of proteins from various sources.

Abbreviations

Butyl-IDA	IDA immobilised by butyl-spacer
Butyl-IDA:Cu(II)	Cu(II)-loaded butyl-IDA
CDI	1,1′-Carbonyldiimidazole
CDI::IDA	CDI-immobilised IDA
CDI::IDA:Cu(II)	Cu(II)-loaded CDI::IDA
CS	Chelating Sepharose FF
CS:Cu(II)	Cu(II)-loaded CS
Cyt c	Cytochrome *c*

DSA	Dog serum albumin
Epi::IDA	Epibromohydrin-immobilized IDA
FPLC	Fast protein liquid chromatography
GLYMO	3-Glycidoxypropyltrimethoxysilane
GLYMO-IDA	GLYMO-immobilised IDA
GLYMO-IDA:Cu(II)	Cu(II)-loaded GLYMO-IDA
HSA	Human serum albumin
IDA	Iminodiacetic acid
IDA:Cu(II)	Cu(II)-loaded IDA
MCIC	Metal chelate interaction chromatography
OVA	Ovalbumin
Propyl-IDA	IDA immobilised through propyl spacer
RNase	Ribonuclease

Acknowledgments

The help from Dr. K.-D. Aumann from the Molecular Structure Research Department at GBF during analysis of contour plots of the proteins is very much appreciated.

Financial support was provided by the Hochschulnachwuchsförderungsprogramm of the German federal ministry of education and research (HSP II).

References

[1] Z. El Rassi and Cs. Horváth, *J. Chromatogr.*, 359 (1986) 241.
[2] Y. Kato, K. Nakamura and T. Hashimoto, *J. Chromatogr.*, 354 1986 511.
[3] T.-T. Yip and T.W. Hutchens, *UCLA Symp. Mol. Cell. Biol., New Ser.*, 80 (1989) 45.
[4] E. Sulkowski, *BioEssays*, 10 (1989) 170.
[5] L. Kågedal, in J.C. Janson and L. Rydén (Editors), *Protein Purification*, VCH, New York, 1989, Ch. 8, p. 227.
[6] E. Sulkowski, *Trends Biotechnol.*, 3 (1985) 1.
[7] F.B. Anspach, *J. Chromatogr. A*, 672 (1994) 35.
[8] S. Chaberek and A.E. Martell, *J. Am. Chem. Soc.*, 74 (1952) 5052.
[9] S. Chaberek and A.E. Martell, *J. Am. Chem. Soc.*, 76 (1954) 215.
[10] E.S. Hemdan, Y.-J. Zhao, E. Sulkowski and J. Porath, *Proc. Natl. Acad. Sci. U.S.A.*, 86 (1989) 1811.
[11] M. Belew and J. Porath, *J. Chromatogr.*, 516 (1990) 333.
[12] J. Porath and B. Olin, *Biochemistry*, 22 (1983) 1621.
[13] E. Sulkowski, in S.K. Sikdar, P.W. Todd and M. Bier (Editors), *Frontiers in Bioprocessing*, CRC Press, Boca Raton, FL, 1989, Ch. 29, p. 343.
[14] Y. Nakagawa, T.-T. Yip, M. Belew and J. Porath, *Anal. Biochem.*, 168 (1988) 75.
[15] L. Andersson, E. Sulkowski and J. Porath, *Bioseparation*, 2 (1991) 15.
[16] L. Andersson, E. Sulkowski and J. Porath, *J. Chromatogr.*, 421 (1987) 141.
[17] D. Schomburg and J. Reichelt, *J. Mol. Graphics*, 6 (1988) 161.
[18] E. Sulkowski, *UCLA Symp. Mol. Cell. Biol., New Ser.*, 68 (1987) 149.
[19] E. Sulkowski, *Makromol. Chem., Macromol. Symp.*, 17 (1988) 335.
[20] M. Belew, T.-T. Yip, L. Andersson and R. Ehrnström, *Anal. Biochem.*, 164 (1987) 457.
[21] R.M. Chicz and F.E. Regnier, *Anal. Chem.*, 61 (1989) 1742.
[22] T. Peters and F.A. Blumenstock, *J. Biol. Chem.*, 242 (1967) 1574.
[23] F.B. Anspach, K.K. Unger, J. Davies and M.T.W. Hearn, *J. Chromatogr.*, 457 (1988) 195.
[24] F.B. Anspach, K.K. Unger, P. Stanton and M.T.W. Hearn, *Anal. Biochem.*, 179 (1989) 171.
[25] F.B. Anspach, G. Altmann and W.-D. Deckwer, *Biotechnol. Appl. Biochem.*, in press.
[26] Z. El Rassi, Y. Truei, Y.-F. Maa and Cs. Horváth, *Anal. Biochem.*, 169 (1988) 172.
[27] G. Lindeberg, H. Bennich and Å. Engström, *Int. J. Peptide Protein Res.*, 38 (1991) 253.
[28] B. Lönnerdal and C.L. Keen, *J. Appl. Biochem.*, 4 (1982) 203.
[29] B.H. Arve and A.T. Liapis, *AIChE J.*, 33 (1987) 179.
[30] D.J. Winzor and J. de Jersey, *J. Chromatogr.*, 492 (1989) 377.
[31] P.-O. Larsson, M. Glad, L. Hansson, M.-O. Mansson and K. Mosbach, *Adv. Chromatogr.*, 21 (1982) 41.
[32] P.D.G. Dean, W.S. Johnson and F.A. Middle, *Affinity chromatography —A Practical Approach*, IRL Press, Oxford, 1985, p. 34.
[33] P.E. Stein, A.G.W. Leslie, J.T. Finch and R.W. Carrell, *J. Mol. Biol.*, 221 (1991) 941.
[34] N. Borkakoti, D.S. Moss and R.A. Palmer, *Acta Crystallogr., Sect. B*, 38 (1982) 2210.
[35] K.K. Unger, B. Anspach, R. Janzen, G. Jilge and K.D. Lork, in Cs. Horváth (Editor), *High-Performance Liquid Chromatography —Advances and Perspectives*, Vol. 5, Academic Press, San Diego, CA, 1988, p. 2.
[36] F.B. Anspach, A. Johnston, H.-J. Wirth, K.K. Unger and M.T.W. Hearn, *J. Chromatogr.*, 499 (1990) 103.

[37] A. Carsana, E. Confalone, M. Palmieri, M. Libonati and A. Furia, *Nucleic Acid Res.*, 16 (1988) 5491.
[38] E. Margoliash, E.L. Smith, G. Kreil and H. Tuppy, *Nature*, 192 (1961) 1125.
[39] R.E. Canfield, *J. Biol. Chem.*, 238 (1963) 2698.
[40] Y.-J. Zhao, E. Sulkowski and J. Porath, *Eur. J. Biochem.*, 202 (1991) 1115.
[41] P.P. Minghetti, D.E. Ruffner, W.J. Kuang, O.E. Dennison, J.W. Hawkins, W.G. Beattie and A. Dugaiczyk, *J. Biol. Chem.*, 261 (1986) 6747.
[42] J.R. Brown, *Fed. Proc.*, 34 (1975) 591.
[43] S.L.C. Woo, W.G. Beattie, J.F. Catterall, A. Dugaiczyk, R. Staden, G.G. Brownlee and B.W. O'Malley, *Biochemistry*, 20 (1981) 6437.

ELSEVIER

Journal of Chromatography A, 676 (1994) 267–275

JOURNAL OF CHROMATOGRAPHY A

Cross-linked N,N-dimethylaminopropylacrylamide spherical particles for selective removal of endotoxin

Chuichi Hirayama*, Masayo Sakata, Yasuhiro Yugawa, Hirotaka Ihara

Department of Applied Chemistry, Faculty of Engineering, Kumamoto University, 2-39-1 Kurokami, Kumamoto 860, Japan

First received 30 November 1993; revised manuscript received 14 March 1994

Abstract

Spherical polymer adsorbents for endotoxin adsorption were prepared by suspension copolymerization of N,N-dimethylaminopropylacrylamide (DMAPAA) with N-allylacrylamide (AAA). The amino-group contents and the pore size of the adsorbents were easily adjusted by changing the monomer ratio and diluent ratio. The more amino groups are introduced, the larger is the endotoxin-adsorbing capacity of the adsorbent, and the smaller the pore size (molecular mass exclusion, M_{lim}) of the adsorbent, the less acidic proteins such as bovine serum albumin are adsorbed. When M_{lim} was smaller than 300 (as the molecular mass of polysaccharide) and the amino group content was 4.5 mequiv./g, the DMAPAA–AAA adsorbent showed a high endotoxin-removing activity at an ionic strength of $\mu = 0.05$–0.4 and pH 5–9. The adsorbent was also able to remove endotoxin from a protein solution, naturally contaminated with endotoxin, at $\mu = 0.05$ without affecting the recovery of the protein. The adsorbent can be completely regenerated by washing with 0.2 *M* sodium hydroxide followed by 2.0 *M* sodium chloride.

1. Introduction

Removal of endotoxin (lipopolysaccharide, LPS) from substances used as drugs is very important, as its potent biological activity causes pyrogenic and shock reactions in mammals on intravenous injection even in nanogram amounts [1–3]. Endotoxin, a constituent of the cell wall of Gram-negative bacteria, is a potential contaminant of physiological fluids and aqueous solutions and a very stable molecule which resists extreme temperatures and pH values. For removing endotoxin from solutions of high-molecular-mass compounds, such as proteins, adsorption techniques are used.

Recently, some endotoxin adsorbents, immobilized histidine [4–6] and polymyxin-Sepharose [7], have become commercially available. Although these adsorbents have high capacities for adsorbing endotoxin, adsorption of acidic proteins such as bovine serum albumin (BSA) also occurs at a low ionic strength of $\mu = 0.05$ and neutral pH. As the ionic strength increased, the adsorption of BSA by the adsorbents decreased, and at a high ionic strength ($\mu = 0.2$–0.8) adsorption of endotoxin was also very slight [5].

We attempted, therefore, to develop endotoxin adsorbents capable of retaining a high endotoxin-removing activity over a wide range of ionic strength. We have reported that aminated poly(γ-methyl L-glutamate) (PMLG) spheres

* Corresponding author.

0021-9673/94/$07.00
SSDI 0021-9673(94)00264-A

having diaminoethane as a ligand have a high endotoxin-removing activity even at a high ionic strength ($\mu = 0.2$–0.8) [8,9]. Further, we found that the interaction of various proteins with the aminated PMLG adsorbent decreased with decrease in the pore size of the spheres [10]. However, this adsorbent is unsatisfactory with respect to complete regeneration because it is generally considered that PMLG, having esteratic sites (–CO–O– bonds), is gradually hydrolysed in an alkaline solution, one of the solvents used for regeneration.

In this work, we attempted to develop novel endotoxin adsorbents that can be produced on a large scale and can be easily regenerated many times. This paper describes the synthesis of novel spherical copolymers from N,N-dimethylaminopropylacrylamide (DMAPAA) (monomer), having amino groups [CH_2=CHCONH(CH_2)$_3$ · N(CH_3)$_2$], and N-allylacrylamide (AAA) (water-soluble cross-linking agent) (CH_2=CHCONHCH$_2$CH=CH_2), being highly soluble in the monomer by one-step polymerization. We describe also the characteristics and applications of the spherical copolymers for the selective removal of endotoxin and the regeneration of this adsorbent.

2. Experimental

2.1. Materials

Purified endotoxin (*Escherichia coli* UKT-B) was purchased from Wako (Osaka, Japan) and other endotoxins from Difco (Detroit, MI, USA). Limulus ES-J test Wako (Limulus amoebocyte lysate) was a product of Wako.

Immobilized histidine (Pyro Sep) was purchased from Daicel (Tokyo, Japan). N,N-Dimethylaminopropylacrylamide (DMAPAA) monomer (Kohjin, Tokyo, Japan) and N-allylacrylamide (AAA) cross-linking agent (Kohjin) were purified by vacuum distillation at 131°C/1 mmHg and 115°C/0.7 mmHg, respectively.

Proteins were purchased from Wako. Endotoxin-free water was kindly supplied by the Chemo-Sero-Therapeutic Research Institute (Kumamoto, Japan). All other chemicals were of analytical-reagent grade.

2.2. Synthesis of adsorbents

DMAPAA monomer, AAA as a cross-linking agent, 1-hexanol as a diluent and 2 mass-% azobisisobutyronitrile as an initiator were mixed at room temperature. The mixture was added to a 25 mass-% anhydrous sodium sulphate solution containing 1% sodium carboxymethylcellulose, which were suspended by stirring. The suspension was heated at 80°C for 12 h. The DMAPAA–AAA (DAA) copolymer particles obtained were washed successively with water, hot water, methanol and ethanol.

DAA particles with diameters of 44 to 105 μm were used as adsorbents.

2.3. Determination of amino group contents of adsorbents

Amino groups were determined by pH titration and elemental analysis as described previously [8].

2.4. Determination of the pore size of the adsorbent

The prepared DAA adsorbents were packed into a stainless-steel column (150 × 5 mm I.D.). The chromatograph included a JASCO Model 880-PU pump and a Shodex SE-51 refractometric monitor. The pore size (molecular mass exclusion, M_{lim}) of the matrix in the adsorbent was calculated from calibration graphs obtained by size-exclusion chromatography (SEC). Homogeneous series of pullulan and maltose were used as permeable substances. The calibration graphs were obtained by plotting the average molecular masses against the peak elution volumes. The M_{lim} value was determined by extrapolating the linear part of the graph as described previously [11,12].

2.5. Adsorption of endotoxin

The adsorption of endotoxin was measured by a batchwise method as follows. The adsorbent was washed and equilibrated with various buffers with different ionic strengths as described previously [9]. A 0.2–0.3-g portion of wet adsorbent was suspended in 2–3 ml of an endotoxin solution. The suspension was shaken for 2 h at 25°C and filtered through a Millipore filter (0.8 μm) to remove the adsorbent. The endotoxin content of the filtrate was determined. The apparent dissociation constant (K_d) between endotoxin and adsorbent was calculated from the adsorption isotherm as described previously [5,6].

2.6. Reproducibility of adsorbent

The reproducibility of the adsorbent was determined with a frontal column as follows. A 0.7-ml portion of wet adsorbent was packed in a sterilized glass column (10 × 0.3 cm I.D.) and the column was washed with 20 ml of 2.0 *M* sodium chloride and then equilibrated with 0.02 *M* phosphate buffer (pH 7.0, $\mu = 0.05$). An endotoxin solution (1000 ng/ml, purified LPS from *E. coli* UKT-B) was passed through the column at a flow-rate of 0.2 ml/min at room temperature. Fractions of 25 ml were collected and the endotoxin concentration in each fraction was determined.

The column was reused after washing with 20 ml of 0.2 *M* sodium hydroxide, 2.0 *M* sodium chloride and endotoxin-free water.

2.7. Endotoxin assay

Endotoxin was assayed by the Limulus test involving turbidimetric time assay at 660 nm with a Toxinometer ET-201 (Wako) [13]. Purified endotoxin (*E. coli* UKT-B) was used as the standard. Limulus ES-J test Wako was used as the reagent for the reaction.

2.8. Protein assay

The protein concentration was measured with a UV-160 spectrophotometer (Shimadzu) at 280 nm (proteins other than cytochrome *c*) or 410 nm (cytochrome *c*).

3. Results and discussion

3.1. Effects of various factors on the endotoxin-adsorbing activity of adsorbents

The endotoxin-adsorbing activities of the adsorbents were examined by the batchwise method with various kinds of buffers. Two kinds of standard LPS, from *E. coli* UKT-B and O111:B4, were used as endotoxin-containing samples.

The effects of amino-group contents or M_{lim} of DMAPAA–AAA (DAA) adsorbents on the adsorption of endotoxins were investigated at pH 7.0 and ionic strength $\mu = 0.05$. The results are given in Table 1. DAA adsorbents with pore sizes <300–40 000 as M_{lim} and amino-group content [$-N(CH_3)_2$] of 1.1–5.1 mequiv./g were prepared. The amino-group content and M_{lim} of the adsorbents were easily adjusted by changing the DMAPAA (monomer) ratio and 1-hexanol (diluent) ratio in the suspension copolymerization; the amino-group content increased from 1.1 to 5.1 mequiv./g with increase in the monomer ratio from 10 to 90 mol-%, and M_{lim} increased from <300 to 45 000 with increase in the diluent ratio (to the DMAPAA–AAA solution) from 0 to 200 vol.-%. Each adsorbent satisfactorily adsorbed endotoxin from endotoxin solutions. When the amino-group content of the adsorbent was 4.5–5.1 mequiv./g (DAA-70–0, -90–0, -70–100, -70–200), the residual concentration of each endotoxin after treatment was below 10 pg/ml.

Fig. 1 shows an electron micrograph of a typical example of DAA adsorbents prepared from DMAPAA and AAA by one-step polymerization without a diluent. The adsorbents were spherical particles with a diameter of about 100 μm.

For selective adsorption of endotoxin, it is necessary to reduce cationic and hydrophobic interactions of the adsorbent with substances such as proteins. The effects of the ionic strength and M_{lim} of the adsorbent on the adsorption of

Table 1
Adsorption of endotoxin by various DAA adsorbents

Adsorbent							Residual concentration of endotoxin after treatment (pg/ml)	
Type	Molar ratio		Diluent[a] (%, v/v)	M_{lim}[b]	Amino-group content[c] (mequiv./g)	S_d[d] (wet-ml/dry-g)		
	DMAPAA (mol%)	AAA (mol%)					*E. coli* UKT-B	*E. coli* O111:B4
DAA-10–0	10	90	0	<300	1.1	2.2	350 000	174 000
DAA-30–0	30	70	0	<300	2.3	2.6	175 000	65 000
DAA-50–0	50	50	0	<300	3.8	2.8	50 000	150
DAA-70–0	70	30	0	<300	4.5	4.3	<10	<10
DAA-90–0	90	10	0	<300	5.1	7.9	<10	<10
DAA-70–100	70	30	100	10 000	4.4	9.0	<10	<10
DAA-70–200	70	30	200	43 000	4.5	23.8	<10	<10

[a] % (v/v) of *n*-hexanol to DMAPAA–AAA solution.
[b] Value reduced as molecular mass of polysaccharide.
[c] Amino groups introduced into the adsorbent.
[d] Degree of swelling in water.
[e] Adsorption of endotoxin by the adsorbent was determined by the batchwise method with 0.3 g of wet adsorbent and 3 ml of endotoxin solution (*E. coli* LPS, 500 ng/ml, pH 7.0, $\mu = 0.05$).

BSA, an acidic protein, were examined with various adsorbents at ionic strengths $\mu = 0.05$–0.4. The adsorbents with an amino-group content of 4.5 mequiv./g and M_{lim} of <300–43 000 were used and the results are shown Fig. 2. Little BSA was adsorbed by the DAA-70–0 adsorbent ($M_{lim} < 300$) at any ionic strength. The BSA-adsorbing capacity of the other adsorbents decreased with increase in the ionic strength. At a low ionic strength ($\mu = 0.05$), the adsorption rate of BSA increased from 0 to 98% with increase in M_{lim} of the adsorbent from <300 (DAA-70–0) to 43 000 (DAA-70–200). Im-

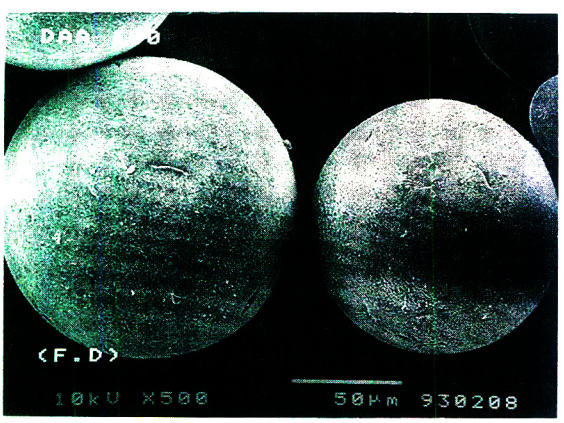

Fig. 1. Electron micrograph of DAA adsorbents prepared without a diluent. The amino-group content of adsorbents was 4.5 mequiv./g. The scale bar represents 50 μm.

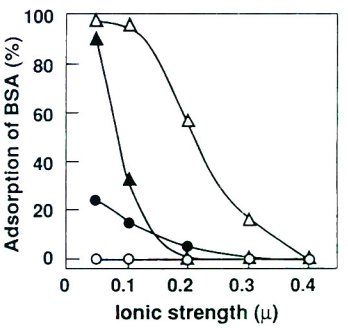

Fig. 2. Effects of ionic strength and M_{lim} on adsorption of BSA by various adsorbents. The adsorption of BSA was determined by the batchwise method with 0.3 g of each wet adsorbent and 3 ml of a BSA solution (500 μg/ml, pH 7.0, $\mu = 0.05$–0.4). Adsorbent, M_{lim}: (○) DAA-70–0, <300; (●) DAA-70–100, 10 000; (△) DAA-70–200, 43 000; (▲) immobilized histidine, 100 000. Amino-group contents: DAA adsorbents, 4.5 mequiv./g; immobilized histidine, 0.3 mequiv./g.

mobilized histidine with a large pore size (M_{lim} 100 000) also showed high adsorption of BSA at a low ionic strength of $\mu = 0.05$. The other DAA (DAA-10–0, -30–0, -50–0, -90–0) adsorbents with $M_{lim} < 300$ hardly adsorbed BSA, just like DAA-70–0. Little γ-globulin (a neutral protein) or cytochrome *c* (a basic protein) was adsorbed by any adsorbent under any conditions (data not shown).

These results suggest that DAA-10–0, -30–0, -50–0, -70–0 and -90–0 can adsorb endotoxins without affecting the recovery of the proteins. However, DAA-10–0, -30–0 and -50–0 are unsatisfactory with respect to endotoxin-adsorbing capacity and DAA-90–0 is disadvantageous with a high flow-rate in the chromatographic process because of its high degree of swelling (S_d) of 7.8, as shown in Table 1. In contrast, the DAA-70–0 adsorbent with an S_d of 4.3 (similar to that of an aminated PMLG sphere [14]) is expected to show a higher flow-rate resistance than Sepharose gels.

The adsorption isotherms for DAA-70–0 (amino-group content 4.5 mequiv./g) and immobilized histidine (amino-group content 0.3 mequiv./g) adsorbents were determined in phosphate buffer (pH 7.0, $\mu = 0.05$) by changing the concentration of endotoxin (*E. coli* O111:B4 LPS) with the batchwise method. The endotoxin adsorption of each adsorbent increased with increasing concentration of endotoxin. Fig. 3 shows the Scatchard plots [6] derived from these adsorption isotherms. According to these plots, the adsorption capacities and dissociation constants (K_d) were calculated to be 0.81 mg endotoxin/g wet adsorbent and $8.5 \cdot 10^{-10}$ *M* in the DAA-70–0 adsorbent and 0.21 mg and $1.1 \cdot 10^{-9}$ *M* in the immobilized histidine, when the aggregation mass of endotoxins was estimated as 10^6. The adsorption capacity of the DAA-70–0 adsorbent was about four times larger than that of the immobilized histidine although both of the adsorbents showed similar K_d values. These results indicate that a high amino-group content increased substantially the endotoxin-adsorbing activity of the DAA-70–0 adsorbent.

The adsorption of endotoxins originating from various Gram-negative bacteria by the DAA-70–0 adsorbent were investigated, and the results are given in Table 2. When adsorption of endotoxin was measured in water, the DAA-70–0 adsorbent showed a high endotoxin-adsorbing activity for various purified endotoxins. Under the conditions of pH 7.0 and $\mu = 0.1$, the residual concentrations of endotoxin originating from *E. coli* UKT-B and O111:B4 decreased

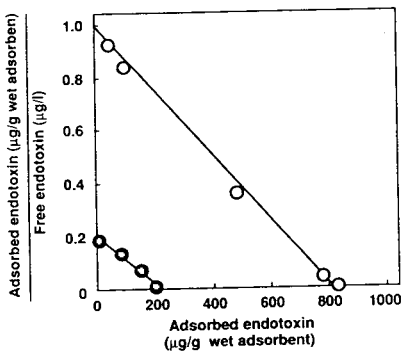

Fig. 3. Scatchard plots derived from adsorption isotherms of endotoxin on (○) DAA-70–0 adsorbent and (●) immobilized histidine. The adsorption of endotoxin was determined by the batchwise method with 0.2 g of the wet adsorbent and 2 ml of an endotoxin solution (*E. coli* O111:B4 LPS, 10^3–10^6 ng/ml, pH 7.0, $\mu = 0.05$).

Table 2
Adsorption of endotoxins originating from various Gram-negative bacteria by DAA-70–0 adsorbent

Endotoxin[a]	Residual concentration of endotoxin after treatment[b] (pg/ml)	
	Water	Buffer (pH 7.0, $\mu = 0.1$)
Escherichia coli UKT-B	<10	<10
Escherichia coli O111:B4	<10	<10
Escherichia coli O127:B8	<10	5600
Escherichia coli O55:B5	<10	100
Salmonella typhosa O901	<10	50
Salmonella typhimurium	<10	600
Bordetella pertussis Tohama	<10	80

[a] The purified endotoxin was dissolved in water and phosphate buffer (pH 7.0, $\mu = 0.1$) at a concentration of 500 ng/ml.

[b] The adsorption of endotoxin was determined by the batchwise method with 0.3 g of wet adsorbent and 3 ml of an endotoxin solution.

from 500 to less than 10 pg/ml, but all other endotoxins were not completely removed.

The effects of pH and ionic strength on the removal of endotoxin by DAA-70–0 and immobilized histidine were investigated in various kinds of buffers and the results are shown in Fig. 4a and b. Each residual concentration of endotoxin increased with increasing ionic strength at any pH. When the ionic strength was adjusted to $\mu = 0.05$, both adsorbents removed endotoxin satisfactorily at around neutral pH. When the ionic strength was increased ($\mu = 0.1$–0.4), the endotoxin-removing activity of immobilized histidine decreased considerably at any pH value (Fig. 4b). DAA-70–0 adsorbent was able to decrease the residual concentration of endotoxin from 100 ng/ml to less than 100 pg/ml at $\mu =$ 0.05–0.2 and pH 6–8 (Fig. 4a).

The effects of pH on the removal of endotoxin from a BSA solution containing endotoxin (endotoxin 100 ng/ml as *E. coli* O111:B4 LPS, BSA 500 μg/ml) with DAA-70–0 adsorbent or immobilized histidine were examined at an ionic strength of $\mu = 0.05$ (Fig. 5a and b). The DAA-70–0 adsorbent satisfactorily removed endotoxin from a BSA solution without affecting the recovery of BSA over a wide pH range from 5 to 8, as shown in Fig. 5a. In contrast, the immobilized histidine had a high endotoxin-removing activity over a wide pH range from 5 to 8, but

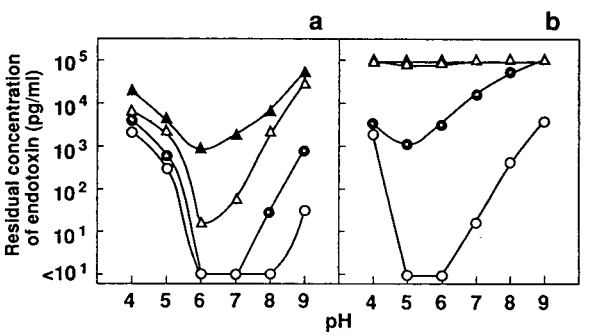

Fig. 4. Effects of pH and ionic strength on removal of endotoxin by (a) DAA-70–0 adsorbent and (b) immobilized histidine. The removal of endotoxin was determined by the batchwise method with 0.3 g of the wet adsorbent and 3 ml of an endotoxin solution (*E. coli* O111:B4 LPS, 100 ng/ml, pH 4–9, $\mu = 0.05$–0.4). Ionic strength: $\mu =$ (○) 0.05, (●) 0.1, (△) 0.2 and (▲) 0.4.

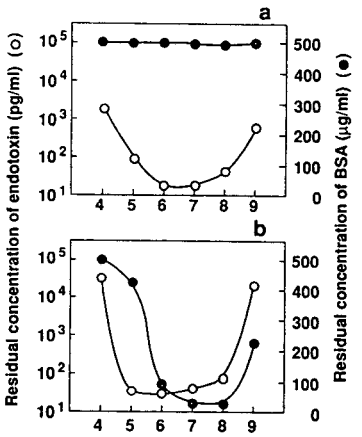

Fig. 5. Effects of pH (*x*-axes) on removal of endotoxin from a BSA solution containing endotoxin with (a) DAA-70–0 adsorbent and (b) immobilized histidine. The removal of endotoxin was determined by the batchwise method with 0.3 g of wet adsorbent and 3 ml of a BSA solution (endotoxin 100 ng/ml as *E. coli* O111:B4 LPS, BSA 500 μg/ml, pH 4–9, $\mu = 0.05$). ○ = Endotoxin; ● = BSA.

the residual concentration of BSA also decreased from 500 to less than 10 μg/ml, as shown in Fig. 5b. As the ionic strength increased ($\mu = 0.2$) the adsorption of BSA by immobilized histidine decreased (Fig. 2), but this was accompanied by a decrease in the adsorption of endotoxin at any pH value (Fig. 4b). Immobilized histidine therefore cannot remove endotoxin from a BSA solution (500 μg/ml) at any ionic strength or any pH.

On the basis of these results (Figs. 2–5), we assumed that the adsorption of endotoxin and BSA by the adsorbent was induced by cooperation of cationic and weakly hydrophobic properties. The charge of the DAA adsorbent is cationic at pH < 10 because of the amino groups originating from the DAA copolymer. The adsorption of endotoxin was dependent on pH and ionic strength, as shown in Figs. 4 and 5. This suggests that the ionic interaction participates in binding between the adsorbent and endotoxins. The adsorption, being independent of the ionic strength, suggests a hydrophobic interaction; the DAA adsorbent can retain the high endotoxin-removing activity even at a high ionic strength of $\mu = 0.1$–0.4 (Fig. 4a). Immobilized histidine adsorbed endotoxin mainly by ionic interaction at a

low ionic strength, as it adsorbed little endotoxin at high ionic strengths, $\mu = 0.2$–0.4 (Fig. 4b). Presumably, the high endotoxin-removing activity of the DAA adsorbent is related to the ionic interaction between the cationic region of the adsorbents and the anionic region (the phosphoric acid group) of endotoxin, and to the weak hydrophobic interaction between the alkyl chain region of the adsorbent and the lipid region of endotoxin.

It seems that the adsorption of BSA by the adsorbent is induced by the cationic properties. The charge of BSA is anionic at pH values greater than its p*I* (4.9), and also the adsorption of BSA by the adsorbents is dependent on the ionic strength, as shown in Fig. 2. This suggests the participation of the ionic interaction in binding between the adsorbent and BSA; however, the DAA-70–0 adsorbent with $M_{lim} < 300$, which is less than the molecular mass of BSA, adsorbed little BSA at any pH value (Fig. 5a). The adsorption of BSA increased with increase in M_{lim} of the DAA adsorbent, at a low ionic strength, as shown in Fig. 2. Immobilized histidine with large pore sizes ($M_{lim} = 100\,000$) adsorbed a considerable amount of BSA at pH values greater than the p*I* (4.9) of BSA (Fig. 5b). These results show that adsorption of BSA is caused by entry of the BSA molecules into the pores of the adsorbent. Much endotoxin, however, was adsorbed by the DAA-70–0 adsorbent. We reported previously [10] that endotoxin cannot enter the pores of the adsorbent with $M_{lim} <$ 300 because endotoxin aggregates to form supermolecular assemblies ($M_{lim} > 1\,000\,000$). Therefore, we assume that endotoxin is adsorbed also on the surface of the DAA-70–0 adsorbent but BSA can hardly be adsorbed on it.

3.2. Removal of endotoxin from various protein solutions

Table 3 shows the selective removal of endotoxin with the DAA-70–0 adsorbent from various useful protein solutions containing natural endotoxin. BSA, myoglobin, γ-globulin and cytochrome *c* were used as test samples at various concentrations. The proteins were naturally contaminated with endotoxin at concentrations from 500 to 32 000 pg/ml. When the endotoxin adsorption was measured at pH 7.0 and $\mu = 0.05$, a high recovery of protein was obtained with each sample solution after removal of endotoxin. It is essential to eliminate endotoxin or at least to decrease it to a concentration of 100 pg/ml from the fluid to be used for intravenous injection [5], because of its potent biological activity eliciting pyrogenic and shock reactions in mammals [1]. As shown in Table 3, the DAA-70–0 adsorbent was able to remove endotoxin from any sample to a level below 100 pg/ml without loss of the proteins.

3.3. Adsorption capacity and regeneration

The endotoxin-adsorbing capacity of DAA-70–0 adsorbent was determined by frontal chromatography. An endotoxin solution (*E. coli* O111:B4 LPS, 1000 ng/ml) was applied to a column (10 × 0.3 cm I.D.) of the DAA-70–0

Table 3
Removal of endotoxin from various protein solutions with DAA-70–0 adsorbent

Sample (500 μg/ml)	Concentration of endotoxin (pg/ml)		Endotoxin removed (%)	Recovery of protein (%)
	Before treatment	After treatment		
BSA	32 000	80	99	99
Myoglobin	500	20	96	99
γ-Globulin	8400	50	99	99
Cytochrome *c*	800	20	98	100

The endotoxin removed was determined by the batchwise method with 0.5 ml of wet DAA-70–0 adsorbent ($M_{lim} < 300$, amino-group content 4.5 mequiv./g) and 5 ml of a sample solution (pH 7.0, $\mu = 0.05$).

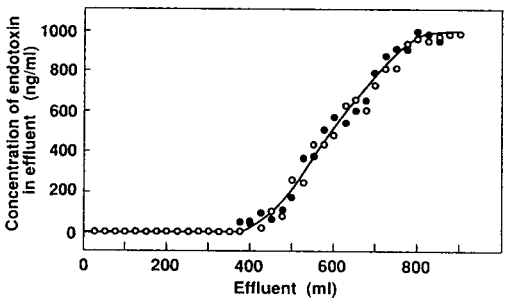

Fig. 6. Adsorption capacity of DAA-70–0 adsorbent for endotoxin (*E. coli* O111:B4 LPS, 1000 ng/ml, pH 7.0, μ = 0.05) in frontal chromatography on a 10 × 0.3 cm I.D. glass column. ○ = First use; ● = fifth use (reused after treatment with 20 ml of 0.2 *M* sodium hydroxide solution followed by 20 ml of 2 *M* sodium chloride solution).

adsorbent. As shown in Fig. 6, the adsorbent was gradually saturated with endotoxin. When the endotoxin-saturated column was washed with 20 ml of a 0.2 *M* sodium hydroxide solution followed by 20 ml of 2 *M* sodium chloride solution, the graph of the adsorbing capacity of the regenerated column was similar to that of the fresh column. We also repeated the column reuse and the 0.2 *M* NaOH treatment five times. As shown in Fig. 6, the curve of the adsorbing capacity of the five-times regenerated column was similar to that of the fresh column. These results show that the DAA adsorbent can be completely regenerated by the 0.2 *M* NaOH treatment. The adsorption capacity of 1 ml of the DAA-70–0 adsorbent was 0.87 mg of endotoxin (*E. coli* O111:B4 LPS) at pH 7.0 and at an ionic strength of $\mu = 0.05$ in the column method. Minobe *et al.* [5] found that the endotoxin-adsorbing capacity of 1 ml of immobilized histidine was 0.53 mg (*E. coli* O128:B12 LPS) at an ionic strength of $\mu = 0.02$. We also found that the adsorbing capacity of 1 ml of the aminated PMLG adsorbent ($M_{lim} = 20\,000$, amino-group content 3.2 mequiv./g) was over 2 mg of endotoxin (*E. coli* O111:B4 LPS) even at a high ionic strength, $\mu = 0.17$, as reported previously [9]. Although the adsorption capacity is lower than that of the aminated PMLG adsorbent, the DAA-70–0 adsorbent can satisfactorily remove endotoxin from a protein solution naturally contaminated with endotoxin, as shown in Table 3.

For practical application, the ease of regeneration is important, and the DAA-70–0 adsorbent can easily be reused, as shown in Fig. 6. The aminated PMLG adsorbent can also be reused after washing by the same method as used for the DAA-70–0 adsorbent. We suspect, however, that the aminated PMLG adsorbent will be gradually hydrolysed in a 0.2 *M* sodium hydroxide solution (one of the solvents used for washing) because the adsorbent ha⌣ free –CO–O– bonds originating from PMLG. In contrast, the DAA adsorbent, being composed of –CONH– bonds from DMAPAA and AAA, is considered to keep its entire structure in 0.2 *M* sodium hydroxide solution. It seems that this favourable property permits the DAA column to be reused many times.

4. Conclusion

The present results indicate that adsorption technique using the DAA adsorbent can remove endotoxin from a naturally contaminated protein solution without affecting the recovery of the protein. In addition, the DAA adsorbents have the following advantages: (1) they are prepared by one-step polymerization; (2) the amino-group content of the adsorbent is easily adjusted by changing the molar ratio of the monomer; and (3) they can be completely regenerated by washing with several kinds of solutions.

References

[1] S.I. Morse, *Adv. Appl. Microbiol.*, 20 (1976) 9.
[2] D.C. Morrison and R.J. Ulevitch, *Am. J. Pathol.*, 93 (1978) 527.
[3] D. Fumerola, *Cell. Immunol.*, 58 (1981) 216.
[4] S. Minobe, T. Sato, T. Tosa and I. Chibata, *J. Chromatogr.*, 262 (1983) 193.
[5] S. Minobe, T. Watanabe, T. Sato and T. Tosa, *Biotechnol. Appl. Biochem.*, 10 (1988) 143.
[6] H. Matsumae, S. Minobe, K. Kindan, T. Watanabe and T. Tosa, *Biotechnol. Appl. Biochem.*, 12 (1990) 129.

[7] T.E. Karplus, R.J. Ulevitch and C.B. Wilson, *J. Immunol. Methods*, 105 (1987) 221.
[8] C. Hirayama, H. Ihara and X. Li, *J. Chromatogr.*, 530 (1990) 148.
[9] C. Hirayama, M. Sakata, Y. Ohkura, H. Ihara and K. Ohkuma, *Chem. Pharm. Bull.*, 40 (1992) 2106.
[10] C. Hirayama, M. Sakata, H. Ihara, K. Ohkuma and M. Iwatsuki, *Anal. Sci.*, 8 (1992) 805.
[11] K.A. Granath and P. Flodin, *Makromol. Chem.*, 48 (1961) 160.
[12] H. Ihara, T. Yoshinaga and C. Hirayama, *J. Chromatogr.*, 362 (1986) 197.
[13] H. Ohishi, Y. Hatoyama, H. Shiraishi and K. Yanagisawa, *Yakugaku Zasshi*, 105 (1985) 300.
[14] C. Hirayama and H. Ihara, *Anal. Sci.*, 7 (1991) 527.

ELSEVIER

Journal of Chromatography A, 676 (1994) 277–285

JOURNAL OF CHROMATOGRAPHY A

Electrolytic conductivity detector for selective detection of chlorine-containing compounds in liquid chromatography

R. Wiesiollek, K. Bächmann*

Technische Hochschule Darmstadt, Fachbereich Chemie, Eduard Zintl-Institut, Hochschulstr. 10, D-6100 Darmstadt, Germany

First received 8 June 1993; revised manuscript received 15 March 1994

Abstract

The use of an electrolytic conductivity detector for chlorine-specific HPLC detection is described. The use of a miniaturized LC system with flow-rates up to 60 μl/min allows the entire column effluent to be fed into the detector. The design of the laboratory-made interface supporting the vaporization process by nebulizing the eluent is described in detail. Various parameters were evaluated to determine the performance of the coupling, also applied to environmental analysis. The detector is shown to be sensitive to 52–123 pg of chlorine in chlorine-containing compounds eluted by normal-phase HPLC.

1. Introduction

High-performance liquid chromatography (HPLC) is often limited by the lack of appropriate detectors specific to a class of compounds. Especially in environmental analysis, selective detection is desirable for minimizing extensive sample clean-up procedures. Various attempts have been made to improve the performance of HPLC detection by interfacing GC detectors to an LC system.

In recent years, papers have been published on flame ionization, photoionization, nitrogen–phosphorus, flame photometric and electron-capture detection (ECD) [1–4]. ECD has been used on-line with moving-wire systems [5] and with nebulizing [6] and vaporizing interfaces [7]. With a recent miniaturized version (with a 200 × 0.7 mm I.D. column) the detection limits for favourable electron-capturing compounds (chloroanilines) were of the order of 0.2–10 pg [8].

A chlorine-selective flame-based detector using the indium(I) chloride emission band at 360 nm was described by Folestad *et al.* [9] for microbore LC (20–70 μl/min). Under non-retaining conditions, the detection limit for 1,1,2-trichloroethane is 0.39 ng of injected compound, provided that quenching effects by organic modifiers are avoided and pure water is used as the mobile phase. The use of electrolytic conductivity detection (ELCD) with an instrument designed for GC has the advantage of low sensitivity for non-halogenated interferents. This means that most of the sample clean-up associated with other types of detectors can be eliminated.

In the ideal case, the detector response is proportional to the chlorine content of a compound; this offers the possibility of quantitative determination without calibration for each compound in question.

* Corresponding author.

0021-9673/94/$07.00
SSDI 0021-9673(94)00288-K

Basic research in this field was carried out by Shepherd *et al.* [10] using a segmented stream splitter to reduce the eluent flow reaching the detector. The development of miniaturized HPLC allows the introduction of the entire effluent into the GC detector.

The performance of the HPLC–ELCD system was investigated by varying parameters such as eluent flow-rate, interface position, reaction gas flow and reaction temperature. Various applications of HPLC–ELCD under normal-phase conditions are demonstrated and discussed.

2. Experimental

2.1. Apparatus

HPLC system

A syringe pump (LDC/Milton Roy) was used for delivering pulse-free flow-rates in the range 1–500 μl/min. The narrow-bore column employed (300 × 1 mm I.D.) was packed with 5-μm NH_2-Nucleosil (Grom, Herrenberg, Germany). Injections were made with a Rheodyne Model 7010 injection valve equipped with a 2 or 4-μl external sample loop.

Detector

The detection system consisted of a Model ROK 3/30 horizontal tube furnace (Heraeus, Hanau, Germany) including a quartz pyrolysis tube (350 × 1 mm I.D.), a Tracor Model 700A differential conductivity cell and a Tracor Model 700 control unit (Techmation, Düsseldorf, Germany). Data analysis was performed with a Shimadzu, C-R3A integrator.

Interface

The design of the laboratory-made interface is shown in the inset in Fig. 1. The front part of the pyrolysis tube has an extended inner diameter (3.5 mm I.D.). The stainless-steel capillary (20 cm × 0.1 mm I.D.) from the analytical column enters the tube through a Swagelok tee-piece (1/4 in.) and stops where the pyrolysis tube begins to narrow. The capillary end has a hand-filed tip so that the resulting orifice acts as a restrictor for a liquid stream down to 10–20 μl/min. Thus, the column effluent can be nebulized for supporting the vaporization process. The

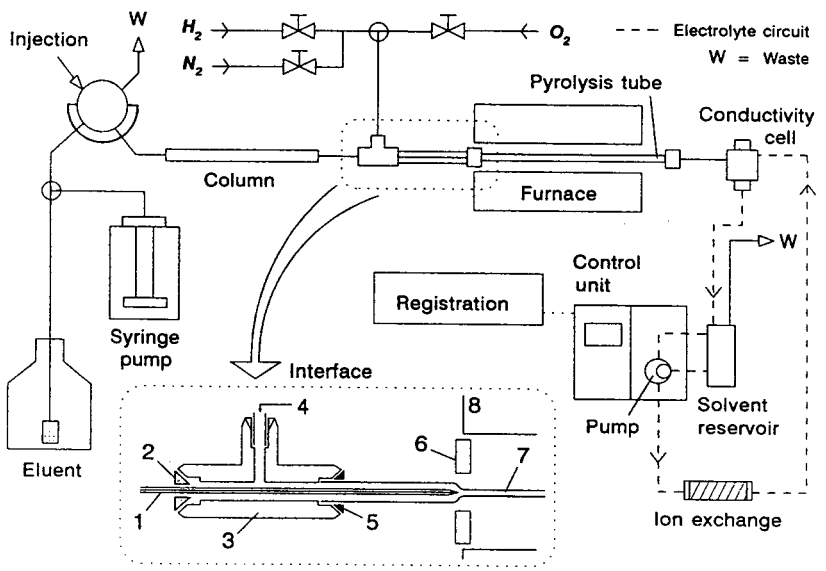

Fig. 1. Schematic diagram of the HPLC–ELCD system. Interface details: 1 = LC capillary; 2 = PTFE ferrule; 3 = tee-piece; 4 = reaction gas inlet; 5 = graphite ferrule; 6 = ceramic ring; 7 = quartz tube; 8 = furnace.

performance of the interfaced ELCD instrument was compared with that of a variable-wavelength UV detector (Model 575; Applied Biosystems, Weiterstadt, Germany).

2.2. Chemicals

The solvents used were of analytical-reagent grade from Merck (Darmstadt, Germany) and Baker (Deventer, Netherlands). They were used as received, except for *n*-pentane and *n*-hexane, which were purified by refluxing over a dispersion of 45% sodium in paraffin (Fluka, Buchs, Switzerland) and subsequent distillation [11]. Tetrachloromethane and 1,1,1-trichloroethane (analytical-reagent grade) were obtained from Merck; all other compounds used as solutes were analytical reagent grade products from Fluka, Riedel-de Haën (Seelze, Germany), Aldrich (Steinheim, Germany) and Polyscience (Niles, IL, USA).

High-purity hydrogen (99.999%) was used as the reaction gas. All solvents used as eluents were previously degassed under vacuum.

3. Results and discussion

The physical nature, in particular the detector transparency and evaporation properties, of the mobile phase and the volume of the eluent transferred into the detection unit are key factors for successful LC interfacing. The on-line-coupling of a GC detector to a liquid chromatograph requires continuous effluent vaporization. The constancy of this process has a direct influence on the detection limits. Favourable evaporation conditions, however, should agree with the conditions required by the chromatographic process and with the parameters demanded for the detector operation.

3.1. HPLC solvent and flow-rate

In spite of the detector selectivity, the solvent flow, which has to be evaporated, produces a background noise depending on the solvent used, the impurities and the flow-rate. The combustion products of the eluent act as interfering compounds, which are constantly present in the detector and can increase the limit of detection for halogenated compounds.

To compare the interfering properties of possible eluents, solutions of tetrachloromethane in methanol, acetonitrile and *n*-pentane were prepared. The solutions were directly injected (4 μl in each instance) into the detector via a GC injection port and a fused-silica capillary (250 × 0.53 mm I.D.) as transfer line, heated at 100°C. Hydrogen acted as the carrier gas (50 ml/min) and the reaction gas (150 ml/min). This resulted in a higher sensitivity with the alkane as solvent, especially where lower concentrations were concerned (Fig. 2). It is also seen that a non-linear relationship exists with methanol and acetonitrile as solvents at a concentration range that is more than two orders of magnitude smaller than that which was investigated by Shepherd *et al.* [10].

The baseline noise with a continuous solvent flow increases with increase in flow-rate. The best results were observed with alkanes as eluents. To achieve the highest signal-to-noise ratios, the flow-rates, or at least the fraction of the LC effluent reaching the detector, should not exceed 60–80 μl/min, as can be seen from Table 1.

A further disadvantage of increased flow-rates

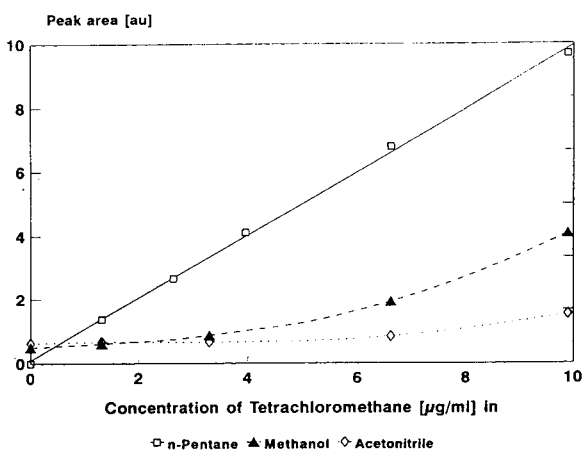

Fig. 2. Influence of the solvent on the chlorine sensitivity. For conditions, see text.

Table 1
Influence of the eluent flow-rate on the signal-to-noise ratio

Eluent flow-rate (μl/min)	Signal-to-noise ratio	Eluent flow-rate (μl/min)	Signal-to-noise ratio
10	74	90	51
30	77	110	36
50	75	130	32
70	60	150	28

Eluent, *n*-pentane; reaction temperature, 1000°C; hydrogen flow-rate, 200 ml/min; injections (without separation column), 4 ng of tetrachloroethylene.

is a greater deposition of carbon in the furnace tube. The extent of this deposition depends on the eluent used and its carbon content. A flow-rate of 40 μl/min of *n*-hexane gives a distinct carbon deposition in the furnace tube after only 20 min, whereas no carbon is found with methanol as solvent, even after 40 min.

To decrease the detector load, a miniaturized LC system with a column of 1 mm I.D. was employed. Typical flow-rates of 5–50 μl/min allow the entire column effluent to be fed into the detector.

The increase in volume that occurs on converting the liquid eluent into vapour is, compared with the reaction gas flow, negligible at these flow-rates. In spite of greater carbon deposition, further investigations were confined to normal-phase chromatography with alkanes as solvents, because of a more sensitive determination.

Moreover, cleaning of the reaction tube by burning the carbon deposits can be carried out easily by changing the reaction gas to oxygen for 30 min when the eluent flow is turned off. The conductivity cell should be removed for this operation. Although no effect on sensitivity was observed over an operating period of 7 days (with an average of 2–4 h operation daily), this cleaning procedure was performed every 2 days.

Great variations in solvent purity were observed, although the same brands and grades were employed. Whereas single charges of *n*-hexane or *n*-pentane could be used as received from the suppliers, most of them show high noise levels (when used as eluents) and give peaks (when injected as solvents). Sensitive and reproducible results could be obtained after purification of the alkanes in the above-described manner.

3.2. Hydrogen flow-rate

According to manufacturers' recommendations, operation in the halogen mode requires a hydrogen-flow-rate of 50 ml/min. This adjustment cannot be applied for the LC-coupled system, because the eluent has to react additionally. The theoretical consumption of hydrogen, assuming that methane is produced exclusively, which is a coarse approach, because other reaction products are also formed, is 43 ml/min at an *n*-hexane eluent flow-rate of 50 μl/min. This excess demand should be considered to achieve complete decomposition of the analyte.

In fact, the effect of an insufficient supply of reaction gas is observed. This is particularly apparent with aromatic chlorine compounds with a high carbon content. Distinctly diminished signals of di- and trichlorobenzenes are obtained at flow-rates below 80 ml/min, whereas varying the hydrogen flow-rate between 10 and 100 ml/min has no observable effect on the sensitivity for tetrachloromethane and tetrachloroethylene.

Further, as a result of a more efficient decomposition, increased hydrogen flow-rates (200 ml/min as compared with 75 ml/min at an *n*-pentane eluent flow-rate of 50 μ/min) decrease both the baseline noise and the carbon deposition in the pyrolysis tube. Above 300 ml/min, however, increased hydrogen flow-rates decrease the residence time in the reaction tube, which results in diminished signals. Hence a hydrogen flow-rate of 200 ml/min was routinely employed.

3.3. Reaction temperature

The efficiency of the thermal fragmentation also depends on the reaction temperature. Fig. 3 shows the temperature profiles of the response for three chlorinated compounds at an eluent flow-rate of 20 μl/min. With increasing furnace temperature, the detector response increases to a maximum. Unlike in its GC application, higher

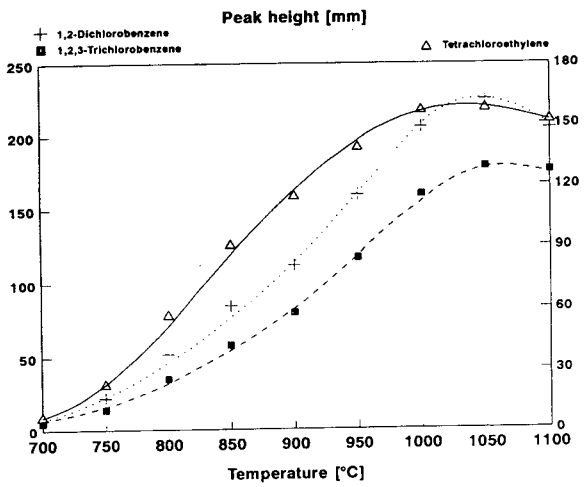

Fig. 3. Effect of reaction temperature on detector response.

furnace temperatures are required to obtain the maximum response. Further, because of the higher dissociation energy of the aromatic C–Cl bonds, the temperature must be sufficiently high to ensure that there is no difference in the response to aliphatic and aromatic compounds. Discriminating effects between the two groups are eliminated at a furnace temperature of 1050°C. In consideration of the working life of the furnace, however, a temperature of 1000°C was chosen for most experiments.

3.4. Conductivity solvent

The flow-rate of the solvent determines the concentration of the absorbed ions. Thus the detector response decreases with increasing flow-rate. Occasional carbon deposits in the conductivity cell may cause flow changes. To minimize variations in sensitivity, the correct volume flow, set at 0.6 ml/min, was checked daily. Undiluted ethanol was used as a conductivity solvent instead of alcohol–water mixtures, which tend to change their composition owing to gradual evaporation. In spite of the on-line coupled modification, the electrolyte is continuously circulated through the ion-exchange resin (Fig. 1) without any deterioration in sensitivity even after several weeks. Replacement of the resin and solvent is necessary when the background noise increases significantly.

3.5. Selectivity

As specific detector, the ELCD instrument responds only to compounds that contain elements for which it is tuned. The selectivity is determined by the products formed in the furnace tube. Under reductive conditions (in the halogen mode hydrogen is used as reaction gas) strong acids are produced by the decomposition of organic halogen compounds. The low response of interfering compounds is due to poor solubility or low ionization of their pyrolysis products in the conductivity solvent. In spite of the selective properties of the detector, a large excess of interfering compounds can lead to systematic errors. To quantify the selectivity under coupling conditions, the chlorine response is compared with the responses to other heteroatomic compounds, which produce corresponding hydrogen compounds such as NH_3, H_2S and H_2O.

Solutions of these compounds in *n*-pentane (10 μl/ml) were injected into the solvent stream (40 μl/min). The separation column was removed for this operation. The response data shown in Fig. 4 are expressed in terms of peak areas related to the amount injected. Under the described conditions, a selectivity of 10^4–10^6 for organic-bound chlorine relative to the investigated compounds is achieved.

3.6. Interface

The interface must provide for an efficient transfer of analyte molecules from the LC outlet into the detector, while the contribution to band broadening must be minimized.

The most important parameters influencing the interface performance are the temperature and the shape of the interface. As far as the geometry is concerned, the interface must project into an opening of 1.5 mm because of the pyrolysis tube diameter. Further, the interface construction includes the reaction gas feed implied by the detection method. A possible later

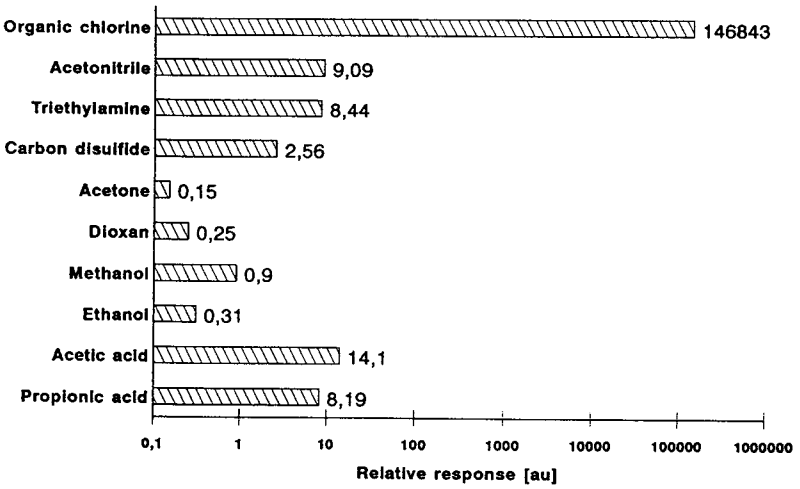

Fig. 4. Relative detector responses to various heteroatomic compounds.

supply would cause an additional band broadening, or a make-up gas stream as in the GC mode. The position of the liquid–vapour transition is determined by the interface temperature. It can be regulated by varying the position of the interface with respect to the heating zone of the furnace.

Different possibilities of solvent evaporation can be discussed. At low temperatures, the liquid flows until the capillary end and evaporates after leaving the capillary. In the case of a non-restricting orifice, this happens more as a result of the reaction gas stream passing by and would be a completely insufficient transfer for non-volatile solutes. At sufficiently high temperatures, the interface would be used under conditions of inside-capillary evaporation. With extremely volatile solvents (*e.g.*, *n*-pentane) however, the "solvent concurrent evaporation" effect is risked with this operation. In this instance, the solvent evaporates at the liquid front, whereas high-boiling compounds are retained at the inner wall of the capillary.

All these effects are indicated when operating the interface without eluent nebulization. The measurements were made at various interface positions with solutes of different volatility. For high temperatures (>400°C), the stainless-steel capillary projected 30 mm into the heating zone of the furnace. To avoid inside-capillary evaporation, the capillary tip was set at a distance of 10 mm from the furnace front. Exact temperatures at the capillary orifice inside the interface cannot be ascertained because of the cooling reaction gas jacket. This resulted in small and broadened peaks for hexachlorobenzene, whereas no band-broadening effects were observed for more volatile compounds (perchloroethylene or 1,2 dichlorobenzene). For 2,2′,3,4,4′,5,5′-heptachlorobiphenyl, no signal could be obtained with the crude capillary outlet under the various temperature conditions.

In contrast, high-pressure nebulization of the eluent permits the transfer even of the less volatile investigated compounds without evident band broadening; note peaks 2 and 4 in Fig. 5. The contribution of the interface to band broadening is identical with that which can be obtained with a UV detector equipped with a low-volume detector cell (0.5 μl) under identical chromatographic conditions, including the length and inner diameter of all connecting tubings. A liquid jet transports the solute molecules into zones of sufficiently high temperature. In order to achieve a steeper temperature gradient, the furnace aperture is diminished by a ceramic ring,

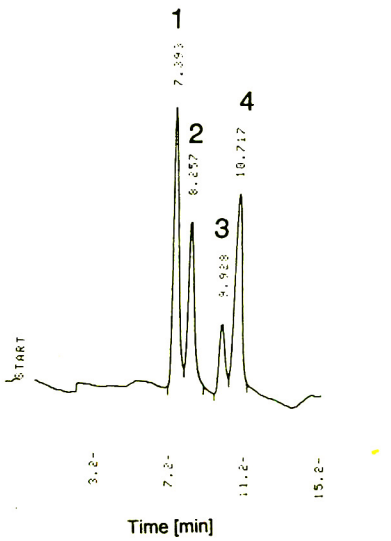

Fig. 5. ELCD chromatogram of an organochlorine standard mixture; Column, 5-μm Nucleosil NH_2 (300 × 1 mm I.D.); eluent, *n*-pentane (30 μl/min); hydrogen flow-rate, 200 ml/min; furnace temperature, 1000°C. Peaks: 1 = tetrachloroethylene (4 ng); 2 = hexachlorobenzene (4 ng); 3 = 1,2-dichlorobenzene (4 ng); 4 = 2,2′,3,4,4′,5,5′-heptachlorobiphenyl (5 ng).

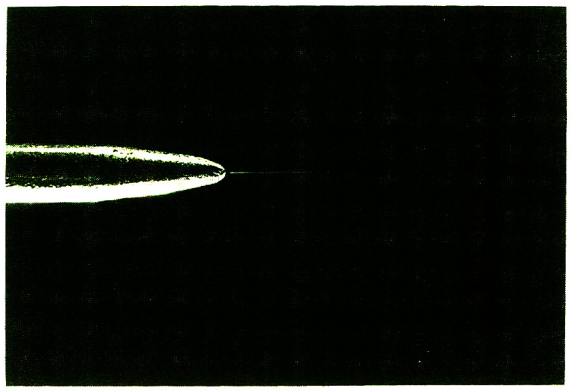

Fig. 6. Photograph of the nebulizing capillary tip and the liquid jet produced at an *n*-pentane flow-rate of 30 μl/min. For dimensions, see capillary diameter of 1.6 mm. The furnace and the quartz tube are removed.

which allows the capillary tip to reach up to the furnace front (Fig. 1).

The condition for a jet disintegrating into a spray of droplets can be evaluated by the equation [12]

$$d < \sqrt[3]{\frac{2\rho F^2}{\pi^2 \sigma}}$$

where d is the orifice diameter, F is the solvent flow-rate, ρ is the density and σ the surface tension of the liquid. Thus, the prepared stainless-steel capillary produces a continuous jet at an *n*-pentane flow-rate of 30 μl/min if the orifice of the capillary end has a diameter of 13 μm or less. This calculation can be verified by examination of a cut-off of the capillary tip using a scanning electron microscope: A photograph of the liquid jet at an *n*-pentane flow-rate of 30 μl/min is shown in Fig. 6.

Possible pneumatic nebulization with hydrogen as nebulizer gas would require such high gas flow-rates that they would not be compatible with operation of the conductivity cell.

3.7. Detector performance and application

The limits of detection for some selected compounds are summarized in Table 2. In order to determine the chlorine response under coupled conditions, the sensitivity for the investigated compounds, obtained from the slope of the calibration graphs, is divided by the chlorine content. The relative values in Table 2 show the linear response to the content of chlorine in the molecule. Assuming a normal peak width of *ca.* 35s, the chlorine sensitivity found is in the 2–3 pg/s range, which is also specified in GC use.

The present set-up is suitable for analysing solid or aqueous environmental samples, subsequent to enrichment, using liquid–liquid or liquid–solid extraction. The organic extracts can be directly injected into the system. The advantage of the specific detection, which does not exist with other HPLC detectors, is shown in Fig. 7, which compares the ELCD and UV traces for a contaminated soil extract; the characterization of the signals obtained with

Table 2
Characteristics of some selected chlorinated organic compounds

Compound	Limit of detection (3s) (pg)	Relative standard deviation ($n = 4$) (%)	Chlorine content (%)	Relative chlorine sensitivity
1,3-Dichlorobenzene	205	2.8	48	1.00[a]
1,2-Dichlorobenzene	257	3.8	48	1.07
1,2,3-Trichlorobenzene	209	3.2	59	0.97
Hexachloroethane	58	1.0	90	0.96

[a] Defined.

ELCD as 1,2- and 1,3-dichlorobenzene was achieved by comparison with reference data (GC–MS analysis).

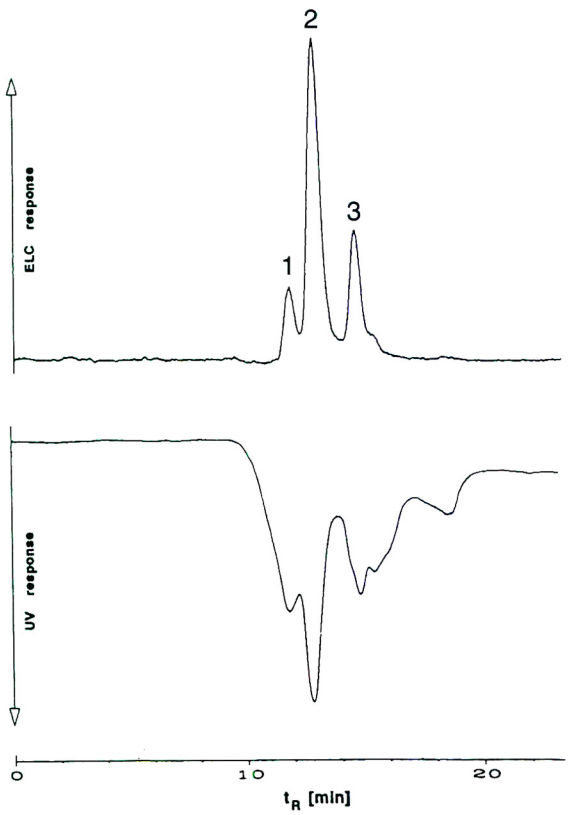

Fig. 7. LC–UV and LC–ELCD traces for a soil extract. Sample, 7.5 g soil; solvent, 5 ml of *n*-hexane; extraction period, 1 h; UV detection at 205 nm. Peaks: 1 = unidentified halogenated aliphatic; 2 = 1,3-dichlorobenzene; 3 = 1,2-dichlorobenzene.

4. Conclusions

The on-line coupling of a electrolytic conductivity detector to a miniaturized LC system has been successfully accomplished. The interface is based on nebulizing the total column effluent, while the contribution to band broadening is negligible. The minimum detectable amounts of chlorine (52–123 pg) are about 1000 times lower than those found in earlier studies.

The described HPLC–ELCD interfacing offers a very useful extension to the available range of the LC detectors and has its advantage in areas where thermal instability and low volatility make analysis by GC difficult. Compared with ECD, ELCD has the advantage of a direct proportionality between the response and the chlorine content of a compound. This can also be an interesting aspect for application as an extended parameter of extractable organic halogen compounds (EOX), with the possibility of sample characterization.

Further investigations on chromatographic optimization (shortening of extra-column tubings, use of polar modifiers and phase separators for coupling to reversed-phase chromatography) should improve the chromatographic resolution and increase the possibilities of identification and application.

5. Acknowledgement

We are grateful to the Umweltbundesamt for financial support.

6. References

[1] H. Veening, P.P.H. Tock, J.C. Kraak and H. Poppe, *J. Chromatogr.*, 352 (1986) 345.
[2] J.N. Driscoll, D.W. Conron, P. Ferioli, I.S. Krull and K.H. Xie, *J. Chromatogr.*, 302 (1984) 43.
[3] J.C. Gluckman, D. Barcelo, G.J. de Jong, R.W. Frei, F. Maris and U.A.Th. Brinkman, *J. Chromatogr.*, 367 (1986) 35.
[4] Ch. E. Kientz and A. Verweij, *Int. J. Environ. Anal. Chem.*, 30 (1987) 255.
[5] R.J. Maggs, *Column*, 2, No. 4 (1968) 5.
[6] G. Nota and A. Palombari, *J. Chromatogr.*, 62 (1971) 153.
[7] A. de Kok, R.B. Geerdink and U.A.Th. Brinkman, *J. Chromatogr.*, 252 (1982) 101.
[8] F.A. Maris, A. van der Vliet, R.B. Geerdink and U.A.Th. Brinkman, *J. Chromatogr.*, 347 (1985) 75.
[9] S. Folestad, B. Josefsson and P. Marstorp, *Anal. Chem.*, 59 (1987) 334.
[10] M.J. Shepherd, M.A. Wallwork and J. Gilbert, *J. Chromatogr.*, 261 (1983) 213.
[11] U.A.Th. Brinkman, P.M. Onel and G. de Vries, *J. Chromatogr.*, 171 (1979) 424.
[12] P.J. Arpiono and C. Beaugrand, *Int. J. Mass Spectrom. Ion Processes*, 64 (1985) 288.

ELSEVIER

Journal of Chromatography A, 676 (1994) 287–295

JOURNAL OF CHROMATOGRAPHY A

Determination of carbon sources in fermentation media using high-performance anion-exchange liquid chromatography and pulsed amperometric detection

Wayne K. Herber*, R.S. Robin Robinett

Cellular and Molecular Biology, Merck and Co., West Point, PA 19486, USA

First received 23 November 1993; revised manuscript received 30 March 1994

Abstract

The technique of high pH anion-exchange chromatography method with pulsed amperometric detection (HPAEC–PAD) has been adapted for the rapid determination of common carbohydrates present in fermentation broths. Simple water dilution of filtered fermentation broth samples was the sole sample preparation step required. The samples were analyzed using a Dionex CarboPac PA1 column with 150 m*M* NaOH as the mobile phase at a flow-rate of 1 ml/min and a total run time of 20 min. A gradient method was also developed to resolve species which exhibited similar t_R in the isocratic procedure. Among the analytes examined in this study were ethanol, glycerol, galactose, glucose, mannose, fructose, raffinose, ribose and lactose. Examples from several microbial fermentations using chemically defined or complex medium are presented.

1. Introduction

Fermentations are complex processes designed to control the growth and productivity of microorganisms or cultured cells. The productivity of the fermentation process is directly influenced by environmental parameters such as pH, temperature, dissolved oxygen, and other nutritional factors.

Thus, definition of the nutrient composition of fermentation medium is essential to the understanding of the physiology of fermentation processes. Carbohydrates are one of the most important classes of nutrients that can affect microbial growth. An understanding of carbon catabolism is critical to optimization of culture conditions. The concentration of the preferred carbohydrate utilized by the microorganism can vary widely depending upon the type of fermentation as well as the stage of culture growth (e.g., from 1–5 mg/l to 100 g/l in batch cultures). Clearly, analysis of carbohydrates is a critical element of medium optimization and for productivity improvements of fermentation processes.

Many analytical techniques have been used to quantitate carbohydrate concentration in fermentation broths. Historically, enzyme-based or chemical identity assays have been used to detect individual saccharides [1]. However, sample throughput is limited, the technique is cumbersome, and the assays are specific for a single saccharide. More recently, flow injection analysis has been tested as an on-line process monitoring

* Corresponding author.

0021-9673/94/$07.00
SSDI 0021-9673(94)00374-I

technique [2]. Some drawbacks of this technology are the limitation of one analyte per channel and the extensive training necessary to allow the use of this technology. HPLC analysis affords a more comprehensive picture of the carbohydrate constituents in media. This technology has been used extensively for analysis of defined and complex fermentation media [3]. Commonly, refractive index (RI) detection is utilized for carbohydrate determination as direct UV detection is not practical [4]. However, since gradient methods cannot be used with RI detection, resolution may be compromised. To overcome this problem, post-column derivatization has been investigated by some groups [5,6]. Bell and Newman [7] found that solid-phase extraction of the fermentation sample was necessary to remove broth matrix interferences prior to HPLC–RI analysis.

To the authors' knowledge, an alternative HPLC technology that has not been applied to fermentation broth analysis is high-performance anion-exchange chromatography (HPAEC) in combination with pulsed amperometric detection (PAD). HPAEC–PAD has been widely applied as a sensitive detection system for alcohols, monosaccharides and oligosaccharides in biological samples such as soil [8], dairy products [9], peat samples [10] and fruit juices [11]. The successful application of HPAEC–PAD for the determination of carbohydrates in numerous biological samples led us to investigate and develop this technique for ion chromatographic determination of common carbohydrates used in fermentation. Carbon sources of wide interest in fermentation technology include, but are not limited to, the following compounds: ethanol, glycerol, galactose, glucose, mannose, fructose, raffinose, ribose and lactose.

This report describes the method development, optimization and validation of chromatographic methods to monitor carbohydrates in fermentation broth without the need for excessive sample pretreatment. The utility of this analysis was documented by application to a variety of microbial fermentations employing chemically defined media or complex nutrient sources, several examples of which are illustrated.

2. Experimental

2.1. Chemicals

Sodium hydroxide (50%, w/w) was obtained from Fisher Scientific (Malvern, PA, USA). HPLC-grade glacial acetic acid was obtained from J.T. Baker (Phillipsburg, PA, USA). All stock carbohydrate standards were prepared from analytical-grade material obtained from either Pfanstiehl (Waukegan, IL, USA) or Fluka (Ronkonkoma, NY, USA).

2.2. Carbohydrate chromatographic system and eluents

Isocratic

Component analysis was performed using a Dionex ion chromatography system (Sunnyvale, CA, USA) that contained a gradient pump, PAD system, autosampler and data-handling system. The actual separation was accomplished using a CarboPac PA1 analytical column (Dionex, 250 × 4 mm) and a CarboPac PA1 guard column (Dionex, 50 × 4 mm) with a 150 m*M* NaOH mobile phase. The method was isocratic with a flow-rate of 1 ml/min. A PAD system equipped with a gold electrode was used for detection. The PAD settings were: $E1 = 0.05$, $E2 = 0.65$, $E3 = -0.95$; $T1 = 2$, $T2 = 2$, $T3 = 5$ and range = 2. A 50-μl sample was injected using the filled-loop mode. The total run time was 20 min.

Gradient

The aforementioned analytical system was used for a gradient elution method by changing appropriate conditions. The mobile phase components were distilled water (A) and 50 m*M* NaOH–2 m*M* acetic acid (B). The gradient conditions were: A–B (94:6) held constant for 13.8 min; varied linearly to 100% B over the next 11.2 min; and then returned to A–B (94:6) over an additional 16 min. The PAD settings were: $E1 = 0.05$, $E2 = 0.60$, $E3 = -0.65$; $T1 = 5$, $T2 = 2$, $T3 = 1$ and range = 2.

Data system

A Dionex advanced computer interface (ACI) Model III was used for data transfer to an AST

Premium 486/33TE computer. Data reduction and processing were accomplished using Dionex AI-450 software (version 3.20).

Preparation of standards and samples

Stock carbohydrate standards were prepared at a concentration of 10 mg/ml using Milli-Q water and were stored at −70°C. Dilutions of stock standards to prepare 10, 25, 50, 100, 250 and 500 μg/ml working standards were made daily. Fermentation samples were prepared by diluting 0.22-μm-filtered broth with Milli-Q water; dilutions of at least 1:50 were used.

3. Results and discussion

The objective of the study was to develop an HPAEC–PAD method for the determination of carbohydrate concentration in fermentation broths. While establishing the sensitivity and linear range of the assay, we were especially concerned with the wide range of carbohydrate concentrations (1 mg/l to 100 g/l) that can occur during the course of a microbial fermentation. To accommodate this magnitude of change, we employed the least sensitive PAD setting that allowed for a broad range of sensitivity. The working limit of detection for most analytes was 10 μg/ml under these conditions. These detection limits could be reduced to ca. 10 pg/ml by adjusting the PAD settings appropriately, as reported by other investigators [12,13]. The concentration of these analytes in fermentation media usually exceeds this range (10 μg/ml) by several orders of magnitude. It was determined that simple dilution with water (commonly 10- to 400-fold) was required to perform the analysis, thus, method sensitivity was not stressed.

To determine if the isocratic method could be adapted for fermentation broth analysis, analytes of interest were evaluated. These included ribose, trehalose, fructose, galactose, mannose, glucose, rhamnose, sucrose, lactose, maltose, raffinose, ethanol, glycerol, ribitol, galactitol and sorbitol. Because of the wide variety of fermentation media that were potentially available and to simplify assay protocol, a common matrix for the standards was necessary. Water was chosen as the first approximation for the matrix because the starting concentrations of most carbohydrates of interest in fermentation broths were in the g/l range and considerable dilution with water was necessary for analysis. To define the HPLC parameters for separation and quantitation, mixtures of known standards in water were examined.

Fig. 1 illustrates the resolution of a mixture of components (each present at 50 μg/ml) using the isocratic method. Hardy et al. [14] reported that the order of elution of simple carbohydrates and polyols was affected by the accessibility of polyanions to functional groups attached to the stationary phase; thus, there is not a strict relationship between t_R and molecular mass. Alcohols exhibited the shortest t_R followed by monosaccharides, disaccharides, then trisaccharides. Chromatographic parameters, including t_R, response factor (1/sensitivity), sensitivity (peak area/concentration), column capacity factor (k') and working range of linearity are listed in Table 1.

For some applications, glucose and galactose

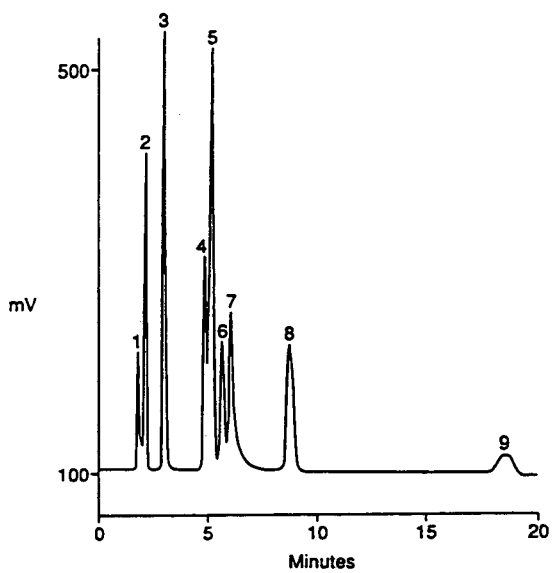

Fig. 1. Chromatogram of standard mixture of alcohols and carbohydrates: separation by the isocratic method. Injection volume, 50 μl. Peaks: 1 = ethanol (1000 μg/ml); 2 = glycerol; 3 = sorbitol; 4 = mannose; 5 = galactose; 6 = fructose; 7 = ribose; 8 = lactose; 9 = maltose (all at 100 μg/ml).

Table 1
HPLC parameters for eleven carbohydrates and five alcohols generated using the isocratic carbohydrate method

Carbohydrate	M_r	t_R (min)[a]	Response factor	Sensitivity	k'	Range of linearity (μg/ml)
D-Ribose, C.P.	150.13	5.57	0.000091	1105	2.71	10–500
Trehalose dihydrate, C.P.	179.90	3.28	0.00078	1280	1.19	10–500
D-Fructose, C.P.	180.16	5.20	0.00078	1288	2.47	10–500
D-Galactose, C.P.	180.16	4.78	0.00070	1422	2.19	10–500
D-Mannose, C.P.	180.16	4.43	0.00061	1632	1.95	10–500
Glucose	180.16	4.72	0.00061	1649	2.15	10–500
L-Rhamnose monohydrate, C.P.	182.17	3.20	0.00047	2117	1.13	10–500
Sucrose	342.30	10.03	0.00448	223	5.69	25–500
Lactose monohydrate	360.31	8.25	0.00181	553	4.50	10–500
Maltose monohydrate, C.P.	360.31	19.57	0.00713	140	12.05	25–500
Raffinose, C.P.	594.52	17.93	0.00463	216	10.95	10–500
Ethanol	46.06	1.65	0.03264	31	0.10	500–5000
Glycerol	92.09	1.80	0.00024	4091	0.20	10–250
Ribitol	152.15	2.63	0.00038	2647	0.75	10–250
Galactitol	182.17	2.62	0.00038	2644	0.75	10–500
Sorbitol, N.F.	182.17	2.62	0.00039	2566	0.75	10–500

Data were obtained using 100 μg/ml standards; ethanol at 1000 μm/ml. C.P. = Chemically pure, N.F. = national formulary.
[a]Based on chromatograms from 100 μg/ml samples.

separation was important. As these analytes cannot be resolved using the isocratic method, a gradient method was optimized to resolve these two species which have the same molecular mass (Fig. 2). In practical terms, this did not hamper analysis of fermentation media since most samples could be analyzed using the isocratic method. Chromatographic parameters for the gradient separation are listed in Table 2. The data listed in Tables 1 and 2 are comparable to values reported by other investigators [14,15].

The linearity of response was investigated for all analytes listed in Tables 1 and 2. Representative plots for seven saccharides and two polyols are depicted in Fig. 3. Using either method, the linearity of response for most analytes was between 10 and 500 μg/ml (Tables 1 and 2). This relatively large standard curve range was selected to accommodate the large variability in analyte concentrations expected to occur in fermentation broths. A cubic fit of the data was used to obtain a better quantitation of standards.

To ensure that water was a good approximation of the medium background, and that

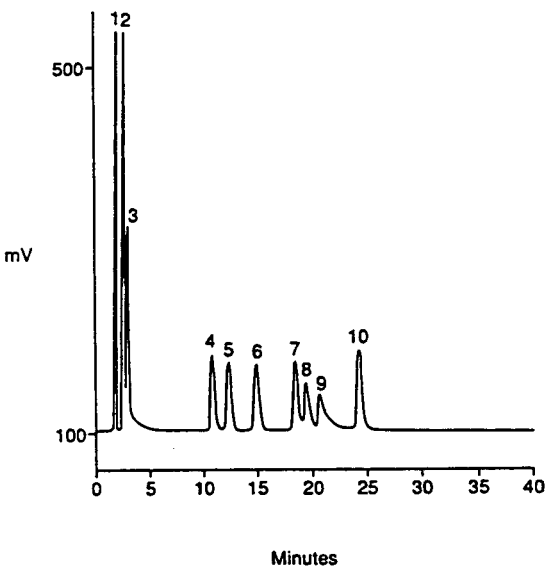

Fig. 2. Chromatogram of standard mixtures of alcohols and carbohydrates: separation by the gradient method. Injection volume, 50 μl. Peaks: 1 = ethanol (1000 μg/ml); 2 = glycerol; 3 = sorbitol; 4 = mannose; 5 = galactose; 6 = fructose; 7 = ribose; 8 = lactose; 9 = maltose; 10 = lactose (all at 100 μg/ml).

Table 2
HPLC parameters for ten carbohydrates and five alcohols generated using the gradient carbohydrate method

Carbohydrate	M_r	t_R (min)[a]	Response factor	Sensitivity	k'	Range of linearity (μg/ml)
D-Ribose, C.P.	150.13	22.30	0.00007	13 662	13.87	10–500
Trehalose dihydrate, C.P.	179.90	2.83	0.00008	12 164	0.89	10–500
D-Fructose, C.P.	180.16	19.38	0.00006	15 508	11.92	10–250
D-Galactose, C.P.	180.16	11.45	0.00005	19 952	6.63	10–500
D-Mannose, C.P.	180.16	17.95	0.00005	19 444	10.97	10–500
Glucose	180.16	13.85	0.00005	19 248	8.23	10–500
L-Rhamnose monohydrate, C.P.	182.17	10.08	0.00005	19 019	5.72	10–500
Sucrose	342.30	13.25	0.00018	5 480	7.83	25–500
Lactose, monohydrate	360.31	22.98	0.00007	13 608	14.32	10–500
Raffinose, C.P.	594.52	21.75	0.00009	10 619	13.50	10–500
Ethanol	46.06	1.62	0.03175	31	0.08	250–5000
Glycerol	92.09	1.73	0.00003	38 776	0.15	10–500
Ribitol	152.15	2.47	0.00003	28 739	0.65	10–500
Galactitol	182.17	2.40	0.00004	22 341	0.60	10–500
Sorbitol, N.F.	182.17	2.52	0.00005	20 963	0.68	10–500

Data were obtained using 100 μg/ml standards; ethanol at 1000 μg/ml.
[a]Based on chromatograms from 100 μg/ml samples.

standards exhibited the same characteristics in fermentation medium, potential interferences from medium components were examined. Interferences from compounds with ionizable groups should be minimized by dilution. Concentrations for most analytes (2.5 μg/ml), other than the predominant carbohydrate species, were below the limit of detection with the PAD settings used. When an alkaline pH mobile phase is used, a PAD system equipped with a gold electrode is sensitive to analytes that contain oxidizable functional groups such as hydroxyls, amines and sulfides [16,17]. Carboxylic acids and inorganic species are transparent in such a system. Other organic compounds that would be converted to anions under the alkaline conditions used for chromatography were also potential sources of interference. Thus, certain amino acids, nucleosides, and choline (all with relatively high dissociation constants, $pK_a > 10.5$) were tested as potential interfering compounds by spiking water with 250 μg/ml standards. At these levels only proline, arginine and lysine exhibited any noticeable detector response (data not shown). These compounds did not present an interference problem because the normal concentration of these amino acids was <2–5 μg/ml and at these levels they were undetectable. To confirm that medium components posed no interference, spike recovery studies in various complex media were performed. Equivalent analyte concentrations were detected in water spiked with analyte, media spiked with analyte then diluted, and diluted media spiked with analyte when either a representative alcohol, pentose, hexose or disaccharide was used (data not shown).

The intraday accuracy of the method was tested by assaying a galactose standard six times. The relative standard deviations (R.S.D.s) of retention times or peak heights were 1.8 and 0.2% for galactose at 10 and 500 μg/ml, respectively. Interday accuracy has been monitored for over two years with R.S.D.s of 5.6 and 0.5% for the 10 and 500 μg/ml galactose standard, respectively. Intraday and interday reproducibility studies have also been performed for five additional analytes (glucose, ribose, ethanol, glycerol and lactose) with similar results (data not shown).

To ensure assay performance during fermentation sample analysis, quality control (QC) samples were analyzed approximately every ten

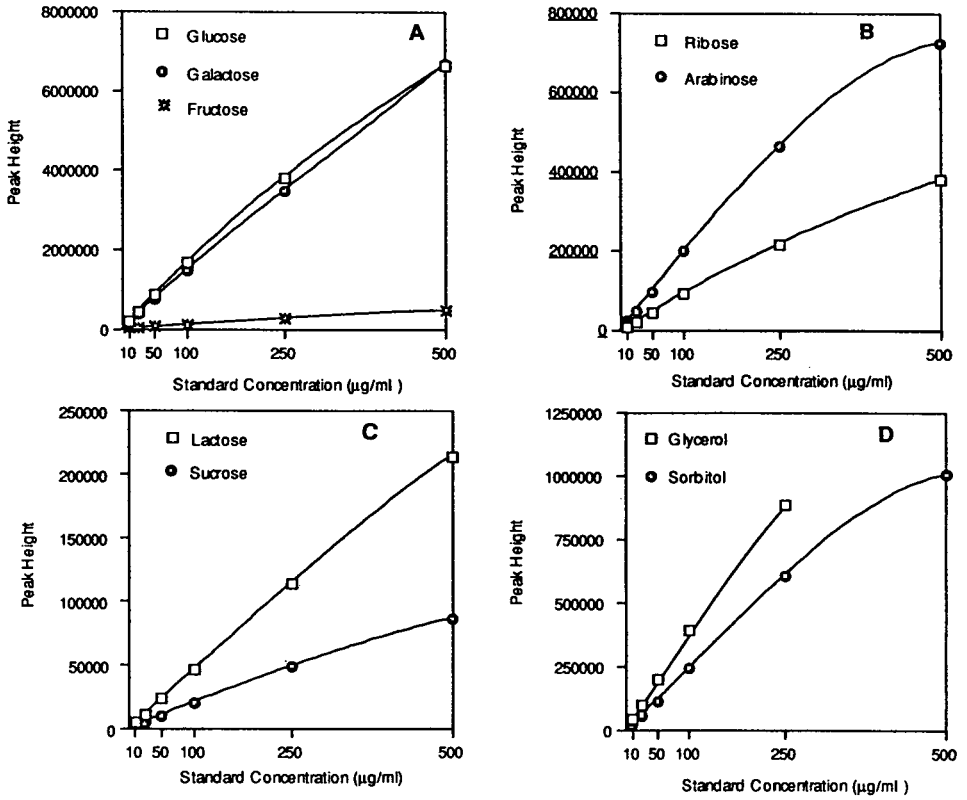

Fig. 3. Typical calibration curves for (A) three hexoses (glucose, galactose, fructose), (B) two pentoses (ribose, arabinose), (C) two disaccharides (lactose, sucrose) and (D) two alcohols (glycerol, sorbitol). Standard curve ranges: 10 to 500 μg/ml for hexoses, pentoses, disaccharides and sorbitol; 10 to 250 μg/ml for glycerol. $R^2 > 0.9999$ for all analytes.

fermentation samples. QC samples were 100 μg/ml galactose in water. For each fermentation sample set, the variability of the QC samples was determined. Typical variation for QC samples was R.S.D. $< 5\%$ with actual values being $< \pm 5\%$ of the nominal QC value. The limiting factor for run size was the sample schedule (software limitation), not QC variation. Accuracy was observed to vary with the type of fermentation medium used, thus the minimum recommended dilution was established for each medium.

The utility of the system for analyzing fermentations broths was demonstrated by monitoring carbohydrate profiles of several different fermentations. Several examples are depicted in Figs. 4–6. Fig. 4 depicts the chromatograms from two recombinant *Escherichia coli* fermentations generated using the isocratic method. The upper panel is an analysis of a filtered broth sample from a chemically defined fermentation medium with glucose (peak 1) as the sole carbon source; the lower panel is a sample from a complex medium formulation with glycerol (peak 2) as the primary carbon source. In both cases a simple 1:50 dilution with water was the only sample pretreament. The chromatogram generated from the chemically defined medium sample shows that except for the glucose peak, virtually no other components are detectable. While several minor peaks were detected in the complex medium, the major peak was glycerol (peak 2), the principal carbon source.

Fig. 5 presents a representative time course of the chromatograms from a fermentation of *Haemophilus influenzae* b cultivated in complex medium with glucose as the major carbon

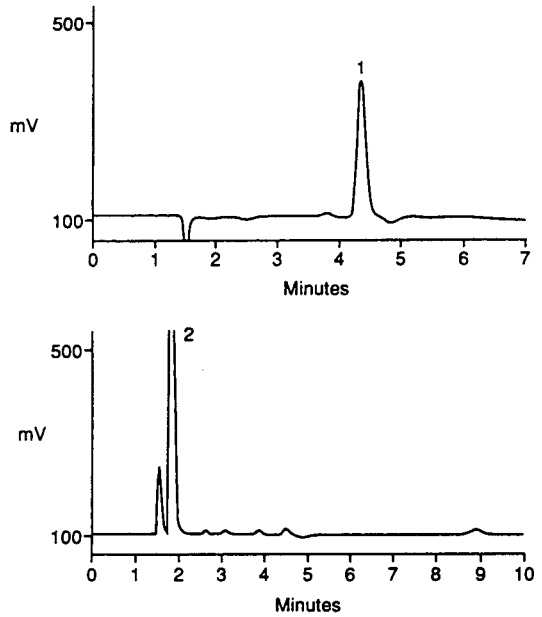

Fig. 4. Representative chromatograms showing isocratic analysis of carbohydrates in an *E. coli* fermentation using chemically defined medium with glucose (peak 1) as the major carbon source (top) or complex medium with glycerol (peak 2) as the major carbon source (bottom).

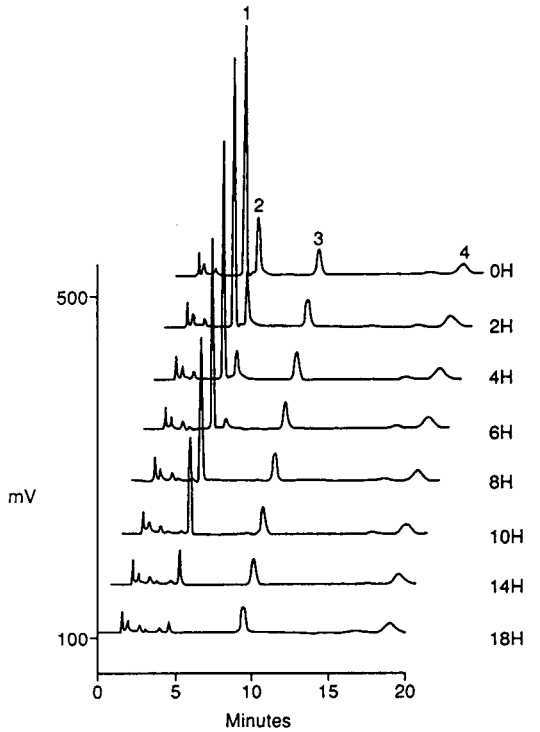

Fig. 5. A time course of representative chromatograms showing isocratic analysis of carbohydrates in a *H. influenzae* fermentation using complex medium with glucose as the major carbon source. Peaks: 1 = glucose; 2 = fructose; 3 = ribose; 4 = maltose. H = Hours.

source. These were generated using the isocratic method. Two major monosaccharides are reduced in concentration during the course of the fermentation. One can infer that glucose (peak 1) and ribose (peak 2) are coordinately metabolized during the period of 18 and 8 h, respectively. Note also the relative stability of the minor peak such as sucrose (peak 3) over the same time course.

The concentration of the maltose (peak 4) did not change during this period but in this series of chromatograms, maltose exhibited an t_R of ca. 19.2 min which does not agree with the 19.6 min t_R as listed in Table 1. This finding illustrated a notable feature of the method. Over time, with repeated injections of complex medium samples, the t_R of disaccharides such as maltose and raffinose tended to decrease. The column performance was restored by washing the column with 1 *M* NaOH for 30 min. This phenomenon was attributed to the loss of column binding sites due to interference from complex medium components [18]. An altered t_R of other analytes that elute sooner than 15 min was not observed.

Fig. 6 illustrates the fermentation time course of a recombinant *Saccharomyces cerevisiae* grown in chemically defined medium containing galactose (peak 1) and glucose (peak 2) at starting concentrations of 89 and 20 g/l, respectively. As shown, the concentration of galactose in the broth decreased by 86% during the fermentation, while glucose is virtually depleted from the broth by 16 h.

A gradient chromatography method, which has an extended run time, was required to resolve these two main analytes. From a practical viewpoint, to maximize ample throughput the isocratic method was utilized for analysis of fermentation samples after glucose exhaustion (e.g., >16 h, data not shown).

HPAEC–PAD can be used for direct detection

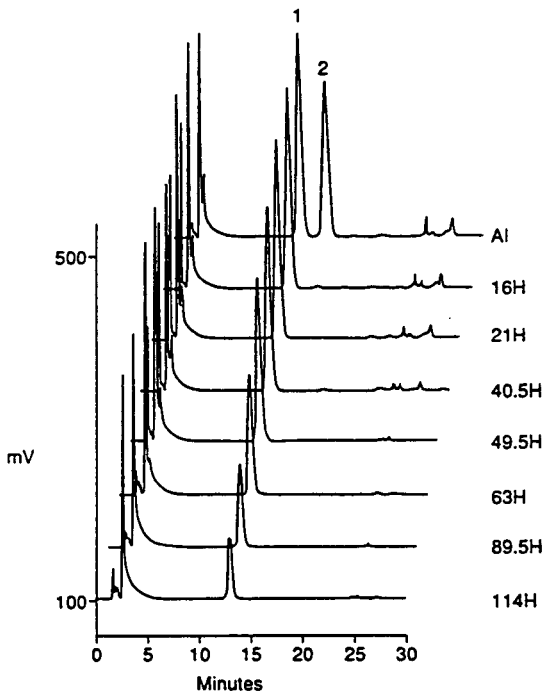

Fig. 6. A time course of representative chromatograms showing gradient analysis of carbohydrates in a *S. cerevisiae* fermentation using chemically defined medium with two principal carbon sources, galactose (peak 1) and glucose (peak 2). H = Hours. AI = After inoculation.

of common carbon sources in fermentation media with only 0.22-μm filtration of fermentation broths and ca. 100-fold dilution of the filtered broth as the sole sample preparation steps. The system can be used for fermentation broths of various composition (either chemically defined or complex) with neither extraction, sample derivatization, nor ashing required. As fermentation broths can contain a variety of components, we were especially concerned about interferences from high ion levels, complex organic components and metabolic by-products. The majority of the components in fermentation media have relatively low pK_a values; thus, the only analytes which would be ionized in alkaline mobile phases are those with high pK_a values such as certain amino acids and nucleoside bases. No interference was observed due to media components. The system proved to be rugged, with greater than 1000 injections prior to column cleanup (defined as change in t_R of standards by 10%). The system has been in continuous use for three years with no major problems in over 10 000 injections. Samples from multiple fermentations constituting different media formulations have been analyzed without compromising the accuracy of the system. In comparison to other analytical methodologies for obtaining carbohydrate concentration in fermentation broth, this system is straightforward and simple. Biologically relevant information about carbohydrate metabolism is critical to the understanding of microbial physiology. Moreover, the central role of carbon metabolism in microbial fermentation processes is the basis for many on-line process control strategies. Thus, the dilute and shoot feature of this method makes on-line sampling/analysis an attractive option for future studies.

Acknowledgements

We express our thanks to R. Ellis, H. George, R. Greasham, J. Hennessey and W. Miller for helpful discussions.

References

[1] E.A. Dawes, D.J. McGill and M. Midgley, *Methods Microbiol.*, 6A (1971) 53–216.
[2] S. Chung, X. Wen, K. Vilholm, M. De Bang, G. Christian and J. Ruzicka, *Anal. Chim. Acta*, 249 (1991) 77–85.
[3] A. Plaga, J. Stumpfel and H. Fielder, *Appl. Microbiol. Biotechnol.*, 32 (1989) 45–49.
[4] F. Weigang, M. Reiter, A. Jungbauer and H. Katinger, *J. Chromatogr.*, 497 (1989) 59–68.
[5] A. Coquet, J.-L. Veuthy and W. Haerdi, *Anal. Chim. Acta*, 252 (1991) 173–179.
[6] N.C. van de Merbel, I.M. Kool, H. Langeman, U.A.Th. Brinkman, A. Kohlhorn and L.C. de Rijke, *Chromatographia*, 33 (1992) 525–532.
[7] R.G. Bell and K.L. Newman, *J. Chromatogr.*, 632 (1993) 87–90.
[8] D.A. Martens and W.T. Frankenberger, Jr., *Chromatographia*, 29 (1990) 7–12.
[9] J. van Riel and C. Olieman, *Carbohydr. Res.*, 215 (1991) 39–46.
[10] S. Mou, Q. Sun and D. Lu, *J. Chromatogr.*, 546 (1991) 289–295.

[11] C. Corradini, A. Cristalli and D. Corradini, *J. Liq. Chromatogr.*, 16 (1993) 3471–3485.
[12] M.R. Hardy and R.R. Townsend, *Proc. Natl. Acad. Sci. U.S.A.*, 85 (1988) 3289–3293.
[13] Y.C. Lee, *Anal. Biochem.*, 189 (1990) 151–162.
[14] M.R. Hardy, R.R. Townsend and Y.C. Lee, *Anal. Biochem.*, 170 (1988) 54–62.
[15] D.P. Lee and M.T. Bunker, *J. Chromatogr. Sci.*, 27 (1989) 496–503.
[16] W.R. LaCourse and D.C. Johnson, *Carbohydr. Res.*, 215 (1991) 1159–1178.
[17] D.C. Johnson and W.R. LaCourse, *Anal. Chem.*, 62 (1990) 589A–597A.
[18] *Installation Instructions and Troubleshooting Guide for CarboPac PA1 Column; Document No. 034441, Rev. 02,* Dionex, Sunnyvale, CA, 1991.

ELSEVIER

Journal of Chromatography A, 676 (1994) 297–302

JOURNAL OF CHROMATOGRAPHY A

Liquid chromatographic separation of the enantiomers of cyclic β-amino esters as their N-3,5-dinitrobenzoyl derivatives

William H. Pirkle*, William E. Bowen, Duc V. Vuong

School of Chemical Sciences, University of Illinois, P.O. Box 44-5, Urbana, IL 61801-3731, USA

First received 25 January 1994; revised manuscript received 12 April 1994

Abstract

A variety of cyclic N-3,5-dinitrobenzoyl β-amino esters has been synthesized and resolved by chiral HPLC. The β-amino esters were derived from β-lactams formed by the [2 + 2] cycloaddition of N-chlorosulfonyl isocyanate with simple olefins. Chromatographic separation of the enantiomers of these N-(3,5-dinitrobenzoyl)-β-amino esters on three π-basic chiral stationary phases is described and the origin of the observed chiral recognition considered.

1. Introduction

A chiral stationary phase (CSP) derived from a conformationally restricted β-amino acid, CSP 1, was developed in these laboratories several years ago [1]. Despite the greater distance between two of the potential recognition sites, CSP 1 has broader analyte scope and generally affords larger separation factors than its α-amino acid analogue, N-(3,5-dinitrobenzoyl)phenylglycine [2]. It is presumed that greater degrees of recognition site preorganization and conformational rigidity are present and are responsible for CSP 1's improved performance. To explore this hypothesis, a series of cyclic (and thereby conformationally restricted) β-amino acids were prepared and the enantiomers of their 3,5-dinitrobenzamide derivatives were examined chromatographically on three CSPs, each of which has a somewhat different conformational preference. Should large separation factors be encountered for the enantiomers of one or more of the analytes in this series, one might, in view of the reciprocity often noted for chiral recognition [3], use this information to aid in the development of a still more efficacious β-amino acid-derived CSP. The understanding one might gain concerning the relationship between structure and chiral recognition using this series of analytes would be an added benefit.

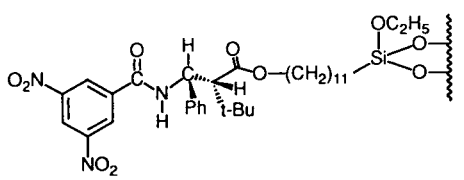

CSP 1

The synthetic route used to prepare the β-lactam precursor of CSP 1 is not suitable for the preparation of cyclic β-amino acids [1,4]. A convenient method for the rapid synthesis of small quantities of β-lactams (and the derivative β-amino acids) is the [2 + 2] cycloaddition of

* Corresponding author.

0021-9673/94/$07.00
SSDI 0021-9673(94)00352-A

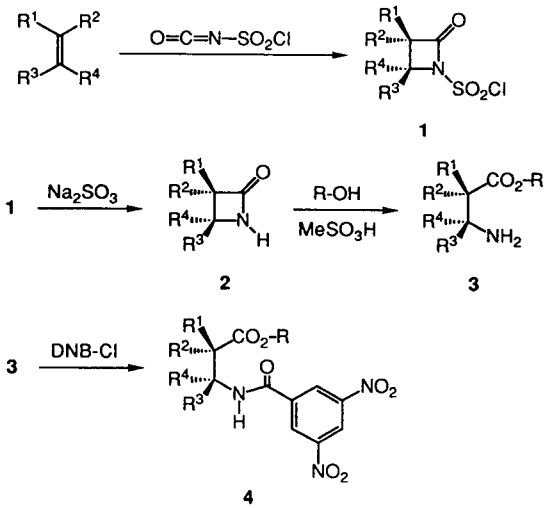

Fig. 1. The synthetic sequence used to prepare racemic analytes **5–14**.

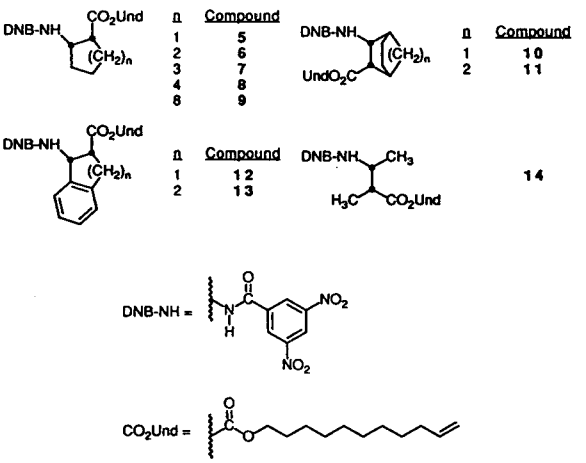

Fig. 2. N-(3,5-Dinitrobenzoyl) β-amino esters synthesized for use in this study.

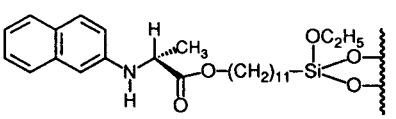

CSP 2

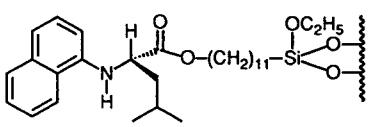

CSP 3

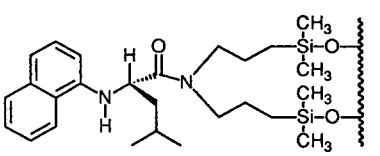

CSP 4

N-chlorosulfonyl isocyanate (CSI) to simple olefins, either cyclic or acyclic (see Fig. 1) [5]. The [2 + 2] cycloaddition reaction proceeds with net retention of the stereochemistry of the starting olefin. Hence, either *cis* or *trans* disubstituted β-lactams can be obtained.

The N-chlorosulfonyl β-lactams, **1**, obtained by [2 + 2] cycloaddition of the isocyanate to an alkene, were hydrolyzed to give the corresponding β-lactams, **2**. These were then ring opened, esterified and acylated as previously described to give the N-3,5-dinitrobenzoyl (DNB) amino esters, **4** [1]. The compounds synthesized by this route are shown in Fig. 2.

The liquid chromatographic separation of the enantiomers of the DNB derivatives of a series of acyclic β-amino acids on several π-basic CSPs was reported earlier [6,7]. The chromatographic separation of the enantiomers of derivatized β-amino acids by liquid chromatography [8,9], ligand-exchange chromatography [10–13], gas chromatography [11], diastereomeric derivatization [14–16] and mobile phase additives [17] have been reported elsewhere. In this study, DNB β-amino esters were evaluated on π-basic CSPs 2–4. CSPs 2 and 3 are commercially available (see Experimental). The synthesis and evaluation of CSP 4 are being reported elsewhere.

2. Experimental

2.1. Equipment

Chromatography was performed with an Alcott 760 HPLC pump, a Rheodyne Model 7125 injector with a 20-μl sample loop, a 250 × 4.6 mm stainless-steel column packed with either CSP 2, 3 or 4, a LDC Analytical UV Monitor D

fixed-wavelength detector (254 nm), a Rudolph Research Autopol III automatic polarimeter using a 2-dm flow-cell and a Hewlett-Packard HP 3394A integrator.

CSPs 2 and 3 are available from Regis (Morton Grove, IL, USA).

2.2. Chemicals

The CSI, undecenyl alcohol and olefins were purchased from Aldrich. Chromatography solvents were generously provided by EM Science. The normal-phase void volume was determined using tri-*tert.*-butylbenzene [18].

2.3. General synthetic approach

The β-lactams were synthesized according to published procedures or minor modifications thereof [19–22]. The ring opening of the β-lactams and esterification of the resulting β-amino acids was accomplished by heating a 1:1.2:1.2 molar ratio of β-lactam, undecenyl alcohol and methanesulfonic acid, respectively, in benzene at reflux overnight with azeotropic removal of the water formed. The resulting reaction mixture was washed successively with saturated $NaHCO_3$ and brine, dried over $MgSO_4$, filtered and isolated in vacuo. The crude amino ester was then acylated with 3,5-dinitrobenzoyl chloride according to standard procedure [1]. Compounds were purified by silica gel flash chromatography or preparative TLC with an ethyl acetate–hexane solvent system.

3. Results and discussion

The enantiomers of each of the DNB β-amino esters studied were successfully resolved by each of the three CSPs examined, see Table 1. In most cases, baseline (or better) resolution of the enantiomers was obtained. The enantiomers of the five-, six- and seven-membered rings, **5–7**, are the most readily separated by these CSPs. Analytes having still larger rings (*e.g.* **8** and **9**) are less well resolved. The decrease in the separation factors of the enantiomers of a larger-ringed analyte is presumably due to the increased degree of conformational flexibility. This is believed to result in a loss of preorganization and to lead to a blend of retention processes which causes increased retention of the least-retained enantiomer and reduced retention of the more retained enantiomer.

The relative placement of interaction sites and the rigidity of two of the smaller ringed analytes was altered either by incorporation of a bridge, **10** and **11**, or by fusing a benzo substituent, **12** and **13**, onto the cyclic analytes. Increased ana-

Table 1
Separation of the enantiomers of N-3,5-dinitrobenzoyl β-amino esters

Compound	CSP 2			CSP 3			CSP 4		
	k'_1	α	Sign[a]	k'_1	α	Sign[a]	k'_1	α	Sign[a]
5	1.88	1.63	(+)	1.51	3.76	(−)	1.13	6.72	(−)
6	2.45	1.87		2.27	3.67		1.19	9.40	
7	2.01	2.07	(+)	1.89	4.57	(−)	1.08	10.3	(−)
8	1.89	1.57	(+)	1.79	2.77	(−)	1.13	5.36	(−)
9	1.76	1.56		2.19	2.28		1.35	2.94	
10	2.11	1.52	(+)	1.76	2.55	(−)	1.02	4.67	(−)
11	3.00	1.17		2.17	1.99		0.91	5.08	
12	3.28	1.16	(−)	1.99	2.78	(+)	2.53	1.66	(+)
13	2.93	1.60	(+)	2.60	1.50	(+)	3.76	1.06	(−)
14	1.89	1.31	(−)	1.65	2.30	(+)	1.38	3.96	(+)

Chromatographic conditions: mobile phase, 2-propanol–hexane (20:80); flow-rate, 2.0 ml/min.
[a] The sign of rotation at 589 nm of the most retained enantiomer is given.

lyte rigidity may be either beneficial or detrimental to chiral recognition by a given selector. Should a structural change in an analyte more heavily populate a conformation having good spatial complementarity of its interaction sites with those of the selector, one can increase the retention of the more retained enantiomer while diminishing the retention of the least-retained enantiomer. By locking the analyte enantiomers into an unfavorable (for chiral recognition) conformation, rigidity can reduce or destroy the selectors' ability to distinguish between the enantiomers.

The enantiomers of the bridged **10** and **11** exhibit separation factors adequate for resolution but smaller than those of their monocyclic counterpart, **6**. In retrospect, it seems likely that, to some extent, the rigid bridge interferes sterically with the selector–analyte interactions principally responsible for chiral recognition. Benzo analogues **12** or **13** show less enantioselectivity on CSPs 2–4 than do the monocyclic analogues **5** and **6**. The added benzo substituent may function as an additional interaction site, either leading to non-chiral retention or to an alternative and opposite-sense chiral recognition process. In fact, **12** and **13** exhibit larger separation factors on CSP 3 than on CSP 4, **13** being best resolved on CSP 2. The order of elution of the enantiomers of **13** from CSP 4 differs from that noted on CSPs 2 and 3. This aspect of chromatographic behavior is not consistent with the general trends observed in Table 1 and seems to support the contention that the benzo substituent can alter the (otherwise) dominant recognition process.

The structurally simple non-cyclic analyte, **14**, prepared for comparative purposes, is well resolved by all three CSPs, demonstrating that the enantiomers of simple DNB β-amino esters bearing sterically small substituents can be separated by CSPs 2–4.

The separation factors for the enantiomers of most DNB β-amino esters on CSPs 2 and 3 are much smaller those found for simple DNB α-amino esters under similar chromatographic conditions [7,23]. This is more or less to be expected, since a greater distance and a larger number of bonds between interaction sites typically leads to greater conformational flexibility and less preorganization. Similar considerations apply to chiral selectors. While CSPs 2 and 3 are essentially the same mechanistically, a claim consistent with a body of experimental data [24–26], the latter often show significantly larger separation factors for the enantiomers of DNB α-amino acid derivatives than do the former. CSP 3 is conformationally more rigid and apparently better preorganized to accommodate the more retained enantiomer of the DNB derivative of either an α- or β-amino acid (see Table 1).

Although in a slightly different spatial arrangement, the necessary (for chiral recognition) interaction sites present in DNB α-amino acid derivatives are also present in DNB β-amino acid derivatives. There is no reason to suspect that the chiral recognition processes of the two are conceptually much different even though the enantioselectivity shown by the latter is reduced for the aforementioned reasons. The chiral recognition process proposed to account for the ability of CSPs 2–4 to "recognize" the enantiomers of DNB β-amino esters involves face to face $\pi-\pi$ interaction of the electron-rich naphthyl group and the electron-poor DNB group, a hydrogen bond between the aryl NH and the terminal carbonyl of the β-amino ester and a second hydrogen bond between the DNB amido hydrogen and the terminal carbonyl of the α-amino acid derivative of the CSP. These processes must occur simultaneously (Fig. 3) for the more retained enantiomers of these analytes.

The preceding chiral recognition mechanism readily accounts for the greater enantioselectivity of CSP 4 relative to CSP 3. The amide carbonyl oxygen of CSP 4 bears a higher electron density than that of the ester carbonyl oxygen of CSP 3 and is hence a better hydrogen bond acceptor. By moderately increasing the strength of an interaction essential to the chiral recognition process, one expects to increase enantiodiscrimination. The data in Table 1 are consistent with this argument. The separation factors for the enantiomers of every analyte (with the exception of **12** and **13**) are greater on CSP 4 than on CSP 3.

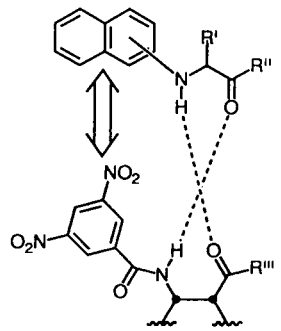

Fig. 3. A generic chiral recognition mechanism proposed to account for the separation of the enantiomers of DNB β-amino esters on CSPs 2-4.

As is the case with most brush-type CSPs, CSPs 2-4 generally exhibit good chromatographic efficiency and resolution factors (R_s) sufficient for complete separation of the enantiomers of these analytes. For example, the resolutions of one of the less-well separated analytes, compound **11**, on these phases (CSP 2, $R_s = 1.2$; CSP 3, $R_s = 3.5$; CSP 4, $R_s = 8.6$) are of a magnitude adequate for most analytical and preparative applications. Compound **13** does show a decrease in resolution from CSPs 2 to 4 (CSP 2, $R_s = 4.0$; CSP 3, $R_s = 3.3$; CSP 4, $R_s = 0.61$) consistent with the previously noted unusual chromatographic behavior of this analyte.

The depiction of CSP 4 shows (*S*)-N-(1-naphthyl)leucine di-*n*-propyl amide doubly linked to the silica support. This is an idealized picture, a mixture of linkage modes doubtless occurs. A selector tethered by both trimethylene legs, as is CSP 4, is expected to manifest a degree of rigidity not present in CSP 3. Plausibly, "two-legged" attachment may lead to a greater spacing between the strands of bonded phase than occurs with "one-legged" attachments, a point under study. Strand spacing can influence the level of enantioselectivity afforded by a given immobilized selector.

Conclusions

The enantiomers of a variety of DNB β-amino esters have been chromatographically separated on three π-basic CSPs. From the ease of separation observed, it is likely that the enantiomers of a wide variety of substituted β-amino acids derivatives can be resolved by CSPs 2–4. The chiral recognition mechanism earlier advocated as responsible for the separation of the enantiomers of α-amino acid derivatives on CSPs 2 and 3 also accounts for the differential affinities shown toward the enantiomers of β-amino acid derivatives by these CSPs. From the magnitudes of the separation factors observed, one presumes that separation of the enantiomers of C-terminal amides of DNB β-amino acids will be separated easily using CSPs 2–4.

CSPs corresponding to analytes **12** and **13** have been synthesized and their performance will be reported in due course.

Acknowledgements

This work was supported by grants from the National Science Foundation and Eli Lilly and Co. Chromatography solvents were generously provided by EM Science.

References

[1] W.H. Pirkle and J.E. McCune, *J. Chromatogr.*, 441 (1988) 311.
[2] W.H. Pirkle and J.E. McCune, *J. Chromatogr.*, 471 (1989) 271.
[3] W.H. Pirkle, C.J. Welch and B. Lamm, *J. Org. Chem.*, 57 (1992) 3854.
[4] D.C. Ha, D.J. Hart and T.K. Yang, *J. Am. Chem. Soc.*, 106 (1984) 4819.
[5] D.N. Dhar and K.S.K. Murthy, *Synthesis*, (1986) 437.
[6] O.W. Griffith, E.B. Campbell, W.H. Pirkle, A. Tsipouras and M.H. Hyun, *J. Chromatogr.*, 362 (1986) 345.
[7] W.H. Pirkle, T.C. Pochapsky, G.S. Mahler, D.E. Corey, D.S. Reno and D.M. Alessi, *J. Org. Chem.*, 51 (1986) 4991.
[8] Y. Okamoto, Y. Kaida, R. Aburatani and K. Hatada, *J. Chromatogr.*, 477 (1989) 367.
[9] T. Miyazawa, Y. Shindo, T. Yamada and S. Kuwata, *Anal. Lett.*, 26 (1993) 457.
[10] V.A. Davankov, Y.A. Zolotarev and A.A. Kurganov, *J. Liq. Chromatogr.*, 2 (1979) 1191.

[11] J. Wagner, E. Wolf, B. Heintzelmann and C. Gaget, *J. Chromatogr.*, 392 (1987) 211.
[12] S. Yamazaki, T. Takeuchi and T. Tanimura, *J. Chromatogr.*, 540 (1991) 169.
[13] N. Ôi, H. Kitahara and F. Aoki, *J. Chromatogr.*, 631 (1993) 177.
[14] T. Yamada, S. Nonomura, H. Fujiwara, T. Miyazawa and S. Kuwata, *J. Chromatogr.*, 515 (1990) 475.
[15] T. Miyazawa, H. Iwanaga, T. Yamada and S. Kuwata, *Anal. Lett.*, 26 (1993) 367.
[16] M. Lobell and M.P. Schneider, *J. Chromatogr.*, 633 (1993) 287.
[17] W.F. Lindner and I. Hirschböck, *J. Liq. Chromatogr.*, 9 (1986) 551.
[18] W.H. Pirkle and C.J. Welch, *J. Liq. Chromatogr.*, 14 (1991) 1.
[19] E.J. Moriconi and P.H. Mazzocchi, *J. Org. Chem.*, 31 (1966) 1372.
[20] H. Bestian, H. Biener, K. Clauss and H. Heyn, *Liebigs Ann. Chem.*, 718 (1968) 94.
[21] T. Durst and M.J. O'Sullivan, *J. Org. Chem.*, 35 (1970) 2043.
[22] F.M. Hauser and S.R. Ellenberger, *Synthesis*, (1987) 324.
[23] W.H. Pirkle, K.C. Deming and J.A. Burke, *Chirality*, 3 (1991) 183.
[24] W.H. Pirkle and T.C. Pochapsky, *J. Am. Chem. Soc.*, 109 (1987) 5975.
[25] W.H. Pirkle, J.A. Burke and S.R. Wilson, *J. Am. Chem. Soc.*, 111 (1989) 9222.
[26] K.C. Deming, *Ph.D. Thesis*, University of Illinois at Urbana-Champaign, Urbana-Champaign, IL, Aug. 1989.

ELSEVIER

Journal of Chromatography A, 676 (1994) 303–309

JOURNAL OF CHROMATOGRAPHY A

Enantiomer separation of amino acids on a chiral stationary phase derived from L-alanyl- and pyrrolidinyl-disubstituted cyanuric chloride

Ching-Erh Lin*, Chen-Hsing Lin

Department of Chemistry, National Taiwan University, Taipei, Taiwan

First received 2 March 1993; revised manuscript received 8 March 1994

Abstract

A silica-based chiral stationary phase derived from L-alanyl- and pyrrolidinyl-disubstituted cyanuric chloride was prepared for the enantioseparation of methyl esters of N-(3,5-dinitrobenzoyl)amino acids. The chromatographic results show that effective and efficient enantioseparation was achieved on this chiral stationary phase. Rationales purporting to account for liquid chromatographic observations of chiral recognition are examined.

1. Introduction

Owing to the increasing awareness of the importance of separating enantiomers, interest in the separation of enantiomers by high-performance liquid chromatography has grown dramatically during the past decade [1–5]. The efficient separation and resolution of enantiomers from racemic mixtures can be achieved by utilizing chemically bonded chiral stationary phases (CSPs) [6–9]. For the successful resolution of enantioseparation on CSPs, the molecular structures of the chiral moieties of the CSP and the enantiomeric analytes must be complementary in some fashion so that at least three simultaneous, preferential and distinct interactions prevail between them [10]. A CSP capable of preferentially retaining one of a pair of enantiomers should exhibit at least one preferential interaction that is stereochemically dependent. The preferential interactions important for enantioselectivity cause a differential retention of the enantiomeric analytes. As the extent of these interactions depends on the molecular structures of enantiomeric analytes, an appropriate derivatization of chiral molecules may become a determining factor for the effective and selective resolution of enantiomeric analytes.

The design of effective and selective CSPs is often aided by understanding the mechanism of chiral recognition. Recently, the origin of chiral recognition has been investigated by many researchers using empirical [11–20] and/or computational [21–29] methods. In this way, chiral recognition models pertaining to the mode of operation of those CSPs become better understood.

As the high-performance liquid chromatographic separation of enantiomers on some *s*-triazine derivatives of amino acid dipeptide es-

* Corresponding author.

0021-9673/94/$07.00
SSDI 0021-9673(94)00266-C

ters, tripeptide esters and (*S*)-1-(α-naphthyl)-ethylamine chiral stationary phases [30–32] demonstrated the practicability of using the *s*-triazine ring as a linking unit, we considered that in the design of new chiral stationary phases the chiral selector can be composed of an amino acid and an *s*-triazine derivative possessing strong π-basic character for the chiral separation of amino acids. In this work, a CSP composed of an L-alanyl- and pyrrolidinyl-disubstituted *s*-triazine derivative was prepared and the enantioselectivities of some amino acids on this CSP column were examined. Rationales purporting to account for liquid chromatographic observations of chiral recognition were considered.

2. Experimental

2.1. Chemicals and reagents

Pyrrolidine, cyanuric chloride, N,N-dicyclohexylcarbodiimide and 3,5-dinitrobenzoyl chloride were purchased from Merck. The silica gel used was Nucleosil (pore size 10 nm; particle size 10 mm; surface area 350 m^2/g) obtained from Macherey–Nagel. 3-Aminopropyltriethoxysilane (APS) and N-methylmorpholine were obtained from Janssen. N-Hydroxysuccinimide was purchased from Aldrich and amino acids from Sigma. Synthesis reagents for preparing the chiral stationary phase and the derivatization of chiral analytes were purchased from various suppliers and were used as received. 2-Propanol and *n*-hexane of LC grade were purchased from Mallinckrodt. Water was purified by ion exchange followed by treatment in a Milli-Q water purification system (Millipore).

2.2. Preparation of chiral stationary phase

Pyrrolidinyl-substituted cyanuric chloride

A solution of sodium carbonate (0.021 mol) and pyrrolidine (0.02 mol) in water (70 ml) kept in an ice-bath near 0°C was added with agitation to a solution of cyanuric chloride (0.02 mol) in acetone (30 ml). After the mixed solution had reacted at 0°C for 1 h, the product was filtered, washed well with cold water several times and then dried over P_4O_{10} at reduced pressure. The product yield is about 85%.

L-Alanyl- and pyrrolidinyl-disubstituted cyanuric chloride

A solution of sodium carbonate (0.021 mol) and L-alanine (0.01 mol) dissolved in water (100 ml) was added with agitation to a solution of pyrrolidinyl-substituted cyanuric chloride (0.01 mol) dissolved in acetone (30 ml). The mixed solution was reacted near 50°C for 2 h. The solution was filtered to remove the precipitate, then the clear filtrate was neutralized with dilute HCl solution until substantial precipitation occurred, with the filtrate in the ice-bath. The precipitate was collected by filtration, washed several times with water and then dried over P_4O_{10} at reduced pressure. The yield of the product was about 55%.

Silane-modified silica gels

The preparation of silane-modified silica gels was described previously [33]. The silane used was 3-aminopropylsilane.

Chemically bonded chiral stationary phase

After adding N-hydroxysuccinimide (0.005 mol) to a solution of L-alanyl- and pyrrolidinyl-disubstituted cyanuric chloride (0.005 mol) dissolved in tetrahydrofuran (THF) (100 ml) in an ice-bath at 0°C, N,N-dicyclohexylcarbodiimide (DCC) (0.005 mol) was slowly added with agitation. Reaction proceeded at 0°C for 1 h, then at room temperature for a further 24 h. The solution product was obtained by filtering off unwanted dicyclohexylurea, in which APS-modified silica gel (3 g) was suspended and to which N-methylmorpholine (1 ml) was added. The reaction proceeded at 0°C for 1 h, then at room temperature for a further 48 h with agitation. The product was collected by filtration, washed thoroughly with THF, methanol, water and methanol successively, then dried over P_4O_{10} at reduced pressure. Fig. 1 displays the reaction scheme for the preparation of this chiral stationary phase.

2.3. Apparatus and chromatography

The chromatographic system and the column-packing apparatus were described previously [32]. Mixtures of 2-propanol and *n*-hexane (typi-

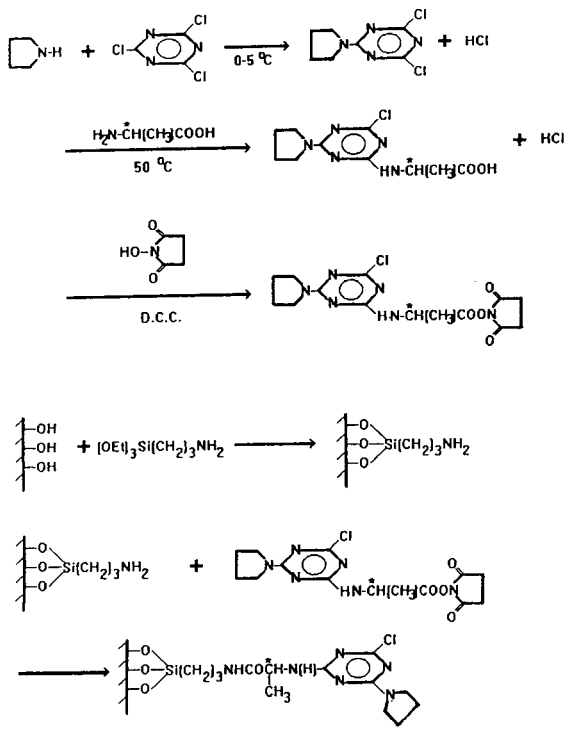

Fig. 1. Reaction scheme for the preparation of chiral stationary phase.

cally 20:80, v/v) were used as the mobile phase and were filtered through a 0.45-μm membrane filter and degassed by ultrasolic vibration. The flow-rate was 1.0 ml/min. The detector was operated at 254 nm. Elemental analyses of the chiral stationary phase and the corresponding silane-modified silica gel were performed with a Perkin-Elmer Model 240C elemental analyser.

3. Results and discussion

3.1. Characterization of the stationary phase

The nitrogen contents of APS-modified silica and chiral stationary phase obtained from elemental analyses were 1.29 and 3.31%, respectively. The loading capacities determined from the nitrogen contents for APS-modified silica and chiral stationary phase were 0.92 and 0.33 mmol/g, respectively. The loading capacity of APS-modified silica (X) was calculated with the equation

$$X\,(\text{mmol}) = \text{N}\,(\%) \times 1000/(14 \times 100)$$

and the loading capacity of the chiral stationary phase (Z, in mmol/g) was calculated with the equation

$$\text{N}\,(\%) = (14X + 5 \times 14Z) \times 10^{-3} \times 100/ [1 + (M) - 18)Z] \times 10^{-3}$$

where M is the molecular mass of pyrrolidinyl- and L-alanyl-disubstituted cyanuric chloride. By comparing the loading capacity of the APS-modified silica with that of the chiral entity, we found that only 36% of the amino groups on the APS-modified silica surface were converted into the chiral moiety.

3.2. Enantioseparation of amino acids

Table 1 presents the results of the enantiomeric separation of methyl esters of 3,5-dinitrobenzoyl amino acids on this chiral stationary phase. Fig. 2 shows typical chromatograms of the enantiomeric separation of valine and leucine. Except for proline, which shows no chiral selectivity, most of the amino acids listed in Table 1 showed excellent enantioselectivity. In most instances, baseline separation of the enantiomers of amino acids was achieved using 2-propanol–*n*-hexane (20:80, v/v) as the eluent.

As shown in Table 1, the capacity factors of the enantiomers of amino acids having an alkyl substituent attached to the chiral carbon decrease with increasing chain length of the alkyl group, but the enantioselectivity indicated by the α values seems to be unaffected by variation of the chain length of the alkyl group. In contrast, the enantioselectivities of amino acids with a branched-chain alkyl group are larger than those of amino acids with a linear alkyl group. This may indicate that a small but stereochemically significant steric interaction exists between the branched-chain alkyl group of the chiral selectrand and the methyl group of the chiral selector.

Among the chiral analytes tested, the enantiomers of amino acids with substituents other than an alkyl group were retained longer in the

Table 1
Chromatographic separation of methyl esters of N-(3,5-dinitrobenzoyl)amino acids on L-alanyl- and pyrrolidinyl-disubstituted cyanuric chloride-derived CSP

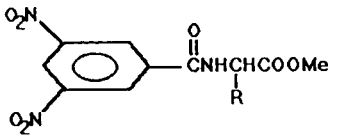

Amino acid	R	k_1' [a]	α	Configuration[b]
Alanine	CH_3	3.65	1.36	*R*
Aminobutyric acid	CH_3CH_2	2.78	1.45	*R*
Norvaline	$CH_3CH_2CH_2$	2.31	1.39	*R*
Norleucine	$CH_3CH_2CH_2CH_2$	2.09	1.35	*R*
Valine	$(CH_3)_2CH$	2.38	1.54	*R*
Leucine	$CH_3CH(CH_3)CH_2$	2.01	1.44	*R*
Isoleucine	$CH_3CH_2CH(CH_3)$	2.03	1.49	*R*
Phenylglycine	C_6H_5	4.46	1.20	*R*
Phenylalanine	$C_6H_5CH_2$	3.95	1.53	*R*
Tyrosine	$HOC_6H_5CH_2$	10.78	1.62	*R*
Tryptophan	$C_8H_5(NH)CH_2$	11.89	1.55	*R*
Aspartic acid	CH_3OOCCH_2	6.63	1.28	*R*
Glutamic acid	$CH_3OOCCH_2CH_2$	5.85	1.40	*R*
Methionine	$CH_3SCH_2CH_2$	5.02	1.46	*R*
Threonine	$HOCH(CH_3)$	6.53	1.17	*R*
Proline	–	3.45	1.00	–

Eluent, 2-propanol–*n*-hexane (20:80, v/v); flow-rate, 1 ml/min.
[a] Capacity factor of the first-eluted enantiomer.
[b] Absolute configuration of the first-eluted enantiomer.

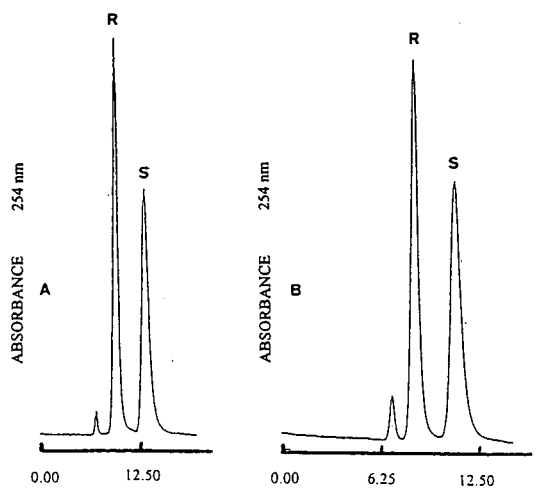

Fig. 2. Enantioseparation of methyl esters of N-(3,5-dinitrobenzoyl)amino acids: (A) valine; (B) leucine. Eluent, 2-propanol–*n*-hexane (20:80, v/v); flow-rate, 1 ml/min.

column than those of amino acids with alkyl substituents, particularly for amino acids with aromatic substituents such as tyrosine and tryptophan. Hence the involvement of the additional $\pi-\pi$ interaction between amino acids with aromatic substituents and the chiral stationary phase is clear. As indicated in Table 1, the α values for phenylglycine, phenylalanine, tyrosine and tryptophan were 1.20, 1.53, 1.62 and 1.55, respectively. The remarkable difference in the enantioselectivity between phenylglycine and phenylalanine, tyrosine or tryptophan reveals that the relative orientation of the aromatic substituent and the structural compatibility between these chiral analytes and the chiral stationary phase plays a significant role in the enantioseparation.

The capacity factors of amino acids with a carboxyl group such as aspartic acid and glutamic acid esters were found to be twice as large as those of amino acids with an alkyl group. This

effect is probably due to hydrogen bonding between the carbonyl group of the chiral analytes and the secondary amino group of the chiral stationary phase. However, as reflected by the smaller α value of aspartic acid than that of amino acids with alkyl substituents, this interaction could not be considered as a preferential interaction contributing to the formation of diastereomeric complexes.

The structural difference between threonine and valine clearly indicates that the presence of a hydroxyl group in threonine causes an increased capacity factor, because of hydrogen bonding with the carbonyl group of the chiral stationary phase. However, as reflected by the smaller α value of threonine than that of valine, the existence of this interaction seems not to favour chiral recognition also.

The enantiomers of N-(3,5-dinitrobenzoyl)-derivatized proline molecule cannot be resolved on this chiral stationary phase. The reasons are unknown; perhaps the absence of an acidic NH group in the derivatized proline prevents hydrogen bonding.

3.3. Chiral recognition mechanism

In accordance with previous reports [11–13], the design of the present chiral stationary phase is based on the following three preferential interactions: (a) $\pi-\pi$ interaction involving the 3,5-dinitrobenzoyl group of the chiral selectrand and the pyrrolidinyl-substituted *s*-triazine ring of the CSP, (b) hydrogen bonding involving the carbonyl group in the carboxyl ester group of the chiral selectrand and the secondary amino group belonging to the amino acid of the chiral selector and (c) hydrogen bonding involving the secondary amino group in the amide linkage of the chiral selectrand and the carbonyl group in the amide linkage of the chiral selector. Fig. 3 shows the preferential interactions existing between the chiral selectrand and the chiral selector. However, as mentioned by several researchers [34–36], these preferential interactions may not be the sole determining factors for chiral discrimination. Additional interactions, such as the steric interaction between the substituent group attached to the chiral centre of the chiral selectrand and the alkyl group attached to the chiral centre of the chiral selector, may also be involved to some extent in the chiral recognition process.

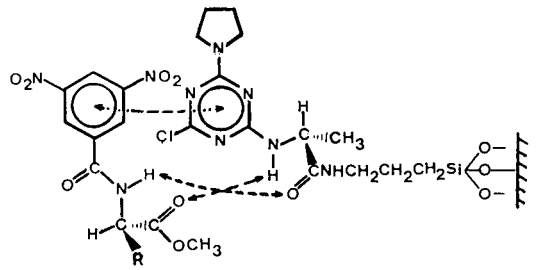

Fig. 3. Preferential interactions between methyl ester of an N-(3,5-dinitrobenzoyl)amino acid and the chiral stationary phase.

In order to establish whether the $\pi-\pi$ interaction involving the 3,5-dinitrobenzoyl group in the chiral selectrand and the pyrrolidinyl-substituted *s*-triazine ring in the chiral selector is essential for chiral recognition, we examined the effect of various π-acceptor substituents on the enantioseparation of methyl esters of benzoyl-derivatized amino acids so that the role played by the 3,5-dinitrobenzoyl group of the chiral selectrand in chiral recognition could be evaluated. Table 2 presents the chromatographic results of the dependence for various derivatized methionine methyl esters and those of valine methyl esters. According to Table 2, the replacement of a 3,5-dinitrobenzoyl group by a 3-nitrobenzoyl group or a benzoyl group greatly decreases the enantioselectivity. For instance, the α value decreased from 1.46 to 1.13 and 1.00 on replacement by a 3-nitrobenzoyl and a benzoyl group, respectively. This effect is simply due to the decrease in the $\pi-\pi$ interaction between the *s*-triazine ring of the chiral selector and the benzoyl group of the chiral selectrand. Our chromatographic data thus clearly indicate the necessity for the presence of a pyrrolidinyl-substituted *s*-triazine ring in the chiral selector and the importance of the interaction between π-acceptor and π-donor groups in the chiral discrimination process. This result is consistent with the findings of Pirkle and co-workers [11–13].

Table 2
Effect of different π-acceptor substituents on the enantioseparation of methylesters of benzoyl-derivatized amino acids

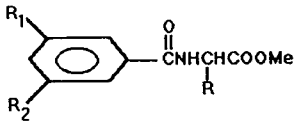

R_1	R_2	R = $CH_2CH_2SCH_3$			R = $CH(CH_3)_2$		
		k'_1	k'_2	α	k'_1	k'_2	α
NO_2	NO_2	5.02	7.35	1.46	2.38	3.67	1.54
H	NO_2	3.26	3.69	1.13	1.55	1.83	1.18
H	Cl	1.34	1.34	1.00	0.66	0.62	1.00
H	H	1.45	1.45	1.00	0.64	0.64	1.00

Eluent, 2-propanol–*n*-hexane (20:80, v/v); flow-rate, 1 ml/min.

The important role played by the ester group of the chiral analytes in the chiral discrimination has been demonstrated by Salvadori *et al.* [37], based on the fact that the replacement of an ester group with a cyano group greatly decreases the α value. We obtained additional evidence to support the important role of the ester group in the chiral recognition by comparing the chromatographic resolution of the enantiomers of 3,5-dinitrobenzoylamino acids with that of 3,5-dinitrobenzoylamine [38]. As the absence of the carbonyl group in 3,5-dinitrobenzoylamine excludes the formation of hydrogen bonding between the carbonyl group of the chiral selectrand and the secondary amino group of the chiral moiety of the chiral stationary phase, no chiral discrimination was achieved on this CSP for 3,5-dinitrobenzoylamines.

The role of the secondary amino group in the chiral analytes is seen by comparing the chromatographic results of the enantioseparation of esters of 3,5-dinitrobenzoyl amino acids possessing an acidic NH group with that of the ester of 3,5-dinitrobenzoylproline. The inability to achieve enantioseparation of the proline ester is probably due to the absence of an acidic NH group, because no hydrogen bonds could be formed between the chiral analyte and the chiral stationary phase. Although this hydrogen bonding is considered as the third preferential interaction, such an interaction may not be essential for the chiral discrimination, because no enantioseparation of amino acids was achieved on the chiral stationary phase derived from L-phenylglycyl- and pyrrolidinyl-disubstituted cyanuric chloride, despite the three major preferential interactions persisting between the CSP and the methyl ester of 3,5-dinitrobenzoylphenylalanine [38]. In other words, the results reveal that the enantiomers of an amino acid may be unable to be discriminated by these three preferential interactions alone. Instead, as was demonstrated in Table 1, steric repulsion between the substitutional group attached to the chiral centre of the chiral analyte and the substituent group attached to the chiral centre of the chiral stationary phase needs to be taken into consideration as a significant discrimination interaction in the chiral recognition process.

4. Conclusions

The chiral stationary phase derived from an L-alanyl- and pyrrolidinyl-disubstituted cyanuric chloride could provide excellent enantioselectivities for most of the racemates of amino acids tested, except proline. Although the π–π interaction and the two hydrogen bondings between chiral analytes and the chiral stationary phase are considered to be the three major preferential interactions between the chiral selector and chiral selectrands, the hydrogen bonding between the secondary amino group of the chiral

analytes and the carbonyl group of the chiral stationary phase may not be essential for the chiral discrimination. Instead, the steric interaction between the substituent group attached to the chiral centre of the chiral selectrands and the methyl group linked to the chiral centre of the chiral stationary phase should play a significant role in the chiral discrimination.

Acknowledgement

We thank the National Science Council of the Republic of China for financial support.

References

[1] M. Zief and L.J. Crane (Editors), *Chromatographic Chiral Separations*, Marcel Dekker, New York, 1988.
[2] W.J. Lough (Editor), *Chiral Liquid Chromatography*, Chapman and Hall, New York, 1989.
[3] A.M. Krstrulovic (Editor), *Chiral Separations by HPLC*, Wiley, New York, 1989.
[4] D. Stevenson and I.D. Wilson (Editors), *Recent Advances in Chiral Separations*, Plenum Press, New York, 1990.
[5] S. Ahuja (Editor), *Chiral Separations by Liquid Chromatography*, American Chemical Society, Washington, DC, 1991.
[6] W.H. Pirkle, D.W. House and J.M. Finn, *J. Chromatogr.*, 192 (1980) 143.
[7] V.A. Davankov, A.A. Kurganov and A.S. Bochkov, *Adv. Chromatogr.*, 22 (1983) 71.
[8] D.W. Armstrong, *J. Liq. Chromatogr.*, 7 (1984) 353.
[9] D.W. Armstrong, *Anal. Chem.*, 59 (1987) 84A.
[10] C.E. Dalgliesh, *J. Chem. Soc.*, 137 (1952) 3940.
[11] W.H. Pirkle, T.C. Pochapsky, G.S. Mahler, D.E. Corey, D.S. Reno and D.M. Alesi, *J. Org. Chem.*, 51 (1986) 4991.
[12] W.H. Pirkle and T.C. Pochapsky, *J. Am. Chem. Soc.*, 108 (1986) 352.
[13] W.H. Pirkle, K.C. Deming and J.A. Burke, III, *Chirality*, 3 (1991) 183.
[14] W.H. Pirkle and T.C. Pochapsky, *J. Am. Chem. Soc.*, 108 (1986) 5627.
[15] W.H. Pirkle and T.C. Pochapsky, *J. Am. Chem. Soc.*, 109 (1987) 5975.
[16] P. Shan, T.B. Hsu and L.B. Rogers, *J. Chromatogr.*, 396 (1987) 31.
[17] W.H. Pirkle, J.A. Burke, III and R. Wilson, *J. Am. Chem. Soc.*, 111 (1989) 9222.
[18] R. Dappen, G. Rihs and C.W. Mayer, *Chirality*, 2 (1990) 185.
[19] P. Salvadori, C. Pini, C. Rosini and G. Uccello-Barretta, *J. Am. Chem. Soc.*, 112 (1990) 2707.
[20] X.-J. Lu, L.B. Rogers and J.A. de Haseth, *Anal. Chem.* 63 (1991) 2939.
[21] K.B. Lipkowitz, D.A. Demeter, R. Zegarra, R. Larter and T. Darden, *J. Am. Chem. Soc.*, 110 (1988) 3446.
[22] K.B. Lipkowitz and R. Zegarra, *J. Comput. Chem.*, 10 (1989) 595.
[23] R.E. Boehm, D.E. Martire and D.W. Armstrong, *Anal. Chem.*, 60 (1988) 522.
[24] M.G. Still and L.B. Rogers, *Talanta*, 36 (1989) 35.
[25] S. Topiol and M.J. Sabio, *J. Chromatogr.*, 461 (1989) 129.
[26] K.B. Lipkowitz, R. Zegarra and B. Baker, *J. Comput. Chem.*, 10 (1989) 718.
[27] K.B. Lipkowitz and B. Baker, *Anal. Chem.*, 62 (1990) 770.
[28] S. Topiol and M. Sabio, *Chirality*, 3 (1991) 56.
[29] U. Norinder and E.G. Sundholm, *J. Liq. Chromatogr.*, 10 (1987) 2825.
[30] M. Oi, M. Nagase and Y. Sawada, *J. Chromatogr.*, 292 (1984) 427.
[31] N. Oi, H. Kitahara, Y. Inda, M. Horiba and T. Doi, *Bunseki Kagaku*, 30 (1981) 254.
[32] N. Oi, M. Horiba and H. Kitahara, *Bunseki Kagaku*, 28 (1979) 607.
[33] C.E. Lin, C. Chen, C.H. Lin, M.H. Yang and J.C. Jiang, *J. Chromatogr. Sci.*, 27 (1989) 665.
[34] S. Topiol and M. Sabio, *J. Am. Chem. Soc.*, 111 (1989) 4109.
[35] A. Berthod, H.L. Jin, A.M. Stalcup and D.W. Armstrong, *Chirality*, 2 (1990) 38.
[36] L. Oliveros, C. Minguillon, B. Desmazieres and P.L. Desbene, *J. Chromatogr.*, 589 (1992) 53.
[37] P. Salvadori, D. Pini, C. Rosini, G. Uccello-Barretta and C. Bertucci, *J. Chromatogr.*, 450 (1988) 163.
[38] C.C. Lin and C.E. Lin, in preparation.

ELSEVIER

Journal of Chromatography A, 676 (1994) 311–319

JOURNAL OF CHROMATOGRAPHY A

Determination of amino acids by ion-pair liquid chromatography with post-column derivatization using 1,2-naphthoquinone-4-sulfonate☆

J. Saurina, S. Hernández-Cassou*

Departament de Química Analítica, Universitat de Barcelona, Diagonal 647, 08028 Barcelona, Spain

First received 2 November 1993; revised manuscript received 5 April 1994

Abstract

A new chromatographic method for the determination of amino acids is proposed. The method is based on the separation of amino acids by means of ion-pair liquid chromatography and post-column derivatization using 1,2-naphthoquinone-4-sulfonate. The analytical column was a Spherisorb ODS 2. Amino acids were separated by an elution gradient with four linear steps based on increasing the concentration of 2-propanol. Two eluents were used to create the gradient profile: eluent A was an aqueous solution of 20 m*M* H_3PO_4 + 20 m*M* $H_2PO_4^-$ + 15 m*M* dodecyl sulfate and eluent B was a mixture of aqueous (25 m*M* H_3PO_4 + 25 m*M* $H_2PO_4^-$ + 18.5 m*M* dodecyl sulfate)–2-propanol (1:1, v/v). The injection volume was 100 μl and the total flow-rate for the mobile phase was 0.8 ml/min. The chromatographic outlet was coupled on-line to the two-channel derivatization system which delivered reagent and buffer solutions. The reaction took place at 65°C in a reaction coil of 4 m × 1.1 mm I.D. The spectrophotometric detection was performed at 305 nm. The separation of common amino acids was done in 90 min, although an additional period of 15 min was required to stabilize the column. The repeatability of the method for lysine is 2.1% and the reproducibility is 2.6%. The detection limit for lysine is 0.09 nmol. The linear range for lysine is up to 32 nmol with a correlation coefficient of 0.999. The method was applied to the determination of amino acids in animal feed and powdered milks. The results of the method are in good agreement with those obtained with the standard amino acid autoanalyzer method.

1. Introduction

The analysis of amino acids is usually done by liquid chromatography. A chemical derivatization is required to improve the detection since most common amino acids are not readily detected by spectroscopy. For this purpose pre- and post-column derivatization methods can be used. Advantages and disadvantages of pre- and post-column labelling have been pointed out [1,2]. Phenylisothiocyanate [3,4], *o*-phthaldialdehyde (OPA) [5,6], dansyl chloride [7], dabsyl chloride [8] and 9-fluorenylmethylchloroformate [9,10] are most popular reagents for pre-column derivatization.

However, only a few post-chromatographic methods are described in the literature. Ninhydrin has been used successfully for post-

* Corresponding author.

☆ Presented at *Euroanalysis VII, Edinburgh, 5–11 September 1993.*

0021-9673/94/$07.00
SSDI 0021-9673(94)00391-L

column derivatization of amino acids [11–15], since it was proposed by Spackman et al. [11]. The ninhydrin stream reacts with the chromatographic eluate to give a derivative detected by visible spectroscopy at 570 and 440 nm. Some commercial amino acid analyzers are based on this reaction. In another study [13], ninhydrin has been added to the mobile phase prior the separation. In this case, the labelling reaction is developed by heating the solution emerging from the column in a reaction coil at 140°C. Hence, an additional channel to pump the reagent is not required. 1,2,3-Perinaphthindantrione has been used in the same way [13]. OPA has also been employed in post-column systems for both spectrophotometric and fluorimetric detection of primary amino acids [16–20]. A reducing agent is added to develop the reaction, which takes place at room temperature in a reaction coil coupled on-line to the chromatographic system. However, OPA is not suitable for the analysis of imino acids such as proline or hydroxyproline. Recently, hollow-fibre membrane reactors have been used in the reaction between OPA and amino acids [21–23]. Fluorescamine [24,25], 4-chloro-7-nitrobenzo-2-oxa-1,3-diazole [26] and 4-fluoro-nitrobenzo-2-oxa-1,3-diazole [27] are other fluorogenic labelling agents for post-column derivatization.

Amino acids can be separated by cation-exchange chromatography or by reversed-phase ion-pair chromatography. In cation-exchange chromatography the separation is performed on a sulfonic resin, using a mobile phase based on a lithium or sodium cation elution gradient together with an increasing-pH gradient. In ion-pair chromatography, the ion pairs formed between the acidic form of amino acids and an anionic surfactant are separated on a reversed-phase column. This type of separation should be preferred because reversed-phase columns are cheaper and live longer is higher than sulfonated columns.

In this work, a new chromatographic method for the spectrophotometric determination of amino acids is proposed. The method is based on the separation of amino acids by ion-pair high-performance liquid chromatography and the subsequent derivatization on-line with 1,2-naphthoquinone-4-sulfonate (NQS). The stationary phase is C_{18}-modified silica. The mobile phase is a phosphoric/dihydrogenphosphate buffer solution containing dodecyl sulfate as surfactant and 2-propanol as a solvent. In order to optimize the separation and to decrease the time of analysis an elution gradient of 2-propanol has been used. The outlet of the analytical column is coupled on-line to the derivatization system in which the reaction between amino acids and NQS takes place. The optimum conditions to develop this reaction in flow systems have been previously described [28,29]. NQS reacts with amino acids in basic medium giving a derivative which is spectrophotometrically detected at 305 nm and 480 nm. NQS has advantages over other reagents mentioned above, since it is soluble in water, reacts with primary and secondary amino groups under milder conditions and is quite cheap.

Finally, this chromatographic method has been applied to the determination of amino acids in extracts of commercial powdered milks and animal feed.

2. Experimental

2.1. Reagents

Phosphoric acid (Carlo Erba, analytical grade), sodium dihydrogenphosphate (Carlo Erba, analytical grade), sodium dodecyl sulfate (SDS) (Merck, analytical grade) and 2-propanol (Probus, HPLC grade) were the constituents of the mobile phase.

Amino acids (analytical grade) were supplied by Merck.

Sodium NQS (Aldrich, analytical grade) was used to prepare a $1.2 \cdot 10^{-3}$ *M* solution in 0.1 *M* hydrochloric acid. This solution is stable for at least two weeks.

Buffer stock solution of 0.015 *M* sodium hydrogencarbonate (Scharlau, analytical grade) + 0.185 *M* sodium carbonate (Scharlau, analytical grade) was used to neutralize the

solution emerging from the column and adjust pH for the development of the reaction.

Commercial powdered milk and animal feed samples were obtained from Cooperativa Agropecuaria de Guissona (Lleida, Spain).

2.2. Apparatus

A LKB Bromma 2152 LC controller connected with two LKB Bromma 2150 HPLC pumps was used to pump the eluents and to generate the elution gradient. Samples were injected by means of a Spark Holland Promis automatic injection system. The analytical column was a Spherisorb ODS 2 (150 mm × 4.6 mm I.D., 5 μm of particle size). The column was held at 50°C using an Spark Holland SPH 99 column thermostat. The detector was a Waters 486 tunable absorbance detector with a flow cell of 10 mm path length and 8 μl of dead volume. Data acquisition was performed with a Perkin-Elmer (PE) Nelson 900 Series interface coupled to a microcomputer. Data were stored on floppy disks for further calculations. The equipment for amino acid analysis using the standard method was a Pharmacia LKB autoanalyzer, Model Alpha Plus (Series Two).

2.3. Chromatographic procedure

The experimental set-up used in this study is shown in Fig. 1. Two different mobile phases were prepared: eluent A was an aqueous solution of 20 m*M* phosphoric acid + 20 m*M* sodium dihydrogenphosphate + 15 m*M* SDS, while eluent B was a mixture of aqueous (25 m*M* phosphoric acid + 25 m*M* sodium dihydrogenphosphate + 18.5 m*M* SDS)–2-propanol (4:1, v/v). The elution gradient profile for the chromatographic separation of amino acids was as follows: step 1: time = 0–10 min, % eluent B = 0; step 2: time = 10–85 min, % eluent B = 0–100 (linear); step 3: time = 85–88 min, % eluent B = 100–0 (linear); step 4: time = 88–90 min, % eluent B = 0. The injection volume was 100 μl and the total flow-rate of the mobile phase was set at 0.8 ml/min. The column outlet was coupled on-line to the two-channel derivatization system, in which the NQS reagent and carbonate/hydrogencarbonate solutions were pumped by means of a peristaltic pump (Scharlau HP4) using standard Tygon tubing. Reagent and buffer solutions merged in a mixing chamber. The reaction coil of 4 m × 1.1 mm I.D. was placed in a thermostatic bath (SBS TFB-3) at 65°C. The spectrophotometric detection was performed at 305 nm. The pH of the final reagent solution emerging from the mixing chamber was sufficiently basic to neutralize the chromatographic effluent and provide the proper medium for the development of the reaction (pH 9.7). This final reagent solution cannot be prepared directly as a stock solution because NQS quickly decomposes in basic medium, so it has to be generated on-line with the flow system [28,29].

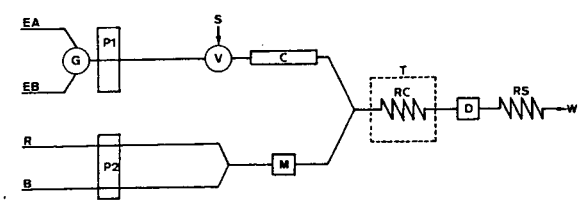

Fig. 1. Flow system scheme. P1 = HPLC pump; P2 = peristaltic pump; G = gradient programmer; V = injection valve; C = analytical column; M = mixing chamber; RC = reaction coil; T = thermostatic bath; D = detector; RS = restrictor; EA = eluent A; EB = eluent B; R = reagent (NQS); B = buffer; S = sample; W = waste.

2.4. Autoanalyzer procedure

The amino acid autoanalyzer is based on the ninhydrin method [11]. Amino acids were separated in a column of 20 cm × 4 mm I.D. packed with a cation-exchange resin Ultropac 7 (8 μm particle size). The column temperature was varied from 20 to 75°C with a Peltier heating/cooling system. The elution is performed by means of a lithium citrate buffer with increasing pH and ionic strength. The chromatographic eluate reacts with ninhydrin in a reaction coil of 0.3 mm I.D. which was contained in a heater jacket at 135°C. The amino acid derivatives were detected spectrophotometrically at 570 and 440

nm using a flow cell of 8 μl volume and 15 mm pathlength.

2.5. Sample treatment

A 2-g amount of feed sample (or 1 g of powdered milk) were subjected to a solid–liquid extraction with 50 ml of 0.01 *M* hydrochloric acid in order to recover free amino acids. The extraction was performed for 60 min in a conical flask by means of magnetic stirring. The extract was centrifuged at 13 000 rpm for 30 min. Solutions obtained in this way were stored in the fridge.

Solutions injected into both HPLC system and amino acid analyzer were prepared from 1000 μl of extract solutions and 100 μl of 10 m*M* norleucine as internal standard, and by filtering through an Ultrafree-MC low-binding cellulose membrane (10 000 NMWL) from Millipore.

3. Results and discussion

3.1. Study of separation conditions

The effect of the concentration of phosphoric acid in the mobile phase on the retention time was studied by varying the concentration of the acid from 1 to 50 m*M*. Concentrations of dihydrogenphosphate and SDS were kept constant at 20 and 15 m*M*, respectively. The retention time of amino acids increased markedly with acidity in the range 1 to 10 m*M*, while from 10 to 50 m*M* the variation was less noticeable. The value chosen for further experiments was 20 m*M*.

Fig. 2 shows the influence of the SDS concentration in the mobile phase on the retention time of alanine. The SDS concentration was varied from 1 to 30 m*M*. The concentrations of phosphoric acid and dihydrogenphosphate were maintained at 20 m*M*. At SDS concentrations higher than 5 m*M*, the retention time of Ala continuously decreases with surfactant concentration. With these conditions, this fact can be attributed to the formation of micelles in the system. The value chosen for the SDS concentration was 15 m*M*.

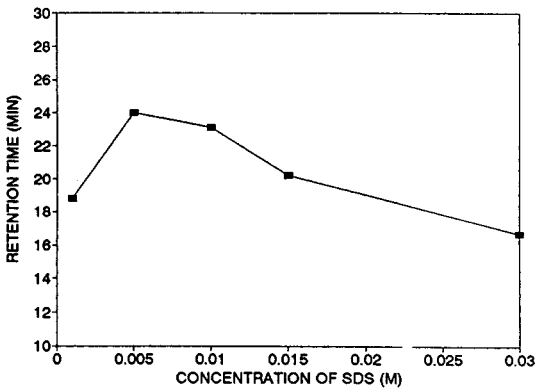

Fig. 2. Effect of the SDS concentration on the isocratic elution of alanine. Amount injected, 100 nmol; reaction coil, 6 m × 1.1 mm I.D.; reaction coil temperature, 65°C; eluent, phosphate buffer (20 m*M* H_3PO_4 + 20 m*M* $H_2PO_4^-$ + SDS)–methanol (4:1, v/v). Other conditions are given in the text.

In these preliminary studies, methanol was added to the mobile phase as solvent to facilitate the elution of amino acids. However, the retention times for several amino acids such as Trp, His, Lys or Arg were too long even at high ratios of methanol/water. In order to reduce the time of analysis methanol was substituted by 2-propanol. Fig. 3 shows the chromatograms for the isocratic elution of several amino acids at three percentages of 2-propanol in the mobile phase. By comparing the common amino acids of this figure (Ala and Pro in Fig. 3a and b, and Nle and Trp in Fig. 3b and c), there is a marked decrease in the retention time with increasing the percentage of 2-propanol. On the basis of these results, different elution gradients were investigated in order to optimize the separation of common amino acids. Fig. 4 shows the chromatogram obtained under the gradient profile chosen. This separation takes 90 min although a further 15 min are required to stabilize the column before the next injection.

3.2. Study of post-column reaction conditions

The most characteristic factors that affect the post-column derivatization of amino acids with NQS were pH, concentration of NQS, tempera-

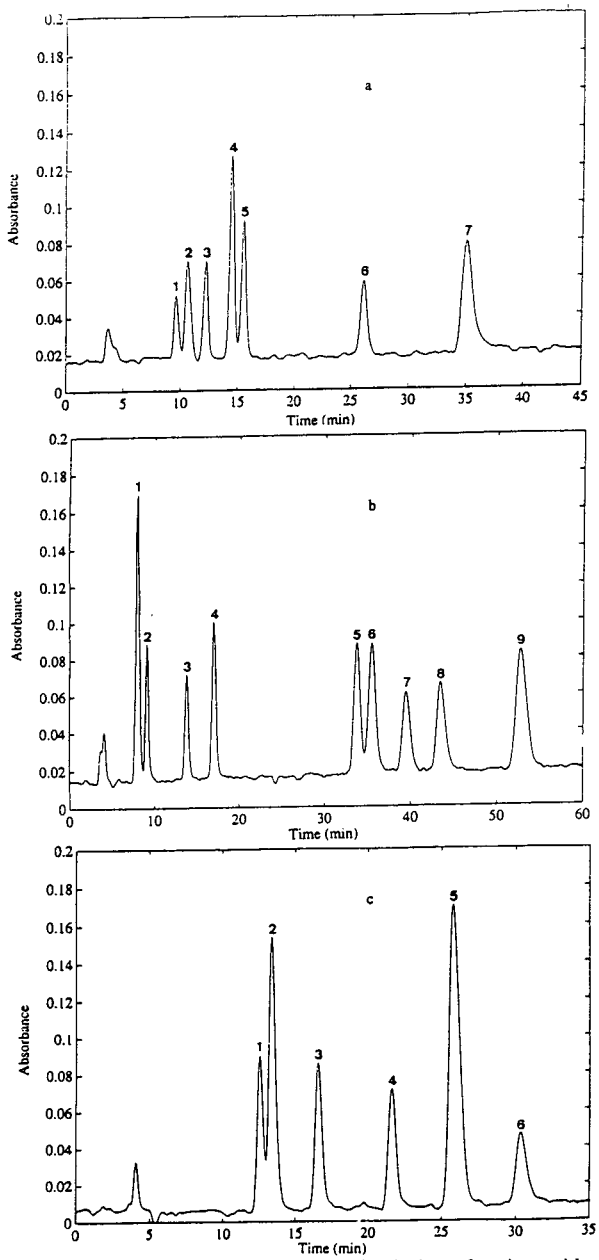

Fig. 3. Chromatograms of the isocratic elution of amino acids at different percentages of 2-propanol in the mobile phase. Injected amounts: Tyr 20 nmol and each other amino acid 40 nmol. Eluent: phosphate buffer (20 m*M* H_3PO_4 + 20 m*M* $H_2PO_4^-$ + 15 m*M* SDS)–2-propanol. Other conditions are given in the text. (a) 0% (v/v) of 2-propanol; peaks: 1 = Asp; 2 = Ser; 3 = Glu; 4 = Gly; 5 = Thr; 6 = Ala; 7 = Pro. (b) 10% (v/v) of 2-propanol; peaks: 1 = Pro; 2 = Asp; 3 = Tyr; 4 = Met; 5 = Ile; 6 = Phe; 7 = Leu; 8 = Nle; 9 = Trp. (c) 20% (v/v) of 2-propanol; peaks: 1 = Nle; 2 = Trp; 3 = His; 4 = Orn; 5 = Lys; 6 = Arg.

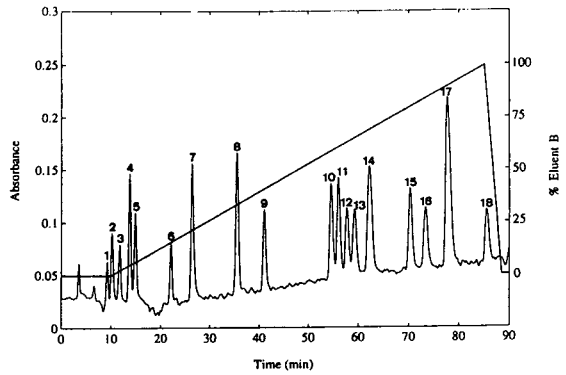

Fig. 4. Chromatogram of amino acids using the elution gradient chosen. Injected amounts: 40 mmol of each amino acid. Peaks: 1 = Asp; 2 = Ser; 3 = Glu; 4 = Gly; 5 = Thr; 6 = Ala; 7 = Pro; 8 = Tyr; 9 = Met; 10 = Ile; 11 = Phe; 12 = Leu; 13 = Nle; 14 = Trp; 15 = His; 16 = Orn; 17 = Lys; 18 = Arg. Line = elution gradient profile.

ture and dimensions of the reaction coil. The experimental conditions for the development of the reaction in flow systems were reported previously [28,29]. In this study, those conditions have been adapted to the new post-column system as follows.

As the separation is performed at pH 2.5 and the reaction between NQS and amino acids occurs at pH 9 to 10, a 0.185 *M* carbonate + 0.015 *M* hydrogencarbonate solution was used as buffer. Under these conditions the pH in the reaction coil was 9.6.

The dimensions of the reaction coil influence both the sensibility and the separation of the method. Reaction coils of 1.1 mm I.D. worked satisfactorily while with the other ones assayed (0.7, 0.5 and 0.35 mm I.D.) the baseline was instable with a high level of fluctuation. This instability was probably due to the incomplete mixing of the chromatographic effluent and the reagent solution. Fig. 5 shows the effect of the length of the reaction coil on the peak height. Maximum absorbance was mostly obtained for a reaction coil of 5 m, although in the range from 4 to 8 m the absorbance was nearly constant. The influence of the length of the reaction coil on the chromatographic resolution of five pairs of close peaks is shown in Fig. 6. From this figure, it can

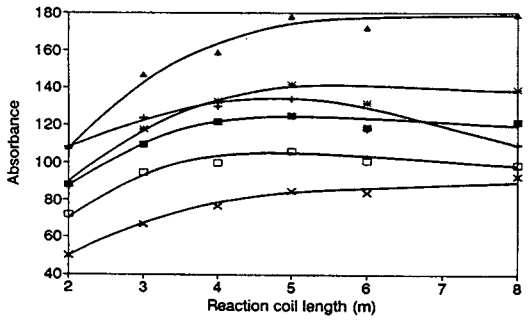

Fig. 5. Influence of the reaction coil on the absorbance at 305 nm. Injected amounts: 40 nmol of each amino acid. Other conditions are given in the text. ■ = Gly; + = Pro; * = Tyr; □ = Trp; × = His; ▲ = Lys.

be seen that peaks become wider and the resolution decreases as coil length increases. Finally, a reaction coil of 4 m × 1.1 mm I.D. was chosen on the basis of a suitable compromise between peak height and peak resolution.

The peak height increases continuously from room temperature to 70°C and remains virtually constant in the range 70–90°C. Thus, although the maximum absorbance was attained in the range indicated, the reaction was developed at 65°C in order to prevent the formation of bubbles in the system.

The effect of SDS and 2-propanol contained in the mobile phase on the post-column reaction was also studied. For this purpose a non-chromatographic system was used, in which solutions with different concentrations of SDS and 2-propanol were pumped to simulate the chromatographic eluate. In the range of concentrations studied [0 to 30 m*M* SDS and 0 to 40% (v/v) of 2-propanol] the absorbance was unaffected. In consequence, the final concentrations chosen for SDS and 2-propanol were those previously selected in the study of separation conditions.

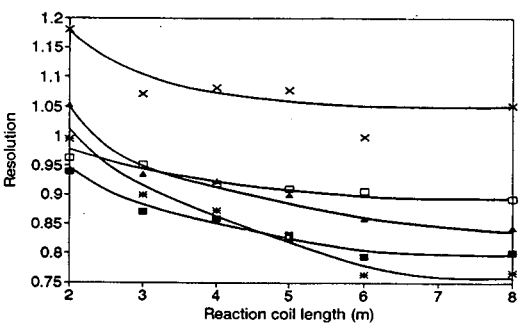

Fig. 6. Influence of the reaction coil on the chromatographic resolution of pairs of close peaks. For conditions see Fig. 5. ■ = Asp–Ser; * = Gly–Thr; □ = Ile–Phe; × = Phe–Nle; ▲ = Nle–Leu.

3.3. Figures of merit

In order to establish the figures of merit for the proposed method a preliminary study was performed to determine which of the following chromatographic parameters provided the best precision: peak area, peak height, peak $\text{area}_{\text{amino acid}}/\text{peak area}_{\text{internal standard}}$ and peak $\text{height}_{\text{amino acid}}/\text{peak height}_{\text{internal standard}}$. The internal standard was $4 \cdot 10^{-4}$ *M* norleucine. Results indicated that the use of Nle as internal standard to perform the calculations did not contribute significatively to the improvement of the results. The lowest R.S.D.s were obtained using the peak height, thus, this parameter was selected for further determination of the figures of merit.

The characteristics of the method at 305 nm, under the optimum conditions described above, are summarized in Table 1. The repeatability of the method was studied by injecting six times consecutively a standard solution of amino acids. The reproducibility on different days was also calculated by injecting the same standard solution for six days. In this case, fresh solutions of reagent, carbonate buffer and eluents A and B were prepared daily. Repeatability and reproducibility were studied both for peak height and retention time. The limit of detection was calculated for a signal-to-noise ratio of 3. In general, for all amino acids tested, the repeatability is better than 4%, the reproducibility better than 5% and the detection limits vary between 0.09 and 0.33 nmol.

3.4. Determination of amino acids in powdered milks and animal feed samples

The proposed method was applied to the determination of the contents of free amino acids

Table 1
Figures of merit for the proposed method at 305 nm under optimum conditions

Amino acid	Retention time		Peak height		Linear range (nmol)	Detection limit (nmol)
	Repeatability (R.S.D., %)	Reproducibility (R.S.D., %)	Repeatability (R.S.D., %)	Reproducibility (R.S.D., %)		
Ser	0.8	1.5	1.7	3.4	Up to 40	0.16
Gly	0.2	1.5	1.9	4.1	Up to 40	0.10
Pro	0.1	0.9	1.6	1.5	Up to 40	0.08
Tyr	0.1	0.8	2.2	3.7	Up to 40	0.11
Met	0.1	1.0	4.1	5.0	Up to 40	0.20
Trp	0.1	0.9	3.8	5.2	Up to 40	0.14
His	0.1	0.5	3.9	4.6	Up to 40	0.26
Lys	0.1	0.6	2.1	2.6	Up to 32	0.09
Arg	0.2	0.4	2.2	4.9	Up to 40	0.33

in feed and powdered milks for animal nourishing. Some essential amino acids such as lysine and methionine are usually added during the elaboration process of this kind of samples in order to correct their lack in proteins used as raw material. Thus, samples were subjected to the solid–liquid extraction previously described, in order to recover the free amino acids.

Fig. 7 shows the chromatograms of the aqueous extracts of a powdered milk and a feed

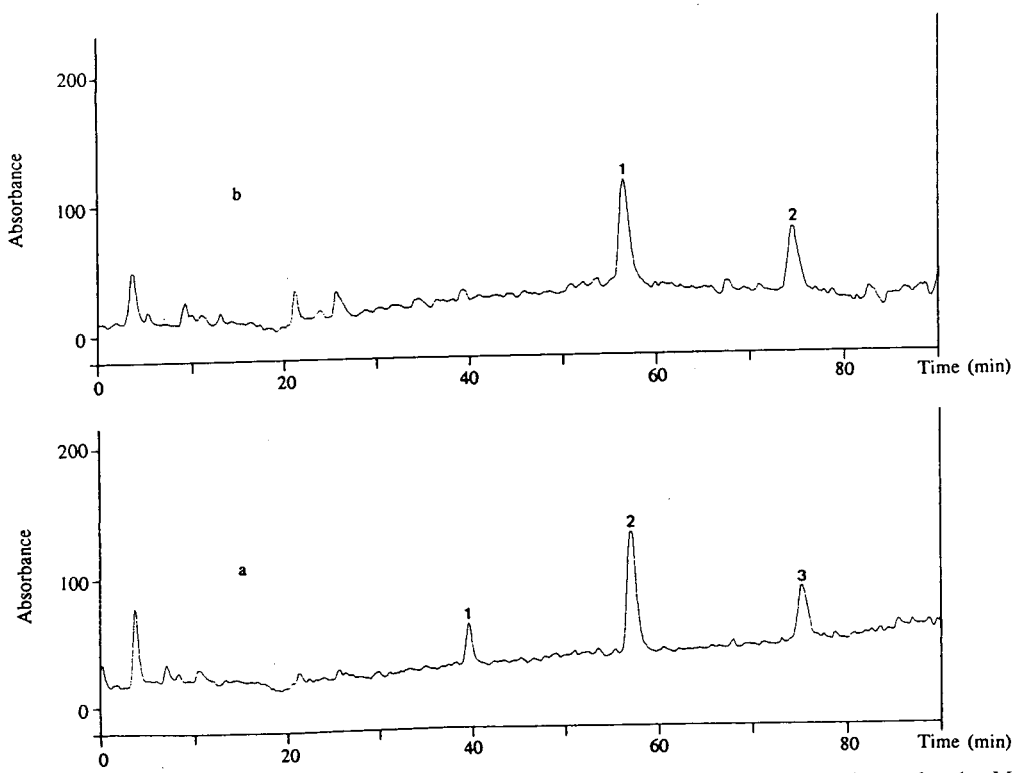

Fig. 7. Chromatograms of extract solutions under optimum conditions. (a) Powdered milk sample; peaks: 1 = Met; 2 = Nle; 3 = Lys. (b) Feed sample; peaks: 1 = Nle; 2 = Lys.

Table 2
Determination of amino acids in feed and powdered milks by the proposed method (NQS method) and the standard method

Sample	Amino acid (g amino acid/100 g sample)			
	Methionine		Lysine	
	NQS method	Standard method	NQS method	Standard method
Milk 1	0.151	0.156	0.056	0.055
Milk 2	0.166	0.168	0.121	0.123
Feed 1	– [a]	– [a]	0.066	0.069
Feed 2	– [a]	– [a]	0.139	0.137

[a]Not present in the sample.

sample, respectively. Although they show that other amino acids (such as proline, arginine and alanine) are present in the samples, the aim of this analysis is focused on the control of the essential amino acids added in the elaboration process, and as a consequence only Lys and Met have been quantified in the samples. Results obtained using the proposed method were compared with those from the standard amino acid analyzer in order to test the accuracy of the method. From Table 2, there is a good agreement between both methods.

4. Conclusions

Sodium NQS is an useful reagent for amino acid analysis using UV–visible spectroscopy. The use of NQS in post-column labelling shows advantages over reagents for pre-column labelling (phenylisothiocyanate, dansyl and dabsyl chlorides and 9-fluorenylmethylchloroformate) because NQS is water soluble and cheaper. In pre-column derivatization methods, the labelling reaction is usually carried out by means of batch procedures. However, the proposed method involves the on-line post-column derivatization, thus the automation is easy, the sample preparation is minimized and problems deal with derivative instability are overcome. OPA and fluorescamine fail in the labelling of secondary amino acids, while NQS reacts with both primary and secondary amino acids. In comparison with the standard method for amino acid determination based on ninhydrin post-column labelling, NQS reacts under milder conditions and dual-wavelength detection is not required in this case. The separation is performed on a reversed-phase column which is cheaper than the cation-exchange columns used in the ninhydrin method. Although the method has been employed in the analysis of feed and powdered milks, it can be easily adapted to other kind of routine samples.

Acknowledgements

The authors thank Dr. I. Casals and co-workers from "Serveis Científico-Tècnics de la Universitat de Barcelona" for their help in the chromatographic study, and to Cooperativa Agropecuaria de Guissona for providing the samples. J.S. also thanks the Ministerio de Educación y Ciencia for a FPI grant. This work has been partially financed by DGICYT project PB90-0821.

References

[1] H. Lingeman and W.J.M. Underberg (Editors), *Detection-Oriented Derivatization Techniques in Liquid Chromatography*, Marcel Dekker, New York, 1990.
[2] E. Heftmann (Editor), *Chromatography: Fundamentals and Applications of Chromatography and Related Differential Migration Methods, Part B: Applications*, Elsevier, Amsterdam, 5th ed., 1992.

[3] R.L. Heinrikson and S.C. Meredith, *Anal. Biochem.*, 136 (1984) 65.
[4] V. Fierabracci, P. Masiello, M. Novelli and E. Bergamini, *J. Chromatogr.*, 570 (1991) 285.
[5] D.W. Hill, F.H. Walter, T.D. Wilson and J.D. Stuart, *Anal. Chem.*, 54 (1979) 1338.
[6] R. Schuster, *J. Chromatogr.*, 431 (1988) 271.
[7] L. Zecca and P. Ferrario, *J. Chromatogr.*, 337 (1985) 391.
[8] E.H.J.M. Jansen, R.H. van der Berg, R. Both-Miedema and L. Doorn, *J. Chromatogr.*, 553 (1991) 123.
[9] S. Einarsson, B. Josefsson and S. Largerkvist, *J. Chromatogr.*, 282 (1983) 609.
[10] P.A. Haynes, D. Sheumack, J. Kibby and J.W. Redmond, *J. Chromatogr.*, 540 (1991) 177.
[11] D.H. Spackman, W.H. Stein and S. Moore, *Anal. Chem.*, 30 (1958) 1190.
[12] P.B. Hamilton, *Anal. Chem.*, 35 (1963) 2055.
[13] J.N. LePage and E.M. Rocha, *Anal. Chem.*, 55 (1980) 1360.
[14] T. Hori and S. Kihara, *Fresenius' Z. Anal. Chem.*, 330 (1988) 253.
[15] J.A. Grunau and J.M. Swiader, *J. Chromatogr.*, 594 (1992) 165.
[16] M. Roth and A. Hampai, *J. Chromatogr.*, 83 (1973) 535.
[17] A. Fiorino, G, Frigo and E. Cucchetti, *J. Chromatogr.*, 476 (1988) 83.
[18] R.B. Ashworth, *J. Assoc. Off. Anal. Chem.*, 70 (1987) 248.
[19] H.K. Radjai and R.T. Hatch,. *J. Chromatogr.*, 196 (1980) 319.
[20] M. Fujiwara, Y. Ishida, N. Nimura, A. Toyama and T. Kinoshita, *Anal. Biochem.*, 166 (1987) 72.
[21] G.I. Tous, J.L. Fausnaugh, O. Akinysoye, H. Lackland, P. Winter-Cash, F.J. Vitorica and S. Stein, *Anal. Biochem.*, 179 (1989) 50.
[22] J. Haginaka and J. Wakai, *J. Chromatogr.*, 396 (1987) 297.
[23] J. Haginaka and J. Wakai, *Anal. Biochem.*, 171 (1988) 398.
[24] M.C. Miedel, J.D. Hulmes and Y.C.E. Pan, *J. Biochem. Biophys. Methods*, 18 (1989) 37.
[25] A.L.L. Duchateau and M.G. Crombach, *Chromatographia*, 24 (1987) 37.
[26] M. Ahnoff, I. Grundevik, A. Arfwidsson, J. Fonsellus and B.A. Persson, *Anal. Chem.*, 53 (1981) 485.
[27] Y. Watanabe and K. Imai, *Anal. Chem.*, 55 (1983) 1786.
[28] J. Saurina and S. Hernández-Cassou, *Anal. Chim. Acta*, 281 (1993) 593.
[29] J. Saurina and S. Hernández-Cassou, *Anal. Chim. Acta*, 283 (1993) 414.

ELSEVIER

Journal of Chromatography A, 676 (1994) 321–330

JOURNAL OF CHROMATOGRAPHY A

Ion-pair high-performance liquid chromatography of cysteine and metabolically related compounds in the form of their S-pyridinium derivatives

Stanisław Sypniewski, Edward Bald*

Department of Chemical Technology and Environmental Protection, University of Łódź, 91-416 Łódź, Poland

First received 21 December 1993; revised manuscript received 17 March 1994

Abstract

A procedure was developed for converting cysteine, glutathione, homocysteine, acetylocysteine, N-(2-mercaptopropionyl)glycine and its metabolite 2-mercaptopropionic acid into their S-pyridinium derivatives for determination by paired-ion reversed-phase high-performance liquid chromatography. The thiol compounds were derivatized with 2-chloro-1-methylpyridinium iodide within a few minutes at room temperature. The thiol group reacted smoothly with the reagent in the pH 8.2 buffer to form an S-pyridinium derivative showing strong UV absorption with a maximum at 314 nm. The reaction mixture was injected directly into a chromatograph without purification and detected spectrophotometrically at 314 nm. The six thiols in the pmol range were separated and determined in a single run on an octadecyl-bonded silica column under isocratic conditions using 0.175 *M* citrate buffer containing 10 mmol/l sodium octanesulphonate (pH 2.8), acetonitrile and methanol (82:6:12, v/v/v) as the mobile phase. Linear calibration graphs were obtained for concentrations of the thiols between 1 and 50 μmol/l. The detection limits ranged from 0.75 pmol for acetylocysteine to 2.1 pmol for 2-mercaptopropionic acid and the relative standard deviations were equal to or better than 9.0% at the 1 μmol/l thiol level and 0.86% at the 50 μmol/l level. Optimum derivatization reaction conditions and HPLC separation conditions were elucidated.

1. Introduction

Cystein and metabolitically related amino acids are substances of great biological importance. L-Cysteine participates in a number of biochemical processes that depend on the particular reactivity of the thiol group. The high nucleophilicity of the thiol function facilitates the role of cysteine as an active site, covalent catalyst, among others in papain and glyceraldehyde-3-phosphate dehydrogenase [1], and allows the cysteine residue of glutathione to accept and detoxify electrophiles during mercapturic acid biosynthesis [2,3] and peroxide reduction [4] or free radical scavenging [5]. Interest in both the physiological and pharmacological roles of SH-containing amino acids has resulted in the development of a number of different methods for their separation and determination.

Most analytical procedures for biological aminothiols involve some form of derivatization followed by separation by a chromatographic method, mostly high-performance liquid chromatography (HPLC), with various detection tech-

* Corresponding author.

0021-9673/94/$07.00
SSDI 0021-9673(94)00275-E

niques. Most of the methods presented up to 1986 have been described in reviews [6,7]. These methods include UV measurement with precolumn derivatization [8,9], fluorimetric detection of monobromobimane (mBrB) derivatives [10–12], *o*-phthalaldehyde (OPA) derivatives [13], derivatives of halosulphonylbenzofurazans (SBD-F and SBD-Cl) [14,15], dansylaziridine [16], N-substituted maleimide [17] and a recycling postcolumn reaction using glutathione reductase and Ellman's reagent [18], detection by the sulphydryl–disulphide exchange reaction in the postcolumn system [19,20] and electrochemical detection [21,22]. More recent publications report data on enlargement of the bimane family of reagents by introducing *p*-sulphobenzoyloxybromobimane [23] as a membrane-impermeable reagent for the derivatization of thiols, likewise a fluorogenic oxazole-based [24] reagent, chiral derivatization with 2,3,4,6-tetra-O-acetyl-β-D-glucopyranosyl isothiocyanate for UV detection [25] and electrochemical detection after derivatization with 3,5-di-*tert*-butyl-1,2-benzoquinone [26] or silver nitrate [27] or without derivatization [28,29].

In spite of the popularity of various precolumn derivatization methods, there have been many reports describing various shortcomings of the procedures, and to date no one method has been shown to overcome all the problems. For example, OPA gives a derivative with cysteine, unlike with the other amino acids containing a primary amino group, with minimal fluorescence [13]. This problem may be overcome by oxidizing cysteine to cysteic acid, which when reacted with OPA–2-mercaptoethanol (MCE) yields a derivative with fluorescent properties similar to those of the other amino acid derivatives [13]. However, the conditions for these two reaction are very different, one being oxidizing and the other reducing, and it is difficult to obtain between-run reproducibility of cysteine derivatization with OPA–MCE following its oxidation; moreover, this procedure makes impossible the determination of cysteine in the presence of cystine without pretreatment of the sample with an SH-blocking reagent [30]. Many of the techniques suffer from incomplete reactions owing to the presence of some solvents or common buffer salts, and highly absorbing hydrolysis products, by-products or the reagent itself, unless an extraction step is incorporated into the procedure prior to the chromatographic analysis [26] or the molar excess of reagent is carefully limited.

In a search for an ideal derivatization reagent or highly automated techniques that are readily available, which could relax the criteria for a practical reagent, we focused our studies on developing a new reagent for the HPLC of aminothiols that minimizes or eliminates the drawbacks mentioned above. Recently we published results on the determination by spectrophotometry of cysteine and related compounds in the form of their S-pyridinium derivatives with the use of 2-chloro-1-methylpyridinium iodide (2-CMPI) as a derivatization reagent [31]. In this paper we report the usefulness of 2-CMPI as a UV derivatization reagent for the separation and determination of biologically important aminothiols by means of ion-pair HPLC.

2. Experimental

2.1. Apparatus

The HPLC system consisted of a Hewlett-Packard Series 1050 isocratic pump, a Hewlett-Packard Series 1050 variable-wavelength detector and a Hewlett-Packard HP 3394A integrator. The samples were injected using a Rheodyne Model 7125 injection valve fitted with a 20-μl loop. The column (250 × 4.0 mm I.D.) was prepacked with 5-μm diameter Spherisorb ODS-2 and operated at a flow-rate of 0.7 ml/min. The analytical column was fitted with a clean-up column (20 × 2.1 mm I.D.) packed with ODS Hypersil (30 μm). UV spectra were recorded on a Carl Zeiss Jena UV–Vis spectrophotometer (1-cm cells).

2.2. Chemicals and reagents

Reduced glutathione (GSH) and L-cysteine (CSH) were obtained from Reanal (Budapest,

Hungary) and DL-homocysteine (HSH), N-acetyl-L-cysteine (ACSH), N-(2-mercaptopropionyl)glycine (MPG) and 2-mercaptopropionic acid (PrSH) from Fluka (Buchs, Switzerland). Ion-pairing reagents (sodium 1-butane-, 1-hexane-, 1-octane- and 1-decanesulphonate) were supplied by Sigma (St. Louis, MO, USA). Other chemicals were purchased from Baker (Deventer, Netherlands).

2-Chloro-1-methylpyridinium iodide (2-CMPI) was prepared as described previously [32]. For aminothiol derivatization prior to HPLC, a 0.01 *M* aqueous solution of 2-CMPI was used.

Standard thiol solutions

Stock standard solutions (0.01 *M*) of the aminothiol compounds were prepared in water or dilute HCl and assayed with HMB [33]. Working standard solutions were prepared daily by dilution with water containing 1 mmol/l of EDTA.

Buffers

Citrate and phosphate buffers of various ionic strength and pH were prepared with purified water. At each pH value, the electrode was calibrated with standard pH solutions. After controlling the pH, the buffers were filtered through a 0.2-μm filter under vacuum.

2.3. Sample derivatization

In a 10-ml calibrated flask were placed an aliquot of sample and 3 ml of 0.1 *M* phosphate derivatization buffer (pH 8.1), then 1 ml of working reagent solution was added. The flask was stoppered, mixed by inversion and put aside for 15 min. The mixture was then diluted to volume with water and a 20-μl aliquot was injected into the liquid chromatographic system. The derivatization procedure was applied to working standard solutions of aminothiols to obtain a calibration graph.

2.4. Assay procedure

An aliquot of the sample solution was subjected to the derivatization procedure and 20 μl of the final analytical solution were injected into the liquid chromatograph in triplicate. The peak areas were measured and the amount of each analyte of the sample was then calculated by interpolation on the calibration graph.

2.5. Chromatography

HPLC separation were carried out under isocratic conditions on a Spherisorb ODS-2 reversed-phase column operated at a flow-rate of 0.7 ml/min. For routine determination of five aminothiols (GSH, CSH, HSH, ACSH and MPG) in a single run, a mobile phase consisting of 0.175 *M* citrate buffer containing 10 mmol/l of sodium octanesulphonate (pH 2.8) and methanol (80:20, v/v) and a detector wavelength of 314 nm were found to be appropriate, allowing an adequate separation of the five S-pyridinium derivatives. With more complicated mixtures, *e.g.*, when 2-mercaptopropionic acid (PrSH, metabolite of MPG) was present, the mobile phase was modified by addition of 6% of acetonitrile at the expense of methanol. Excess reagent elutes last in the form of a small peak (low ε at the recommended analytical wavelength) and does not interfere with the chromatogram (see Fig. 9).

3. Results

3.1. Optimization of aminothiol derivatization

The proposed derivatization reaction, shown in Fig. 1, takes advantage of the high nucleophilicity of thiols; they react rapidly in aqueous solution with 2-chloro-1-methylpyridinium iodide (2-CMPI) to form stable thioethers (S-pyridinium derivatives). These derivatives exhib-

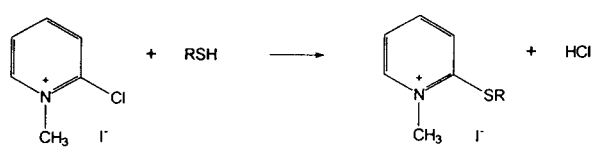

Fig. 1. Reaction of aminothiols (RSH) with 2-chloro-1-methylpyridinium iodide (2-CMPI).

it a well defined maximum at 314 nm in the UV spectrum as a consequence of the bathochromic shift from the reagent maximum (Fig. 2). Of the three functionalities of the amino acids potentially able to undergo nucleophilic attack at the 2-position of the pyridinium ring, in aqueous solution, unlike in anhydrous conditions [34], only the sulphydryl group reacts. This means that no multiple derivatives are formed, as was demonstrated previously [31].

Buffer type and pH

The yields of the aminothiol derivative formation in standard mixtures were studied using 0.1 *M* phosphate derivatization buffers with pH ranging from 7 to 10. Derivative yields for glutathione *versus* time and reaction pH are plotted in Fig. 3a and demonstrate that the recoveries reach a maximum after 5 min in the pH range 8.1–9.0, but at lower pH the reaction is slower. At higher pH (data not shown), the reagent tends to hydrolyse to 1-methyl-2-pyridone (MP) with an absorption maximum at 290 nm. For subsequent assays, 0.1 *M* phosphate derivatization buffer of pH 8.1 was used. Under these conditions, MP would not be expected to

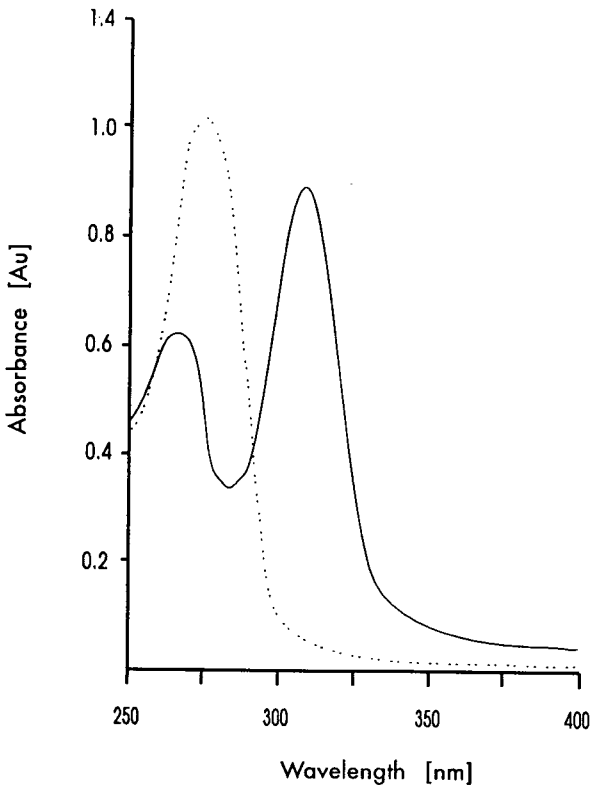

Fig. 2. Absorption spectra of 0.8 μmol of GSH (solid line) and a blank solution (dotted line) treated according to the proposed derivatization procedure. Cells with an optical path length of 1 cm were used.

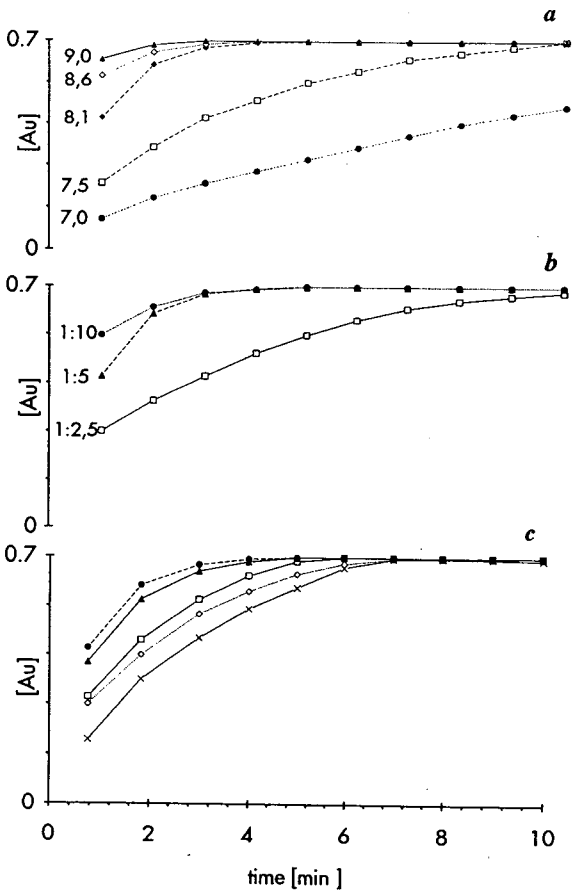

Fig. 3. Kinetics of aminothiol derivative formation in 0.1 *M* phosphate derivatization buffer performed by spectrophotometry; 0.8 μmol of each aminothiol, λ = 314 nm. (a) Effect of derivatization buffer pH and time on aminothiol derivative yields for glutatione. Molar ratio of the reagent to glutathione = 5. (b) Effect of reagent excess and time on aminothiol derivative yields for glutathione in 0.1 *M* phosphate derivatization buffer (pH 8.1). (c) Time course of the reaction of 2-CMPI with several aminothiols (pH 8.1). Fivefold reagent excess with respect to each aminothiol. × = ACSH; □ = CSH; ● = GSH; ◇ = HSH; ▲ = MPG.

interfere in the separation of the target thiols in the calibration range. However, with concentrations of thiols close to the detection limit, when the reagent excess is high, an MP peak appears on the chromatogram (see Fig. 9c).

Effect of the reagent excess and time of the reaction on aminothiol derivative yield

Fig. 3b shows that using a fivefold molar excess of the reagent with respect to glutathione afforded a maximum yield after 3 min, and increasing the excess of reagent beyond this level had no effect on the recoveries. With a 2.5-fold molar excess the derivative was obtained in 60% yield, and in 96% yield after 10 min. The reaction was found to slow with an increase in ionic strength of the reaction environment (0.0–2.0 mol/l range checked, NaCl added; data not shown). As can be seen in Fig. 3c, the rates of 2-CMPI derivative formation decrease in the order GSH > MPG > CSH > HSH > ACSH.

3.2. Derivative stability

Peak areas for the derivatized aminothiols (reaction mixture kept at ambient temperature or in a refrigerator at 4°C) were monitored for at least 10 days and no significant changes were observed. Hence the aminothiol derivatives have sufficient stability to allow for manual or automated chromatographic analysis.

3.3. Optimization of chromatographic conditions for separation of aminothiol derivatives

Highly ionic compounds, such as the present S-pyridinium derivatives of aminothiols could not be satisfactorily separated under standard reversed-phase conditions owing to their very short retention times. They elute close to the solvent front (Fig. 4a), which makes any separation or determination impossible. The only useful alternative was an ion-pair approach. In addition to pH, the effect of the organic modifier, the pairing ion concentration of the eluent and the lipophilicity (length of the alkyl chain) of the pairing ion on retention and resolution were studied.

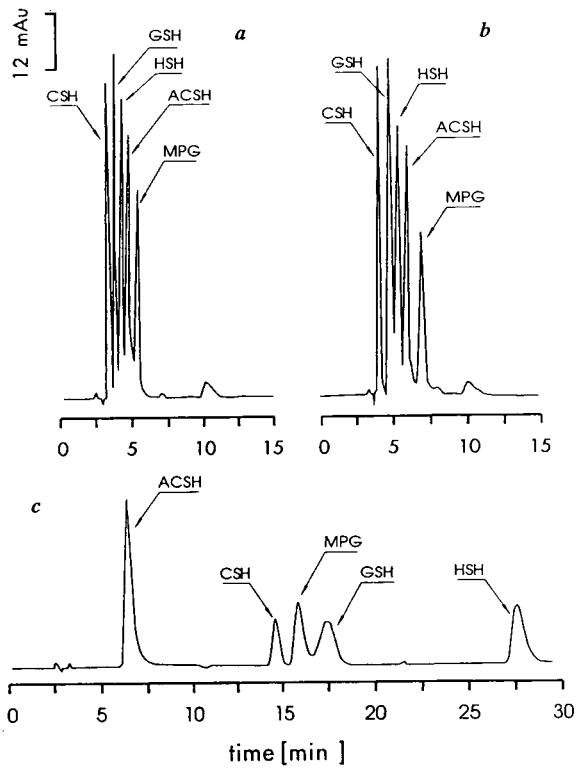

Fig. 4. Chromatograms of the derivatized aminothiol mixture obtained with 0.1 *M* citrate buffer (pH 2.8)–methanol (80:20, v/v) mobile phase containing (a) no ion-pair reagent, (b) 12 mmol/l of B-6 and (c) 10 mmol/l of B10.

Effect of buffer pH and ionic strength

The effect of pH was studied within the range 2.5–7.5, which was imposed by well known fact that outside this range a silica-based stationary phase (ODS-2) could be seriously damaged by aqueous buffer–mobile phase systems. We investigated the effect of the pH of the mobile phase containing 8 mmol/l of octanesulphonate on the capacity factors of all solutes concerned. As can be seen from Fig. 5, the capacity factors of all the solutes increase with decreasing pH in the range 2.5–3.0. In the pH range 3.0–7.5 the capacity factors of HSH and CSH increase and the other three (ACSH, MPG and GSH) elute very close to the void volume, having capacity

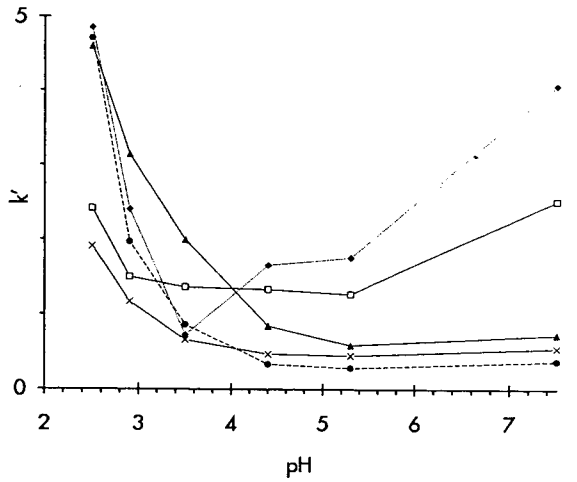

Fig. 5. Variation of the capacity factors of a mixture of aminothiol derivatives as a function of the eluent pH. Mobile phase: 0.1 *M* citrate buffer containing 8 mmol/l of B-8–methanol (80:20, v/v). Symbols as in Fig. 3 except ◆ = HSH.

factors smaller then 1. Therefore, we chose a mobile phase of pH 2.8 for routine HPLC target thiol determination, fulfilling the first criterion for good chromatographic separation, $1 < k' < 10$.

The effect of the ionic strength of the citrate buffer in the concentration range 0.05–2 *M* was also studied. An increase in the ionic strength of the buffer decreased the retention (data not shown), and the concentration of 0.175 *M* chosen constitutes a necessary compromise between maximum detectability and chromatographic resolution.

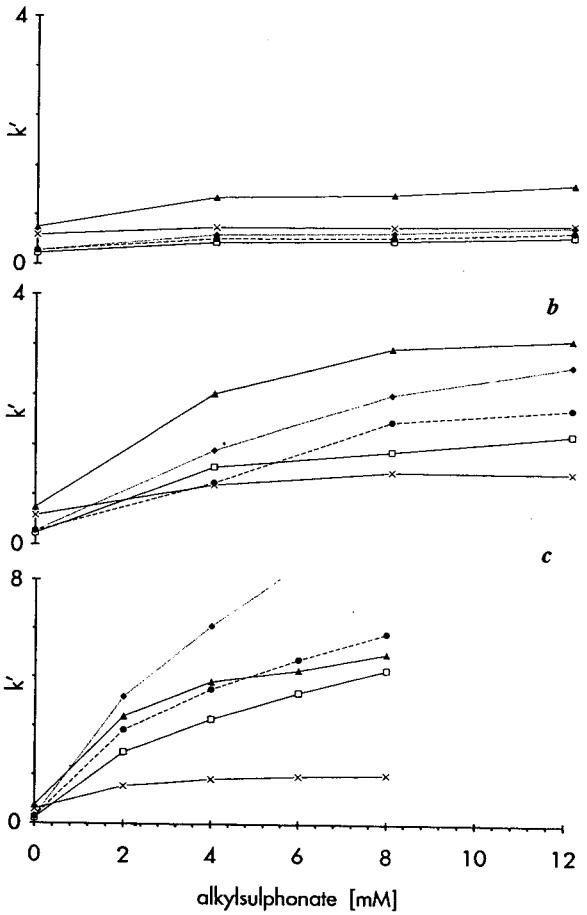

Fig. 6. Capacity factors (k') of aminothiol derivatives as a function of mobile phase sulphonate concentration: (a) hexanesulphonate; (b) octanesulphonate; (c) decanesulphonate. Mobile phase as in Fig. 4. Symbols as in Fig. 5.

Lipophilicity and concentration of ion-pair agent

The use of four alkanesulphonate pairing ions [1-butane- (B-4), 1-hexane- (B-6), 1-octane- (B-8) and 1-decanesulphonate (B-10)] of different lipophilicity was evaluated. The mobile phase concentration of the pairing ions was varied from 1 to 12 m*M*. In Fig. 6 the solute capacity factors are plotted against the mobile phase sulphonate concentration. In the case of sodium hexanesulphonate (B-6) only N-(2-mercaptopropionyl)-glycine (MPG) becomes more retained in the B-6 concentration range 4–12 m*M*, and the capacity factors of the four remaining analytes were virtually unchanged (Figs. 4b and 6a). A similar situation occurred when B-4 as an ion-pair agent was added (data not shown). Sodium octanesulphonate (B-8) enhanced the retention of all solutes and in the concentration range 8–12 m*M* (Figs. 6b and 7a) the capacity factors and resolutions guarantee a good chromatographic separation ($1 < k' < 10$, $R_s > 1.5$). When B-8 was replaced with B-10 a dramatic increase in retention was observed in all instances except ACSH and owing to the high k' values broad peaks were formed, worsening the quantification (Figs. 4c and 6c).

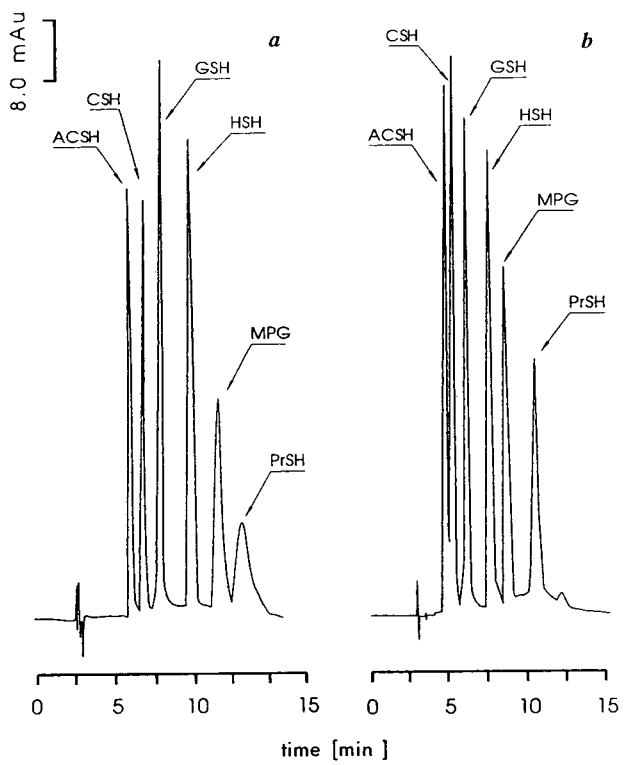

Fig. 7. Chromatograms obtained during the optimatization of the composition of the ternary mobile phase for the separation of six derivatized biological thiols. Mobile phase: (a) methanol–0.175 *M* citrate buffer containing 10 mmol/l of B-8 (20:80, v/v); (b) acetonitrile–0.175 *M* citrate buffer containing 10 mmol/l of B-8 (14:86, v/v).

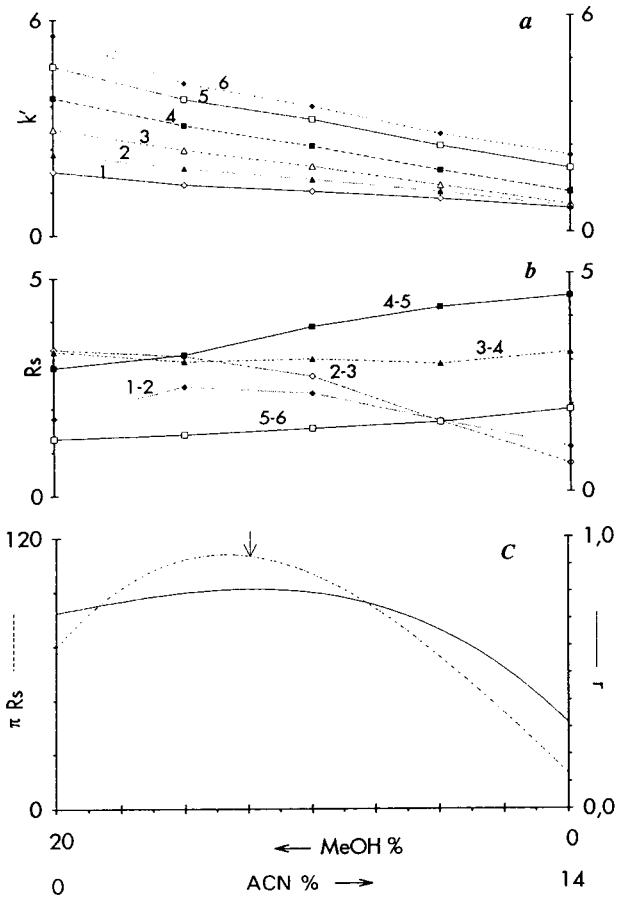

Fig. 8. Final phase selection diagrams for the ternary optimization problem of the separation of six biological thiols: (a) variations of capacity factors; (b) variations of resolutions; (c) response lines of resolution product (πR_s) and normalized resolution product (r). Composition of aqueous component of the mobile phase as in Fig. 7. 1 = ACSH; 2 = CSH; 3 = GSH; 4 = HSH; 5 = MPG; 6 = PrSH.

Effect of organic modifier

Organic modifiers such as acetonitrile, methanol, 2-propanol and tetrahydrofuran were added to the mobile phase in order to check their influence on the separation quality. Addition of 2-propanol and tetrahydrofuran caused tailing and broadening of the peaks of MPG and its metabolite PrSH, so these solvents were not considered further. As expected, an increase in acetonitrile content, at the expense of methanol, maintaining the same solvent strength, produced a linear decrease in all k' values. This is shown in Fig. 8a, where 100% methanol (far left) represents the mobile phase methanol–buffer (20:80, v/v) and 100% acetonitrile (far right) represents acetonitrile–buffer (14:86, v/v). Chromatograms corresponding to these two extreme mobile phase compositions obtained during the optimization procedure are shown in Fig. 7a and b. The best binary separation is achieved with 20% methanol (Fig. 7a), but still a better separation of the tailing peaks of MPG and PrSH would be desirable. The plots of R_s values for several pairs of peaks *versus* ternary solvent compositions are shown in Fig. 8b. These plots show that with an increasing content of acetonitrile in the mobile phase up to 50% of methanol does not cause

much change in resolution, and further increases in acetonitrile concentration lead to poorer resolution of less retained solutes (ACSH, CSH and GSH) and improved resolution of more retained solutes (HSH, MPG and PrSH).

For the prediction of the optimum ternary mobile phase composition, a phase selection diagram (Fig. 8c) was constructed from the chromatograms shown in Fig. 7 and three others, using the criteria r (normalized resolution product) and πR_s (resolution product). The r and πR_s values for the given chromatograms were calculated according to the following equations [35]:

$$r = \prod_{i=1}^{n-1} \left(\frac{R_{si,i+1}}{\bar{R}_s} \right)$$

$$\pi R_s = \exp\left(\sum \ln R_s \right)$$

$$R_s = \frac{k'_2 - k'_1}{k'_1 + k'_2 + 2} \cdot \frac{\sqrt{N}}{2}$$

where n is the number of peaks, k' the capacity factor, N the number of theoretical plates, R_s the resolution and $\bar{R}_s$ the average R_s value.

The point marked with an arrow in Fig. 8c corresponds to the final optimum composition. The chromatogram shown in Fig. 9a was run to verify the optimum composition. This chromatogram is the final result of the procedure, and it does indeed yield a satisfactory distribution of the peaks over the chromatogram.

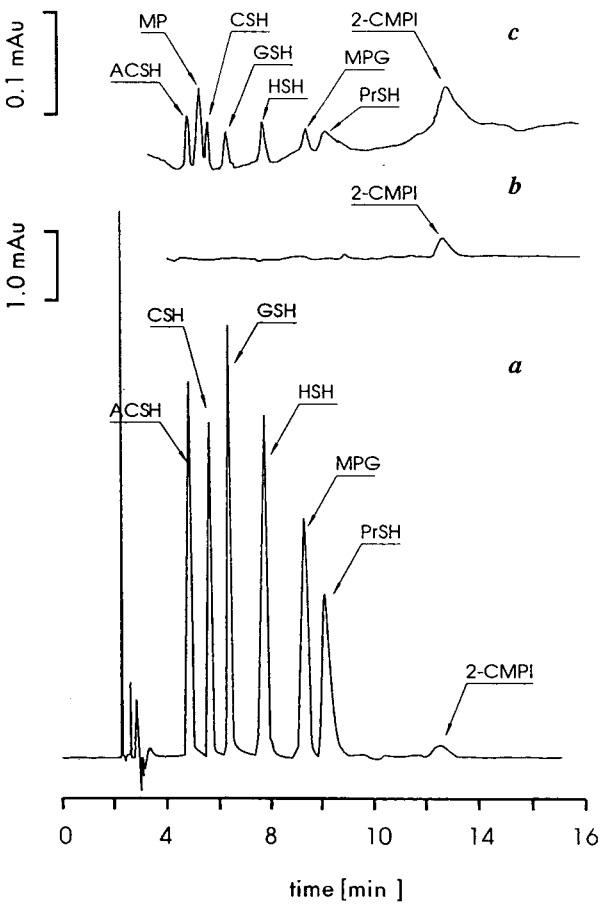

Fig. 9. Optimized chromatography for the derivatized biological thiol standard mixture: (a) 1 nmol for injection (2-CMPI to thiol ratio = 7:1); (b) blank; (c) 4 pmol for injection (2-CMPI to thiol ratio = 1750:1). Mobile phase: acetonitrile–metahnol–0.175 *M* citrate buffer containing 10 mmol/l of octanesulphonate (6:12:82, v/v/v). Detection wavelength: 314 nm.

3.4. Analytical parameters

A linear calibration graph was obtained over the range 1–50 μmol/l with relative standard deviations ≤9.2% at the 1 μmol/l and ≤0.86% at the 50 μmol/l thiol level. The correlation coefficients for response linearity were ≥0.99885. The detection limits ranged from 0.75 pmol for ACSH to 2.1 pmol for PrSH. Detailed data are given in Table 1.

4. Discussion

A six-component mixture of biologically important thiols was taken as an example to demonstrate the usefulness of the method. All the solutes are considered to be of interest and must be separated from each other. The method introduces a new reagent for derivatization of biological thiols for HPLC with superior properties to those of some currently employed reagents, and permits the separation and determination of the six compounds at the pmol level in a single isocratic HPLC run.

Table 1
Analytical parameters

Thiol[a]	Correlation coefficient[b]	Relative standard deviation (%)[c]	Detection limit (pmol)[d]
ACSH	0.99930	2.71; 0.86	0.75
CSH	0.99951	1.28; 0.75	0.94
GSH	0.99997	1.04; 0.79	0.88
HSH	0.99974	1.56; 0.72	0.79
MPG	0.99885	1.15; 0.70	1.5
PrSH	0.99979	9.21; 0.57	2.1

Detection wavelength, 314 nm.
[a] Samples of standard thiol mixtures were in the concentration range 1–50 μmol/l.
[b] $n = 6$.
[c] For bottom and top of the calibration range; $n = 5$.
[d] As calculated from a 4-pmol injection (Fig. 9c) of final analytical solution and based on a signal-to-noise ratio of 3.

The reagent possesses several advantages: high selectivity as it reacts only with thiol group and no multiple derivatives are formed with sulphur amino acids; high reactivity even in the presence of dissolved salts; compatibility with aqueous samples; lack of interference with the chromatogram due to a bathochromic shift of the absorption maximum in the UV spectrum from 275 nm (reagent) to 314 nm (derivative), ensuring a resolution of better than 1.5 for all peaks of interest; low rate of hydrolysis under the recommended conditions; the absorption maximum of the derivatives (analytical wavelength of the detector) falls in the region (314 nm) where common impurities of solvents are UV transparent; and a simple derivatization procedure and high stability of derivatives, allowing automation. Quantitative conversion to S-pyridinium adducts simply requires the addition of the reagent to a buffered sample followed by a few minutes of waiting.

The disadvantage of this method, compared with direct liquid chromatographic approaches with the use of electrochemical detection, is its inability to determine disulphide metabolites, unless they are converted into the corresponding thiols using a reductant such as tri-*n*-butylphosphine and subsequent derivatization of the sulphydryl to form an ultraviolet chromophore in a parallel run.

With regard to sensitivity, owing to the relatively high molar absorptivity of S-pyridinium derivatives ($\varepsilon = 1 \cdot 10^4$ l mol^{-1} cm^{-1}) the method can compete with HPLC methods using fluorescence detection generally considered as one order of magnitude more sensitive than those with UV detection. The detection limits with the recommended method are almost the same as those with bimane (*ca.* 1 pmol) [12] or ammonium-7-fluorobenzo-2-oxa-1,3-diazole-4-sulphonate (0.1–1.4 pmol) [14], lower than those with dansylaziridine (*ca.* 15 pmol) [16] or ethacrynic acid (30 pmol) [9] and higher than those with an oxazole-based reagent (*ca.* 1 fmol) [24].

Such a powerful derivatization reagent for biological thiols as 2-chloro-1-methylpyridinium iodide is likely to find numerous applications in analytical chemistry and biochemistry. In this work the usefulness of the reagent was tested for the separation and determination of compounds in standard solutions, but experiments on the analysis of biological samples are near the completion and will be presented elsewhere.

Acknowledgements

The authors thank Professor Mieczsław Wroński for the donation of aminothiol samples and valuable discussions. This work was partly supported by Grant No. 505/384 and 505/467 from the University of Łódź.

References

[1] A.N. Glazer and E.L. Smith, in P.D. Boyer (Editor), *The Enzymes*, Vol. 3, Academic Press, New York, 3rd ed., 1971, p. 502.

[2] S.S. Tate, in W.B. Jacoby (Editor), *Enzymatic Basis of Detoxification*, Vol. 2, Academic Press, New York, 1980, p. 95.

[3] W.B. Jakoby, J.L. Stevens, M.W. Duffel and R.A. Weisiger, *Rev. Biochem. Toxicol.*, 6 (1984) 97.

[4] L. Flohé, *Ciba Found. Symp.*, 65 (1979) 95.

[5] A. Meister and M.E. Anderson, *Annu. Rev. Biochem.*, 52 (1983) 711.

[6] A. Russo and E.A. Bump, *Methods Biochem. Anal.* 33 (1988) 185.

[7] K. Imai, T. Toyo'oka and H. Miyano, *Analyst*, 109 (1984) 1365.

[8] D.J. Red, J.R. Babson, P.W. Beatty, A.E. Brodie, W.W. Ellis and D.W. Potter, *Anal. Biochem.*, 106 (1980) 55.

[9] V. Cavrini, R. Gatti, A.M. DiPietra and M.A. Raggi, *Chromatographia*, 23 (1987) 680.

[10] E.M. Kosower, B. Pazhenchevsky and E. Hershkowitz, *J. Am. Chem. Soc.*, 100 (1978) 6516.

[11] N.K. Burton and G.W. Aherne, *J. Chromatogr.*, 382 (1968) 253.

[12] R.C. Fahey, G.L. Newton, R. Dorian and E.M. Kosower, *Anal. Biochem.*, 111 (1981) 357.

[13] M. Roth, *Anal. Chem.*, 42 (1971) 880.

[14] T. Toyo'oka and K. Imai, *J. Chromatogr.*, 282 (1983) 495.

[15] T. Toyo'oka, H. Miyano and K. Imai, *104th Annual Meeting of the Pharmaceutical Society of Japan, Sendai, March, 1984, Abstracts*, p. 558.

[16] E.P. Lankmayr, K.W. Bunda, K. Muller and F. Nachtman, *Fresenius' Z. Anal. Chem.*, 295 (1979) 371.

[17] Y. Kanaoka, *Yakugaku Zasshi*, 100 (1980) 973.

[18] A.J. Alpert and H.F. Gilbert, *Anal. Biochem.*, 144 (1985) 553.

[19] J.F. Studebaker, S.A. Slocum and E.L. Lewis, *Anal. Chem.*, 50 (1978) 1500.

[20] J. Nishiyama and T. Kuninori, *Anal. Biochem.*, 138 (1984) 95.

[21] K. Iriyama, T. Ivamoto and M. Yoshiura, *J. Liq. Chromatogr.*, 9 (1986) 995.

[22] E.G. DeMaster and B. Redfern, *Methods Enzymol.*, (1987) 110.

[23] G.L. Newton, J.A. Aquilera, R.C. Fahey, J.F. Ward, A.E. Radkowsky and E.M. Kosower, *Anal. Biochem.*, 201 (1992) 30.

[24] T. Toyo'oka, H.P. Chokshi, R.G. Carlson, R.S. Givens and S.M. Lunte, *Analyst*, 118 (1993) 257.

[25] S. Ito, A. Ota, K. Yamamoto and Y. Kawashima, *J. Chromatogr.*, 626 (1992) 187.

[26] Y. Imai, S. Ito and K. Fujita, *J. Chromatogr.*, 420 (1987) 404.

[27] T. Kuninori and J. Nishiyama, *Anal. Biochem.*, 197 (1991) 19.

[28] L.A. Smolin and J.A. Schneider, *Anal. Biochem.*, 168 (1988) 374.

[29] D. Shea and W.A. MacCrehan, *Anal. Chem.*, 60 (1988) 1449.

[30] J.D.H. Cooper and D.C. Turnell, *J. Chromatogr.*, 227 (1982) 158.

[31] W. Ciesielski and E. Bald, *Chem. Anal. (Warsaw)*, 36 (1991) 607.

[32] E. Bald, *Talanta*, 27 (1980) 281.

[33] M. Wroński, *Talanta*, 24 (1977) 347.

[34] E. Bald, K. Saigo and T. Mukaiyama, *Chem. Lett.*, (1975) 1163.

[35] P.J. Schoenmakers, *Optimisation of Chromatographic Selectivity*, Elsevier, Amsterdam, 1986, Ch. 4.

ELSEVIER

Journal of Chromatography A, 676 (1994) 331–335

JOURNAL OF CHROMATOGRAPHY A

Rapid, automated, two-dimensional high-performance liquid chromatographic analysis of immunoglobulin G and its multimers

Timothy K. Nadler, Sandeep K. Paliwal, Fred E. Regnier*

Chemistry Department, Purdue University, West Lafayette, IN 47907, USA

First received 25 October 1993; revised manuscript received 11 March 1994

Abstract

It is important to determine the amount of IgG multimers in immunoglobulin-containing pharmaceuticals because these aggregates can cause adverse reactions in patients. Previous methods for determining aggregates either suffered from interference of other proteins or required fraction collection and sample purification. A new, automated two-dimensional approach has been developed in which size-exclusion chromatography is performed in the first dimension followed by protein A affinity chromatography in the second dimension. This method is robust in that the aggregates are not disturbed by a preliminary purification step. Further, the presence of contaminating proteins has no effect on the analysis since affinity chromatography is used to determine the presence of IgG in the second dimension. The entire automated two-dimensional analysis can be performed in *ca.* 1 h.

1. Introduction

Intravenous immunoglobulin G (IgG) has been used for clinical purposes such as hypo and agammaglobulinaemia, antibiotic therapy and thrombocytopenia [1–4]. However, dimers and aggregates of IgG have harmful side effects which include anaphylaxis and dyspnea [5]. The cause of these side effects is thought to be due to the activation of the complement reaction as postulated by Barandum *et al.* [6]. Others have also mentioned the possibility of harmful side effects due to aggregates [7]. IgG dimers and aggregates are often formed during pasteurization of the pharmaceutical. Pasteurization is often a necessary step, and therefore, it is important to monitor levels of IgG aggregates in pharmaceuticals which contain immunoglobulin.

A number of methods for the quantitation of IgG dimers have already been published [8–10]. However, these techniques suffer from either interference of albumin aggregates [7] and/or the necessity of collecting fractions for rechromatography. The more recent paper [10] uses a two-stage HPLC separation in which IgG is first separated from the albumin by ion-exchange chromatography and then analyzed for dimers and aggregates by size-exclusion chromatography (SEC). The disadvantage of this approach is that there can be some dissociation of the IgG aggregates during the ion-exchange step. Thus, the results may not reflect the solution concentration of the aggregates. Light scattering may also be

* Corresponding author.

0021-9673/94/$07.00
SSDI 0021-9673(94)00304-R

used for monitoring IgG aggregation but requires pure IgG samples [11–13].

A new two-dimensional chromatographic analysis is presented which is totally automated and robust. The sample is analyzed by SEC in the first dimension in order to determine molecular size. Fractions from the SEC column are then automatically transferred to the protein A column for determination of IgG. Since protein A affinity chromatography is used in the second dimension, albumin and other contaminating proteins can not interfere with the IgG determination. A sample containing induced IgG dimers was used as a model system to test the method's capability to resolve the aggregate IgG from the monomeric IgG. The system was also challenged with high-molecular-mass serum proteins to show that these non-IgG proteins would not interfere with the aggregate determination.

2. Experimental

2.1. SEC

SEC separations were achieved on a 300 × 8 mm column packed with TSK G3000 SW packing material (TosoHaas, Montgomeryville, PA, USA) on a Shandon column packer (Shandon Southern Instruments, Sewickley, PA, USA) at 2000 p.s.i. (1 p.s.i. = 6894.76 Pa). The mobile phase for SEC was 100 m*M* potassium phosphate with 100 m*M* sodium sulfate both from Mallinckrodt (Paris, KY, USA), pH 7.0.

2.2. Protein A affinity chromatography

The immobilized protein A column, POROS A/M (30 × 4.6 mm) (PerSeptive Biosystems, Cambridge, MA, USA), was packed on a Shandon column packer at 2000 p.s.i. The loading buffer was the same as the SEC buffer and the desorption buffer was 0.3 *M* magnesium chloride (Mallinckrodt) with 2% acetic acid (J.T. Baker, Phillipsburg, NJ, USA).

2.3. Apparatus

A BioCAD perfusion chromatography workstation (PerSeptive Biosystems) was configured for tandem columns with the SEC column as the first column and the protein A column as the second (see Fig. 1).

2.4. IgG dimer induction

To induce dimer formation, 100 μl of 1 mg/ml rabbit anti-(bovine IgG) was incubated with 500 μl bovine IgG 1 mg/ml, both proteins from Sigma (St. Louis, MO, USA). Incubation was at room temperature in 20 m*M* potassium phosphate pH 7.0 for 1 h before use. Excess bovine IgG was used to produce what is expected to be mostly bovine–rabbit heterodimers of IgG with excess bovine IgG monomer remaining (see Fig. 2).

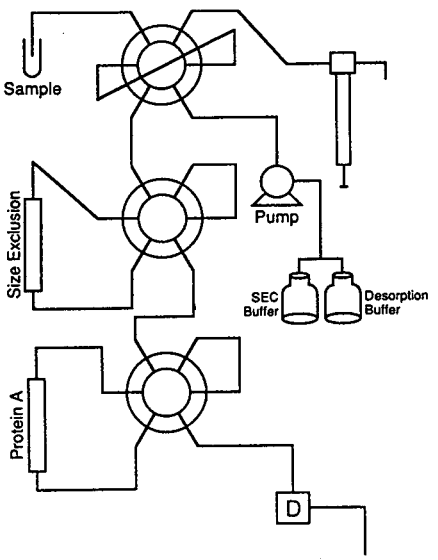

Fig. 1. Column configuration for the two-dimensional separation of IgG monomers and multimers. The SEC column is followed by the protein A column. Switching valves allow either column to be in-line with the mobile phase flow by itself, both columns to be in-line, or both columns to be off-line. Switching both columns off-line allows high-speed pumping of a new mobile phase in order to automate system flushing.

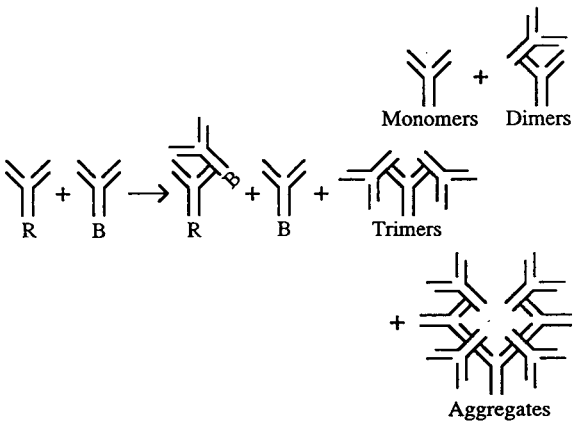

Fig. 2. Antibody reaction in which an excess of bovine IgG, B, is incubated with rabbit anti-(bovine IgG), R, to produce IgG multimers and left over bovine IgG monomers.

2.5. Reconstructed chromatograms

Reconstructed chromatograms were produced by plotting protein A peak areas against fraction volume from the SEC column. In the case of the serum sample, a non-retained peak area accounted for non-IgG protein. It was summed with the area of the retained IgG peak to produce a plot of total protein, and the areas of the IgG peaks were also plotted to produce the IgG reconstructed chromatogram. For the IgG dimers, there was no non-retained peak.

3. Results

3.1. SEC of IgG and induced dimers

Bovine IgG and the rabbit anti-(bovine IgG) were analyzed by SEC. Both eluted with the same retention volume (Table 1) and were judged to be monomeric as determined by the SEC calibration curve (data not shown). However, the induced dimers produced two peaks on the SEC chromatogram indicating that aggregation had indeed occurred and also that some monomers remained (Table 1).

Table 1
Retention times for bovine IgG (B), rabbit anti-(bovine IgG) (R) and multimers on the size-exclusion and protein A columns

Species	SEC retention volume (ml)	Protein A retention time (min)
Bovine IgG	4.5	1.35
Rabbit IgG	4.5	1.46
Aggregate IgG	3.6 and 4.5	1.35 and 1.46

3.2. Protein A chromatography of IgG and induced dimers

Monomeric bovine IgG and rabbit anti-(bovine IgG) were analyzed on the protein A column. Rabbit IgG was found to have a higher affinity for protein A than bovine IgG, eluting later in the desorption gradient (see Table 1).

3.3. Two-dimensional analysis of induced dimers

The BioCAD was configured in the tandem column configuration with the SEC column followed by the protein A column. After injection of the sample, 3 ml of buffer were passed through the SEC column (slightly less than the void volume). Then, a 200-μl fraction was transferred from the SEC column to the protein A column by switching valves. The SEC column was switched off-line and the protein A column eluted with the desorption buffer. Bovine IgG eluted first, followed by rabbit IgG. The protein A column was re-equilibrated with SEC buffer and the SEC column was placed back in line so that another 200-μl fraction could be passed onto the protein A column. Peak areas for the total IgG, rabbit IgG and bovine IgG were calculated and plotted (Fig. 3). The profile of the reconstructed chromatogram for total IgG matched closely with the SEC chromatogram for the dimer mixture as expected. Most of the rabbit IgG eluted as a multimer, because it was the limiting reagent. The bovine IgG was present

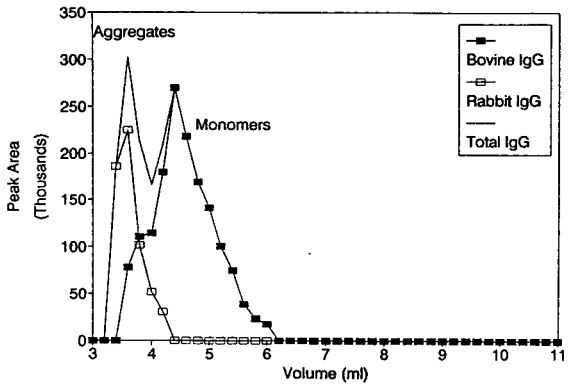

Fig. 3. Reconstructed SEC chromatogram for total IgG, rabbit IgG and bovine IgG.

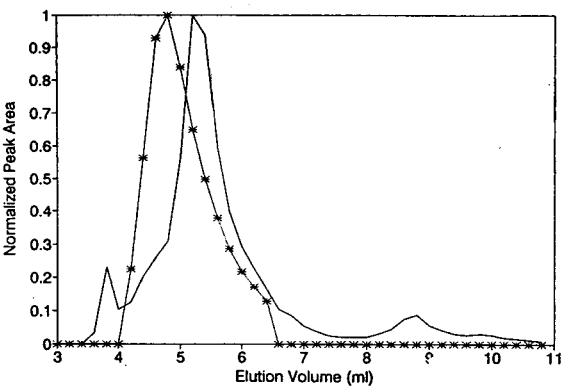

Fig. 4. Reconstructed SEC chromatogram of bovine serum in which total protein is plotted as a solid line and IgG is plotted as a dotted line. From previous work, it is known that the major peak is bovine serum albumin.

partly as an aggregate but was mostly monomeric. Although the dimers were not separated from the other aggregate forms, this separation could be made if the appropriate SEC column were used. The SEC column used in these experiments was chosen for its stability. In order to resolve larger proteins, the pore size of the SEC packing must be larger. Large pores reduce the mechanical strength of the beads which will in turn reduce the life time of the SEC column. Since all forms of IgG aggregates are undesirable, there was no reason to separate them further, especially since doing so would reduce the SEC column life.

3.4. Two-dimensional analysis of serum

To show that the presence of other proteins would not interfere with the dimer determination, the two-dimensional analysis was also applied to a serum sample that contained a number of contaminating proteins, the predominant of which is serum albumin. A reconstructed chromatogram (Fig. 4) of total peak area produces a profile comparable to the SEC chromatogram of serum (data not shown). Plotting area of the IgG peak from the protein A separation yields a peak at $M_r \approx 150\,000$, as expected. No IgG dimers were detected in this serum sample demonstrating that other non-IgG high-molecular-mass proteins would not yield a false positive result for IgG dimers.

4. Discussion

The ratio of rabbit IgG to bovine IgG in the dimer reconstructed SEC chromatogram (Fig. 3) appears to be much greater than one to one in the multimer peak. There are several reasons why one can not determine IgG ratios in this way. First, there is steric hinderance at the bovine IgG Fc region where both the rabbit IgG and protein A can bind. Since rabbit IgG is already bound to the Fc region and the binding is essentially irreversible, the protein A will only bind the Fc region of the rabbit IgG and not the bovine IgG. Second, when the IgG is desorbed from the protein A, the UV absorbance for the rabbit and bovine IgG is summed, because the multimer has not been disrupted. This will result in an overestimation of the rabbit IgG, however it will be an accurate reflection of the total multimer concentration in terms of the aggregates-to-monomer ratio. The primary purpose of plotting both rabbit and bovine IgG is to indicate that all of the rabbit IgG is in the form of multimers while some bovine IgG remains in the monomer form as predicted from the incubation of excess bovine IgG.

It is also important to note that if dimerization occurs through the Fc region, protein A or G may not be appropriate. A more general affinity technique should be applied. Polyclonal antibodies to the specific IgG can be immobilized

and used instead of a protein A or G. The polyclonal antibody to IgG will recognize multiple portions of the molecule whereas protein A and G have a somewhat "monoclonal" interaction with IgG in that they only recognize the Fc region of the IgG molecule.

Detection limits for protein A affinity chromatography have already been determined by previous authors [14,15]. They have found limits on the order of 50 ng. This means that this assay should be able to detect less than 1% aggregate in a 100-μg IgG sample.

5. Conclusions

A robust two-dimensional HPLC determination of IgG and its aggregates has been presented. It is possible to avoid IgG dimer disruption by performing size exclusion in the first dimension followed by protein A affinity chromatography in the second dimension. The analysis may be automated on a single HPLC system and performed in *ca.* 1 h. Further, purity and concentration of IgG may also be determined in the same analysis. It is probably better to use a smaller pore size SEC packing as long as the separation of dimers from aggregates is not important.

Acknowledgements

The authors would like to thank Gretchen Leuck for technical support and valuable discussions. This research was supported by NIH Grant 25431.

References

[1] Y. Mashuho, K. Tomibe, K. Matsuzawa and A. Ohtsu, *Vox Sang.*, 32 (1977) 175.
[2] Y. Mashuho, K. Tomibe, T. Watanabe and Y. Fukumoto, *Vox Sang.*, 32 (1977) 290.
[3] T. Doi, T. Nakajima, M. Nishida and T. Suyama, *Chem. Pharm. Bull.*, 26 (1976) 3492.
[4] M. Kata, K. Kadota and T. Okuda, *Jpn. J. Antibiot.*, 38 (1985) 2688.
[5] IUIS/WHO Notice, *Clin. Exp. Immunol.*, 52 (1983) 417.
[6] S. Barandun, P. Kistler, F. Jeunet and H. Isliker, *Vox Sang.*, 7 (1962) 157.
[7] H. Suomela, H.-J. Himberg and T. Kuronen, *J. Chromatogr.*, 297 (1984) 369.
[8] D.T.S. Law and R.H. Painter, *Mol. Immunol.*, 23 (1986) 331.
[9] J. Andrade and S. Mankarious, presented at the *5th International Symposium on HPLC of Proteins, Peptides and Polynucleotides, Toronto, November 4–6, 1985*, paper No. 1027.
[10] J.K. Lee, F.J. Deluccia, E.L. Kelly, C. Davidson and F.R. Borger, *J. Chromatogr.*, 444 (1988) 141.
[11] B.P. Singh, H.B. Bohidar and S. Chopra, *Biopolymers*, 31 (1991) 1387.
[12] G. Sittampalam and G.S. Wilson, *Anal. Chem.*, 56 (1984) 2170.
[13] G. Sittampalam and G.S. Wilson, *Anal. Chem.*, 56 (1984) 2176.
[14] L. Janis and F.E. Regnier, *Anal. Chem.*, 61 (1989) 1901.
[15] A. Riggin, J.R. Sportsman and F.E. Regnier, *J. Chromatogr.*, 632 (1993) 37.

ELSEVIER

Journal of Chromatography A, 676 (1994) 337–345

JOURNAL OF CHROMATOGRAPHY A

One-step affinity purification of bacterially produced proteins by means of the "Strep tag" and immobilized recombinant core streptavidin

Thomas G.M. Schmidt, Arne Skerra*

Abteilung Molekulare Membranbiologie, Max-Planck-Institut für Biophysik, Heinrich-Hoffmann-Strasse 7, D-60528 Frankfurt am Main, Germany

First received 15 February 1994; revised manuscript received 19 April 1994

Abstract

The "Strep tag" is a nine amino acid peptide with intrinsic streptavidin-binding activity. If this sequence is genetically fused to the C-terminus of a polypeptide the recombinant protein can be directly purified by affinity chromatography from the host cell extract on immobilized streptavidin. However, variations were observed in the suitability of different commercial streptavidin–agarose preparations for this purpose. Therefore, the influence of the source of streptavidin, the coupling chemistry, and the nature of the affinity chromatography resin was investigated. A procedure was developed for the production of recombinant core streptavidin in *Escherichia coli*, followed by its efficient refolding and purification with an overall yield of up to 140 mg functional protein per 1 l bacterial culture. When coupled to activated CH-Sepharose 4B this truncated form of streptavidin showed a performance in the affinity chromatography of Strep tag fusion proteins that was superior to all other combinations tested. In contrast to its conventional preparation from *Streptomyces* strains the recombinant core streptavidin was produced without a proteolytic processing step. Thus, deleterious effects during the streptavidin affinity purification of proteins due to residual proteolytic activity in the immobilized streptavidin were avoided. The versatility of the optimized purification system was demonstrated with five different Strep tag fusion proteins.

1. Introduction

The development of generic purification techniques for recombinant proteins has gained recent interest, particularly because the biochemical characteristics of a gene product are often unknown. In this respect, the use of a short peptide tag with defined affinity properties has the advantage that it does not necessarily interfere with the function of the protein and, therefore, its removal is not needed for in vitro applications [1].

Recently, we described the engineering of a C-terminal peptide tag with intrinsic streptavidin-binding activity, which was termed "Strep tag" [2]. This affinity peptide was shown to be suitable for the efficient single-step purification of a bacterially produced, functional antibody F_v fragment on immobilized streptavidin using mild competitive elution with biotin or its analogues. Furthermore, the Strep tag was employed for the direct and specific detection of the

* Corresponding author.

0021-9673/94/$07.00
SSDI 0021-9673(94)00387-O

protein —on a Western blot or in an enzyme-linked immunosorbent assay (ELISA)— using a commercially available streptavidin–enzyme conjugate.

However, during routine use of this protein purification system significant variations in the ability to bind the Strep tag were observed between different preparations of streptavidin–agarose, even among charges from the same manufacturer. Generally, the biochemical activity of streptavidin is defined and quantified according to its capacity for the binding of biotin, which is not necessarily a valid criterion for the binding of the Strep tag. Therefore, a streptavidin affinity matrix had to be developed with optimized properties for this novel application. The parameters that had to be considered were the composition of the solid support, the coupling chemistry for the immobilization of streptavidin, and, most importantly, the preparation of streptavidin itself.

Commercially produced streptavidin consists of a N- and C-terminally shortened form, called core streptavidin [3], comprising the sequence from Ala^{13} or Glu^{14} to Ala^{138} or Ser^{139} of the mature polypeptide. Core streptavidin is produced via an undisclosed proteolytic digestion protocol from the protein that is naturally secreted by *Streptomyces* strains. In contrast to the full length form, it shows high solubility, reduced tendency towards oligomerization and is extremely resistant to further degradation. In addition, Bayer et al. [4] demonstrated that its binding activity for biotinylated proteins —e.g. alkaline phosphatase— is significantly enhanced, probably due to improved accessibility of the ligand-binding pocket.

Remarkably, an affinity matrix produced with commercial core streptavidin led to degradation during purification of a Strep tag fusion protein, most likely as a result of residual proteolytic activity that was still present in the streptavidin preparation. Therefore, the production of recombinant core streptavidin using *Escherichia coli* as expression host was established together with a simple refolding and purification procedure yielding highly pure and active protein. With this material we developed a standardized purification protocol for Strep tag fusion proteins and present here its application in several examples.

2. Experimental

2.1. Materials

Streptomyces avidinii (ATCC 27419) was obtained from the American Type Culture Collection. *E. coli* strain BL21(DE3) carrying a chromosomal copy of the T7 RNA polymerase gene [5] was provided by H. Reiländer (Max-Planck-Institut für Biophysik, Frankfurt/Main, Germany). *E. coli* K12 strain JM83 (*ara*, Δ(*lac-pro*AB), *rps*L, *Φ*80, *lac*ZΔM15) [6], which was used for the expression of Strep tag fusion proteins, was from our own collection. N-Hydroxysuccinimide (NHS)-activated CH-Sepharose 4B, epoxy-activated Sepharose 6B, as well as Q-Sepharose were purchased from Pharmacia (Uppsala, Sweden), Eupergit C and Eupergit C30N were from Röhm Pharma (Weiterstadt, Germany). The plasmid pLysE for constitutive expression of T7 lysozyme, a natural inhibitor of T7 RNA polymerase [5], was from AMS Biotechnology (Lugano, Switzerland). Commercial streptavidin preparations were samples from Società Prodotti Antibiotici (Milan, Italy) and Amresco (Solon, OH, USA).

2.2. Protein characterization

Sodium dodecyl sulfate–polyacrylamide gel electrophoresis (SDS-PAGE) was performed using standard slab gel methodology with the buffer system of Fling and Gregerson [7], followed by staining with Coomassie Brilliant Blue R 250. The samples were heated to 95°C for 5 min prior to loading onto the gel.

The molar extinction coefficient of recombinant core streptavidin, ϵ_{280}, was determined as 35600 M^{-1} cm^{-1} from measurements of A_{205} and A_{280} according to Scopes [8] with a Perkin-Elmer Lambda 15 UV–Vis spectrophotometer. The measurements were performed in 10 m*M* potassium phosphate pH 7.6 at 20°C and the

peptide bond absorbance at 205 nm was corrected for the tryptophan and tyrosine content. The value agreed almost with that published for proteolytically prepared core streptavidin [9].

The biotin-binding capacity of the recombinant core streptavidin was determined by measuring the ligand-induced quenching of the protein tryptophan fluorescence [10,11]. A 1 μM protein solution (1.8 ml) in 50 mM Tris · HCl pH 8.0 was placed in a quartz cuvette thermostatted at 22°C and a total of 130 μl 20 μM biotin in the same buffer was added in increments of 5 μl. After thorough mixing the tryptophan fluorescence (excited at 295 nm and detected at 350 nm, averaged over 1 s) was measured at each step with a Perkin-Elmer LS50 fluorimeter. All solutions were initially cleared from particles by sterile filtration.

2.3. Preparation and comparison of streptavidin affinity matrices

NHS-Activated CH-Sepharose 4B, epoxy-activated Sepharose 6B, Eupergit C and Eupergit C30N were coupled with 2 mg streptavidin per 1 ml swollen material under conditions as recommended by the suppliers. The binding of a Strep tag fusion protein was then investigated by means of a batch assay. A 15-μl volume of each affinity matrix was dispersed in 50 μl of periplasmic bacterial cell extract containing the D1.3 F_v fragment with the Strep tag fused to the V_H domain [2]. After centrifugation and removal of the supernatant, the material was washed three times with 50 μl 50 mM Tris · HCl pH 8.0 and then incubated with 50 μl of the same buffer containing 1 mM biotin for release of the bound F_v fragment. Finally, the resin was suspended in gel loading buffer and heated for the recovery of residual adsorbed protein. The supernatant from each step was analyzed by SDS-PAGE.

The matrix which was utilized for affinity purification was prepared as follows. NHS-Activated CH-Sepharose 4B was swollen and washed as recommended by the manufacturer. The supernatant was drained and the gel was mixed with twice its volume of a 2.5 mg/ml solution of streptavidin (for the immobilization of 5 mg streptavidin per ml gel) that had been dialyzed against 100 mM sodium carbonate pH 8.0, 500 mM NaCl. After 2 h of gentle shaking at room temperature coupling was complete. The supernatant was decanted and the gel was mixed with 5 volumes of 100 mM Tris · HCl pH 8.0 for the blocking of residual activated groups (overnight at 4°C).

2.4. Preparation of streptavidin from Streptomyces avidinii

Natural streptavidin was isolated from *S. avidinii* as described by Cazin et al. [12] and Suter et al. [13]. After ammonium sulfate precipitation of the protein from the culture supernatant and dissolution of the precipitate in water the sample was further purified via ion-exchange chromatography on Q-Sepharose in 50 mM sodium borate pH 8.5. Essentially pure streptavidin was eluted with 100 mM sodium phosphate pH 7.0.

2.5. Construction of the expression vector pSA1 for the production of recombinant core streptavidin in E. coli

The structural gene encoding core streptavidin was amplified by polymerase chain reaction (PCR) from chromosomal DNA of *S. avidinii* ATCC 27419 using *Pfu* DNA polymerase (Stratagene, Heidelberg, Germany) and the oligodeoxynucleotides 5′-GAT ATA *CAT ATG* GAA GCA GGT ATC ACC GGC ACC TGG TAC and 5′-CGG ATC *AAG CTT* ATT AGG AGG CGG CGG ACG GCT TCA C with phosphorothioate bonds at their 3′ termini according to Skerra [14]. The italicized *Nde*I and *Hin*dIII restriction sites were used for direct insertion of the gene fragment into the appropriately cut T7 expression vector pRSET5a [15] following standard methodology [16]. The resulting plasmid pSA1 is depicted in Fig. 1 together with the amino acid sequence of the gene product. The three codons following the start methionine codon —which was positioned in front of the core streptavidin sequence— were modified at their wobble positions for optimal

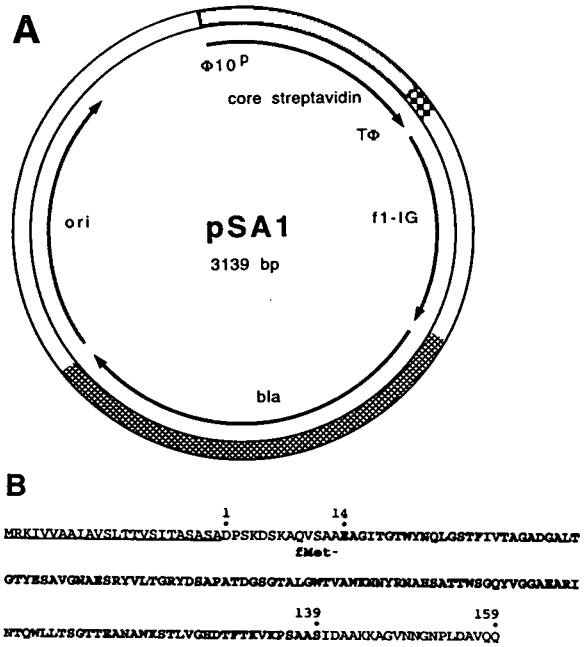

Fig. 1. (A) The expression plasmid pSA1. The structural gene encoding core streptavidin was placed under transcriptional control of the gene 10 promoter of the bacteriophage T7 and ends upstream of the TΦ terminator [5]. Additional vector elements comprise the origin of replication (ori), the ampicillin resistance gene (bla), and the f1 origin of replication for the preparation of single-stranded plasmid DNA (f1-IG) [15]. (B) Amino acid sequence of pre-streptavidin. The signal sequence, which directs secretion of streptavidin in the original host, *S. avidinii*, is underlined [18]. Numbering of the mature sequence starts at 1. The sequence of core streptavidin encoded on pSA1 begins with Glu^{14} and ends with Ser^{139} and is printed in bold. It has an N-terminal fMet residue added as indicated.

initiation of translation [17]. Otherwise the cloned nucleotide sequence was identical to that published by Argaraña et al. [18] as reconfirmed by dideoxy sequencing [19] of the whole insert.

2.6. E. coli expression, refolding and purification of core streptavidin

A single colony of *E. coli* BL21(DE3) freshly transformed with the plasmids pLysE and pSA1 was used for inoculating 20 ml Luria-Bertani (LB)-broth containing 30 μg/ml chloramphenicol and 100 μg/ml ampicillin. After incubation overnight at 37°C the culture was transferred to 1 l of the same medium in a shaking flask prewarmed at 37°C. At an A_{550} of 0.6 expression was induced by the addition of 0.5 m*M* isopropyl-β-D-thiogalactopyranoside (IPTG) (final concentration) and shaking was continued for 16 h. Cells were harvested by centrifugation (4200 *g*, 15 min, 4°C) and washed with 25 ml ice-cold 50 m*M* Tris·HCl pH 8.0, 500 m*M* sucrose. After centrifugation (20 000 *g*, 30 min, 4°C) the cells were resuspended in 15 ml ice-cold 50 m*M* Tris·HCl pH 8.0, 1 m*M* EDTA and passed three times through a French pressure cell at 16 000 p.s.i. (1 p.s.i. = 6894.76 Pa). The homogenate was centrifuged (20 000 *g*, 30 min, 4°C) in order to sediment the streptavidin inclusion bodies. After washing with 10 ml ice-cold 50 m*M* Tris·HCl pH 8.0, 1 m*M* EDTA the inclusion bodies were dissolved in 8 ml 6 *M* guanidine·HCl (practical grade, Sigma, Deisenhofen, Germany) pH 1.5. The solution was dialyzed twice for 4 h in the cold against 100 ml 6 *M* guanidine·HCl pH 1.5 in order to remove traces of biotin [20]. Refolding was then accomplished by rapid dilution into 250 ml of phosphate-buffered saline (PBS) (4 m*M* KH_2PO_4, 16 m*M* Na_2HPO_4, 115 m*M* NaCl) at 4°C. The mixture was incubated for a minimum of 3 h at 4°C and cleared by centrifugation (20 000 *g*, 30 min, 4°C). Solid ammonium sulfate was slowly added in the cold to a saturation of 40% (62.7 g). After incubation for 3 h at 4°C precipitated contaminating proteins and monomeric, incompletely refolded core streptavidin were removed by centrifugation (20 000 *g*, 30 min, 4°C). Then, the ammonium sulfate saturation of the supernatant was raised to 70% (adding 59 g). After overnight incubation at 4°C, the precipitated tetrameric core streptavidin was recovered (20 000 *g*, 60 min, 4°C) and resuspended in 10 ml PBS-buffered 2.2 *M* ammonium sulfate for removal of residual impurities, which became soluble under these conditions. After centrifugation (20 000 *g*, 30 min, 4°C) the recombinant core streptavidin was dissolved in PBS buffer. The solution was finally cleared by centrifugation (30 000 *g*, 30 min, 4°C) and stored at 4°C. Routinely, between 1.2 and 1.4 g purified core

streptavidin were obtained from 10 l *E. coli* culture in this way.

2.7. *E. coli expression of Strep tag fusion proteins*

In order to demonstrate their purification via streptavidin affinity chromatography five different Strep tag fusion proteins were produced: the antibody D1.3 F_v fragment with the Strep tag fused to the V_H domain [2], retinol-binding protein (RBP) [21], chicken egg-white cystatin [22], *Pseudomonas aeruginosa* azurin [23] and *Escherichia coli* cytochrome b_{562} [24]. The structural genes were introduced into the bacterial expression vector pASK60-Strep [2] except for the F_v fragment, whose production was accomplished using the plasmid pASK68-D1.3 (an optimized version of pASK46-p111 [2] with improved control elements that will be described elsewhere). All proteins became thus fused to the *Omp*A signal peptide —directing secretion to the periplasm of *E. coli*— at their N-terminus and to the Strep tag —comprising the amino acid sequence Ser–Ala–Trp–Arg–His–Pro–Gln–Phe–Gly–Gly— at their C-terminus (cf. the cloning strategies previously outlined [2]). The resulting mature polypeptide sequences were as follows: RBP: Glu^{1} to Cys^{174} plus two intervening Pro residues and the Strep tag; cystatin: Gly^{9} to Gln^{116} plus the Strep tag; azurin: Ala^{1} to Lys^{128} plus the Strep tag; cytochrome b_{562}: Ala^{1} to Arg^{106} plus two intervening Pro residues and the Strep tag. For protein production, a 100-ml culture of *E. coli* JM83 harbouring the appropriate expression plasmid was grown at 22°C (37°C for cytochrome b_{562}) in LB medium containing 100 μg/ml ampicillin (with the addition of 50 μg/ml hemin (Sigma) in the case of cytochrome b_{562}). At an A_{550} of 0.5 IPTG was added to a final concentration of 0.5 m*M* (expression conditions for RBP were modified due to the presence of a second plasmid, pASK61, as described by Müller and Skerra [21]). After 3 h of induction, cells were collected (4200 *g*, 15 min, 4°C) and the pellet was resuspended in 1 ml ice-cold 100 m*M* Tris · HCl pH 8.0, 500 m*M* sucrose, 1 m*M* EDTA and kept on ice for 30 min. The spheroplasts were removed by centrifugation (microfuge, 4°C, 15 min) and the supernatant was recovered as the periplasmic cell fraction.

2.8. *Streptavidin affinity chromatography of Strep tag fusion proteins*

A column containing 0.5 ml CH-Sepharose 4B coupled with 5 mg/ml recombinant core streptavidin was equilibrated with 5 ml 100 m*M* Tris · HCl pH 8.0, 1 m*M* EDTA. Then the periplasmic cell fraction (1 ml) containing the Strep tag fusion protein was applied and the column was washed with up to 5 ml 100 m*M* Tris · HCl pH 8.0, 1 m*M* EDTA (no EDTA in the case of the metallo-proteins azurin and cytochrome b_{562}). The bound recombinant protein was specifically eluted with 2 ml 1 m*M* biotin dissolved in the same buffer. The Strep tag fusion protein was almost quantitatively recovered in a volume of 1 ml under these conditions. All steps were performed at 4°C using gravity flow. Alternatively, a solution of 5 m*M* diaminobiotin (Sigma) was used for elution, permitting regeneration of the affinity column by washing with 10 ml 100 m*M* Tris · HCl pH 8.0.

3. Results and discussion

3.1. *Production of functional core streptavidin using E. coli as expression host*

For expression in *E. coli* the structural gene encoding residues Glu^{14} to Ser^{139} of streptavidin was PCR-amplified from *S. avidinii* chromosomal DNA and inserted into the T7 promoter vector pRSET5a [15] yielding pSA1 (Fig. 1). Expression conditions were essentially as described earlier by Sano and Cantor [20] for a genetic fusion between the non-truncated streptavidin and the N-terminal part of the T7 gene 10 protein. For the preparation of the correctly folded, tetrameric core streptavidin from the inclusion bodies an optimized refolding and purification procedure was developed (Fig. 2A). The method is simple, without a chromatograph-

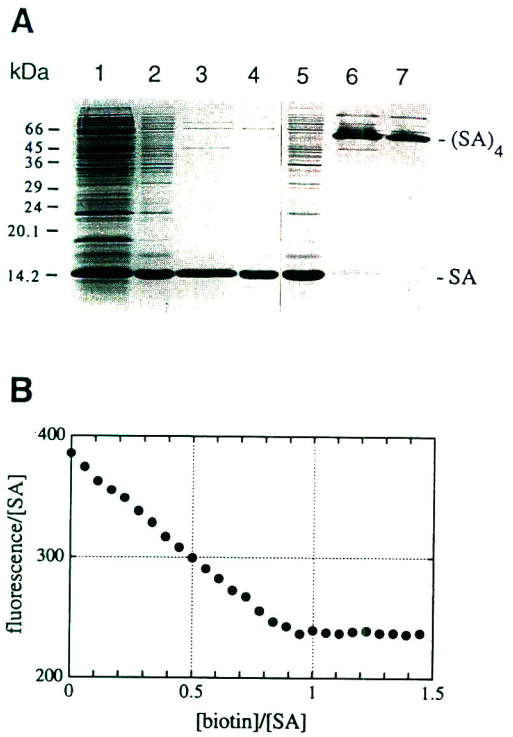

Fig. 2. (A) Purification and refolding of the recombinant core streptavidin. A 15% SDS-PAGE is shown with samples (equivalent portions) from different stages during the preparation. Lanes: 1 = total cell protein of *E. coli* BL21(DE3)(pLysE)(pSA1) 16 h after induction of expression; 2 = sedimented inclusion bodies; 3 = protein solution after renaturation; 4 = purified core streptavidin after fractionated ammonium sulfate precipitation; 5–7 = same samples as in 2–4 without heat treatment prior to SDS-PAGE. Under these conditions the core streptavidin tetramer remains intact [26]. Thus the correctly folded state of the recombinant protein in the final preparation was confirmed (lane 7) whereas small amounts of monomeric streptavidin were still present after refolding (lane 6). kDa = kilodalton, SA = streptavidin. (B) Biotin binding assay with the recombinant core streptavidin. The tryptophan fluorescence is plotted versus the relative amount of biotin added. The two almost linear segments of the curve were fitted separately and from the intercept a ratio of 0.88 bound biotin molecules per core streptavidin monomer was calculated.

ic step, can be easily scaled up and leads to pure and highly soluble core streptavidin, which can be directly used for coupling to, e.g., NHS-activated CH-Sepharose 4B. The final yield of the functional core streptavidin was up to 140 mg per 1 l *E. coli* culture.

Sequencing of the four N-terminal residues revealed that the start methionine residue was not removed by the Met-aminopeptidase as could have been expected from the presence of glutamic acid as the penultimate residue [25]. In order to assess the biochemical activity of the *E. coli*-produced core streptavidin its biotin-binding capacity was determined by fluorescence titration. Reproducibly a value of 0.88 bound biotin molecules per subunit was found (Fig. 2B).

3.2. Choice of the activated resin for the coupling of streptavidin

Four different activated chromatography supports were tested: (i) NHS-activated CH-Sepharose 4B, (ii) epoxy-activated Sepharose 6B, (iii) Eupergit C (epoxy-activated) and (iv) Eupergit C30N (epoxy-activated). After coupling with recombinant core streptavidin the affinity matrices were compared in a batch assay for the specific binding of a bacterially expressed F_v fragment with the Strep tag fused to the C-terminus of the V_H domain [2] from periplasmic protein extract. It was found that the epoxy-activated Sepharose 6B did not bind the Strep tag fusion protein at all whereas the remaining affinity matrices bound the protein equally well (data not shown). However, the two Eupergit supports gave rise to a substantial background of non-specifically bound host cell proteins that were slowly released throughout the assay. A similar effect was not observed for the NHS-activated CH-Sepharose 4B, which thus appeared to be the support of choice for the streptavidin affinity chromatography of Strep tag fusion proteins.

3.3. Comparison of differently prepared streptavidin samples

Initially it was attempted to use natural streptavidin produced by *S. avidinii* in order to prepare affinity matrices that could be used for the purification of Strep tag fusion proteins. The protein was isolated from the culture supernatant of this Gram-positive bacterium and coupled to NHS-activated CH-Sepharose 4B. However,

when the periplasmic *E. coli* extract containing the F_v fragment with the Strep tag was applied to the affinity column only modest retardation was observed with respect to other periplasmic proteins.

This finding was in contrast to earlier results obtained with streptavidin–agarose purchased from Biomol (Hamburg, Germany) under otherwise unchanged conditions, where almost all of the recombinant F_v fragment bound specifically to the column and was then eluted in pure form with 2-iminobiotin [2]. The diminished affinity for the Strep tag observed here was thus attributed to the presence of N- and C-terminal extensions in the natural streptavidin compared to commercial preparations, which consist of the proteolytically truncated core streptavidin [3,4,26]. The improved sterical accessibility of the biotin-binding site in core streptavidin [4] might also be important for the binding of the Strep tag, which is likely to occupy the same pocket on the streptavidin surface [27].

Consequently, two commercial preparations (SPA and Amresco) of core streptavidin were used for coupling to NHS-activated CH-Sepharose 4B. In both cases satisfactory binding activity was observed in purification experiments with several different Strep tag fusion proteins. Unexpectedly however, when a larger amount of immobilized streptavidin was used (5 mg streptavidin per ml gel, SPA or Amresco) significant proteolytic degradation of the Strep tag fusion protein was observed (Fig. 3A). The proteolytic activity, that was obviously present in the affinity matrix (and not in the protein extract), could be inhibited by treatment of the streptavidin Sepharose with phenylmethanesulfonyl fluoride (PMSF) prior to use. Most likely, a contamination with proteases from the preparation process for core streptavidin was responsible for this effect.

In contrast, no protein degradation was detected during the purification of several different Strep tag fusion proteins (see below) when the *E. coli*-derived recombinant core streptavidin was employed (Fig. 3B). Thus, the combination of recombinant core streptavidin with NHS-activated CH-Sepharose 4B as support (cf. above)

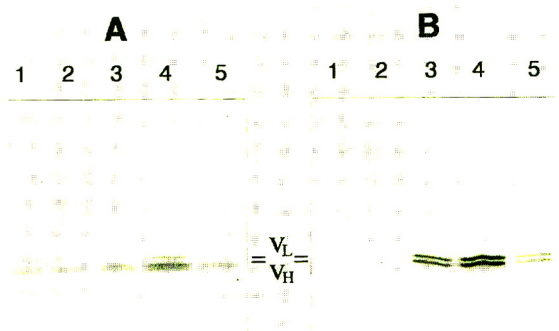

Fig. 3. Proteolytic degradation during purification of a Strep tag fusion protein using immobilized commercial core streptavidin (A) compared to recombinant core streptavidin (B). Affinity chromatography was performed with a periplasmic *E. coli* cell extract containing the D1.3 F_v fragment with the Strep tag at the C-terminus of the V_H domain. The streptavidin was coupled to NHS-activated CH-Sepharose 4B at 5 mg protein per ml gel in each case. Both chromatography experiments were performed in parallel under identical conditions (essentially similar as in the optimized protocol described in the Experimental section). Aliquots from five consecutive fractions collected during elution of the bound F_v fragment were subjected to 15% SDS-PAGE (lanes 1–5). Only small quantities of the intact V_L domain could be detected in (A) (lane 4) and a likely degradation product eluted almost constantly over the range investigated. In contrast elution of stoichiometric amounts of the two immunoglobulin domains V_H and V_L, which make up the F_v fragment, was observed in (B).

led to optimal performance in the streptavidin affinity chromatography of Strep tag fusion proteins.

3.4. A standardized protocol for the purification of Strep tag fusion proteins

In order to permit the rapid purification of different Strep tag fusion proteins on a small scale a standardized procedure was established. For cloning and expression the previously described vector pASK60-Strep [2] was used. pASK60-Strep was designed for secretion of the gene product into the periplasm of *E. coli* and carries a cassette for insertion of the corresponding structural gene permitting concomitant C-terminal fusion with the plasmid-encoded Strep tag. After induction of expression and preparation of the periplasmic cell extract streptavidin affinity chromatography was performed

in a single step as described in the Experimental section.

The purification of five different Strep tag fusion proteins, the D1.3 F_v fragment, RBP, chicken egg-white cystatin, *Pseudomonas aeruginosa* azurin and *E. coli* cytochrome b_{562}, according to this scheme is shown in Fig. 4. The periplasmic host proteins were washed off quickly in every case whereas the homogeneous Strep tag fusion proteins were eluted in the presence of biotin. This demonstrates the low non-specific binding of the affinity matrix. For cytochrome b_{562} weaker retardation on the column was observed but this protein could still be specifically eluted in concentrated form when the amount of washing buffer was reduced (see Fig. 4E). Due to the intense red colour of the holo-protein it was possible to follow visibly its binding and elution so that the cytochrome can be used for the quick control of newly prepared batches of the streptavidin Sepharose.

The streptavidin affinity chromatography was performed under native buffer conditions and a solution of 1 m*M* biotin was usually used for the elution of the bound Strep tag fusion protein. However the extremely high affinity of this ligand for streptavidin prevented re-use of the column. This could be avoided when a solution of 5 m*M* diaminobiotin, a much weaker-binding chemical analogue of biotin [28], was used instead. With this compound elution of the Strep tag fusion protein was only slightly less efficient (Fig. 5) and the column could be regenerated several times without loss of activity. The use of diaminobiotin turned out to be a clear improvement compared to 2-iminobiotin [2] or lipoic acid described before in the case of the purification of the bilin-binding protein [29].

In conclusion all components necessary for the Strep tag purification methodology were optimized and its successful application was demonstrated in a number of cases. Both the recombinant production of core streptavidin in *E. coli* and the use of diaminobiotin for elution in the chromatography make an important contribution to the economic aspect of this method, permitting its use even on a larger scale.

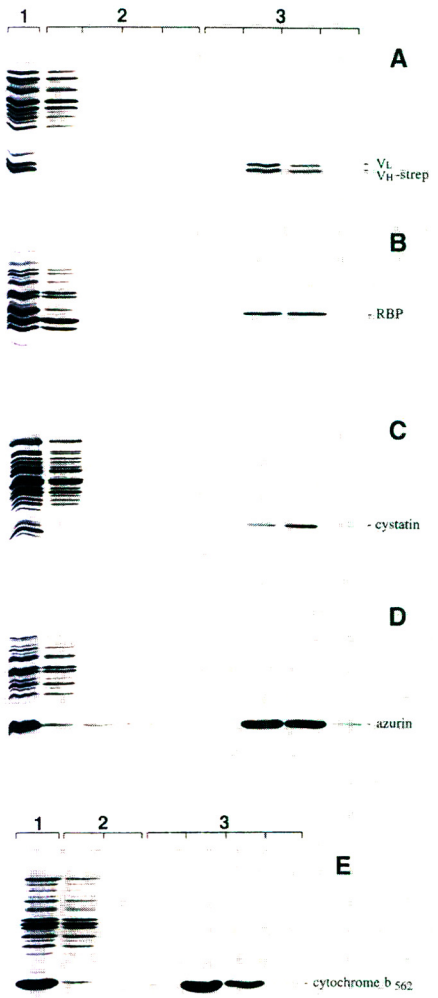

Fig. 4. The one-step purification of various Strep tag fusion proteins via streptavidin affinity chromatography: the D1.3 F_v fragment (A), retinol-binding protein (B), chicken egg-white cystatin (C), *Pseudomonas aeruginosa* azurin (D) and *E. coli* cytochrome b_{562} (E). Chromatography was performed under standardized conditions as described in the Experimental section. After application of the periplasmic *E. coli* cell extract containing the Strep tag fusion protein the column was washed with 5 ml buffer and the effluent was collected in four fractions of 1.25 ml. Then the bound protein was eluted with 1 m*M* biotin and four fractions of 0.5 ml were collected. 20-μl samples of each fraction were subjected to 15% SDS-PAGE. Lanes: 1 = periplasmic protein solution; 2 = washing fractions; 3 = elution fractions. In the case of the cytochrome (E) only 2 ml buffer were used for washing and the effluent was collected in two fractions of 1 ml. Then the bound protein was eluted as above.

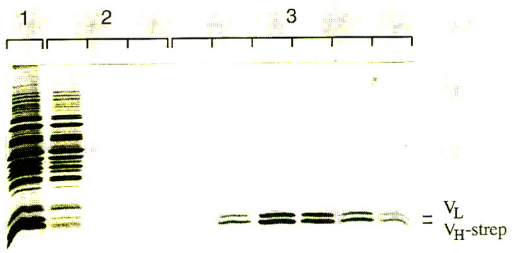

Fig. 5. Use of diaminobiotin for elution of the bound Strep tag fusion protein. The streptavidin affinity chromatography of the bacterial periplasmic cell extract containing the D1.3 F_v fragment was performed as in Fig. 4A except that 3 ml 5 m*M* diaminobiotin was used for elution. Samples (20 μl) of each fraction were subjected to 15% SDS-PAGE. Lanes: 1 = periplasmic protein solution; 2 = washing fractions (fractions 2 and 3 were pooled); 3 = elution fractions.

Acknowledgements

The authors wish to thank F. Lottspeich for N-terminal protein sequencing of the recombinant streptavidin, H.N. Müller for the expression plasmid encoding the RBP-Strep tag fusion protein, E. Auerswald for his synthetic gene encoding chicken egg-white cystatin, and L.-O. Essen for help in some experiments. This work was supported by a pre-doctoral fellowship from the Ministère des Affaires Culturelles, Luxembourg to T.G.M.S. and a grant from the Deutsche Forschungsgemeinschaft to A.S.

References

[1] H.M. Sassenfeld, *Trends Biotechnol.*, 8 (1990) 88.
[2] T.G.M. Schmidt and A. Skerra, *Prot. Eng.*, 6 (1993) 109.
[3] A. Pähler, W.A. Hendrickson, M.A. Gawinowicz Kolks, C.E. Argaraña and C.R. Cantor, *J. Biol. Chem.*, 262 (1987) 13933.
[4] E.A. Bayer, H. Ben-Hur, Y. Hiller and M. Wilchek, *Biochem. J.*, 259 (1989) 369.
[5] F.W. Studier, A.H. Rosenberg, J.J. Dunn and J.W. Dubendorff, *Methods Enzymol.*, 185 (1990) 60.
[6] C. Yanisch-Perron, J. Vieira and J. Messing, *Gene*, 33 (1985) 103.
[7] S.P. Fling and D.S. Gregerson, *Anal. Biochem.*, 155 (1986) 83.
[8] R.K. Scopes, *Anal. Biochem.*, 59 (1974) 277.
[9] N.M. Green, *Methods Enzymol.*, 184 (1990) 51.
[10] N.M. Green, *Biochem. J.*, 90 (1964) 564.
[11] C.F. Chignell, D.K. Starkweather and B.K. Sinha, *J. Biol. Chem.*, 250 (1975) 5622.
[12] J. Cazin, Jr., M. Suter and J.E. Butler, *J. Immunol. Methods*, 113 (1988) 75.
[13] M. Suter, J. Cazin, Jr., J.E. Butler and D.M. Mock, *J. Immunol. Methods*, 113 (1988) 83.
[14] A. Skerra, *Nucleic Acids Res.*, 20 (1992) 3551.
[15] R. Schoepfer, *Gene*, 124 (1993) 83.
[16] J. Sambrook, E.F. Fritsch and T. Maniatis, *Molecular Cloning: A Laboratory Manual*, Cold Spring Harbor Laboratory, Cold Spring Harbor, NY, 2nd ed., 1989.
[17] T.D. Schneider, G.D. Stormo, L. Gold and A. Ehrenfeucht, *J. Mol. Biol.*, 188 (1986) 415.
[18] C.E. Argaraña, I.D. Kuntz, S. Birken, R. Axel and C.R. Cantor, *Nucleic Acids Res.*, 14 (1986) 1871.
[19] S. Tabor and C.C. Richardson, *Proc. Natl. Acad. Sci. U.S.A.*, 84 (1987) 4767.
[20] T. Sano and C.R. Cantor, *Proc. Natl. Acad. Sci. U.S.A.*, 87 (1990) 142.
[21] H.N. Müller and A. Skerra, *J. Mol. Biol.*, 230 (1993) 725.
[22] E.A. Auerswald, G. Genenger, I. Assfalg-Machleidt, J. Kos and W. Bode, *FEBS Lett.*, 243 (1989) 186.
[23] G.W. Canters, *FEBS Lett.*, 212 (1987) 168.
[24] H. Nikkila, R.B. Gennis and S.G. Sligar, *Eur. J. Biochem.*, 202 (1991) 309.
[25] P.-H. Hirel, J.-M. Schmitter, P. Dessen, G. Fayat and S. Blanquet, *Proc. Natl. Acad. Sci. U.S.A.*, 86 (1989) 8247.
[26] E.A. Bayer, H. Ben-Hur and M. Wilchek, *Methods Enzymol.*, 184 (1990) 80.
[27] P.C. Weber, M.W. Pantoliano and L.D. Thompson, *Biochemistry*, 31 (1992) 9350.
[28] N.M. Green, *Adv. Protein Chem.*, 29 (1975) 85.
[29] F.S. Schmidt and A. Skerra, *Eur. J. Biochem.*, 219 (1994) 855.

ELSEVIER

Journal of Chromatography A, 676 (1994) 347–354

JOURNAL OF CHROMATOGRAPHY A

Ion-pair reversed-phase liquid chromatography with fluorimetric detection of pesticides

F. García Sánchez*, A. Navas Díaz, A. García Pareja

Departamento de Química Analítica, Facultad de Ciencias, Universidad de Málaga, 29071-Málaga, Spain

First received 6 December 1993; revised manuscript received 16 May 1994

Abstract

The pesticides asulam, propoxur, coumatetralyl, biphenyl-2-ol and thiabendazole were separated by ion-pair reversed-phase liquid chromatography with fluorescent detection. The mobile phase contained methanol, acetic acid and sodium cholate as ion-pair reagent. In addition, tetramethylammonium hydrogensulphate and triethylamine were added to elute the pesticides. Separations were accomplished in less than 20 min. Interferences from nineteen pesticides were studied and recoveries from synthetic mixtures ranging from 90 to 110%. Recoveries from spiked apples and wheat grains ranged from 94 to 105% with relative standard deviations between 1.4 and 9.2% and detection limits between 0.1 and 1.9 ng.

1. Introduction

The pesticides asulam, propoxur, coumatetralyl, biphenyl-2-ol and thiabendazole are a contact herbicide, a non-systemic insecticide, an anticoagulant rodenticide and two fungicides, respectively. Their mixtures can be found in fruits, vegetables, cereals and other types of crops as a consequence of the pre- and post-harvest treatment with a variety of chemicals such as herbicides and insecticides in the pre-harvest step and with fungicides and rodenticides in the storage step of the total harvest process. Although liquid chromatography (LC) [1–7] and gas chromatography (GC) [8–13] have been used for their separation and detection in several other mixtures, the above mixture has not been resolved.

Because the thermal lability of asulam and coumatetralyl and the high melting point of thiabendazole impede their GC investigation, LC is the technique of choice. Reversed-phase LC on a C_{18} column does not separate the mixture. However, as anionic, cationic and zwitterionic molecules can all potentially undergo ion-pair formation with appropriate counter-ionic reagents, the scope of LC can be extended. In ion-pair systems, a secondary chemical equilibrium is superimposed on the physical distribution of a solute between the mobile and stationary phases and consequently method development is generally more flexible and facilitates the determination of compounds using the reversed-phase mode [14].

Charged surfactants are used as the counter ions in the mobile phase. A great variety of surface-activity achiral compounds of different hydrophobicity are available as counter-ion re-

* Corresponding author.

0021-9673/94/$07.00
SSDI 0021-9673(94)00466-M

agents. Recently, new chiral surfactants such as bile salts have extended the scope of separations. Bile salts are used in micellar LC [15–19] but no data were found for their use as ion-pair reagents in LC. They differ from the typical long-chain alkyl micelle-forming surfactants previously employed as ion-pair reagents in that they have a rigid cholesterol-like steroidal ring structure and possess hydrophobic and hydrophilic faces.

We report in this paper a rapid, ion-pair reversed-phase LC method with a bile salt, sodium cholate, as organic counter ion for the separation and determination of pesticides. The separation was achieved by using gradient elution and the determination by using fluorimetric detection, with a total analysis time of 20 min.

2. Experimental

2.1. Instrumentation

The measurements were performed with a Merck–Hitachi (Darmstadt, Germany) liquid chromatograph consisting of an L-6200 pump, an AS-4000 autosampler, an L-4250 UV–visible detector and a D-6000 interface. Integration was carried out with a PC/AT computer and the instrumental parameters were controlled by Hitachi–Merck HM software. A Perkin-Elmer (Beaconsfield, UK) LS-50 fluorescence detector, placed in series with and after the UV–visible spectrophotometer, was equipped with a xenon discharge lamp and two monochromators. Fluorescence Data Manager (FLDM) software (LC program) and an RS232C interface were used to send information to an external computer. For graphical recording, an NEC Silenwriter2 S60P laser printer was connected to the spectrofluorimeter.

A Model KNK-3000 gas chromatograph (Konik Instruments, Barcelona, Spain) equipped with a flame ionization detector was used with the following conditions: splitless injector (240°C, 0.8 min); injection volume, 1 μl; detector temperature, 280°C; fused-silica column, BP5 (SGE, Victoria, Australia) stationary phase (5% diphenyl–dimethylsiloxane), 25 m × 0.22 mm I.D., 0.25-μm film thickness; temperature programme: 120°C for 2 min, increased to 240°C at 8°C/min and held at 240°C 40 min; carrier gas, helium at 11.6 ml/min; and make-up gas, nitrogen at 24 ml/min.

2.2. Chemicals and reagents

Sodium cholate, sodium dodecyl sulphate (SDS), cetyltrimethylammonium bromide (CTAB) and triethylamine (TEA) were obtained from Sigma (St. Louis, MO, USA) and tetramethylammonium hydrogensulphate (TMA) and acetic acid from Merck (Darmstadt, Germany). Methanol was of LiChrosolv gradient grade (Merck) and acetone of analytical-reagent grade (Merck). The pesticides asulam (purity 99.9%), propoxur (99.9%) and coumatetralyl (96%) were purchased from Dr. S. Ehrenstorfer (Augsburg, Germany), biphenyl-2-ol (>99%) from Merck and thiabendazole (Pestanal, 99%) from Riedel-de Haën (Hannover, Germany).

Stock standard solutions of asulam ($4.34 \cdot 10^{-3}$ M), propoxur ($4.78 \cdot 10^{-3}$ M), coumatetralyl ($3.42 \cdot 10^{-3}$ M), biphenyl-2-ol ($5.87 \cdot 10^{-3}$ M) and thiabendazole ($4.97 \cdot 10^{-3}$ M) were prepared by dissolving the compounds in methanol and stored at 4°C. Working standard solutions were prepared by dilution with methanol.

Solutions of sodium cholate ($7 \cdot 10^{-3}$ M) SDS ($3.5 \cdot 10^{-3}$ M), CTAB ($1 \cdot 10^{-4}$ M) and tetramethylammonium hydrogensulphate ($1 \cdot 10^{-2}$ M) were prepared in doubly deionized water. These solutions were filtered through 0.2-μm nylon membrane filters.

2.3. Extraction procedure for apples

A 250-g amount of apples was chopped in a food chopper and 15 g were transferred into a blender cup and blended with 50 ml of acetone containing 0.3 ml of orthophosphoric acid at high speed for 3 min. The homogenate was filtered through a fritted-glass Büchner funnel (coarse porosity) under reduced pressure and the filter cake washed with 5 ml of acetone. The filtrate was transferred into a 50-ml volumetric flask and

diluted to volume with acetone. An aliquot of 1 ml of the extract in acetone was diluted with methanol to a final volume of 5 ml. This solution was used for analysis.

2.4. Extraction procedure for wheat grain

Portions of 10 g of representative wheat grain samples were washed with 20 ml of acetone in order to eliminate any impurities present. The pesticides were extracted by adding 20 ml of acetone and sonicating for 5 min. The solution was filtered through a fritted-glass Büchner funnel (coarse porosity) under reduced pressure and the filter cake was washed with acetone. The filtrate was evaporated to dryness on a rotary evaporator. The residue was dissolved in methanol (5 ml) and this solution was used for analysis.

2.5. LC operating conditions

The pesticide samples were analysed using a Spherisorb S5 ODS-2 reversed-phase column (20 cm × 4.6 mm I.D.; 5-μm particle size) from Phase Separations (Deeside, UK). The injection volume was 20 μl for the standard methanolic solutions and samples and the flow-rate was 1 ml/min. The mobile phase composition and wavelength programme for fluorimetric detection are detailed in Table 1. The peak-area response was measured at the retention times of asulam (1.85 min), propoxur (3.74 min), coumatetralyl (6.19 min), biphenyl-2-ol (7.95 min) and thiabendazole (15.97 min). A calibration graph was constructed using the responses.

2.6. Recovery test

Apples samples were spiked with a solution of pesticides in methanol of composition asulam, coumatetralyl and propoxur 200 mg/l, biphenyl-2-ol 50 mg/l and thiabendazole 12.5 mg/l and left for 30 min before extraction. Wheat grains were washed with 20 ml of acetone in order to eliminate any impurities present and spiked with a solution of pesticides in methanol of composition asulam, coumatetralyl and propoxur 20 mg/l, biphenyl-2-ol 5 mg/l and thiabendazole 1.25 mg/l. After thorough mixing, the grains were left for 30 min before extraction. The apple and grain extracts in acetone were transferred into 50- and 10-ml volumetric flasks, respectively, and diluted to volume with acetone. Aliquots of these solutions were diluted with methanol to a final volume of 5 ml. These solutions were used for analysis.

3. Results and discussion

The structures of asulam, propoxur, coumatetralyl, biphenyl-2-ol and thiabendazole are shown in Fig. 1 [20]. These compounds possess

Table 1
Mobile phase composition and wavelength programme

Time (min)	Methanol (%)	Ion-pair mixture 1[a] (%)	Ion-pair mixture 2[b] (%)	$\lambda_{excitation}$ (nm)	$\lambda_{emission}$ (nm)
0.0	60	40	0	255	342
2.5				272	303
4.5				310	385
6.8				247	340
8.0	60	40	0		
9.0	60	0	40		
10.0				298	342
18.0	60	0	40	298	342

[a] Ion-pair mixture 1: aqueous solution of 7 m*M* sodium cholate, 25 m*M* acetic acid and 5 m*M* tetramethylammonium.
[b] Ion-pair mixture 2: aqueous solution of 7 m*M* sodium cholate, 2.5 *M* acetic acid and 84 m*M* triethylamine.

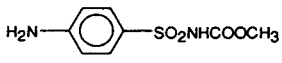

ASULAM
Methyl sulphanilylcarbamate

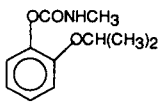

PROPOXUR
2-Isopropoxyphenylmethylcarbamate

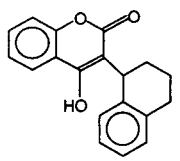

COUMATETRALYL
4-Hydroxy-3-(1,2,3,4-tetrahydro-1-naphthyl) coumarin

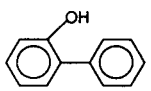

BIPHENYL-2-OL
(1,1'-Biphenyl-2-ol)

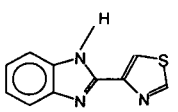

THIABENDAZOLE
2-(thiazol-4-yl) benzimidazole

Fig. 1. Structures of the pesticides.

sufficient natural fluorescence to permit their detection without pre- or postcolumn derivatization steps and so fluorimetric detection was selected.

The retention behaviour was studied on a C_{18} reversed-phase column under a variety of mobile phase conditions including concentrations of organic modifier, ion-pairing reagent and acetic acid, pH and concentrations of TMA and TEA in the mobile phase.

Because of the quenching effect on the fluorescence of the solutes exerted by acetonitrile, the latter was discarded as an organic modifier and methanol was selected. Methanol concentrations below 50% cause turbidity of the mobile phase; concentrations between 50 and 70% give the greatest differences in capacity factor and 60% methanol in the mobile phase was selected as the optimum concentration.

Different surfactants of cationic and anionic character were studied to determine the best ion-pairing reagent. The results indicated that in absence of surfactants asulam and propoxur overlap completely. Alternatively, the use of ion-pairing reagents in the mobile phase separates the compounds. The peak heights obtained with the anionic surfactants sodium cholate and SDS are higher than those with cationic surfactants such as CTAB whereas the retention times with anionic surfactants are similar or shorter than those with cationic surfactants or without surfactants. The greater efficiency was achieved with sodium cholate and this was selected as the ion-pair reagent for the separation. Fig. 2A shows a plot of the capacity factor vs. sodium cholate concentration in the mobile phase, from which it is deduced that all the pesticides can be separated satisfactorily with 2.8 m*M* sodium cholate.

The effect of acetic acid on the capacity factor is summarized in Fig. 2B. Whereas an acetic acid concentration of 10 m*M* in the mobile phase gives the greatest efficiency for the separation of asulam, propoxur, coumatetralyl and biphenyl-2-ol, thiabendazole is strongly retained into the column and 1 m*M* acetic acid in the mobile phase is needed to elute it. This behaviour of thiabendazole is consistent with the behaviour of a weaker acid. As the pH decreases, the retention increases rapidly for coumatetralyl, thiabendazole and asulam and remains constant for propoxur and biphenyl-2-ol. The last two compounds form ion pairs with sodium cholate in a wide pH range, but coumatetralyl requires $pH < 7$ and thiabendazole and asulam $pH < 5$.

Variation in the sodium cholate content of the mobile phase alone does not allow adequate control over the column selectivities for pesticides and an ion-pair mixture of counter ions of different hydrophobicities is used. Therefore, low concentrations of a cationic species such as TMA or TEA were added; this addition to a mobile phase of low pH tends to lower the capacity factors of positively charged solute molecules owing to co-ion repulsive interaction. A 2 m*M* TMA concentration in the mobile phase was selected as the optimum to elute asulam,

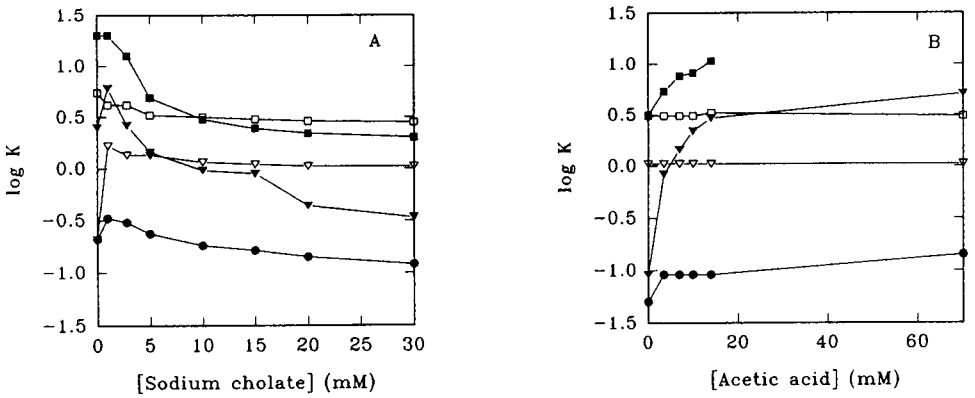

Fig. 2. Effect of mobile phase parameters on the retention of the pesticides: (A) sodium cholate concentration in the mobile phase; conditions, methanol–water (60:40) solution of 25 m*M* acetic acid and 5 m*M* TMA; (B) acetic acid; conditions, methanol–water (60:40) solution of 2.5 m*M* acetic acid and 85 m*M* TEA. ○ = Asulam; ▼ = coumatetralyl; □ = biphenyl-2-ol; ▽ = propoxur; ■ = thiabendazole.

propoxur, coumatetralyl and biphenyl-2-ol. However, the ion-pair mixture of sodium cholate, acetic acid and TMA does not lower the capacity factor of thiabendazole sufficiently and the addition of another hydrophobic reagent, TEA, instead of TMA is needed to elute thiabendazole.

3.1. Calibration graphs and comparison of results with those of GC–FID

The calibration graphs are linear between 1.8 and 200 ng for asulam, 3 and 200 ng for propoxur, 0.6 and 200 ng for coumatetralyl, 0.6 and 100 ng for biphenyl-2-ol and 0.2 and 40 ng for thiabendazole. The lower limit of the linear dynamic range is determined by the detection limit. Typical relative standard deviations (R.S.D.s) are between 0.7 and 5.8%.

The results obtained for propoxur and biphenyl-2-ol by LC were compared with those given by GC. Coumatetralyl, asulam and thiabendazole decomposed on-column and they cannot be determined by GC without a previous derivatization step. Universal flame ionization detection (FID) was used with GC because propoxur and biphenyl-2-ol do not give response with the more commonly used detectors in pesticide residue analysis, such as electron-capture or nitrogen–phosphorus detectors.

The correlation between the LC and GC methods was $r = 0.9998$; the slope of the regression line was 1.0218 and the intercept −4.7792 for propoxur and $r = 0.9999$, slope = 0.9911 and intercept = 2.3364 for biphenyl-2-ol. The detection limits with the LC and GC methods are 2.4 and 2.6 ng, respectively, for propoxur and 0.4 and 2.4 ng, respectively, for biphenyl-2-ol. The R.S.D.s ($n = 3$) using the LC and the GC methods are 2.2 and 1.3%, respectively, for propoxur and 2.6 and 18.5%, respectively, for biphenyl 2-ol. These results indicate that both methods correlated well.

3.2. Application to food samples

Prior to application to real samples, the method was evaluated with synthetic mixtures of the most commonly used pesticides in pre- or post-harvest treatment. Nineteen potential interferents were selected among insecticides, fungicides, rodenticides and herbicides usually found in cereals, fruits, vegetables and other types of crops [7,13]. The synthetic mixtures were prepared using a fixed concentration of the pesticide to be recovered, namely asulam 0.2 μg/ml, coumatetralyl 0.2 μg/ml, biphenyl 2-ol 0.2 μg/ml, propoxur 0.5 μg/ml and thiabendazole 0.1 μg/ml, and adding the potential interferents at several levels. The organophos-

Table 2
Analytical characteristics and recovery of pesticides from spiked foods

Compound	Apples[a]					Wheat grains[a]				
	D_L^b (ng)	C_Q^c (ng)	Concentration range (μg/ml)	Mean recovery (%)	R.S.D. (%)	D_L^b (ng)	C_Q^c (ng)	Concentration range (μg/ml)	Mean recovery (%)	R.S.D. (%)
Asulam	0.8	2.7	0.5–8.0	101.0	5.1	1.9	6.5	0.5–8.0	104.9	2.5
Propoxur	0.9	2.9	0.5–8.0	97.3	3.9	1.4	4.7	0.5–8.0	97.0	1.4
Coumatetralyl	0.6	2.0	0.5–8.0	98.6	3.5	1.0	3.5	0.5–8.0	96.0	2.8
Biphenyl-2-ol	0.1	0.30	0.05–2.0	99.4	6.8	0.3	1.1	0.06–2.0	93.6	2.6
Thiabendazole	0.2	0.6	0.05–0.5	103.1	9.2	0.1	0.4	0.03–0.5	95.9	3.7

[a] $n = 3$.
[b] Detection limit (signal-to-noise ratio = 3).
[c] Quantification limit (signal-to-noise ratio = 10).

phates azinphos-ethyl, chlorpyrifos, dialifos, fenamifos and parathion-methyl were added together, as were the organochlorides chlorfenson, chlorobenzilate, dicofol and tetradifon. Recoveries from these synthetic mixtures ranged from 90 to 110% at a pesticide-to-interferent ratio of 50 for the most of pesticides; organochlorines are the best tolerated and analysis for thiabendazole is least subject to interference from the other pesticides.

To check the usefulness of the procedure, recoveries of the pesticides in apples and wheat grain were determined. These samples were chosen because of their high consumption and to demonstrate the applicability of the procedure to different product matrices.

A number of solvent extraction systems have been used for residue screening procedures. The use of acetone and acetone–water mixtures is the most widely used [13,21–24], simplest and most efficient method to remove organic chemical residues quantitatively from foodstuffs because high concentrations of residues can be extracted.

Apples and wheat grain samples were spiked prior to extraction with a methanolic solution of the pesticides, after checking for the absence of the pesticides under study. After extraction, the samples were subjected to the LC procedure. The chromatograms of apple and wheat grain extracts are reported in Fig. 3. Table 2 gives the results obtained with recoveries ranging from 97 to 103% in apples and from 94 to 105% in wheat grains. The accuracy is excellent. The precision deduced from the R.S.D. values is consistently good; these results were affected by the particularly high R.S.D. for repeatability for low levels of biphenyl-2-ol and thiabendazole in apples. The detection limits, defined as the lowest amount that gave a signal three times higher than the baseline noise, ranged from 0.1 ng for thiabendazole to 1.9 ng for asulam and are higher than those obtained for apples because the wheat grain blanks are affected by a high R.S.D.

4. Conclusions

A mixture of the pesticides asulam, propoxur, coumatetralyl, biphenyl-2-ol and thiabendazole was resolved by ion-pair reversed-phase liquid chromatography. The chiral surfactant sodium

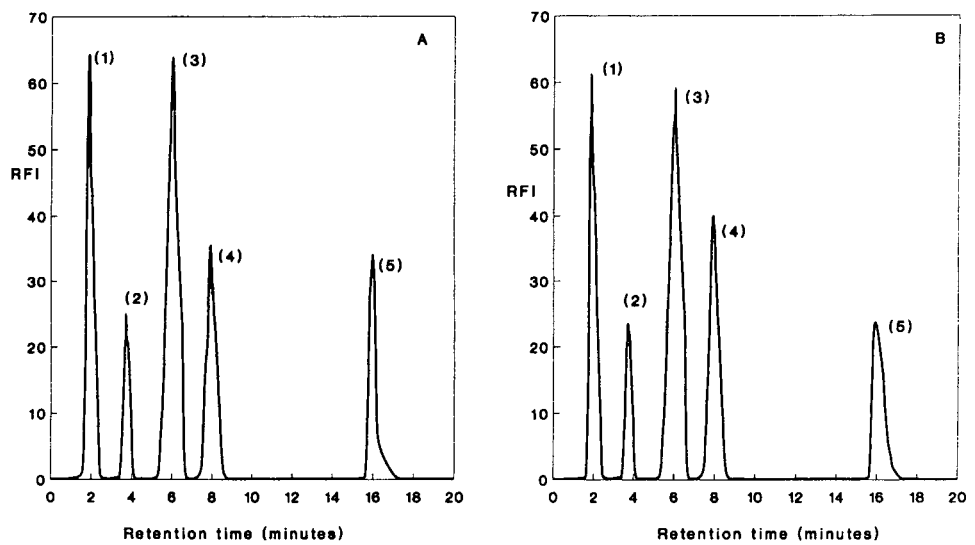

Fig. 3. Chromatograms of (A) apples spiked with (1) 2 μg/ml of asulam, (2) 2 μg/ml of coumatetralyl, (3) 0.5 μg/ml of biphenyl-2-ol, (4) 2 μg/ml of propoxur and (5) 0.10 μg/ml of thiabendazole and (B) wheat grains spiked with (1) 2 μg/ml of asulam, (2) 2 μg/ml of coumatetralyl, (3) 0.5 μg/ml of biphenyl-2-ol, (4) 2 μg/ml of propoxur and (5) 0.125 μg/ml of thiabendazole.

cholate proved its utility as a counter ion in the mobile phase. The method compares well with GC. As the analytical characteristics (ease of applicability, detection limits, precision) show the method is suitable for the analysis of food samples.

Acknowledgement

The authors thank the Comisión Interministerial de Ciencia y Technología (Project PB89-0583) for supporting this study.

References

[1] R.T. Kon, L. Geissel and R.A. Leavit, *Food Addit. Contam.*, 1 (1984) 67.
[2] C.H. Marvin, I.D. Bridle, C.D. Hall and M. Chiba, *Anal. Chem.*, 62 (1990) 1495.
[3] D.M. Gilvydis and S.M. Walters, *J. Assoc. Off. Anal. Chem.*, 73 (1990) 753.
[4] A.R. Long, L.C. Hsieh, C.R. Short and S.A. Barker, *J. Chromatogr.*, 475 (1989) 753.
[5] Y. Kitada, M. Sasaki and K. Tanigawa, *J. Assoc. Off. Anal. Chem.*, 65 (1982) 1302.
[6] A.M. Marti, A.E. Mooser and H. Kock, *J. Chromatogr.*, 498 (1990) 145.
[7] B. Ohlin, *Var Föda, Suppl.*, 38 (1986) 111.
[8] K. Isshiki, S. Tsumura and T. Watanabe, *Agric. Biol. Chem.*, 42 (1978) 2375.
[9] N. Motohashi, H. Nagashima and R. Meyer, *J. Liq. Chromatogr.*, 13 (1990) 345.
[10] S.Y. Szeto and K.M.S. Sundaram, *J. Chromatogr.*, 200 (1980) 179.
[11] R.E. Cline, L.W. Yert and L.L. Needham, *J. Chromatogr.*, 32 (1984) 420.
[12] L. Ogierman, *J. Chromatogr.*, 210 (1981) 83.
[13] A. Anderson and B. Ohlin, *Var Föda, Suppl.*, 38 (1986) 79.
[14] M.T.W. Hearn (Editor), *Ion-Pair Chromatography. Theory and Biological and Pharmaceutical Applications*, Marcel Dekker, New York, 1985.
[15] S. Terabe, M. Shibata and Y. Miyashita, *J. Chromatogr.*, 480 (1989) 403.
[16] R.O. Cole, M.J. Sepaniak and W.L. Hinze, *J. High Resolut. Chromatogr.*, 13 (1990) 579.
[17] R.W. Williams, Jr., Z. Fu and W.L. Hinze, *J. Chromatogr. Sci.*, 28 (1990) 292.
[18] H. Nishi, T. Fukuyama, M. Matsuo and S. Terabe, *Anal. Chim. Acta*, 236 (1990) 281.
[19] A. Dobashi, T. Ono, S. Hara and J. Yamaguchi, *Anal. Chem.*, 61 (1989) 1984.
[20] *The Pesticide Manual —A World Compendium*, British Crop Protection Council, Croydon, 1983.
[21] Y. Aoki, M. Takeda and M. Uchiyama, *J. Assoc. Off. Anal. Chem.*, 50 (1975) 1286.
[22] M.C. Bowman and M. Beroza, *J. Assoc. Off. Anal. Chem.*, 50 (1967) 1228.
[23] M.A. Luke and G.M. Doose, *Bull. Environ. Contam. Toxicol.*, 30 (1983) 110.
[24] L.D. Sawyer, *J. Assoc. Off. Anal. Chem.*, 68 (1985) 64.

ELSEVIER

Journal of Chromatography A, 676 (1994) 355–359

JOURNAL OF CHROMATOGRAPHY A

Stationary phase complexation of polyethers: separation of polyethers with amino-bonded silica gel

Tetsuo Okada*, Toshinori Usui

Faculty of Liberal Arts, Shizuoka University, Shizuoka 422, Japan

Received 23 February 1994

Abstract

Polyethers are retained on a common amino-bonded column by forming complexes with protonated amino groups, and then separated according to the complex formation ability. The fact that counter anions strongly affected the retention indicates that the retention mechanism involves not only complexation with the ammonium groups but also ion-pair formation with counter anions. The practical separation of crown ethers and polyoxyethylene chains involved in a variety of non-ionic surfactants is reported.

1. Introduction

The separation of polyethers is of practical importance because they are often used as hydrophilic groups in various surface-active agents [1]. Apart from practical analysis, the separation of polyethers has some interesting features, *e.g.*, their ability to form complexes with hard metal ions can be evaluated when an ion-exchange resin is used for the separation [2–5] and the partitioning of acyclic polyethers to reversed-phase stationary phases reflects the conformational changes of polyether chains [6,7] and the complexation [8], etc. We therefore believe that it is worth developing a novel separation method for polyethers not only to expedite their practical analysis but also to elucidate the polyether chemistry itself.

Amino groups, which in general have been utilized for the separation of sugars [9,10] as functional groups anchored on the stationary phase, donate lone-pair electrons to hydroxyl groups in sugars in their unprotonated forms. Once amino groups have been protonated, they are expected to play the role of cationic sites and to be complexed by polyethers. Amino-bonded silica gel can therefore differentiate polyethers according to the complexation ability with the corresponding ammonium ion. In this paper, we present preliminary results and describe the practical application of amino-bonded silica gel to the separation of some polyethers.

2. Experimental

The chromatographic system was composed of a Tosoh CCPM computer-controlled pump, a Thomastat thermostated water-bath, a

* Corresponding author.

0021-9673/94/$07.00
SSDI 0021-9673(94)00280-M

Rheodyne injection valve equipped with a 100-μl sample loop and a Tosoh UV-8020 UV–visible detector. The separation column was a Tosoh TSKgel NH_2-60 stainless-steel column (250 mm × 4.6 mm I.D.) packed with 3-aminopropylsilica gel of 5-μm particle size and was used after the amino groups had been completely protonated with a moderately acidic solution (HCl, etc.). Complete protonation was confirmed by measuring the pH of the effluent from the column. Once the amino groups had been protonated, it was not necessary to take disprotonation into account with neutral mobile phases because of the high pK_a values of aliphatic amines. This was verified by the unchanged retention of a particular polyether over a long period; if disprotonation takes place, the retention of polyethers should decrease because the amino group itself did not act as a Lewis acid and was not complexed by any polyethers. The separation column was immersed in water thermostated at 25°C. Methanol, which has been known as a medium favourable for polyether complexation, was used as a mobile phase.

Reagents were of analytical-reagent grade. Methanol was distilled twice. Distilled, deionized water was used throughout. Polyoxyethylenes (POE) were labeled with 3,5-dinitrobenzyl chloride, if necessary. Crown ethers were synthesized according to the literature [11].

3. Results and discussion

3.1. Choice of counter anion

The primary retention mechanism of polyethers on protonated amino-bonded silica gel is their complexation with the ammonium ion sites in the stationary phase. Unfortunately, the solvation of ammonium ions has not been well investigated in comparison with other simple cations. However, it is possible to predict roughly the solvation of an ammonium ion. The similarity of the complexation behaviour and the crystalline ionic size of ammonium ion to those of potassium and rubidium ions implies a resemblance of solvation [12,13], except that the former is a stronger hydrogen-bond donor than the latter.

It has been reported that the complexation of polyethers with a cation is affected by the counter anion. However, in most reported instances, effects of anions are classified into two major types: (1) hydrogen bonding between the anion and a ligand influences the complexation [13]; (2) in low-permittivity solvents, ion-pair formation is related to the complexation. However, our results clearly indicated that the stationary phase complexation is influenced by the nature of the counter anion despite the use of a polar protic solvent.

Table 1 shows the effects of counter anions on

Table 1
Variation of k' of crown ethers with counter anions in the protonated amino-bonded column

Crown ether[a]	k'						
	SO_4^{2-}	AcO^- [b]	Cl^-	Br^-	I^-	SCN^-	ClO_4^-
B15C5	0.98	1.35	1.62	2.88	5.13	6.45	7.08
B18C6	28.2	42.7	31.6	–[c]	–[c]	–[c]	–[c]
DB18C6	4.47	6.46	5.75	11.22	29.5	34.7	40.7
DB21C7	3.39	5.13	3.39	6.61	17.0	24.5	26.3
DB24C8	0.49	0.62	0.10	0.79	1.28	2.82	2.88
DB30C10	0.23	0.33	0.093	0.54	1.45	2.14	2.75

Methanol was used as the mobile phase.

[a] Abbreviations: B15C5 = benzo-15-crown-5; B18C6 = benzo-18-crown-6; DB18C6 = dibenzo-18-crown-6; DB21C7 = dibenzo-21-crown-7; DB24C8 = dibenzo-24-crown-8; DB30C10 = dibenzo-30-crown-10.

[b] Acetate.

[c] Not determined because of extremely strong retention.

the stationary phase complexation of crown ethers as changes in capacity factors. Once the amino groups in the stationary phase have been protonated, they cannot be disprotonated with either pure methanol or methanol containing a neutral salt. The replacement of a counter anion was therefore possible in the usual manner, *i.e.*, by passing the solution of a salt of the anion of interest through the column. It is obviously that large "hydrophobic" anions enhance the stationary phase complexation, whereas small ions, in other words strong hydrogen bond acceptors, lower the retention (use of the term "hydrophobic" is not strictly appropriate; however, as bulky less hydrated ions such as ClO_4^- usually show the hydrophobic properties in water, this term has been used here). This phenomenon will be related to the retention mechanism. Although details are being studied in our laboratory and will be reported in the near future, it appears that ion-pair formation in the stationary phase is strongly related to the mechanism. In the practical sense, ClO_4^- will be the best choice because the retention is the strongest of the counter anions tested (strong retention can be modified by the addition of various components to the mobile phase, whereas it is difficult to alter weak retention by modifying the mobile phase).

3.2. Separation of polyethers

Separation of POE chains contained in nonionic surfactants is of general and practical interest. Therefore, the present method was first applied to this aspect. As is known, the complexation ability of POE is enhanced by the chain length; in complexation with an alkali metal ion, the complexation ability of POE is almost exponentially enhanced with increasing chain length [3]. Such complexation behaviour strongly indicates a need for gradient elution. Various gradient modes can be considered, *e.g.*, the addition of a solvent unfavourable for the complexation (*e.g.*, water is an example of such solvents), increasing the temperature because the complexation is exothermic [5] and the addition of an appropriate cation to the mobile phase [2]. Of these three methods, we selected the last one because of the flexibility of the choice of the cation; as we quantitatively know the complexation of polyether with a cation employed in the mobile phase, we can easily control the retention of polyethers by both selecting an appropriate cation and varying the concentration of the cation.

Fig. 1 shows the separation of POE chains contained in Triton X-100, where ClO_4^- was chosen as the counter anion because of the strong retention ability of the ClO_4^--form stationary phase. Therefore, a perchlorate salt should be used in the gradient solution to keep the stationary phase in the ClO_4^- form. Of various perchlorate salts, we selected potassium perchlorate for this purpose, because K^+ is one of the best cations for polyether complexation, especially for acyclic polyether complexation, and thus permits the facile control of the retention. UV detection can be utilized to detect the elution of POE oligomers in Triton X-100, and therefore gradient elution is applicable in this case. However, other POE-based surfactants such as Brij 35 do not necessarily involve an effective chromophore. A common method, derivatization with 3,5-dinitrobenzoyl chloride, was used in such cases. Figs. 2–4 show the separation of POE chains contained in Brij 35 and other

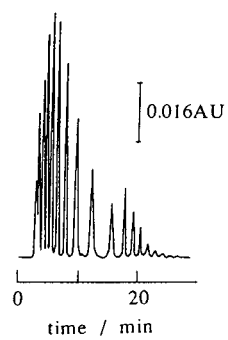

Fig. 1. Separation of POE oligomers contained in Triton X-100. Stationary phase in ClO_4^- form. Sample concentration, 1 mg/ml. Mobile phase, methanol (0–15 min)→5 m*M* $KClO_4$ in methanol (25 min). Detection, UV at 280 nm.

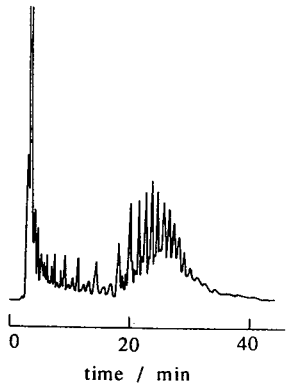

Fig. 2. Separation of POE oligomers contained in Brij 35 [trade-name of POE(23)dodecyl ether]. Stationary phase as in Fig. 1. POE was dinitrobenzylated in advance. Sample concentration, 1 mg/ml. Mobile phase as in Fig. 1. Detection, UV at 250 nm.

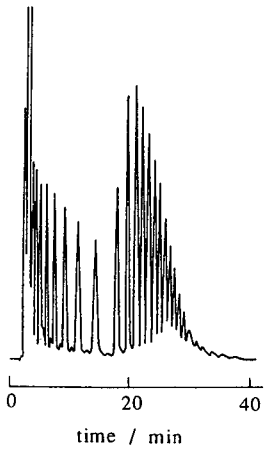

Fig. 4. Separation of POE oligomers contained in POE(20)S. Conditions as in Fig. 2.

POE-based surfactants bearing C_{16} and C_{18} hydrophobic chains.

Some small peaks other than main series of POE chains are visible. Although complete identification was difficult, the comparison of retention times obtained from Figs. 2–4 indicates that these small minor peaks are given by POE chains having different hydrophobic chains. This speculation implies that this separation method can be used for the separation in terms of both hydrophobic and POE chain levels.

Finally, an example of the separation of crown ethers is shown in Fig. 5. Such a separation will not often be needed, but is interesting from a fundamental viewpoint. The selectivity clearly correlates with those of solution complexation with alkylammonium salts; the elution order in DB30C10 < DB24C8 < B15C5 < DB21C7 < DB18C6 < B18C6, and though it was a rough determination, our electrophoretic research [14] indicated that the complexation constants with an ethylammonium ion are 24 < 25 < 25 < 94 < 170 < 370 in the same order. This indicates that

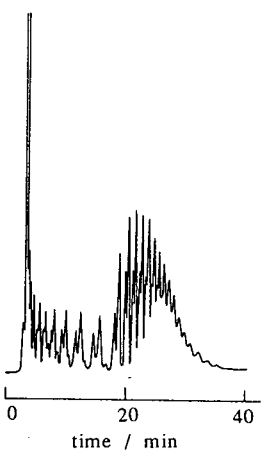

Fig. 3. Separation of POE oligomers contained in POE(20)C. Conditions as in Fig. 2.

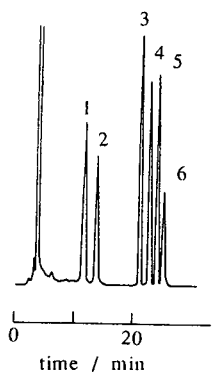

Fig. 5. Separation of crown ethers. Sample concentration, $2.5 \cdot 10^{-5}$ *M*. Mobile phase, methanol (0–25 min)→5 m*M* $KClO_4$ in methanol. Detection, UV at 280 nm. Peaks: 1 = DB30C10; 2 = DB24C8; 3 = B15C5; 4 = DB21C7; 5 = DB18C6; 6 = B18C6. Abbreviations are given in Table I.

the primary retention mechanism is complexation of polyethers with protonated amino groups in the stationary phase. In addition, effects of counter anions should be elucidated, in future work.

Acknowledgements

We thank Tosoh for the gift of the separation column. This work was supported in part by a Grant-in-Aid for scientific research from the Ministry of Education, Science and Culture, Japan.

References

[1] J. Cross, in J. Cross (Editor), *Nonionic Surfactants*, Marcel Dekker, New York, 1987, Ch. 1.
[2] T. Okada, *Anal. Chem.*, 62 (1990) 327.
[3] T. Okada, *Macromolecules*, 23 (1990) 4216.
[4] T. Okada, *J. Chem. Soc., Faraday Trans.*, 87 (1991) 3027.
[5] T. Okada, *J. Chem. Soc., Chem. Commun.*, (1991) 1209.
[6] T. Okada, *Anal. Chim. Acta*, 281 (1993) 85.
[7] W.R. Melander, A. Nahum and Cs. Horváth, *J. Chromatogr.*, 185 (1979) 129.
[8] Cs. Horváth, W.R. Melander and A. Nahum, *J. Chromatogr.*, 186 (1979) 371.
[9] N. Hirata, Y. Tamura, M. Kasai, Y. Yanagihara and K. Noguchi, *J. Chromatogr.*, 592 (1992) 93.
[10] C.A. Chang, *Anal. Chem.*, 55 (1983) 971.
[11] C.J. Pedersen, *J. Am. Chem. Soc.*, 89 (1967) 7017.
[12] R.A. Schwind, T.J. Gilligan and E.L. Cussler, in R.M. Izatt and J.J. Christensen (Editors), *Synthetic Multidentate Macrocyclic Compounds*, Academic Press, New York, 1978, Ch. 6.
[13] R.M. Izatt, J.S. Bradshaw, S.A. Nielsen, J.D. Lamb and J.J. Christensen, *Chem. Rev.*, 85 (1985) 271, and references cited therein.
[14] T. Okada, *Anal. Chem.*, submitted for publication.

ELSEVIER

Journal of Chromatography A, 676 (1994) 361–373

JOURNAL OF CHROMATOGRAPHY A

Thermal field flow fractionation of polytetrahydrofuran

A.C. van Asten, W. Th. Kok, R. Tijssen, H. Poppe*

Laboratory for Analytical Chemistry, University of Amsterdam, Nieuwe Achtergracht 166, 1018 WV Amsterdam, Netherlands

First received 16 February 1994; revised manuscript received 12 April 1994

Abstract

The possibility to fractionate polytetrahydrofuran (PTHF) samples effectively with Thermal Field Flow Fractionation has been investigated. Retention measurements of four standards of different molecular mass were performed in eight organic solvents. When methylethylketone or dioxane were used no retention was found. Highest retention for a given molecular mass was obtained with the solvents toluene and ethylbenzene. However, in ethyl acetate the highest separation speed was observed. Plate height measurements showed that both the thermal and molecular diffusion coefficients of the PTHF standards are very high in ethyl acetate. According to theory, this combination should result in a high separation speed. A baseline separation of two PTHF standards with molecular masses of 67 000 and 282 300 could be obtained in 8 minutes when ethyl acetate was used as the solvent.

1. Introduction

Field Flow Fractionation (FFF) was introduced in the 1960's by Giddings as a fractionation method for polymers and particles [1]. With the use of an external field perpendicular to the laminar flow of a carrier liquid in an open channel, macromolecules are concentrated at one of the channel walls. Due to the high velocity gradient near the channel walls retention and separation are accomplished. A number of different external fields or gradients have been employed to obtain retention in FFF. On the basis of field or gradient used, different subtechniques are distinguished in FFF. The major subtechniques are Thermal, Sedimentation [2], Flow [3] and Electrical [4] FFF.

In Thermal Field Flow Fractionation (ThFFF) a large temperature difference is established across the channel thickness. Due to the so-called thermal diffusion effect, the temperature gradient forces the polymer molecules to concentrate near the cold wall. This selective migration is opposed by molecular diffusion and subsequently retention is determined by the ratio of the thermal and molecular diffusion coefficients. This ratio is also expressed as α/T, where α is the Soret coefficient and T is the temperature.

Although it has been studied for a long time [5], thermal diffusion in liquids is still a largely uncomprehended phenomenon [6]. From ThFFF retention data α/T values can be obtained. Therefore, thermal diffusion coefficients can be determined with ThFFF, provided that molecular diffusion coefficients are measured independently. In this way thermal diffusion coefficients of various polymer–solvent systems have been obtained and with this data the understanding of

* Corresponding author.

0021-9673/94/$07.00
SSDI 0021-9673(94)00381-I

the thermal diffusion phenomenon has increased significantly. For all polymer–solvent systems studied so far it has been found that the magnitude of the thermal diffusion effect is independent of the molecular mass of the polymer [6]. Therefore, the ThFFF fractionation of a given polymer species is based solely on differences in molecular diffusion or mass. Also the branching configuration of the polymer has no influence on the thermal diffusion coefficient [7]. However, the extent of thermal diffusion is strongly dependent on the chemical nature of both the polymer and the solvent [6,8]. Furthermore, it has been found that the thermal diffusion coefficient is temperature dependent [9] and that the thermal diffusion phenomenon is usually not very strong in aqueous solutions [10].

The fact that ThFFF is a powerful tool for the fractionation of synthetic polymers has often been demonstrated [8,11–15]. Recently it has been shown that ThFFF can also be used for particle analysis [16,17]. Due to the fact that adsorption and degradation phenomena are minimal inside the ThFFF channel, polymers of ultra high molecular mass can effectively be analyzed with ThFFF [18]. Furthermore, samples of a broad molecular weight range can be fractionated with sufficient resolution in an acceptable analysis time using temperature programming [19,20]. As retention in ThFFF is also determined by the thermal diffusion coefficient, fractionation occurs not only according to molecular mass but also according to chemical nature [8,21]. Therefore, ThFFF can be used to obtain chemical and structural information of polymer samples [22].

As was stated earlier the extent of thermal diffusion strongly depends on the chemical nature of both the polymer and the solvent. Because a high thermal diffusion coefficient is beneficial for the separation speed, the choice of the solvent is extremely important for the ThFFF analysis of a particular polymer species [8,23]. Giddings et al. [11] demonstrated that PTHF standards could successfully be retained in both tetrahydrofuran (THF) and ethyl acetate. In the work presented here, α/T values for four PTHF standards of different molecular mass have been determined in eight organic solvents, including the two mentioned above. Diffusion measurements are currently being done in order to determine thermal diffusion coefficients for PTHF in the various organic solvents. With the separation of two PTHF standards in a constant run time, the best solvent for the ThFFF analysis of PTHF samples has been found. The effects of polymer concentration and temperature drop on retention have also been investigated.

2. Theory

2.1. Determination of α/T values

The theoretical description of retention in FFF is given in several textbooks and papers [24–26]. The retention ratio, R, defined as the ratio of the void time of the system and the retention time, can be expressed as:

$$R \approx 6\lambda\left[\coth\left(\frac{1}{2\lambda}\right) - 2\lambda\right] \quad (1)$$

where λ is the dimensionless zone thickness, which is equal to the ratio of the mean layer thickness of the concentrated polymer zone and the channel thickness.

The mean layer thickness is defined as the ratio of the molecular diffusion coefficient and the migration velocity towards the accumulation wall caused by the external field or gradient. In ThFFF the migration velocity towards the cold wall, u, is approximated by [27]:

$$u \approx D_T \frac{\Delta T}{w} \quad (2)$$

where D_T is the thermal diffusion coefficient, w is the channel thickness and ΔT is the temperature drop over the channel.

From Eq. (2) it follows that the parameter λ in ThFFF can be approximated by:

$$\lambda \approx \frac{D}{D_T \Delta T} = \frac{1}{\frac{\alpha}{T}\Delta T} \quad (3)$$

where D is the molecular diffusion coefficient, T is the temperature and α is the Soret coefficient.

The retention ratio can easily be measured from the fractogram and with Eqs. (1) and (3) the R value can be converted into a corresponding α/T value. If the molecular diffusion coefficient of the polymer sample in solution is known, the thermal diffusion coefficient can be determined from the α/T value.

However, the use of a temperature gradient in ThFFF leads to theoretical complications. Because both the solvent viscosity and thermal conductivity of an organic solvent are temperature dependent, the ideal flow profile of the carrier liquid and concentration profile of the compressed solute will be disturbed. If empirical relations are used to express the temperature dependence of the solvent viscosity and thermal conductivity, these effects can be theoretically accounted for [28,29]. The temperature dependence of the solvent viscosity, η, can best be expressed as:

$$\frac{1}{\eta} = a_0 + a_1 T + a_2 T^2 + a_3 T^3 \qquad (4)$$

where the coefficients a_i are empirical constants which can be found when viscosity data at various temperatures are fitted according to Eq. (4).

The temperature dependence of the thermal conductivity, κ, is usually described as:

$$\kappa = b_0 + b_1 (T - T_c) \qquad (5)$$

where b_0 and T_c are the thermal conductivity and temperature at the cold wall, respectively.

The parameter b_1, which is frequently denoted as $d\kappa/dT$, is considered to be constant in the working range of the temperature.

The theoretical model describing retention with the use of Eqs. (4) and (5) becomes so complex that a numerical integration routine is necessary to calculate accurate α/T values from the measured retention ratios [29]. In this work the temperature dependence of the solvent viscosity and thermal conductivity has been accounted for. However, the temperature dependence of α/T itself [29] has been ignored and the α/T values have been directly assigned to the temperature in the centre of gravity of the corresponding solute zones [9]. Viscosity and thermal conductivity data were taken from literature to obtain the values of the empirical constants given in Table 1 [9,28,30–32].

2.2. Solvent choice in ThFFF

A time optimization scheme as used in chromatography can also be employed for polymer separation methods [33]. The analysis time, t_a, defined as the time needed to separate two polymer fractions of absolute molecular mass with a given resolution R_s, is determined by the separation requirements and the efficiency and mass selectivity of the fractionation method [8,33]. If the temperature dependence of the solvent viscosity and thermal conductivity is neglected, the analysis time in ThFFF can be expressed as:

$$t_a = \frac{16}{b^2} R_s^2 \left[\frac{M}{\Delta M} \right]^2 \left[\frac{\chi}{R\,(S/b)^2} \right] \frac{w^2}{D} \qquad (6)$$

Table 1
Values of the empirical constants describing the temperature dependence of the solvent viscosity and thermal conductivity

Solvent	a_0	a_1	a_2	$a_3 \times 10^5$	$\kappa(293)$ (W/sK)	$b_1 \times 10^5$ (W/sK^2)
Benzene	6445.30	−80.060	0.2936	−26.477	0.1477	−35.00
Cyclohexane	4081.22	−40.278	0.1094	−2.5481	0.1209	−25.19
Ethyl acetate	3828.96	−49.428	0.1914	−14.130	0.1519	−50.21
Ethylbenzene	2892.92	−35.176	0.1284	−8.3949	0.1322	−24.39
MEK	−227.871	2.8762	−0.01531	12.076	0.1464	−22.68
THF	7622.73	−88.933	0.3344	−32.587	0.1398	−19.89
Toluene	3109.76	−45.318	0.1818	−15.078	0.1320	−27.24

where S is the mass selectivity [11], χ is the λ dependent function in the plate height expression [34], b is a constant approximately equal to 0.5 [6] and M and ΔM are the mean molecular mass and the difference in molecular mass of the two polymer fractions, respectively.

The term $[\chi/(R\,(S/b)^2)]$, which is only a function of the parameter λ, decreases with decreasing λ value. When λ approaches zero, χ can be approximated by $24\lambda^3$ [34], R is equal to 6λ [24] and (S/b) approaches 1 [8]. Under these circumstances Eq. [6] can be simplified to:

$$t_a = \frac{64}{b^2} R_s^2 \left[\frac{M}{\Delta M} \right]^2 \frac{\lambda^2 w^2}{D} = \frac{64}{b^2} R_s^2 \left[\frac{M}{\Delta M} \right]^2 \frac{D}{D_T^2} \left[\frac{w}{\Delta T} \right]^2 \quad (7)$$

The latter expression in Eq. (7) is obtained with the use of Eq. (2). It can be noted that the analysis time is independent of the flow rate of the carrier liquid. The choice of the solvent will influence the thermal and molecular diffusion coefficients [6] and, thereby, the analysis time. For the ThFFF analysis of a particular polymer species the solvent for which the shortest analysis time (i.e. highest separation speed) is obtained (for given separation requirements, temperature gradient and molecular mass range) should be used.

To find the optimum solvent for the ThFFF analysis of PTHF samples, two PTHF standards have been separated in a constant analysis time (or rather a constant run time [23]) in the various organic solvents. The fractograms are given in the Results and Discussion section. By adjusting the flow rate the analysis time has been kept the same for each solvent. In this way differences in separation speed are indicated by differences in resolution. The solvent for which highest resolution is found should be used for the ThFFF analysis of PTHF samples. Mathematically this approach can be visualized by rewriting Eq. (7) to:

$$R_s = \frac{b}{8} \sqrt{t_a} \frac{\Delta M}{M} \frac{\sqrt{D}}{\lambda w} = \frac{b}{8} \sqrt{t_a} \frac{\Delta M}{M} \frac{D_T}{\sqrt{D}} \frac{\Delta T}{w} \quad (8)$$

In earlier work we concluded that using the solvent in which lowest λ values were found for a given molecular mass and temperature drop, would lead to an optimum ThFFF separation performance [8]. Although this conclusion will usually be valid, some extra considerations are in order. Eq. (8) demonstrates that the resolution at constant analysis time is not only influenced by λ but also by D. A high value for the latter parameter can therefore compensate for an unfavourable λ value, and in this way a high separation speed still can be obtained. This is demonstrated in Fig. 1, where the resolution is plotted as a function of the molecular diffusion coefficient for various λ values. Fig. 1 is generally valid because it is based on Eq. (6) rather than on Eq. (8). As can be seen from this figure, a higher λ value can still lead to the same or even better resolution in a constant analysis time, when the molecular diffusion coefficient and, therefore, also the thermal diffusion coefficient are very high.

3. Experimental

3.1. Instrumentation

The T100 Thermal FFF system used in this work was obtained from FFFractionation (Salt Lake City, UT, USA). The experimental set-up for the ThFFF measurements has been described in detail previously [8,23]. A channel thickness of 127 μm was used. The channel length and breadth were 46 cm and 1.6 cm, respectively. The void volume of the channel was equal to 0.75 ml. The eluting polymer zones were detected by means of an Evaporative Light Scattering Detector (Model 2A, Varex, Burtonsville, MD, USA). The outlet of the channel was connected to the detector with the use of a fused-silica capillary with an internal diameter of 100 μm, an external diameter of 360 μm and a length of 1 m (Polymicro Technologies, Phoenix, AZ, USA). In this way a sufficiently large back pressure was created to avoid boiling of the organic solvents inside the ThFFF channel.

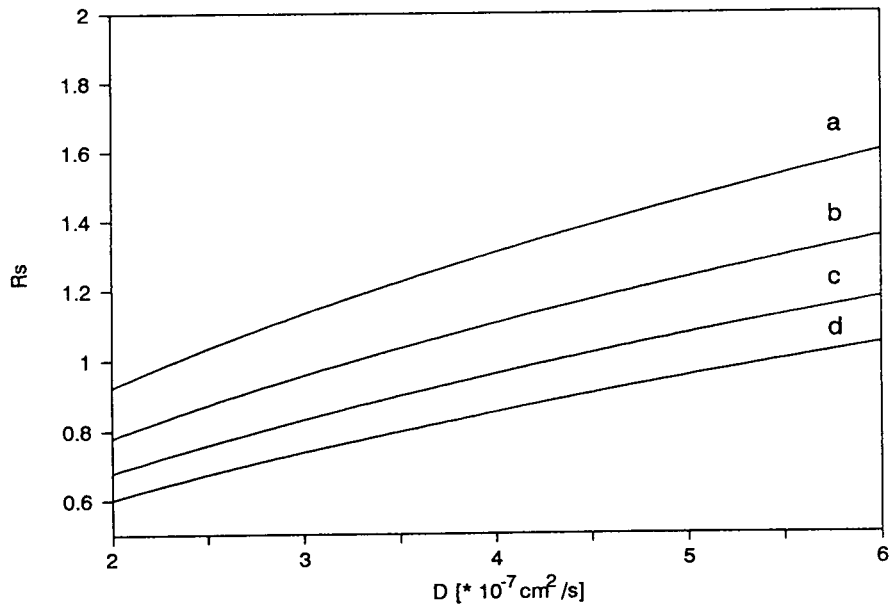

Fig. 1. Resolution at constant analysis time for the separation of two polymer fractions with a mean molecular mass of 175 000 and a difference in molecular mass of 100 000, with $w = 127$ μm, $t_a = 20$ min, and $b = 0.5$. (a) $\lambda = 0.05$; (b) $\lambda = 0.06$; (c) $\lambda = 0.07$; (d) $\lambda = 0.08$

Furthermore, this set-up ensured that the dead volume was negligibly small (0.008 ml).

The α/T measurements of the PTHF standards in the various organic solvents were performed with a temperature drop of 40 K and a cold wall temperature of 298 K. Due to the low retention of the PTHF standards in cyclohexane, a temperature drop of 80 K ($T_c = 302$ K) was used in this case. For all retention measurements the flow rate was set at 0.2 ml/min and a stop flow period of 5 min was employed after injection to allow relaxation. The concentration of the injected solutions of the PTHF standards was usually equal to 0.25 mg/ml. However, for the PTHF standard with a molecular mass of 547 000 the polydispersity was quite high and as a result a higher concentration (0.5 or 0.75 mg/ml) had to be used for this standard. The void time was determined by adding a polystyrene standard with a molecular mass of 580 (0.05 mg/ml) to the samples. For some of the experiments displayed in the figures different experimental conditions have been used, as specified in the corresponding legends.

For the plate height measurements the linear solvent velocities were determined from the void times and the channel length. The channel length was corrected for the distance traversed prior to the relaxation process. For the PTHF standard with a molecular mass of 282 300 a sample concentration of 0.5 mg/ml was used to ensure a sufficiently high signal-to-noise ratio for an accurate determination of the peak width. Sigma values were determined by fitting the signal to a Gaussian curve using the FFFractionation analysis software (version 2.0). In this way also the peak symmetry could be checked.

3.2. Materials

All solvents were of analytical-reagent grade and were filtered (type FH, 0.5 μm, Millipore, Bedford, MA, USA) prior to use. Cyclohexane, dioxane, ethylbenzene and methylethylketone (MEK) were obtained from Merck (Darmstadt, Germany), tetrahydrofuran (THF) and toluene from Janssen Chimica (Geel, Belgium), benzene from Baker (Deventer, The Netherlands) and

ethyl acetate from Lamers and Pleuger ('s Hertogenbosch, The Netherlands). The polystyrene standard (PS) used in this work ($M_r = 580$, $\mu < 1.18$) was supplied by Merck, the PTHF standards ($M_r = 67\,000$, $\mu = 1.08$; $M_r = 99\,000$, $\mu = 1.08$; $M_r = 282\,300$, $\mu = 1.08$; $M_r = 547\,000$, $\mu = 1.35$) by Polymer Laboratories (Church Stretton, Shropshire, UK).

4. Results and discussion

In Table 2 the α/T values measured for the PTHF standards in the various organic solvents are given. The temperature dependence of the solvent viscosity and thermal conductivity was accounted for. The α/T values have been assigned to the temperature in the centre of gravity of the concentrated polymer zones. As the molecular diffusion coefficient decreases with increasing molecular mass, the zone thickness of the concentrated polymer zone is smaller for the standards of a high molecular mass. Because a decrease in zone thickness corresponds to a decrease in T_{cg}, the temperature in the centre of gravity of the solute zone decreases with increasing molecular mass of the PTHF standard. Since in the different solvents the PTHF standards possess different molecular and thermal diffusion coefficients, the observed T_{cg} was also dependent on the solvent used. A high α/T value corresponds to a low λ value and, therefore, to a temperature in the centre of gravity of the solute zone which is almost equal to the cold wall temperature. These considerations do not, of course, apply for the retention measurements of the PTHF standards in cyclohexane, which were performed at a higher temperature drop due to the fact that only very low retention was found in this solvent. No α/T values are given for the PTHF standards in either dioxane or MEK. The reason for this is that insufficient retention was found for the standards in these two solvents, even at a temperature drop of 80 K. The fact that for polystyrene in MEK a very high thermal diffusion coefficient is found [6], is in sharp contrast with these findings and demonstrates the strong influence of the chemical nature of the polymer on the thermal diffusion phenomenon.

For the determination of the α/T values the concentration of the injected samples of the PTHF standards was usually equal to 0.25 mg/ml. Only for the PTHF standard with a molecular mass of 547 000 a higher sample concentration of 0.5 or 0.75 mg/ml was used because of the higher polydispersity of this standard. Because inside the ThFFF channel the polymer zones are compressed into thin layers at the cold wall, in which the concentration is much higher than the concentration of the injected sample,

Table 2
α/T values for PTHF standards in the various organic solvents

Solvent	Molecular mass of the PTHF standards							
	67 000		99 000		282 300		547 000	
	α/T (K^{-1})	T_{cg} (K)	α/T (K^{-1})	T_{cg} (K)	α/T (K^{-1})	T_{cg} (K)	α/T (K^{-1})	T_{cg} (K)
Benzene	0.116	306	0.151	305	0.272	302	0.436	300
Cyclohexane	0.061	318	0.071	316	0.132	310	0.213	307
Ethyl acetate	0.121	307	0.151	306	0.263	303	0.443	301
Ethylbenzene	0.147	306	0.183	305	0.321	302	0.604	301
THF	0.074	311	0.093	310	0.175	306	0.321	303
Toluene	0.136	306	0.179	305	0.316	302	0.537	301

$w = 127$ μm, $\Delta T = 40$ K or 80 K (cyclohexane), $T_c = 299$ K (ethyl acetate, ethylbenzene and toluene), $T_c = 298$ K (benzene), $T_c = 300$ K (THF), $T_c = 302$ K (cyclohexane). Each α/T value is the average of three different measurements, the relative standard deviation is in the order of 2–4%

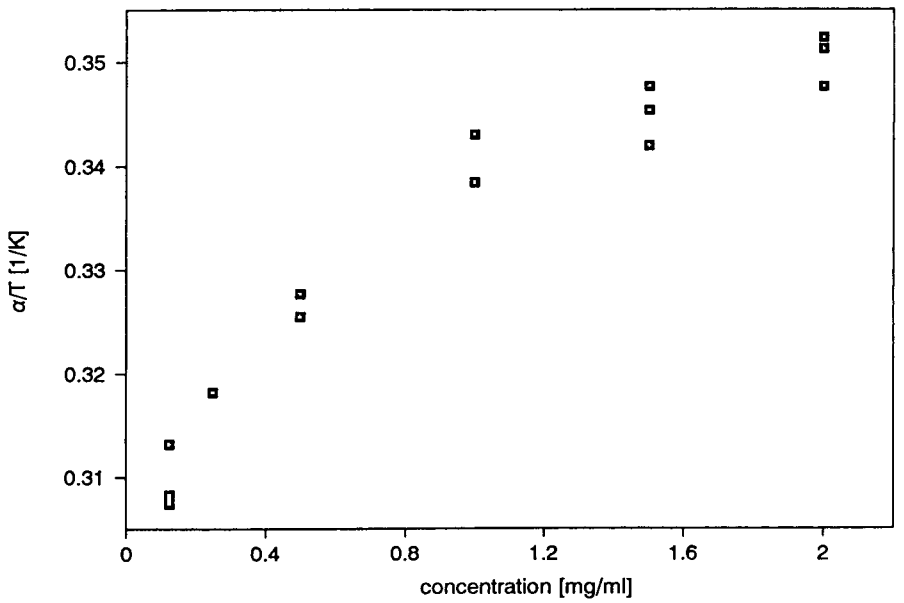

Fig. 2. The influence of the polymer concentration on the α/T value of PTHF 282 300 in toluene, with $w = 127$ μm, $\Delta T = 40$ K, $T_c = 298$ K, t_0 = PS 580 (0.05 mg/ml), flow = 0.3 ml/min, and stop-flow time = 3 min.

concentration overloading can be a severe problem in ThFFF [35,36]. In Fig. 2 the effect of the sample concentration on the measured α/T value is demonstrated. For this system (PTHF M_r = 282 300 in toluene with $\Delta T = 40$ K) the λ value is approximately equal to 0.08. This corresponds initially to a polymer concentration at the cold wall which is more than 12 times higher than the concentration of the injected sample displayed on the x-axis of Fig. 2 [36]. As was also found in previous work [8], retention and thus α/T increased with increasing polymer concentration. This effect cannot be explained by the concentration dependence of the molecular diffusion coefficient because molecular diffusion tends to increase with increasing polymer concentration [37]. The increase in retention with increasing polymer concentration is probably caused by the increasing viscosity in the compressed polymer zone [36]. The concentration profile will lead to a viscosity gradient which will skew the velocity profile of the carrier liquid near the cold wall. As a result the migration velocity will be lower than expected and an apparent increase in retention is observed. Fig. 2 demonstrates that concentration effects are visible even when the polymer concentration is well below 1 mg/ml. Even for the lowest sample concentrations a concentration dependence of α/T was found. For polymer concentrations higher than 1 mg/ml the concentration effect appears to level off and for these solutions a deviation of approximately 12% in the α/T values was found compared to the values obtained at the lowest concentration (0.125 mg/ml).

In Fig. 3 the λ values of the PTHF standards are plotted as function of $M^{-\frac{1}{2}}$ for three solvents. The correlation between the molecular diffusion coefficient and the molecular mass is often expressed according to the empirical relationship $D = A \cdot M^{-b}$, where A and b are constants [6]. The constant b is approximately equal to 0.5 for most polymer–solvent systems. With the use of Eq. (3) it can be seen that the linear relationship (which was found in all solvents) displayed in Fig. 3, indicates that also for PTHF in the various solvents the thermal diffusion coefficient appears to be independent of the molecular mass of the polymer. However, molecular diffusion coefficients should be determined independently

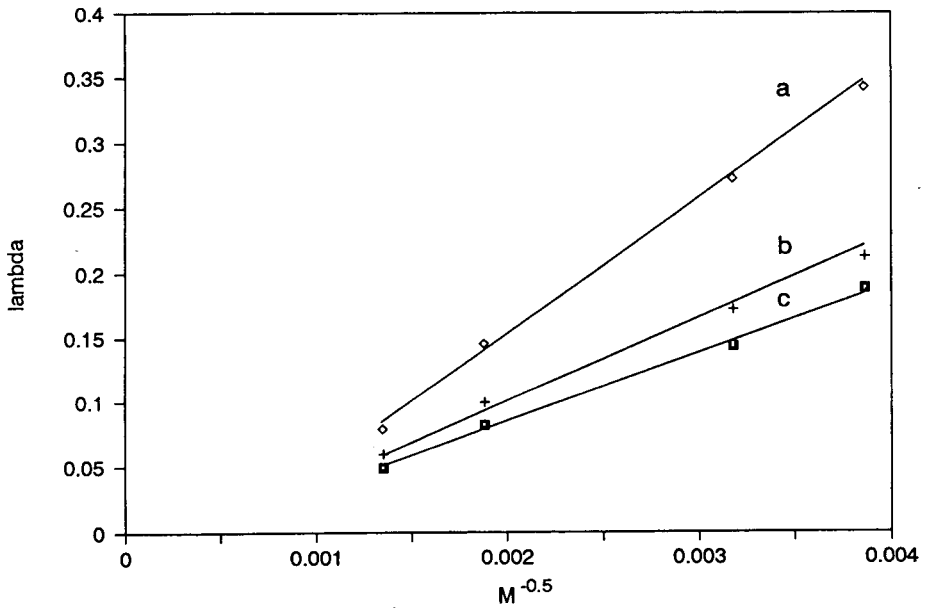

Fig. 3. λ Values of the PTHF standards as function of $M^{-\frac{1}{2}}$. Conditions as given in Table 2. (a) THF; (b) ethyl acetate; (c) toluene.

to verify this conclusion. Just as was found for polybutadiene [8], relatively high λ values (low retention) of the PTHF standards were obtained in THF, whereas highest retention was found in toluene and ethylbenzene.

For the PTHF standard with a molecular mass of 282 300 also the effect of the temperature drop on the λ value in toluene was investigated. The results, given in Fig. 4, are in good agreement with Eq. (3). As was expected a linear relationship was found between the λ value and the reciprocal value of the temperature drop. These results indicate that the measurements are free of systematic errors caused by the set-up. This was also confirmed by the fact that the retention ratio was independent of the flow rate of the carrier liquid.

Next, two PTHF standards with molecular masses of 67 000 and 282 300 were separated in the various organic solvents at a constant run time [23] and temperature gradient. The results are displayed in Fig. 5. The fractionation of the two standards in cyclohexane is not given in Fig. 5 due to the very poor resolution found in this solvent. Going from fractogram a to e, the λ value for a given molecular mass and temperature drop decreases. As a lower λ value corresponds to higher retention, the flow rate had to be increased going from fractogram a to e in order to keep the run time constant. To a first approximation the separation speed is expected to increase with decreasing λ value [see Eq. (8)]. From this point of view the resolution at constant run time is expected to increase going from THF to ethylbenzene and toluene. Although in general this trend can be observed in Fig. 5, two striking features attract attention.

Firstly, it can be seen that, although λ values for a given molecular mass and temperature drop are comparable for PTHF in ethylbenzene and toluene, a higher resolution and thus separation speed was obtained using the latter solvent. The same effect was also found for the ThFFF fractionation of polybutadiene [8]. As the λ values are comparable also the α/T values are identical, and therefore it can be stated that the ratio of D and D_T for a given PTHF standard is the same in toluene and ethylbenzene. However, the individual values of the molecular and thermal diffusion coefficients can still be different in the two solvents. Without the loss of retention, high molecular diffusion (and thus high thermal

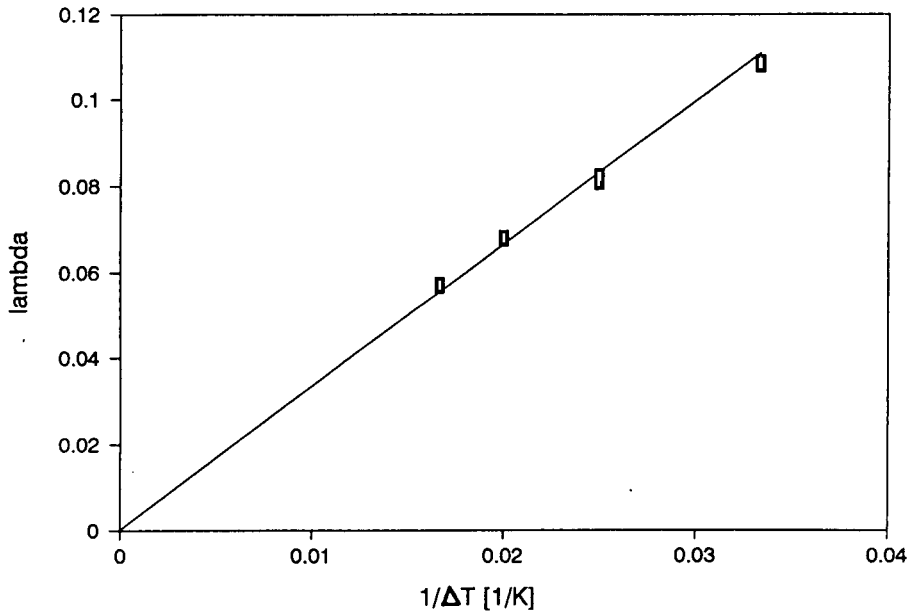

Fig. 4. The effect of ΔT on the λ value for PTHF 282 300 (0.25 mg/ml) in toluene, with $w = 127$ μm, t_0 = PS 580 (0.05 mg/ml), flow = 0.2 ml/min, stop-flow time = 5 min, and $\Delta T = 60$ K ($T_{cg} = 300$ K); $\Delta T = 50$ K ($T_{cg} = 301$ K); $\Delta T = 40$ K ($T_{cg} = 299$ K); $\Delta T = 30$ K ($T_{cg} = 299$ K).

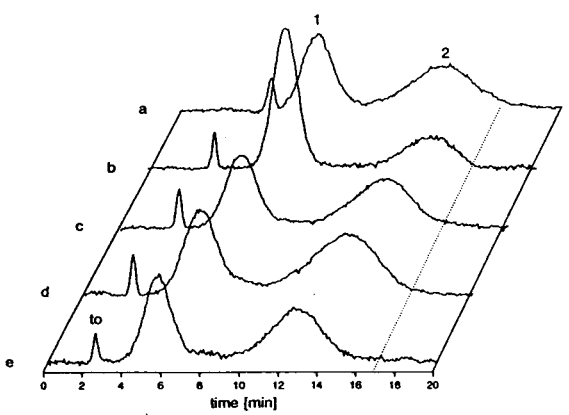

Fig. 5. Separation of a PTHF standard with M = 67 000 (0.33 mg/ml) (1) and a PTHF standard with M = 282 300 (0.5 mg/ml) (2) in various solvents performed at a constant analysis time of 17 min, with $w = 127$ μm, $\Delta T = 80$ K, $T_c = 302$ K, stop-flow time = 2 min, and t_0 = PS 580 (0.03 mg/ml). (a) THF, flow = 0.16 ml/min; (b) ethyl acetate, flow = 0.22 ml/min; (c) benzene, flow = 0.25 ml/min; (d) ethylbenzene, flow = 0.3 ml/min; (e) toluene, flow = 0.3 ml/min.

diffusion) is beneficial for the separation speed in ThFFF [8]. From fractograms d and e in Fig. 5 it can therefore be concluded that both D and D_T for a PTHF standard of a given molecular mass must be lower in ethylbenzene than in toluene. Consequently, it is better to use the latter of the two solvents for the ThFFF analysis of this polymer species.

Secondly, Fig. 5 demonstrates that highest separation speed for the ThFFF fractionation of PTHF samples is obtained when ethyl acetate is used. Although relatively low retention was found for the PTHF standards in this solvent, the highest resolution was obtained for fractogram b. The results displayed in Fig. 5 indicate that for an optimal ThFFF analysis of PTHF samples ethyl acetate is the best solvent to use. As was already explained in the theoretical part, this must be caused by the fact that PTHF standards posses a high thermal diffusion coefficient combined with an even higher molecular diffusion coefficient when they are dissolved in ethyl acetate.

Under normal working conditions the plate

height H, in ThFFF, can be approximated by [13]:

$$H = H_{pd} + \frac{\chi w^2}{D} v \quad (9)$$

where v is the mean linear velocity of the carrier liquid and H_{pd} is the apparent contribution to the plate height caused by the molecular mass distribution of the polymer sample.

Therefore, measuring the plate height at various fluid velocities in principle provides a means to determining both the molecular diffusion coefficient and the polydispersity [13]. In combination with retention measurements also the magnitude of the thermal diffusion coefficient can be estimated.

For the PTHF standard with a molecular mass of 282 300, plate height measurements were performed at various flow rates in THF, benzene, toluene and ethyl acetate. The results are given in Fig. 6. In good agreement with Eq. (9), a linear increase in system dispersion was found with increasing linear solvent velocity. Fig. 6 also demonstrates that with the use of ethyl acetate the lowest plate heights were obtained. For PTHF in ethyl acetate a relatively high λ value was found, which corresponds to a high χ value. Therefore, these low plate heights can only be caused by a high molecular diffusion coefficient.

As was previously mentioned, molecular and thermal diffusion coefficients can be determined from the results in Fig. 6 and Table 2. In this way for PTHF $M_r = 282\,300$ in ethyl acetate a D value of $6.1 \cdot 10^{-7}$ cm^2 s^{-1} and a D_T value of $1.7 \cdot 10^{-7}$ cm^2 s^{-1} K^{-1} was found, whereas for the same standard dissolved in toluene a D value of $2.7 \cdot 10^{-7}$ cm^2 s^{-1} and a D_T value of $0.9 \cdot 10^{-7}$ cm^2 s^{-1} K^{-1} was obtained. This clearly illustrates how for PTHF in ethyl acetate the highest separation speed is obtained, despite the relatively low retention.

The values for D and D_T determined in this way are not very accurate. Firstly, it is known that with the use of an Evaporative Light Scattering Detector a non-linear calibration curve is obtained. With an increase in polymer concentration a more than proportional increase in signal is usually observed [38]. As a result the

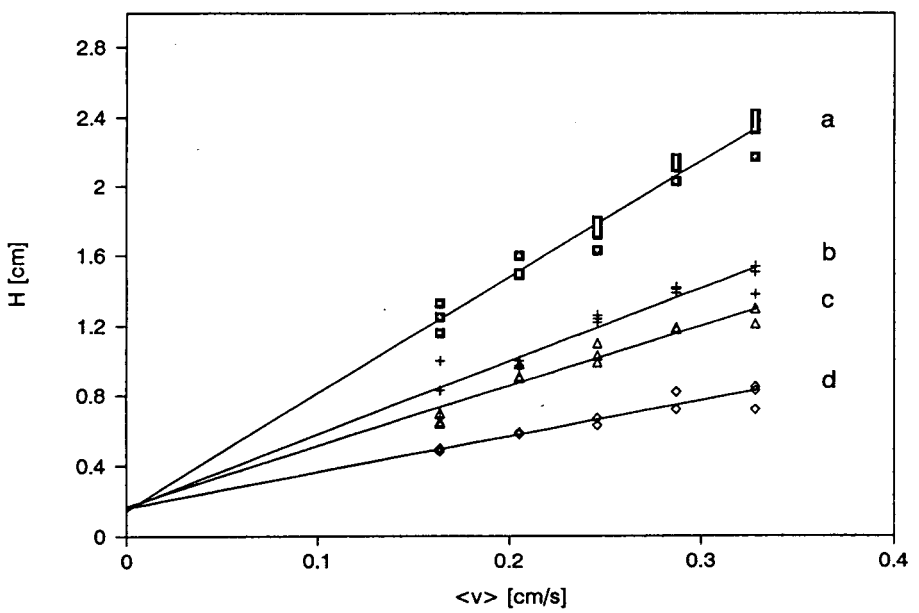

Fig. 6. Plate height as function of the mean linear velocity of the carrier liquid for a PTHF standard with $M_r = 282\,300$ (0.5 mg/ml) in various solvents, with $w = 127$ μm, $\Delta T = 40$ K, $T_c = 298$ K, stop-flow time = 2 min, and t_0 = PS 580 (0.1 mg/ml). (a) THF; (b) benzene; (c) toluene; (d) ethyl acetate.

measured peak width and, therefore, the plate height will be smaller than the actual dispersion of the polymer zone. Secondly, the χ value was determined from the λ value using the relationship given by Giddings et al. [34]. Therefore, no correction was made for the temperature dependence of the solvent viscosity and thermal conductivity and as a result systematically lower χ values have been used [24]. Although the two effects mentioned above counteract each other when the molecular diffusion coefficient is determined from the plate height data, the results must be considered with great care. The large difference in the values found for the diffusion coefficient of the PTHF standard in the two solvents should be verified by an independent technique (e.g. Light Scattering). The results displayed in Figs. 5 and 6 and Table 2 show only qualitatively that the thermal and molecular diffusion coefficients of the PTHF standard are highest in ethyl acetate.

Figs. 5 and 6 clearly demonstrate that for the ThFFF analysis of PTHF samples ethyl acetate is the best solvent to use. Therefore, the maximum separation speed for a given molecular mass range and temperature gradient is fully determined. Even in the most appropriate solvent, separation speeds can differ strongly for different polymer species. For the ThFFF analysis of polybutadiene it is best to use toluene as solvent (n.b. polybutadiene samples do not dissolve in ethyl acetate). However, even with this solvent the separation speed is fairly low and as a result a long analysis time is necessary to obtain a good fractionation [8]. Because of the high molecular and thermal diffusion of PTHF samples in ethyl acetate, a very high maximum separation speed is obtained in this case. This is demonstrated in Fig. 7 with the baseline separation in 8 min of two PTHF standards (M_r = 67 000 and 282 300) in ethyl acetate performed under a reasonable temperature gradient.

One of the objectives of a polymer fractionation method is the accurate determination of the molecular mass distribution of polydisperse materials. With adequate calibration standards and a deconvolution procedure to remove system dispersion from the observed signal, ThFFF can

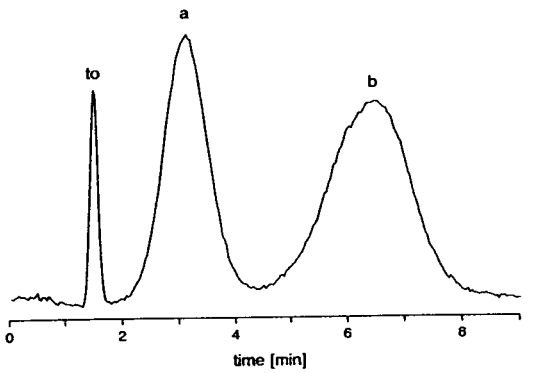

Fig. 7. High speed ThFFF separation of two PTHF standards with (a) M_r = 67 000 (0.25 mg/ml) and (b) M_r = 282 300 (0.5 mg/ml) in ethyl acetate, with w = 127 μm, ΔT = 80 K, T_c = 303 K, flow = 0.5 ml/min, stop-flow time = 2 min, and t_0 = PS 580 (0.05 mg/ml).

be used effectively to obtain such information [39]. When ThFFF is used in combination with a concentration dependent detector and a viscosity detector, molecular mass distributions can even be measured without the need for calibration [15]. However, as was demonstrated by Kirkland and Rementer [15], concentration overloading can be very important in this application. As a result of the polydispersity often a very broad signal is observed for polydisperse materials. This leads to a low signal-to-noise ratio in the fractogram and for an accurate determination of the molecular mass distribution high sample concentrations have to be injected. As was mentioned previously, retention tends to increase with increasing polymer concentration and as a result a systematic error in the determination of the molecular mass distribution can be made. The polydispersity of the PTHF standard with a molecular mass of 547 000 is quite high (μ = 1.35) and as a result broad signals were obtained for this standard. In Fig. 8 the effect of the sample concentration for polydisperse materials is demonstrated with the fractionation of PTHF M_r = 547 000 in toluene ($\lambda \approx$ 0.05). Injection of higher concentrations resulted in a shift of the signal to higher retention, which will lead to a determination of a mean molecular mass which will be systematically too high. Toluene was used as the solvent because lowest

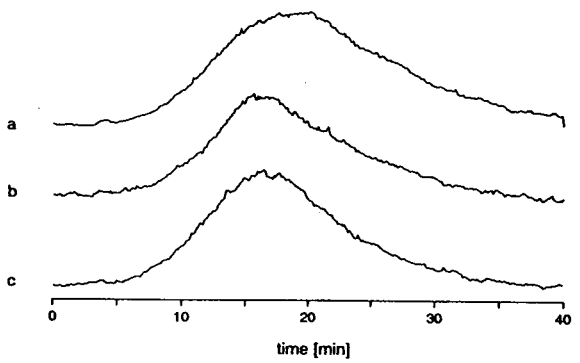

Fig. 8. Effect of polymer concentration on the ThFFF fractionation of a broad PTHF standard with $M_r = 547\,000$ ($\mu = 1.35$) in toluene, with $w = 127\ \mu m$, $\Delta T = 40$ K, $T_c = 299$ K, flow = 0.2 ml/min, and stop-flow time = 5 min. Concentration of injected sample is 5 mg/ml for (a), 2 mg/ml for (b) and 1 mg/ml for (c).

λ values for PTHF were obtained for this combination. Note that the use of ethyl acetate, the optimum solvent for the analysis of PTHF samples in respect to separation speed, also has the advantage that concentration overloading will be less because the compression of the polymer zones at the cold wall is not that strong due to the relatively low retention found for PTHF samples in this solvent. No accurate molecular mass distribution could be obtained from Fig. 8 in combination with the retention data of the other PTHF standards. This was caused by the fact that the other three standards were all of lower molecular mass and calibration with these standards resulted in a large error due to extrapolation.

5. Conclusions

ThFFF can be used effectively for the fractionation and analysis of PTHF samples. For a given temperature gradient and molecular mass, highest retention for the PTHF standards was found when ethylbenzene or toluene were used as the solvents. No retention was observed when the standards were dissolved in dioxane or MEK. The retention measurements of the PTHF standards in the various organic solvents indicated that the thermal diffusion coefficient is independent of the molecular mass of the polymer, as has been observed for other polymer species.

Although only moderate retention for the PTHF standards was measured when ethyl acetate was used as the carrier liquid, highest separation speed was observed when the standards were dissolved in this solvent. Therefore, for the ThFFF analysis of PTHF samples ethyl acetate is the best solvent to use. These results show that low retention for a given molecular mass and temperature gradient does not always correspond to a low separation speed. If low retention is caused by a very high molecular diffusion coefficient, still a very efficient ThFFF fractionation is possible.

Even for polymer concentrations well below 1 mg/ml an increase in retention was observed with increasing sample concentration. Especially when molecular mass distributions of polydisperse materials have to be determined with ThFFF, care should be taken to avoid systematic errors due to concentration effects. The use of ethyl acetate as the carrier liquid for the ThFFF analysis of PTHF samples has the additional advantage that concentration overloading is not very profound due to the relatively low retention found in this solvent.

Acknowledgments

This research was supported by AKZO Research Laboratories (Arnhem, The Netherlands) and Shell Research BV (Amsterdam, The Netherlands).

Symbols

a_i	empirical constants relating solvent viscosity to temperature
b_i	empirical constants relating solvent thermal conductivity to temperature
A,b	empirical constants relating diffusion to molecular mass
D	diffusion coefficient ($m^2\ s^{-1}$)

D_T thermal diffusion coefficient ($m^2\ s^{-1}\ K^{-1}$)
H plate height (m)
H_{pd} polydispersity plate height contribution (m)
M (mean) molecular mass ($g\ mol^{-1}$)
R retention ratio
R_s resolution
S selectivity
T temperature (K)
t_0 unretained time (s)
t_a analysis time (s)
T_c cold wall temperature (K)
u field induced velocity of the polymer molecules in the direction of the accumulation wall ($m\ s^{-1}$)
v mean linear velocity of the carrier liquid ($m\ s^{-1}$)
w channel thickness (m)
α Soret coefficient
ΔT temperature drop (K)
η solvent viscosity (Pa s)
κ solvent thermal conductivity ($J\ s^{-1}\ m^{-1}\ K^{-1}$)
λ dimensionless zone thickness
μ polydispersity
χ λ dependent function in the non-equilibrium term of the plate height equation

References

[1] J.C. Giddings, *Sep. Sci.*, 1 (1966) 123.
[2] M.H. Moon and J.C. Giddings, *Anal. Chem.*, 64 (1992) 3029.
[3] M.A. Benincasa and J.C. Giddings, *Anal. Chem.*, 64 (1992) 790.
[4] K.D. Caldwell and Y.S. Gao, *Anal. Chem.*, 65 (1993) 1764.
[5] H.J.V. Tyrell, *Diffusion and Heat Flow in Liquids*, Butterworths, London, 1961
[6] M.E. Schimpf and J.C. Giddings, *J. Polym. Sci.*, B, 27 (1989) 1317.
[7] M.E. Schimpf and J.C. Giddings, *Macromolecules*, 20 (1987) 1561.
[8] A.C. van Asten, E. Venema, W.Th. Kok and H. Poppe, *J. Chromatogr.*, 644 (1993) 83–94.
[9] S.L. Brimhall, M.N. Myers, K.D. Caldwell, J.C. Giddings, *J. Polym. Sci., Polym. Phys. Ed.*, 23 (1985) 2443.
[10] J.J. Kirkland and W.W. Yau, *J. Chromatogr.*, 353 (1986) 95.
[11] J.C. Giddings, M.N. Myers and J. Janča, *J. Chromatogr.*, 186 (1979) 37.
[12] M. Martin and R. Reynaud, *Anal. Chem.*, 52 (1980) 2293.
[13] M.E Schimpf, M.N. Myers and J.C. Giddings, *J. Appl. Polym. Sci.*, 33 (1987) 117.
[14] J.J. Kirkland, S.W. Rementer and W.W. Yau, *J. Appl. Polym. Sci.*, 38 (1989) 1383.
[15] J. Kirkland and S.W. Rementer, *Anal. Chem.*, 64 (1992) 904.
[16] G. Liu and J.C. Giddings, *Anal. Chem.*, 63 (1991) 296.
[17] G. Liu and J.C. Giddings, *Chromatographia*, 34 (1992) 483.
[18] Y.S. Gao, K.D. Caldwell, M.N. Myers and J.C. Giddings, *Macromolecules*, 18 (1985) 1272.
[19] J.C. Giddings, L.K. Smith and M.N. Myers, *Anal. Chem.*, 48 (1976) 1587.
[20] J.J. Kirkland and W.W. Yau, *J. Chromatogr.*, 499 (1990) 655.
[21] J.J. Gunderson and J.C. Giddings, *Macromolecules*, 19 (1986) 2618.
[22] M.E. Schimpf and J.C. Giddings, *J. Polym. Sci.*, B, 28 (1990) 2673.
[23] A.C. van Asten, G. Stegeman, W. Th. Kok, H. Poppe and R. Tijssen, *Anal. Chem.*, submitted for publication.
[24] J.C. Giddings, *Unified Separation Science*, Wiley, New York, 1991.
[25] J.C. Giddings, *J. Chem. Education*, 50 (1973) 667–669.
[26] J. Janča and K. Kleparnik, *J. Liq. Chromatogr.*, 634 (1993) 149.
[27] J.C. Giddings, M.N. Myers, G.C. Liu and M. Martin, *J. Chromatogr.*, 142 (1977) 23.
[28] J.J. Gunderson, K.D. Caldwell and J.C. Giddings, *Sep. Sci. Technol.*, 19 (1984) 667.
[29] A.C. van Asten, H.F.M. Boelens, W.Th. Kok, H. Poppe, P.S. Williams and J.C. Giddings, *Sep. Sci. Technol.*, 29 (1994) 513.
[30] R.C Reid, J.M. Prausnitz and T.K. Sherwood, *Properties of Gases and Liquids*, McGraw-Hill, New York, 3rd ed., 1977.
[31] D.S. Viswanath and G. Natarajan, *Databook on the Viscosity of Liquids*, Hemisphere Publication Co., New York, 1990.
[32] J.C. Giddings, K.D. Caldwell and M.N. Myers, *Macromolecules*, 9 (1976) 108.
[33] J.C. Giddings, M. Martin and M.N. Myers, *J. Chromatogr.*, 158 (1978) 419.
[34] J.C. Giddings, Y.H. Yoon, K.D. Caldwell, M.N. Myers and M.E. Hovingh, *Sep. Sci.*, 10 (1975) 447.
[35] M.E. Schimpf, *J. Chromatogr.*, 517 (1990) 405.
[36] K.D. Caldwell, S.L. Brimhall, Y. Gao and J.C. Giddings, *J. Appl. Pol. Sci.*, 36 (1988) 703.
[37] W. Mandema and H. Zeldenrust, *Polymer*, 18 (1977) 835
[38] H. Stolyhwo, H. Colin, M. Martin and G. Guiochon, *J. Chromatogr.*, 288 (1984) 253.
[39] M.E. Schimpf, P.S. Williams and J.C. Giddings, *J. Appl. Polym. Sci*, 37 (1989) 2059.

ELSEVIER

Journal of Chromatography A, 676 (1994) 375–388

JOURNAL OF CHROMATOGRAPHY A

Comparison of four methods for the determination of polycyclic aromatic hydrocarbons in airborne particulates ☆

C. Escrivá*, E. Viana, J.C. Moltó, Y. Picó, J. Mañes

Laboratori de Toxicologia, Facultat de Farmàcia, Universitat de València, Avd. Vicent Andrés Estellés s/n, 46100 Burjassot (València), Spain

First received 6 December 1993; revised manuscript received 14 March 1994

Abstract

High-performance liquid chromatography (HPLC) with ultraviolet and fluorescence detection and capillary gas chromatography (GC) with flame ionization and mass spectrometric (MS) detection were used to determine nineteen polycyclic aromatic hydrocarbons (PAHs) in airborne particulates. Sixteen of them are included in the prioritary pollutants list of the US Environmental Protection Agency. Five C_{18}-bonded silica HPLC columns and five GC capillary columns were checked to select the best conditions for the PAH mixtures. Samples were extracted by adding an organic solvent and sonication. The recoveries obtained were >75%. These results are compared with those obtained using Soxhlet extraction. The method was applied to the determination of PAHs at five sampling sites in the city of Valencia during 1 week. The results confirm that the best detection limits are obtained by HPLC–fluorescence, which is also the simplest, shortest and most economical method. In spite of its high maintenance cost, GC–MS in the single-ion monitoring mode is also suitable for the determination of PAHs in real samples using a low-volume system.

1. Introduction

Polycyclic aromatic hydrocarbons (PAHs) are ubiquitous in atmospheric particulates, and with lead constitute the principal pollutants of urban areas. There are two kinds of systems to collect the particulates, high- and low-volume collection bubbler systems. Low-volume systems are more frequently used but the low volume of sample (*ca.* 2 m^3 during a sampling period of 24 h) requires a technique with very high sensitivity and makes the determination of PAHs in atmospheric particulate matter an important analytical problem [1,2].

The analysis of the purified extracts can be carried out using gas and liquid chromatographic methods with different detection devices to achieve simultaneously high resolution, sensitivity and selectivity [3,4].

High-performance liquid chromatography (HPLC) has been the selected technique for PAH determination. Ultraviolet (UV) absorption and fluorescence spectrometry provide sensitive and selective detection for PAHs in HPLC [5–8]. However, not all C_{18} stationary phases provide the same selectivity for PAHs owing to the influence of factors such as the bonded-phase type, silica substrate characteris-

* Corresponding author.

☆ Presented at the *22nd Annual Meeting of the Spanish Chromatography Group, Barcelona, October 20–22, 1993.*

0021-9673/94/$07.00
SSDI 0021-9673(94)00256-9

tics, alkyl chain length and C_{18} ligand density or selectivity [9,10].

Gas chromatography (GC) with capillary columns is also a method of choice for the separation and analysis of complex PAH mixtures with moderate to low molecular masses. Improvements in GC stationary phases have contributed to this [11,12], and a recent comparison of four high-temperature GC columns showed their usefulness in separating PAHs with a molecular mass of 328 [13]. GC with a capillary column has been used in combination with flame ionization detection (FID) [14,15]. However, the use of a quadrupole mass spectrometer operated in single-ion monitoring (SIM) mode is an innovation that allows selective and sensitive detection [16–19].

The analysis step is usually preceded by extraction of the PAHs from the air particulates retained in PTFE or glass-fibre filters. Soxhlet extraction and ultrasonication employing a variety of organic solvents including acetone, benzene, toluene and acetonitrile are the most commonly used processes [20–22].

The main purpose of this study was to develop a method for the routine determination of PAHs in air samples taken with low-volume collection systems. For this purpose, different analytical techniques, HPLC–UV, HPLC–fluorescence, GC–FID and GC–MS-SIM, were compared and different stationary phases for both the HPLC and GC systems were checked. Finally, to demonstrate the applicability of the method to real samples and establish whether the techniques are really suitable for monitoring of PAH contamination in urban areas, PAHs were determined in atmospheric particulate matter sampled at five sites in the city of Valencia.

2. Experimental

2.1. Materials

Organic solvents (acetonitrile, methanol, acetone, cyclohexane, chloroform, dichloromethane, methanol and toluene) were of HPLC grade (Romil, Leics., UK). Ultra-pure water was prepared by ultrafiltration of distilled water with a Milli-Q system (Millipore, Bedford, MA, USA).

Acenaphthene, acenaphthylene, anthracene, benz[*a*]anthracene, benzo[*b*]fluoranthene, 2,3-benzofluorene, benzo[*ghi*]perylene, benzo[*e*]-pyrene, chrysene, dibenzo[*a,h*]anthracene, phenanthrene, fluorene, naphthalene, perylene and pyrene were supplied by Aldrich Chemie (Steinheim, Germany), benzo[*a*]pyrene by Janssen Chimica (Geel, Belgium) and fluoranthene by Scharlau (Barcelona, Spain). Benzo[*k*]-fluoranthene and indeno[1,2,3-*cd*]pyrene were purchased from the Community Bureau of Reference (BCR). (Brussels, Belgium).

These standards were dissolved in acetonitrile at 500 μg/l, although anthracene and benzo[*a*]pyrene solutions contained toluene (20%) and dibenzo[*a,h*]anthracene solution chloroform (20%). Stock mixtures of PAH standards were made up from the individual solutions in acetonitrile.

2.2. Chromatographic determinations

HPLC analyses were carried out with a Shimadzu (Kyoto, Japan) SCL-6A controller equipped with two LC6A pumps, a Rheodyne Model 7125 injector (20-μl loop), an SPD 6A ultraviolet detector, a RF-53 fluorescence detector, a CTO-6AS camera for column thermostating and a C-R4A data processor. The following LC columns were used: two Supelcosil LC-PAH (Supelco, Bellefonte, PA, USA), two Spherisorb ODS-2 (Teknokroma, Middelburg, Netherlands), a Spherisorb C_8 and a Zorbax-CN (Shandon, Runcorn, UK) and a Green Hypersil-PAH (Delta Scientific, Madrid, Spain). The characteristics of the columns and the HPLC conditions are given in Table 1. The use of different mobile phase gradients and different wavelengths in UV or fluorescence detection were checked. The conditions reported in Table 1 were suitable for routine analysis.

GC–FID analyses were performed using a Konik (Sant Cugat del Valles, Spain) Model 3000 gas chromatograph equipped with a flame ionization detector, split–splitless injector and a Spec-

Table 1
Experimental HPLC conditions

Parameter	Column						
	S-PAH (1)	S-PAH (2)	ODS-2 (1)	ODS-2 (2)	C_8	CN	H-PAH
Column length (cm)	25	15	25	25	25	25	10
Column I.D. (mm)	4.6	4.6	4.0	4.0	4.0	3.6	4.6
Particle size (μm)	5	5	5	3	5	5	5
Column temperature (°C)	30	30	30	30	30	30	30
Mobile phase gradient	See below[a]						
UV detection:							
λ (nm)	250	250	250	250	250	250	250
Fluorescence detection:							
λ_{exc} (nm)	290	290	290	290	290	290	290
λ_{em} (nm)	385	385	385	385	385	285	385

[a] Mobile phase gradient in all instances: acetonitrile–water gradient changed from 50:50 through 60:40, 70:30, 80:20 and 90:10 to 100:0, with 5 min at each composition and a 5-min gradient between each.

tra-Physics (San Jose, CA, USA) integrator with double channels and a memory module. The following GC capillary columns were tested: two BP-5 (Scientific Glass Engineering, Sydney, Australia), a BP-10 (Scientific Glass Engineering), a BP-20 (Scientific Glass Engineering) and an RSL-400 (Alltech, Deerfield, IL, USA).

Analyses were also carried out with the same columns on an HP 5970 quadrupole mass spectrometer (Hewlett-Packard, Waldbronn, Germany) connected to an HP 5690A gas chromatograph equipped with a split–splitless injector. The chromatographic data were recorded on an HP 59970 MS Chem-Station.

The characteristics of the columns and the GC conditions are given in Table 2. Various initial temperatures, programming rates and upper isotherm lengths were also tested and the conditions reported in Table 2 were suitable for routine analyses.

2.3. Extraction procedures

The PAHs were extracted ultrasonically with 5 ml of acetonitrile from Whatman filter-papers in a borosilicate glass-stoppered tube. The extracts were filtered through Millipore FHLP 01300 filter-paper. The volume of the extract was reduced to about 0.3 ml by bubbling a gentle stream of nitrogen through the solution at room temperature. The extracts were transferred into a 500-μl volumetric flask and taken up with acetonitrile for direct analysis.

Soxhlet extraction of the PAHs was performed using 250 ml of dichloromethane for 12 h at 60°C. The solvent was then evaporated in an evaporator–concentrator at 40–50°C and the residue was dissolved in 0.5 ml of acetonitrile.

2.4. Sampling

Air samples were collected at five different locations in Valencia in a low-volume collection bubbler system (MCV, Barcelona, Spain), with an aspiration pump equipped with an electric motor and a 2–4 m^3 per 24 h aspiration capacity. Dust was collected in a Whatman filter No. 1 dry aspirater air counter (1.5–3 l/min ± 3%) to provide readings per litre volume of air. The different components were interconnected by glass tubes and plastic parts.

Total suspended particulate matter samples were collected daily in Valencia during 1 week in the spring of 1992. Each sample was collected over a period of 24 h and the air volume of each sample was about 2 m^3.

Table 2
Experimental GC conditions

Parameter	Column				
	BP-5 (1)	BP-5 (2)	BP-10	BP-20	RSL-400
Injector temperature (°C)	285	285	285	285	285
Injector splitless	Yes	Yes	Yes	Yes	Yes
Splitless time (min)	0.7	0.7	0.7	0.7	0.7
Injection volume (μl)	3	3	3	3	3
Column length (m)	25	50	50	25	25
Column I.D. (mm)	0.22	0.22	0.22	0.22	0.22
Film thickness (μm)	25	25	25	25	25
Oven temperature programme	See below[a]				
FID:					
Detector temperature (°C)	300	300	300	300	300
Hydrogen carrier gas flow-rate (ml/min)	1	1	1	1	1
Nitrogen make-up gas flow-rate (ml/min)	35	35	35	35	35
Air (ml/min)	250	250	250	250	250
Hydrogen (ml/min)	35	35	35	35	35
MS:					
Transfer line temperature (°C)	260	260	260	260	260
Source temperature (°C)	200	200	200	200	200
Electron energy (eV)	70	70	70	70	70
Helium carrier gas flow-rate (ml/min)	1	1	1	1	1

[a] Temperature programme in all instances: initial temperature 50°C, held for 0.8 min, then increased at 30°C/min to 100°C (held for 2 min) and at 5°C/min to 280°C (held for 10 min).

3. Results and discussion

3.1. HPLC determination

The selectivity of HPLC for the PAH mixtures is affected by the phase type, particle diameter, column length, mobile phase flow-rate and LC column temperature [13]. In this work, these factors have been studied in detail.

Table 3 shows the resolution values (R_s) for sixteen PAHs obtained with the four stationary phases studied [$R_s = 2\Delta t/(w_{b1} + w_{b2})$], where Δt is the distance between the maxima of the two peaks and w_b the width of the peak at half-height. Fluorimetric detection was used. The concentrations of the standard solutions used were the same as those used for the optimization of extraction procedure with each detector (see below).

The pairs of PAHs acenaphthene–fluorene, benz[a]anthracene–chrysene and benzo[*e*]pyrene–benzo[*b*]fluoranthene were not separated with normal commercial columns of octyl-, octadecyl- and cyanopropyl-bonded silica. This is due to the "monomeric" character of the stationary phase [13]. The retention time of benzo[*b*]fluoranthene is the same as that of its isomer benzo[*k*]fluoranthene using the most polar columns, octyl- and cyanopropylsilica.

Only by using special columns for PAH analyses can the separation of the sixteen PAHs be achieved. The special phases consist of "polymeric" C_{18}-bonded silica and improve the selectivity for the PAHs. With these special columns, values of $R_s > 1.5$ are obtained for the pairs of PAHs. The elution order of the sixteen PAHs studied did not vary with the different LC-columns tested.

The effect of the particle diameter on the resolution of the PAH mixture was studied using the ODS-2 columns. Fig. 1A shows the effect of the particle diameter on the resolution of the

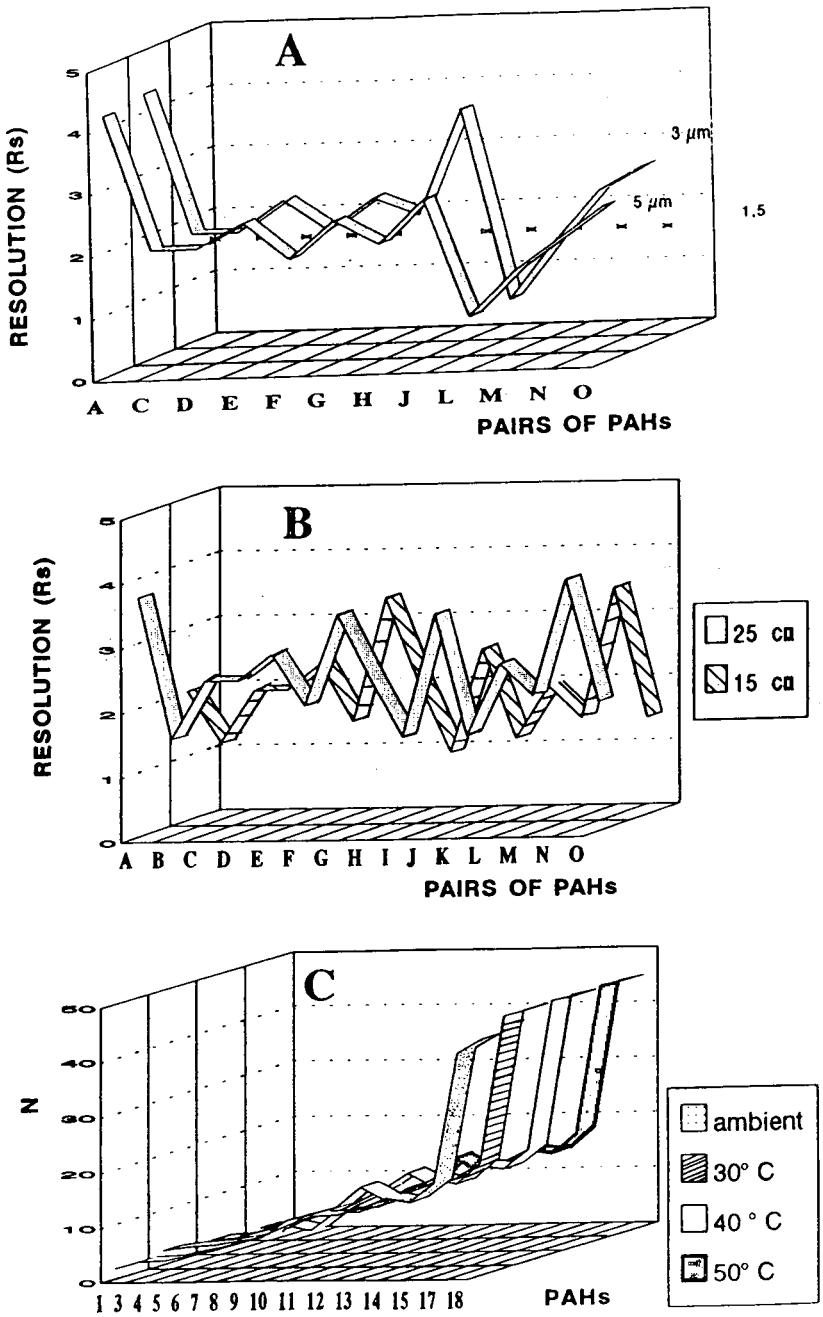

Fig. 1. Effect of instrumental parameters on the selectivity of PAHs. (A) Particle diameter vs. resolution; (B) column length vs. resolution. Pairs of PAHs: A = naphthalene–acenaphthene; B = acenaphthene–fluorene; C = fluorene–phenanthrene; D = phenanthrene–anthracene; E = anthracene–fluoranthene; F = fluoranthene–pyrene; G = pyrene–2,3-benzofluorene; H = 2,3-benzofluorene–benz[*a*]anthracene; I = benz[*a*]anthracene–chrysene; J = chrysene–benzo[*e*]pyrene; K = benzo[*e*]pyrene–benzo[*b*]fluoranthene; L = benzo[*b*]fluoranthene–benzo[*k*]fluoranthene; M = benzo[*k*]fluoranthene–benzo[*a*]pyrene; N = benzo[*a*]pyrene–dibenzo[*a*,*h*]anthracene; O = dibenzo[*a*,*h*]anthracene–benzo[*ghi*]perylene. (C) Column temperature vs. efficiency. For identification of PAHs, see Fig. 2.

Table 3
Resolution (R_s) obtained with the stationary phases tested

Pairs of PAHs	Stationary phase				
	S-PAH	H-PAH	C_8	C_{18}	CN
Naphthalene–acenaphthene	3.7	3.8	3.5	4.1	3.5
Acenaphthene–fluorene	1.5	1.3	0.0	0.0	0.0
Fluorene–phenanthrene	2.4	2.3	1.6	1.6	1.2
Phenanthrene–anthracene	2.4	2.1	0.8	0.8	0.0
Anthracene–fluoranthene	2.8	2.3	2.1	2.1	1.9
Fluoranthene-pyrene	2.0	1.5	0.2	0.2	0.3
Pyrene–2,3-benzofluorene	3.4	3.5	1.5	1.5	1.6
2,3-Benzofluorene–benz[*a*]anthracene	2.4	2.3	1.4	1.4	0.5
Benz[*a*]anthracene–chrysene	1.5	1.5	0.0	0.0	0.0
Chrysene–benzo[*e*]pyrene	3.4	3.5	2.7	2.7	2.8
Benzo[*e*]pyrene–benzo[*b*]fluoranthene	1.5	1.3	0.0	0.0	0.0
Benzo[*b*]fluoranthene–benzo[*k*]fluoranthene	2.6	2.4	0.0	0.0	0.0
Benzo[*k*]fluoranthene–benzo[*e*]pyrene	2.1	2.3	0.7	0.7	1.1
Benzo[*e*]pyrene–dibenzo[*a,h*]anthracene	3.9	2.3	2.4	2.4	0.0
Dibenzo[*a,h*]antracene–benzo[*ghi*]perylene	2.0	1.5	0.9	0.9	0.0

PAHs; acenaphthene–fluorene, benz[*a*]anthracene–chrysene and benzo[*e*]pyrene–benzo[*b*]-fluoranthene were not separated by the ODS-2 columns.

With the same stationary phase and column length, the resolution was improved in some instances (see Fig. 1A). However, the capacity factor was constant. This is due to a change in the peak form; the retention time is the same in both columns but the width of the base of the peak is narrower in the columns with a 3-μm particle diameter. Diminishing the particle size of the stationary phase does not improve the separation of the unresolved PAHs, but the accuracy and reproducibility are better.

In Fig. 1B the effect of the column length is illustrated using 15- and 25-cm Supelcosil-PAH columns. Although the increase in the column length leads to longer analysis times, it provides better resolution. The pairs of PAHs benz-[*a*]anthracene–chrysene and benzo[*e*]pyrene–benzo[*b*]fluoranthene were well separated in the 25-cm column whereas in the 15-cm column the separation was only partial.

The effect of the mobile phase flow-rate on the separation of the PAHs was also studied. Flow-rates of 0.8, 1.0, 1.2 and 1.4 ml/min were tested with the 25-cm Supelcosil-PAH column. A flow-rate between 0.8 and 1.2 ml/min provides a total resolution of the analyte compounds. With a flow-rate of 1.4 ml/min, the peaks corresponding

Table 4
HPLC detection limits (ng) with the fluorescence and UV detection

PAH	Fluorescence	UV
Naphthalene	2.00	16.60
Acenaphthylene	–	22.80
Acenaphthene	0.05	22.80
Fluorene	0.50	3.00
Phenanthrene	0.07	1.60
Anthracene	0.10	1.60
Fluoranthene	2.00	5.00
Pyrene	0.02	6.10
2,3-Benzofluorene	0.02	1.60
Benz[*a*]anthracene	0.01	6.10
Chrysene	0.02	2.20
Benzo[*e*]pyrene	0.03	4.00
Benzo[*b*]fluoranthene	0.05	3.00
Benzo[*k*]fluoranthene	0.05	3.20
Benzo[*a*]pyrene	0.03	6.10
Perylene	–	6.10
Dibenzo[*a,h*]anthracene	0.03	10.00
Benzo[*ghi*]perylene	0.01	8.00
Indenopyrene	–	3.00

Table 5
GC detection limits (DL, ng) with FID and MS-SIM detection and selected ions for SIM

PAH	FID DL	MS-SIM	
		Selected ion (*m/z*)	DL
Naphthalene	3.00	128	0.01
Acenaphthylene	1.00	152	0.02
Acenaphthene	0.90	154	0.02
Fluorene	0.90	166	0.01
Phenanthrene	0.80	178	0.01
Anthracene	0.90	202	0.01
Fluoranthene	0.80	202	0.01
Pyrene	0.80	216	0.01
2,3-Benzofluorene	0.70	228	0.02
Benz[*a*]anthracene	0.70	228	0.03
Chrysene	0.70	252	0.03
Benzo[*e*]pyrene	0.60	252	0.03
Benzo[*b*]fluoranthene	0.70	252	0.02
Benzo[*k*]fluoranthene	0.70	252	0.04
Benzo[*e*]pyrene	0.70	252	0.04
Perylene	0.70	252	0.04
Dibenzo[*a,h*]anthracene	0.50	276	0.04
Benzo[*ghi*]perylene	0.80	278	0.04
Indenopyrene	1.30	276	0.10

to acenaphthene and fluorene and to benz-[*a*]anthracene and chrysene were not separated. Small variations in the flow-rate usually affect the retention times but not the resolution.

The column temperature is an important parameter that can be used to modify selectivity for PAH separation. The Supelcosil-PAH column was thermostated at temperatures of 30, 40 and 50°C. Fig. 1C shows the variation in the column efficacy $[N = 5.545(t_r/W_h)]$ with temperature. The column temperature affected the efficiency of separation. The best results were obtained at 30°C. The temperature must be controlled in order to obtain reproducible retention times.

When these parameters were optimized, two detection systems (fluorescence and UV) were compared. Both detectors provided a linear response for a wide range of amounts injected, and their reproducibilities were similar and lower than 4.2%.

In Table 4, the detection limits with fluorescence and UV detection are compared. For

Table 6
Concentration of the working solution (mg/l) for fluorescence and UV detection

PAHs	Fluorescence	UV
Naphthalene	4.00	80
Acenaphthylene	–	160
Acenaphthene	0.20	80
Fluorene	2.00	16
Phenanthrene	0.10	8
Anthracene	0.40	8
Fluoranthene	4.00	16
Pyrene	0.15	8
2,3-Benzofluorene	0.05	8
Benz[*a*]anthracene	0.01	16
Chrysene	0.07	8
Benzo[*e*]pyrene	0.04	8
Benzo[*b*]fluoranthene	0.20	16
Benzo[*k*]fluoranthene	0.20	8
Benzo[*a*]pyrene	0.04	8
Perylene	–	16
Dibenzo[*a,h*]anthracene	0.02	16
Benzo[*ghi*]perylene	0.10	16
Indenopyrene	–	8

quantification in airborne particulates, fluorescence detection offers far greater sensitivity and, more important, is much more selective than UV detection. Only fluorene and fluoranthene present similar sensitivities with both detection techniques. However, there are three PAHs, acenaphthylene, indoperylene and perylene, that are not fluorescent at the excitation and emission wavelengths used, and they can be detected by UV spectrophotometry at 254 nm. Even the excitation and emission wavelengths can be changed in order to obtain optimum sensitivity and/or selectivity for these individual PAHs.

3.2. GC determination

A comparison of four GC columns with different stationary phases illustrates the usefulness of some of them for the high-resolution separation of PAHs.

The BP-20 and the RSL-400 columns gave low resolution for the pairs phenanthrene–anthracene and benz[*a*]anthracene–chrysene. Moreover, with the BP-20 column the peaks corresponding to the isomers perylene–dibenzo[*a*,*h*]anthracene and benzo[*b*]fluoranthene–benzo[*k*]fluoranthene were unresolved. The probable cause is the polarity of the stationary phase; these phases have polar characteristics and do not retain apolar compounds such as PAHs well.

With the BP-5 and BP-10 columns it was possible to resolve all the PAHs studied. A shorter analysis time was obtained with the BP-5 columns.

The influence of the column length on the

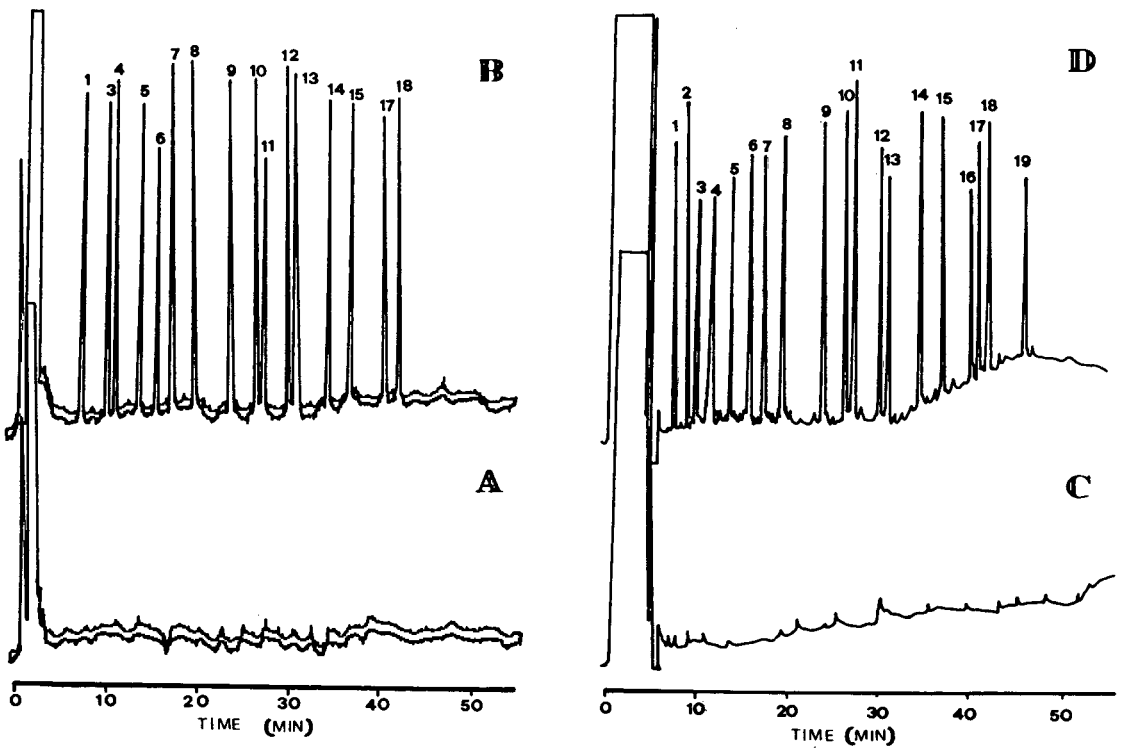

Fig. 2. Chromatograms for the HPLC analysis of 20 μl of an extract obtained by sonication of (A) untreated filter with fluorescence detection, (B) filter treated with sixteen PAHs with fluorescence detection, (C) untreated filter with UV detection and (D) filter treated with nineteen PAHs with UV detection. For concentrations, see Table 6. Peaks: 1 = naphthalene; 2 = acenaphthylene; 3 = acenaphthene; 4 = fluorene; 5 = phenanthrene; 6 = anthracene; 7 = fluoranthene; 8 = pyrene; 9 = 2,3-benzofluorene; 10 = benz[*a*]anthracene; 11 = chrysene; 12 = benzo[*e*]pyrene; 13 = benzo[*b*]fluoranthene; 14 = benzo[*k*]fluoranthene; 15 = benzo[*a*]pyrene; 16 = perylene; 17 = dibenzo[*a*,*h*]anthracene; 18 = benzo[*ghi*]perylene; 19 = indenopyrene.

separation of the PAH peaks was also studied. Increasing the length of the column (from 25 to 50 m) increased the analysis time but did not improve the resolution of the chromatographic peaks.

As a result of this study, the BP-5 column with a length of 25 m was selected for routine analyses because it provided the best separation between the PAHs with the shortest analysis time.

All these experiments were performed using FID; minimum detectable amounts ranging from 0.5 to 1.5 ng (see Table 5) were obtained. FID presented the same problem as UV detection: the sensitivity and selectivity were too low for application to real sample analyses.

To improve the sensitivity, detection with MS-SIM was checked. Table 5 shows the detection limits obtained using FID and MS-SIM for the nineteen PAHs studied. Table 5 also shows the m/z values for the selected ions in MS-SIM.

With GC–MS-SIM, the detection limits were suitable for the determination of PAHs in real samples when they are taken with low-volume systems.

3.3. Extraction procedure

To optimize the extraction procedure using sonication, the following parameters were studied: the organic solvent used in the extraction, evaporation conditions, shaking time and number of extractions.

Recovery experiments were carried out by placing on the Whatman filter 200 μl of the solution listed for each HPLC detector in Table 6. These should be equivalent at air concentrations between 0.4 and 0.002 $\mu g/m^3$ depending on the PAH for fluorescence detection and between 16 and 0.8 $\mu g/m^3$ for UV detection. For GC–FID and GC–MS-SIM, working solutions of 10 and 0.4 mg/l of each compound,

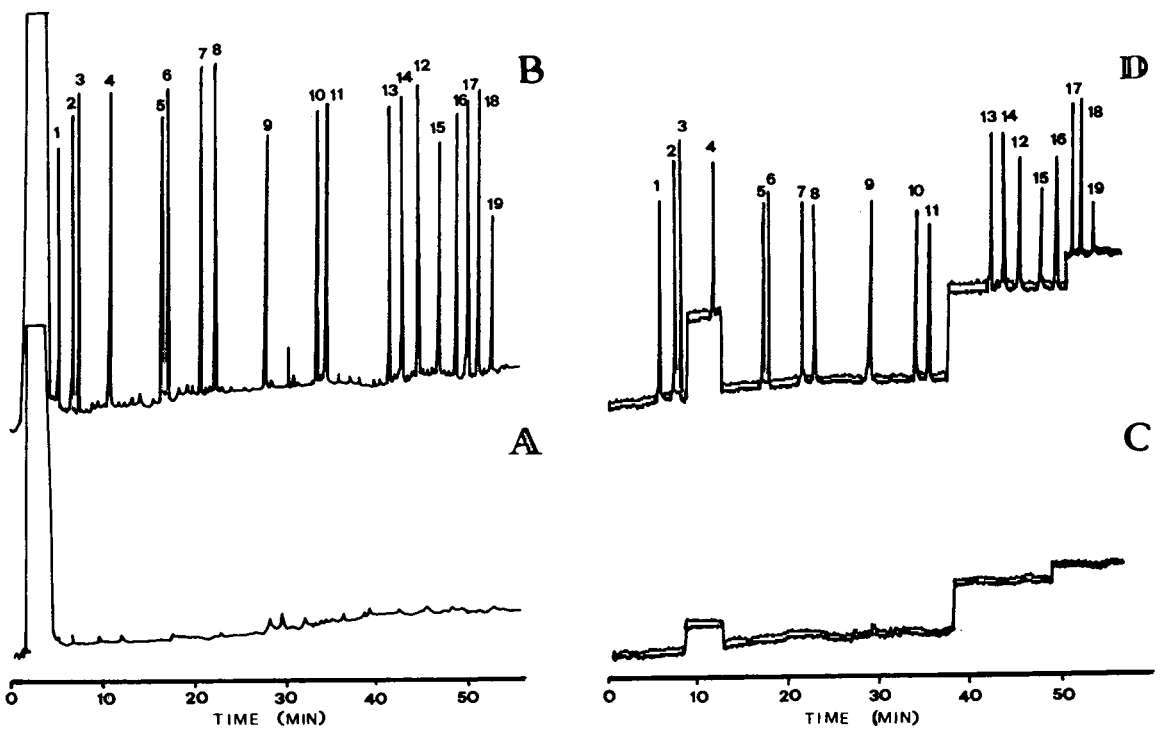

Fig. 3. Chromatograms obtained in the GC analysis of 1 μl of an exact of (A) untreated filter with FID, (B) filter treated with nineteen PAHs with FID, (C) untreated filter with MS-SIM and (D) filter treated with nineteen PAHs with MS-SIM. For concentrations, see text. Peak assignment as in Fig. 2.

respectively, were used. After the organic solvent had been evaporated, the filter was extracted.

First, four organic solvents were tested: dichloromethane, methanol, acetone, cyclohexane and acetonitrile. Methanol and cyclodhexane provided recoveries lower than 59%. Dichloromethane and acetone increased the recoveries to 66% and acetonitrile gave and best results with recoveries of about the 75%.

If the reproducibilities are compared the best results are also obtained with acetonitrile. Therefore, acetonitrile was chosen as the extraction solvent.

The evaporation conditions were checked. The recoveries diminished when the sample was dried. This phenomenon was more evident with the volatile PAHs; for example, naphthalene was not recovered when the organic solvent was evaporated. Evaporation with air and nitrogen streams was also tested; there were no significant differences in the recoveries.

Table 7
Mean recovery ±R.S.D. (%) ($n = 6$) from fortified filters using the sonication and Soxhlet extraction methods

PAH	Sonication	Soxhlet
Naphthalene	65 ± 14	30 ± 15
Acenaphthylene	76 ± 14	30 ± 16
Acenaphthene	80 ± 13	50 ± 10
Fluorene	79 ± 7	40 ± 8
Phenanthrene	99 ± 6	60 ± 9
Anthracene	76 ± 10	60 ± 10
Fluoranthene	84 ± 7	55 ± 12
Pyrene	85 ± 6	55 ± 9
2,3-Benzofluorene	79 ± 9	50 ± 7
Benz[*a*]anthracene	78 ± 5	55 ± 10
Chrysene	75 ± 4	55 ± 12
Benzo[*e*]pyrene	75 ± 4	57 ± 14
Benzo[*b*]fluoranthene	82 ± 4	58 ± 18
Benzo[*k*]fluoranthene	85 ± 4	59 ± 13
Benzo[*a*]pyrene	81 ± 6	50 ± 12
Perylene	82 ± 8	58 ± 11
Dibenzo[*a,h*]anthracene	83 ± 9	59 ± 9
Benzo[*ghi*]perylene	80 ± 6	40 ± 8
Indenopyrene	85 ± 9	48 ± 10

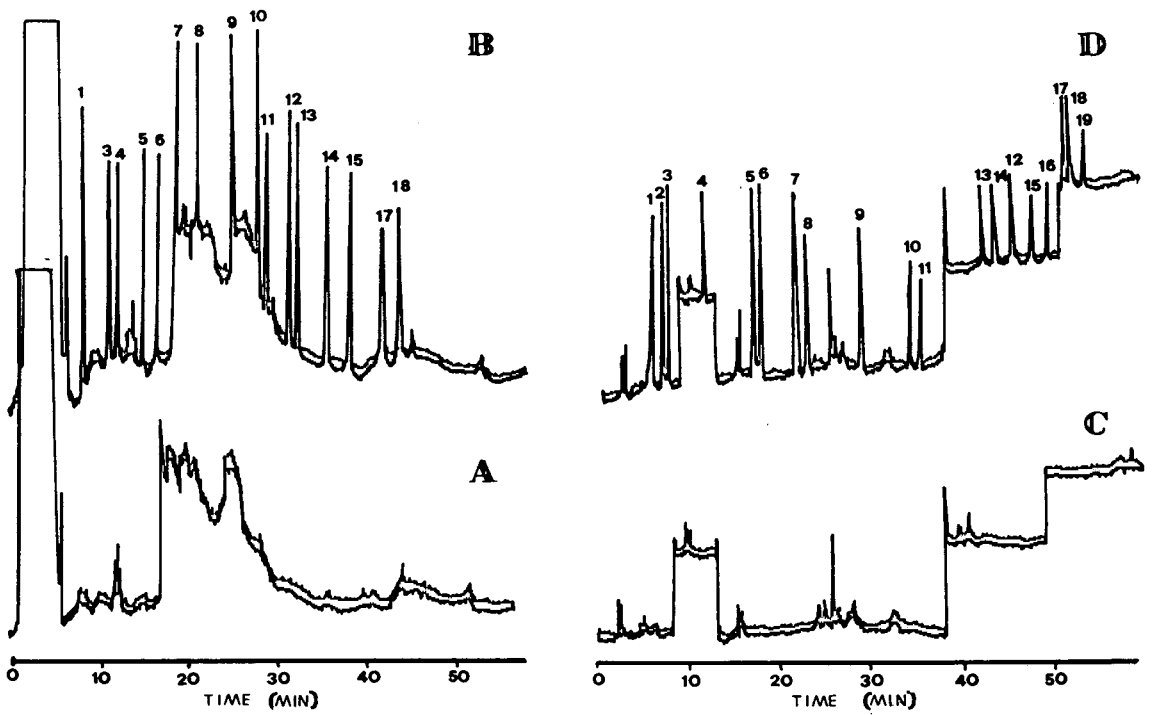

Fig. 4. Chromatograms obtained following Soxhlet extraction of (A) untreated filter by HPLC–fluorescence, (B) treated filter by HPLC–fluorescence, (C) untreated filter by GC–MS-SIM and (D) treated filter by GC–MS-SIM. For concentrations see Table 6 and text. Peak assignment as in Fig. 2.

The next step was to select the ultrasonication time. For this, Whatman No. 1 filter-paper treated with the nineteen PAHs was shaken for 5, 10, 20, 30 or 40 min with acetonitrile. The recoveries increased with shaking time up to 30 min, but shaking for more than 30 min gave lower recovery values.

The number of extractions was also studied. The filter-paper was extracted from one to five times. There was no improvement in the recoveries when the number of extractions was increased. However, the relative standard deviation increased with increase in the number of extractions.

Therefore, for maximum recoveries of PAHs, Whatman filter-papers treated with 5 ml of ethyl acetate in a borosilicate glass-stoppered tube were used. The tubes were placed in an ultrasonic bath for 30 min. The extracts were then filtered through Millipore FHLP 01300 filter-paper. The volume of the extract was reduced to about 0.3 ml by bubbling a gentle stream of nitrogen through the solution at room temperature. The extracts were transferred into a 500-μl volumetric flask and taken up with acetonitrile for direct determination.

Fig. 2A–D illustrate the chromatograms for unspiked filter extract and spiked filter extract analysed by HPLC–fluorescence (Fig. 2A and B) and by HPLC–UV (Fig. 2C and D). In both instances there were no interfering peaks in the blank chromatograms but a difference in sensitivity between the two detectors can be observed (see the concentrations in Table 6).

Fig. 3A–D show the same chromatograms but obtained using GC–FID and GC–MS-SIM. The FID blank (Fig. 3A) showed some interfering peaks, but the MS-SIM blank (Fig. 3C) showed none. Differences in sensitivity between the two detectors can also be observed.

To validate the method, the recoveries obtained were compared with those obtained using

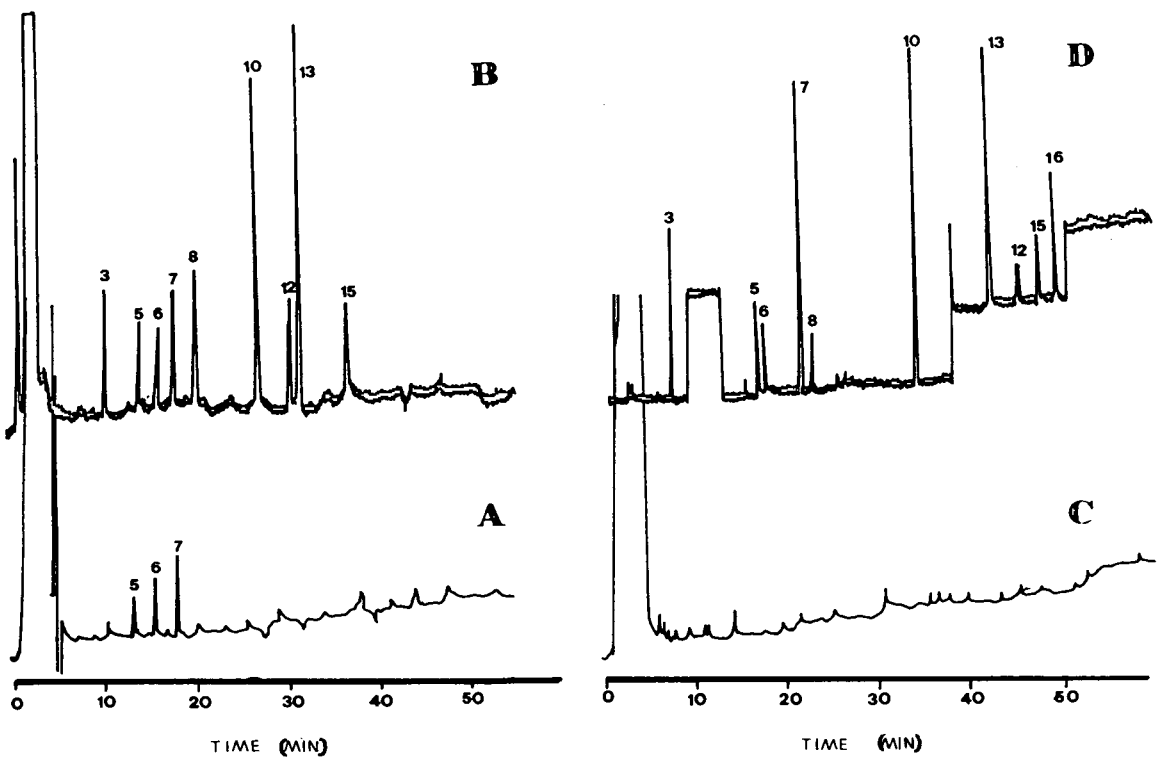

Fig. 5. Chromatogram obtained after sonication extraction of a real samples, (A) by HPLC–UV, (B) by HPLC–fluorescence, (C) by GC–FID and (D) by GC–MS-SIM. Peak assignment as in Fig. 2.

Table 8
Mean weekly values of PAHs (ng/m^3) in air samples in Valencia obtained by HPLC–fluorescence detection (F) and GC–MS (MS)

PAH	Sampling site									
	1		2		3		4		5	
	F	MS	F	MS	F	MS	F	MS	F	MS
Naphthalene	–	–	–	–	–	–	–	–	–	–
Acenaphthylene	–	–	–	–	–	–	–	–	–	–
Acenaphthene	5.7	5.9	7.6	7.5	–	–	9.0	9.0	8.8	8.9
Fluorene	–	–	–	–	–	–	–	–	–	–
Phenanthrene	2.0	1.9	3.8	3.8	10.7	11.0	8.9	9.0	–	–
Anthracene	–	–	–	–	20.3	20.0	–	–	–	–
Fluoranthene	87.8	87.8	70.8	71.2	189.8	191.9	64.2	64.4	–	–
Pyrene	3.3	3.4	1.2	1.3	–	–	–	–	–	–
2,3-Benzofluorene	–	–	–	–	–	–	–	–	–	–
Benz[*a*]anthracene	0.5	0.5	0.7	0.2	1.3	1.4	0.8	0.8	0.4	0.4
Chrysene	–	–	–	–	2.3	2.3	–	–	–	–
Benzo[*e*]pyrene	2.1	2.0	1.2	1.1	3.8	3.7	1.9	1.8	0.8	0.8
Benzo[*b*]fluoranthene	–	–	–	–	–	–	–	–	–	–
Benzo[*k*]fluoranthene	–	–	–	–	–	–	–	–	–	–
Benzo[*a*]pyrene	1.7	1.7	1.5	1.6	6.5	6.5	–	–	–	–
Perylene	–	1.1	–	–	–	–	–	–	–	–
Dibenzo[*a*,*h*]anthracene	1.2	1.1	–	–	–	–	1.3	1.4	–	–
Benzo[*ghi*]perylene	4.4	4.5	4.8	4.9	13.3	13.4	5.7	5.8	2.8	2.8
Indenopyrene	–	–	–	–	–	–	–	–	–	–

Soxhlet extraction. Table 7 shows the recoveries and relative standard deviations.

Continuous Soxhlet extraction used more organic solvent and the extraction time was longer. The recoveries obtained were lower than those obtained by ultrasonic extraction. The use of Soxhlet extraction provides blanks with many interfering peaks, some of which show the same retention times as the PAHs studied. Fig. 4A–D illustrate the chromatograms obtained by HPLC–fluorescence and GC–MS-SIM, which are the most selective detection methods studied. With the other methods the number of interfering peaks and the baseline noise increased because of the low selectivity. These chromatograms demonstrate the need for a clean-up procedure before PAH determination when Sohxlet extraction is used.

To verify the ultrasonication procedure, airborne particulate samples were taken over a period of 1 week at five locations in Valencia. The PAH concentrations were determined using HPLC–fluorescence and GC–MS-SIM. Table 8 shows the concentrations of the nineteen PAHs obtained using the two techniques. The differences were <3%. Although HPLC–fluorescence with fixed excitation and emission wavelengths does not permit the detection of acenaphthylene, indenopyrene and perylene, it should be the detection method of choice, because there were no peaks interfering with those of the PAH compounds present in the chromatogram obtained from environmental samples and the maintenance cost of the system is much lower than that of GC–MS-SIM for routine analysis.

Fig. 5 shows the chromatograms for a real sample obtained using the four systems. With HPLC–UV and GC–FID no peaks were detected.

The levels of PAHs found in the air samples taken at different locations showed a relationship between this concentration and the traffic intensity at the different locations.

4. Conclusions

Of the four techniques studied, HPLC with fluorescence detection is to be preferred for the measurement of PAHs in airborne particulate samples taken with low-volume systems. The results obtained using HPLC–fluorescence are comparable to those obtained with GC–MS-SIM, but the former has the advantage of being economical for use in routine analyses, which is not a characteristic of MS methods.

Using ultrasonic extraction with acetonitrile, the recoveries obtained are better than those found with Soxhlet extraction, the number of interfering peaks is smaller and the simplicity, speed and cost are much improved.

The results show that the level of PAH pollution in Valencia is not alarming, but a clear relationship between traffic intensity and the level of PAHs was found.

Future research will be devoted to the use of HPLC–wavelength-programmed fluorescence detection with the excitation and emission wavelengths changing during the chromatography to achieve optimum sensitivity and/or selectivity for the individuals PAHs. It will also focus on monitoring of PAH levels at different sites in Valencia periodically during the year to establish the pattern of pollution in the city.

Acknowledgement

This work was financially supported by the Agència del Medi Ambient (Generalitat Valenciana).

References

[1] M. Morales Suarez-Varela, C. Escrivá, A. La Orden, J. Mañes, G. Font and A. Llopis, *J. Environ. Pathol. Toxicol. Oncol.*, 10 (1990) 237.
[2] L.B. Ebert (Editor), *Polynuclear Aromatic Hydrocarbons (ACS Symposium Series*, No. 217), American Chemical Society, Washington, DC, 1988.
[3] S.A. Wise, B.A. Benner, G.D. Byrd, S.N. Chesler, R.E. Rebbert and M.M. Schantz, *Anal. Chem.*, 60 (1988) 887.
[4] G. Castello and T.C. Gerbino, *J. Chromatogr.*, 642 (1993) 351.
[5] C. Escrivá, M. Morales, A. la Orden, J. Mañes and G. Font, *Fresenius' J. Anal. Chem.*, 339 (1991) 743.

[6] W. Maher, F. Pellegrino and J. Furlonger, *Microchem. J.*, 39 (1989) 160.
[7] L.C. Sander and S.A. Wise, *Anal. Chem.*, 59 (1987) 2309.
[8] M.W. Dong and A. Greenberg, *J. Liq. Chromatogr.*, 11 (1988) 1887.
[9] L.C. Sander and S.A. Wise, *LC·GC*, 8 (1990) 378.
[10] S.A. Wise, L.C. Sander and W.E. May, *J. Chromatogr.*, 642 (1993) 329.
[11] E. Klasson-Wehler, A. Bergman, B. Kowalski and I. Brandt, *Xenobiotica*, 17 (1987) 477.
[12] S. Sinkkonen, E. Kolehmainen, and J. Koistinen, *Int. J. Environ. Anal. Chem.*, 47 (1992) 7.
[13] A. Bemgard, A. Colmsjö and B.O. Lundmark, *J. Chromatogr.*, 595 (1992) 247.
[14] J.W. Haas, III, M.V. Buchanan and M.B. Wise, *J. Chromatogr. Sci.*, 26 (1988) 49.
[15] A. Bemgard and A. Colmsjö, *J. Chromatogr. Sci.*, 30 (1992) 23.
[16] I.D. Bridle and X.F. Li, *J. Chromatogr.*, 498 (1990) 11.
[17] A. Khesina, M.S. Makhover and I.A. Khitrovo, *Eksp. Onkol.*, 11 (1989) 3.
[18] D.L. Karlesky, M.E. Rollie and J.M. Warner, *Anal. Chem.*, 58 (1988) 1187.
[19] S.A. Wise, B.A. Benner, S.N. Chesler, L.R. Hilpert, C.R. Vogt and W.E. May, *Anal. Chem.*, 58 (1986) 3067.
[20] M.M. Schantz, B.A. Benner, S.N. Chelser, B.J. Koster, K.E. Hehn, S.F. Stone, W.R. Kelly, R. Zeisler and S.A. Wise, *Fresenius' J. Anal. Chem.*, 338 (1990) 501.
[21] A. Sisovic and M. Fugas, *Environ. Monit. Assess.*, 18 (1991) 235.
[22] M. Morales, C. Escrivá, G. Font, A. Llopis and A. la Orden, *Exp. Oncol.*, 14 (1992) 28.

ELSEVIER

Journal of Chromatography A, 676 (1994) 389–398

JOURNAL OF CHROMATOGRAPHY A

Fully automated gas chromatograph–flame ionization detector system for the *in situ* determination of atmospheric non-methane hydrocarbons at low parts per trillion concentration

J.P. Greenberg*, B. Lee, D. Helmig, P.R. Zimmerman

National Center for Atmospheric Research, Boulder, CO, USA

First received 2 February 1994; revised manuscript received 31 March 1994

Abstract

A completely automated gas chromatography–flame ionization detector system with cryogenic sample freeze-out for measuring atmospheric non-methane hydrocarbons was deployed at the Mauna Loa Observatory, Hawaii during the MLOPEX II experiment, September 1991 through August 1992. The system was designed to (1) rapidly trap air samples of up to 4 litres volume to allow for sub-parts per trillion detection limits, (2) eliminate interferences from ambient ozone, water vapor and carbon dioxide, (3) reduce to negligible levels any contamination in the analytical systems, and (4) allow for continuous, unattended operation. The instrumentation consisted of two parallel analytical systems, employing packed and capillary chromatographic columns, which allowed quantification of C_2–C_{10} non-methane hydrocarbons from sub-parts per trillion to parts per million concentrations. A dynamic dilution system was used to calibrate the analytical system over the range of concentrations measured (low parts per trillion to parts per billion) at this site.

1. Introduction

Atmospheric non-methane hydrocarbons (NMHCs) play an important role in the atmospheric chemistry of the troposphere. They are central to the production and destruction of atmospheric oxidants and oxidant precursors, such as OH, O_3, organic peroxides and peroxy radicals [1]. The annual global emissions of NMHCs into the atmosphere exceed that of methane [2], and, therefore, represent a major component of the atmospheric carbon budget. Because of their higher chemical reactivity, however, NMHCs are often found at a few parts per billion (ppb) to low parts per trillion (ppt) levels in the remote troposphere, compared to approximately 1.7 parts per million (ppm) for methane [3].

Atmospheric NMHCs have been measured both by *in situ* analysis and by sample collection in canisters, bags, or adsorbent cartridges, with subsequent laboratory analysis. The latter strategy has disadvantages, which may include artifact formation in the storage medium, storage losses or transformations, sample recovery, and sample size constraints [2]. More recently, measurements have been reported which utilized *in situ* methods [4–6]. The in situ techniques also have revealed analytical problems, which include chemical or chromatographic interferences as a

* Corresponding author.

0021-9673/94/$07.00
SSDI 0021-9673(94)0321-Y

result of simultaneously collected water vapor, ozone, and CO_2. Problems with high blank or background levels have also been noted. For any sampling and analysis strategy, calibration over the entire range of concentrations in the remote troposphere can present problems. These include difficulties in producing and maintaining accurate and stable standards at low concentrations, the unavailability of standards for all NMHCs and other trace gases detected, linearity of detector response, etc. [7]. Finally, experimental requirements in some cases include the continuous operation of sampling and analytical instrumentation on a 24-hour basis for up to several months.

We have designed and successfully deployed a fully automated gas chromatography–flame ionization detection (GC–FID) system for the determination of atmospheric NMHCs at the Mauna Loa Observatory, Hawaii, as part of the Mauna Loa Photochemical Experiment II (MLOPEX II), from September 1991 to August 1992 [8,9]. The analytical system was designed to satisfy the following fundamental criteria: (1) the system should operate unattended on a 24-hour basis, (2) atmospheric samples of volumes of up to 4 litres should be collected in less than 30 minutes and analyzed for C_2–C_{10} NMHCs down to low ppt concentrations, (3) the analytical system should have blanks sufficiently low for the quantitation of the corresponding NMHCs, (4) interferences of water, CO_2, and O_3 should be eliminated, and (5) calibrations should be made over the entire dynamic range of measurements.

2. Experimental

The measurement of atmospheric NMHCs was based upon a two-stage cryogenic sample trapping strategy. The first stage sample trap was designed to rapidly and efficiently trap C_2 and heavier NMHCs; it had sufficient capacity and cross section so that water vapor trapped simultaneously with the sampled air would not impede the sample air flow at cryogenic trapping temperatures. Traps for removal of O_3 and, in some analyses, CO_2 were placed upstream of this trap. The first stage was then heated slowly and NMHCs trapped were quantitatively transferred to a micro-volume, cryogenically cooled second stage trap. The programmed heating of the first stage prevented the bulk of the trapped water vapor from being transferred to the second-stage, analytical trap. The small effective volume (less than 100 μl after packing, see below) and rapid heating of the second stage trap insured that NMHCs would be transferred to the GC analytical column in the smallest possible volume in order to avoid broad peaks early in the chromatogram.

2.1. Components

The NMHC analytical system is depicted in Fig. 1. The sample inlet was located at an elevation of approximately 9 m; the sample line was 12.7 mm O.D., 10.5 mm I.D. (0.5″ O.D., 0.412″ I.D.) electropolished stainless steel tubing. The inlet was fitted with a Teflon filter holder which contained a Teflon coated glass fibre filter, in order to remove particulates. Sample air was continuously pulled through the sample line at a flow rate of approximately 10 l min^{-1} with a diaphragm pump. The sample line was routed very close to the sample collection system inside the laboratory to minimize the distance between the sample line and the sample collection/introduction system to approximately 20 cm.

All tubing from the sample inlet to the sample transfer tubing of the sample collection/introduction system was wrapped with nickel-coated copper braided wire 0.7 mm diameter (Teflon insulated); AC current (approximately 10 A at 7 V) was passed through the wire in order to heat these components to approximately 50°C. Valves V1, V2, E1, E2, and SS were heated to 60°C by individual valve heaters (VALCO Model HA2). The heating of these components reduced blank levels from sample carryover, especially of higher boiling components, to well below equivalent ppt concentrations measured.

Samples were collected in sample traps SL1 and SL2 (Fig. 1). These traps were cooled by

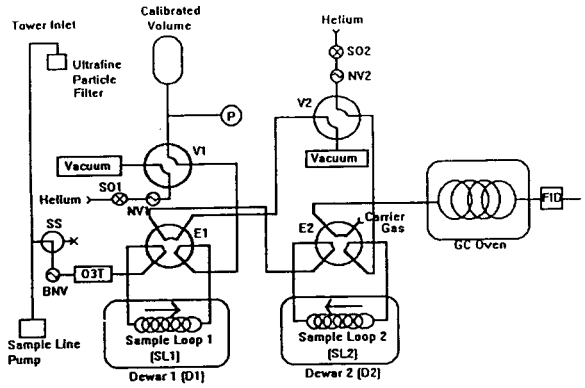

Fig. 1. Schematic of the sample collection/introduction system in the sample collection mode. The system consisted of the following components: 2-position, air actuated switching valves (Valco, Houston, TX, USA): V1 and V2: flow direction valves, 4-port, Models #4UWP (1/4″ tubing ports, 1″ = 2.54 cm) and C4WP (1/16″ tubing ports), respectively; E1 and E2 : 6-port sample trap valves, Models #6WP (1/8″ tubing ports) and #C6WP (1/16″ tubing ports) respectively; SS: stream selector valve, 3-port, Model #C3WP (1/16″ tubing ports). Pumps: sample line pump: diaphragm pump, Model #N035ATP (KNF Neuberger, Princeton, NJ, USA); VP: vacuum pump: Welsh Model #R1405 (Welsh, Skokie, IL, USA) (liquid nitrogen cooled vapor trap placed on low pressure side). Needle valves, shutoff valves (NUPRO, Willoughby, OH, USA); BNV: stainless steel bellows needle valve, Model #SS-4BMW; NV1 and NV2: stainless steel needle valves, Model #SS-SS1; SO: stainless steel bellows pneumatic shut-off valves, Model #SS-4BK-1O. Pressure measurement (MKS Instrument Co., Andover, MA, USA): P: pressure transducer Model #127AA-01000B, power supply and display, Model PDR-C-2C. Miscellaneous: SL1: 1st stage cryogenic sample trap, 16″ × 0.190″ ID stainless steel packed with 0.18–0.23 mm diameter glass beads (Alltech, Deerfield, IL, USA); SL2: 2nd stage cryogenic sample trap, 8″ × 0.085″ I.D. stainless steel packed with 60/80 mesh glass beads; D1 and D2: liquid nitrogen dewars, Model #10LD (Taylor-Wharton, Theodore, AL, USA); O_3T: ozone trap, KI impregnated glass wool Ultrafine particle filter, Teflon coated glass fiber filter, Pallflex T60A20 (Putnam, CT, USA); CV: calibrated volume, 35 litre, electropolished stainless steel, rigid tank.

immersion in liquid nitrogen (Fig. 2). SL1 and SL2 were located inside a plastic pipe (43 mm I.D.), which was placed in a liquid nitrogen dewar. The pipe was sealed on its outside to the top of the dewar, but the inside of the pipe was open to the atmosphere. The bottom end of the pipe extended below the liquid nitrogen level in the dewar. When SL1 or SL2 cooling was required, a level sensing circuit was activated. This circuit closed the dewar vent and pressurized the dewar (10 p.s.i. nitrogen or helium, 1 p.s.i. = 6894.76 Pa) which would force liquid nitrogen up the central tube containing the sample loops. A two-resistor sensing circuit maintained the liquid nitrogen level between the resistors (1 cm apart) by alternately pressurizing and venting the inside of the dewar. The sensors were fixed to appropriate positions on the sample loops. When the loops required heating (for transfer, sample injection, or backflush), the liquid nitrogen level was dropped by venting the dewar to atmospheric pressure. The sample loops were heated electrically by passing 110 V AC current directly through the stainless steel tubing of the trap. Heating rates and temperature setpoints were controlled by temperature controllers (Model #2050, West Instruments, Schiller Park, IL, USA), using a thermocouple sensor attached directly to SL1 or SL2. Separate dewars were used for SL1 and SL2. Cryogen consumption was approximately 2 litres per day for each dewar, when approximately 8 samples were collected daily.

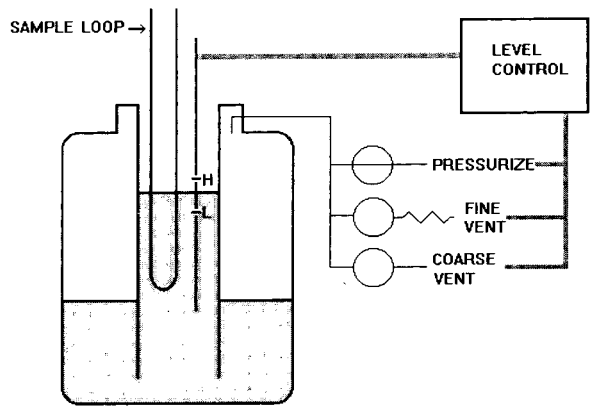

Fig. 2. Schematic of the automated cryo-trapping system. The system is in the activated, level control mode. Liquid nitrogen level is maintained between the high (H) and low (L) resistor level sensors, located 1 cm apart, by pressurizing or venting the dewar headspace.

An ozone trap (O_3T) was installed upstream of SL1 to remove ambient O_3 from the air sampled, since O_3 would also be condensed in SL1 at the cryogenic trapping temperatures and would react with unsaturated NMHCs during

sample heating and transfer from SL1 to SL2 [3]. These traps were prepared by soaking glass wool in a solution of potassium iodide (3 g), methanol (5 ml), water (10 ml) and glycerol (2 ml). The impregnated glass wool was then dried by inserting it in a glass tube and purging it with UHP zero air. The O_3 trap consisted of a short length of stainless steel tubing (51 mm × 5.3 mm I.D.) packed with this impregnated glass wool.

An additional trap (76 mm × 10.5 mm I.D. length stainless steel), packed with Ascarite (NaOH coated silica, A.H. Thomas Co., Philadelphia, PA, USA), was used downstream of the O_3T in the packed column system (see below), in order to remove carbon dioxide (CO_2), which would otherwise interfere with the chromatographic determination of ethane and ethylene. The Ascarite trap was not used with the capillary column system (see below), since a corresponding interference was not found and the Ascarite increasingly removed the higher boiling NMHCs eluting after benzene (retention index 642, DB-1).

NMHC measurements were made by gas chromatography using a Model HP 5890A dual flame ionization detector gas chromatograph (Hewlett-Packard, Palo Alto, CA, USA). Two analytical columns were used: (1) DB-1 fused silica capillary column, 30 m × 0.32 mm I.D., 1 μm film thickness (J and W Scientific, Folsom, CA, USA), −50°C to 200°C at 4°C/min, used for C_3–C_{10} NMHCs; (2) Gas Chrom PICN, 0.14–0.18 mm diameter range (Alltech, Deerfield, IL, USA), 6 m × 0.2 mm I.D. stainless steel packed column, isothermal at 40°C, used for C_2–C_4 NMHCs. Two completely separate automated, analytical systems, one with the capillary and the other with the packed chromatographic column, were operated in parallel, and were used to sample ambient air alternately, every two hours.

Chromatographic signals were sent to HP 3396 integrators; raw signal files were further transferred to and stored by a personal computer, where they were reintegrated using ChromPerfect Ver 3.0 software (Justice Innovations, Palo Alto, CA, USA).

Automation of the sampling process was controlled by a STD-Bus single-board computer (OSC 9600 systems card, Octagon System Corp., Westminster, CO, USA), running STD BASIC III. The automation computer was responsible for initiating and executing the sample collection sequence every two hours on the hour. As illustrated in Fig. 1, sample valves E1 and E2 (to which were attached SL1 and SL2, respectively), flow directing valves (V1 and V2), dewar level control circuitry, and heater power were all switched by a 24-channel digital I/O card (OSC 805 I/O card) controlling standard size OPT022 optically isolated I/O modules mounted on a 24-channel opto relay rack (PB-24 opto rack). GC start, integrator start, and start signals for the West temperature controllers were provided by relay contact closures from an eight-channel relay card (OSC 502 relay card). Sample volumes were determined by analog-to-digital conversion (OSC 860 analog input card) of the pressure of calibrated volumes (CV) from the pressure transducer, P (samples volumes of 2 and 4 litres were approximately 50 and 100 torr above the calibrated volume (CV) pressure at the beginning of the sample collection procedure, respectively). The BASIC automation program was written and compiled on an IBM compatible PC, then downloaded to the Octagon system computer. Diagnostics and housekeeping data were stored on a 256K RAM memory board (OSC 829A 64/256K memory card), before being stored to disk.

Subsequently, the OCTAGON STD-Bus single board computer was replaced by an IBM compatible PC with menu driven software (CONTROL-EG, Quinn Curtis, Needham, MA, USA). This change eliminated the need to write control code in BASIC and considerably reduced the lines of instruction code. It also reduced hardware requirements. All control and sensing in the revised PC system were accomplished using two I/O cards in the PC (Computer Boards Inc., CIO-DIO24 and CIO-DAS08) and one external 16-channel analog input multiplexer board (Computer Boards Inc. CIO-EXP16). Each of the two internal cards had 24 I/O channels which controlled a 24-channel opto relay card (Computer Boards, Inc., SSR-Rack24) with standard size OPTO22 digital I/O

modules. The DAS08 card also had eight A/D channels, several of which were used by the analog input multiplex card for temperature sensing and control, and another two were used for pressure readings on the two parallel analytical channels. In this configuration, the temperatures of SL1 and SL2 were controlled by proportional-integral-differential control (PID) loops run in the background of the Control-EG software.

2.2. Automation sequence

The sample collection/introduction system was completely automated to execute the following sampling sequence:

(1) Initial (default) configuration. The CV was connected to the vacuum pump through switching valve V1 and CV was evacuated to less than 5 torr. Concurrently, the first stage sample trap (SL1) was heated (110°C) and backflushed through the stream selector valve (SS) with UHP helium (50 ml min^{-1}) directed through V1; the second stage sample trap (SL2) was also heated and backflushed with UHP helium (10 ml min^{-1}) directed to vacuum through switching valve V2. Carrier and backflush UHP helium was further purified by passing it through a molecular sieve 5A trap (450 mm × 10.5 mm I.D.) immersed in liquid nitrogen.

(2) Sample collection. SS was switched to the closed (no flow) position, isolating the sample collection system. V1 was switched to connect CV to SL1 on sample valve E1. Simultaneously, the liquid nitrogen level control was activated to immerse SL1 in the cryogen. (The temperature of liquid nitrogen (−196°C) was sufficiently low to trap the lowest boiling NMHCs and immersion in the cryogen eliminated the need to control the trapping temperature.) After a 3-min SL1 temperature equilibration pause, SS was returned to the open (flow) position. The vacuum of the CV pulled sample air from the sample line through a stainless steel bellows needle valve (BNV) used to control sampling rate (125 ml min^{-1}), the ozone trap (O_3T), and SL1. The volume of air pulled through SL1 was related to the pressure change in CV (N_2 and O_2, which constitute approximately 98% of air sampled, pass quantitatively through the trap), which was measured by a pressure transducer (P). A pressure change in CV of 50 torr (used for capillary column system) and 100 torr (used for packed column system) corresponded to approximately 2 and 4 litres air sampled, respectively. At system pressures under approximately 200 torr, liquid nitrogen could be used as a cryogen to trap atmospheric NMHCs without the coincident trapping of atmospheric O_2 and N_2. SL1 had a sufficiently large volume and cross section that lighter NMHCs (ethane, acetylene, ethylene) were trapped at 100% efficiency up to sample flow rates of approximately 200 ml min^{-1} and that simultaneously trapped water vapor would not inhibit sample flows with the large sample volumes passing through SL1.

(3) Sample transfer. After the required volume was passed through SL1, SS was changed to the closed position (no flow). The helium backflush flow through switching valve V2 was stopped by closing shut-off valve SO2 and the position of V2 was changed from the backflush to the SL1–SL2 transfer position. The second stage sample loop (SL2) was then immersed in liquid nitrogen by activating its level control circuit. After SL2 temperature equilibration, the transfer flow of helium through V2 (10 ml min^{-1}) was turned on by opening SO2. E1 position was then changed to put SL1 in series with SL2, the liquid nitrogen level of SL1 was lowered and SL1 was heated to 80°C in 3 min in order to transfer the trapped volatile trace gases to SL2. This slow, controlled heating minimized the transfer of water vapor to SL2, since the water vapor pressure was low over most of the temperature programmed transfer. Coincident with this transfer, the control computer started the HP 5890 gas chromatograph temperature program (contained in its own memory) and the GC oven temperature was lowered to its initial program value (−50°C).

(4) Sample injection. After the sample transfer time expired and the initial oven temperature of the gas chromatograph was reached, sample valve E2 was switched to the inject position, the liquid nitrogen level was lowered and SL2 was

heated to 80°C in approximately 15 s to transfer the sample to the analytical column. The effective dead volume of SL2 after packing with glass beads was less than 100 μl, therefore, minimizing the transfer volume. C_3 and heavier NMHCs were again cryofocused on the GC column. In most samples, the low dead volume of SL2 allowed separation of C_2H_4 from C_2H_6 and C_2H_2 (these NMHCs are not cryofocused on the capillary column). Sample valve E2 was returned to the initial (load) position 45 s after injection. The sample collection/introduction system was returned to its initial default configuration 30 s later. The gas chromatograph continued to execute its temperature program to completion, at which time it held a post-run temperature of 150°C. Detector signals were communicated to the HP 3396 integrator, which was also programmed to store raw data files to a host PC.

2.3. Other analytical details

System blanks were run periodically with zero gas introduced at the beginning of the sample collection system and at the sample inlet atop the tower. Zero gases from high pressure cylinders included UHP nitrogen, UHP helium, and ultrapure zero air. These cylinder zero gases contained numerous trace contaminants, including NMHCs, which were, in some cases, at mixing ratios over 100 ppt. There was considerable variability in the levels of contamination for each of these zero gases and among cylinders of individual zero gases. All required additional purification. Repurification was achieved by passing the zero gas through a molecular sieve 5A trap (450 mm × 10.5 mm I.D.) that was maintained at −80°C in an ethanol–liquid nitrogen bath. The boil-off from the liquid nitrogen tanks was more consistently near appropriate background levels for NMHCs and most other trace gases and was used without additional purification in some tests. Blank levels of NMHCs (and all other trace gases normally detected in routine ambient sampling were negligible (less than 1 ppt) when these repurified zero gases were analyzed.

Experiments were also made to determine the necessity and efficiency of the O_3 traps. O_3 traps were checked at first daily and later weekly. The efficiency of these traps was near 100%, when ambient air (which typically contained 35–45 ppb O_3) was passed through the trap at flow rates up to 1 litre per min (the NMHC sample collection rate was approximately 125 ml min^{-1}). O_3 was measured using a commercial ozone detector (Model #1003-AAS, Dasibi Environmental Corp., Glendale, CA, USA). The traps were efficient for several months under the sampling conditions (up to 25 litres per day or 1.5 m^3 of sample air in a 2 month period). Blank levels for individual NMHCs were not increased by the addition of the O_3 trap and there were no differences in calibration response factors measured with and without the O_3 trap included.

FID signals were processed both with a HP Model 3396-Series II integrator and with ChromPerfect PC software (which allowed for storage of raw signal data and their subsequent reanalysis). The reintegration of the stored raw data file proved essential, since at the low mixing ratios encountered, individual NMHCs often were near their detection limits. The HP 3396 integrator did not conveniently provide adequate integration control. Reintegration of the signal file with ChromPerfect software allowed on-screen baseline placement and integration control, which resulted in satisfactory precision of integration.

3. Calibration and standards

3.1. Standards

Several primary gravimetric standards were used in the course of the experiment: (1) 1 ppm (±1%) propane in nitrogen, National Institute of Standards and Technology (NIST) SRM #1660a; (2) 10.53 ppb (±3%) *n*-butane and 10.30 (±2%) ppb benzene in nitrogen, NIST special mixture; (3) 7-component mixture: ethane, ethylene, acetylene, propane, propylene, *i*-butane, *n*-butane in nitrogen, 15 (±2%) ppm each, Scott Specialty Gases, Plumsteadville, PA, USA; (4) 201 (±2%) ppb 2,2-dimethyl butane

in nitrogen, Scott Specialty Gases. These primary standards were intercompared on a response per carbon basis [7,10,11] and were in agreement within the confidence limits reported by the preparer. In addition to the primary standards, a secondary standard was prepared from the dilution of an aliquot of the 7-component primary standard to the 10 ppb level with zero air.

A dynamic dilution system [12] was used to dilute a flow of the primary 7-component standard to concentrations from 15 ppm down to 650 ppt. These dilutions were used to calibrate the secondary standard made from the 7-component primary standard. The dynamic dilution system was again used to dilute the secondary 7-component standard (approximately 10 ppb for each component) down to 15 ppt/component. High-pressure cylinder ultra-pure zero air (Scott-Marrin, San Bernadino, CA, USA) was used as the diluent gas; however, the NMHC levels in these cylinders were of the order of several tens of ppt for some individual NMHCs and cylinders also contained numerous other trace gas components. Consequently, it was necessary to purify the dilution gas by passing it through a molecular sieve 5A trap (450 mm × 10.5 mm I.D.) immersed in a liquid nitrogen–ethanol bath maintained at −80°C. This additional purification reduced NMHC mixing ratios to levels below 2 ppt and removed most other constituents. Dilutions to lower concentrations were not made because, at dynamic dilution flow rates (> 1 l min^{-1}), the diluent zero air levels of several NMHCs could not be reduced further. (At purification flow rates of the order of 100 ml min^{-1}, used to determine system blanks, sub-ppt levels were obtained for all NMHCs).

3.2. Calibration

Calibration of the NMHC system was performed over the mixing ratio range 15 ppt to 15 ppm and the response of both FID systems proved linear over the entire range (Fig. 3). In addition, we compared the response factors for individual NMHCs (Table 1). The relative response factors measured, when the mixing ratios were expressed as parts per trillion of carbon, are within a few percent of each other. For the calibration of NMHCs sampled, the actual response factor for each individual NMHC in the calibration mixture was used. Where there was no response factor measured for a specific

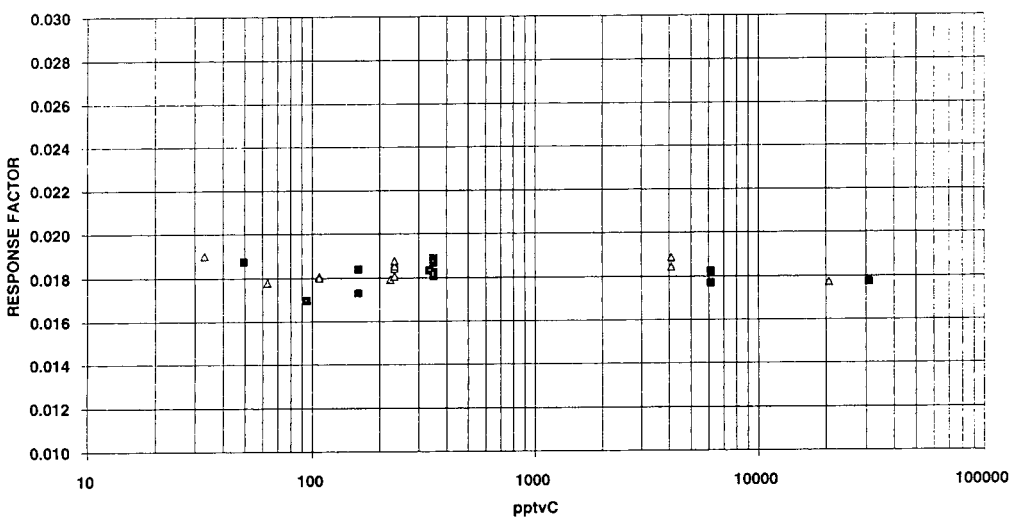

Fig. 3. Response factors calculated for the calibration of ethane (△) and propylene (□), shown in mixing ratios of parts per trillion by volume carbon. The FID system gave a linear response on the pptvC basis over the dynamic range of approximately 30 pptvC (the lowest measured) to 30 ppmvC.

Table 1
Relative FID response factors ($RF_x/RF_{n\text{-butane}}$)

NMHC	Response factor
C_2H_6	1.03 (±0.06)
C_2H_4	1.01 (±0.06)
C_3H_8	1.03 (±0.06)
C_3H_6	0.98 (±0.07)
i-C_4H_{10}	1.02 (±0.06)
C_6H_6	0.98 (±0.03)

RF = [NMHC]/area; concentrations are computed as pptvC. C_2H_6, C_2H_4, C_3H_8, C_3H_6, and i-C_4H_{10} relative response factors were based upon the 7-component NMHC standard; the relative response factor for C_6H_6 was based on the NIST n-butane–benzene standard. Uncertainties were computed from propagation of errors, considering uncertainties in standard calibrations, dilution factors, and standard deviation of area response from multiple analyses of individual components.

NMHC (*i.e.*, the component was not a included in a primary standard), the average of the response factors from Table 1 was used.

3.3. Detection limits and uncertainties

Detection limits for individual NMHCs were determined empirically from the precision of the measurements and are reported as 3 times the uncertainty of the determination for the smallest detected peaks (Table 2). Differences in sample volume, chromatography, and background signal resulted in some differences in the detection limits between the packed and capillary column systems.

Table 2
Detection limits (ppt) for individual NMHCs determined for the system described

NMHC	Packed column	Capillary column
C_2H_6	1	
C_2H_4	1	2
C_2H_2	1	
C_3H_8	0.5	0.5
C_3H_6	0.7	0.5
i-C_4H_{10}		0.4
n-C_4H_{10}	0.4	0.4
n-C_5H_{12}		0.3
C_5H_8		0.3
C_6H_6		0.3
C_7H_8		0.3

Sample sizes were 4 and 2 litres for the packed column and the capillary column systems, respectively.

Uncertainties in the determination of individual NMHCs were determined by a propagation of errors technique, and included errors in the determination of sample volume, temperature, chromatographic integration, and calibration. Uncertainties for NMHCs computed were approximately 5% at mixing ratios above 50 ppt, 7% at 10 ppt, and 10% at 3 ppt (20% for ethylene); errors for acetylene were higher because of incomplete separation from another constituent and sometime were as high as 20%.

4. Conclusion

Concentrations of atmospheric NMHCs measured during the year-long MLOPEXII experiment varied seasonally and diurnally, as well as with synoptic meteorological conditions [8]. These concentrations varied from several thousand ppt for the longest lived NMHC, ethane, to sub-parts per trillion levels for others. Representative chromatograms for the packed column and capillary column techniques are shown in Fig. 4. Numerous peaks corresponding to trace gases other than NMHCs were also detected and appear in these chromatograms. These were often chlorofluorocarbons, aldehydes, and ketones. In cases where identifications were confirmed by *in situ* GC–MS measurements [13], identifications are presented on the chromatograms of Fig. 4. Quantitation of trace species other than NMHCs was not made. Of particular interest in the capillary chromatogram are the occurrence of a series of n-alkyl aldehydes, which appeared as the major features of most chromatograms in samples analyzed on the capillary column. Similar observations have been made by others [14,15]. Actual mixing ratios of these aldehydes may differ from the relative abundances indicated in Fig. 4, since the analytical system was not characterized for the quantitation of aldehydes. Analytical discussions regarding these are presented elsewhere [8].

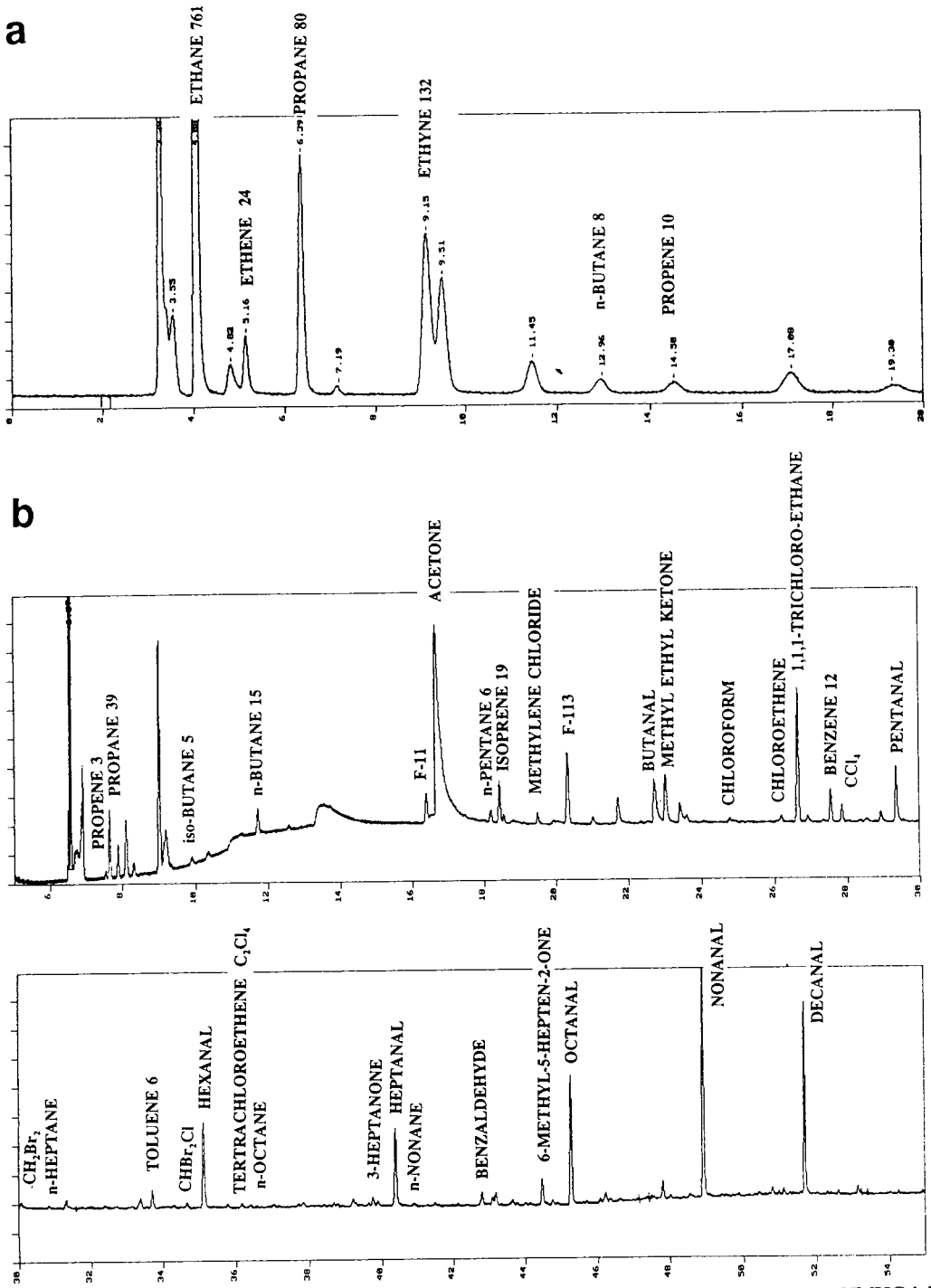

Fig. 4. Sample chromatograms from the MLOPEX II experiment. Mixing ratios in ppt are shown next to NMHC label; other trace gases identified are labeled only. (a) Packed column chromatogram for C_2–C_4 NMHCs, January 29, 1992, 21.00–21.30 local time; (b) capillary column chromatogram for C_3–C_{12} NMHCs, July 22, 1992, 16.00-16.15 local time.

The system described here successfully met the design criteria of continuous, automated, unattended operation; wide dynamic range and sub-ppt detection limits; freedom from water vapor, O_3, and CO_2 interferences; negligible analytical blanks levels; and linear calibration response over the entire range of measurements.

Acknowledgements

We thank E. Ellert, who contributed significantly to the fabrication of the instrument and who wrote the BASIC program instructions to control the instrument. The National Center for Atmospheric Research is sponsored by the National Science Foundation.

References

[1] J.G. Calvert and S. Madronich, *J. Geophys. Res.*, 92 (1987) 2211–2220.
[2] H.B. Singh and P.R. Zimmerman, in J. Nriagu (Editor), *Gaseous Pollutants: Characterization and Cycling*, John Wiley and Sons, New York, 1992, Ch. 5, pp. 177–235.
[3] J.P. Greenberg, P.R. Zimmerman, W.F. Pollock, R.A. Lueb and L. Heidt, *J. Geophys. Res.*, 97, D10 (1992) 10395–10413.
[4] W.C. Kuster, P.D. Goldan, S.A. Monzka and F.C. Fehsenfeld, *EOS Trans. AGU*, 71 (1990) 1228.
[5] N.M. Donahue, *Ph.D. Thesis*, Center for Global Change Science, Massachusetts Institute of Technology, Cambridge, MA, July 1991, Report No. 8.
[6] S.A. Monzka, M. Trainer, P.D. Goldan, W.C. Kuster and F.C. Fehsenfeld, *J. Geophys. Res.*, 98, D1 (1993) 1101–1111.
[7] E.C. Apel, J.G. Calvert and F.C. Fehsenfeld, *J. Geophys. Res.*, in press.
[8] J.P. Greenberg, D. Helmig and P.R. Zimmerman, in preparation.
[9] B.A. Ridley and E. Robinson, *J. Geophys. Res.*, 97, D10 (1992) 10285–10290.
[10] W.A. Dietz, *J. Gas Chromatogr.*, 1 (1967) 68–71.
[11] R.G. Ackman, *J. Gas Chromatogr.*, 6 (1968) 497–501.
[12] P.D. Goldan, W.C. Kuster and D.L. Albritton, *Atmos. Environ.*, 20 (1986) 1203–1209.
[13] D.H. Helmig and J.P. Greenberg, *J. Chromatogr.*, submitted for publication.
[14] Y. Yokouchi, H. Mukai, K. Nakajima and Y. Ambe, *Atmos. Environ.*, Vol. 24A, No. 2 (1990) 439–442.
[15] P. Ciccioli, E. Brancaleoni, M. Frattoni, A. Cecinato and A. Brachetti, *Atmos. Environ.*, 27A, No.12 (1993) 1891–1901.

ELSEVIER

Journal of Chromatography A, 676 (1994) 399–408

JOURNAL OF CHROMATOGRAPHY A

Measurement of vapor-phase organic compounds at high concentrations

Joachim D. Pleil*[,a], Michael L. Stroupe[b]

[a] *Atmospheric Research and Exposure Assessment Laboratory, US Environmental Protection Agency, Research Triangle Park, NC 27711, USA*

[b] *Graseby/Nutech, Durham, NC, USA*

First received 11 January 1994; revised manuscript received 6 April 1994

Abstract

Laboratory, industrial, chemical or other waste products may have constituents that evolve volatile organic compounds (VOCs) at very high concentrations. These could pose human health risks during handling, storage and disposal of the waste through inhalation, dermal exposure or explosion. Additionally, the release of VOCs can adversely impact the tropospheric chemistry, and in the case of halogenated compounds, the stratospheric ozone chemistry as well. Very precise and accurate methods exist for measurement of VOCs at trace levels; however, these are inappropriate for the high levels in waste headspace, which often approach saturation vapor pressure. This paper presents an inlet system and analytical method for gas chromatography–mass spectrometry designed specifically for measuring VOC concentrations greater than 10 ppm (v/v) in a gas matrix. The technique is shown to be effective for measuring selected common solvents including alcohols, ketones, halogenated hydrocarbons and aromatic compounds in an air matrix in stainless-steel sampling canisters. This work was performed under a Cooperative Research and Development Agreement between the US Environmental Protection Agency and Graseby/Nutech Corporation.

1. Introduction

The handling, storage and disposal of mixed wastes is subject to a variety of environmental laws and regulations, health and safety rules and transportation regulations. Often there are reporting requirements for potential hazards such as toxicity and flammability due to volatile organic compounds (VOCs) that are present in the gaseous headspace of the waste materials. For purposes of waste characterization, this headspace can be considered as representative of the VOC concentration within the overall waste volume. Thus depending upon the contents of the waste container, concentrations of VOCs can range from a very low part per billion by volume (ppbv) level, as from slowly leaking secondary containment, up to levels in the percent by volume range, where the contents are at saturation vapor pressure from free liquid evaporation. The minimum reporting requirement for compounds of interest is typically 10 to 100 parts per million by volume (ppmv).

Sampling methods for mixed waste headspace generally involve the capture of a gas sample in a bag or rigid container (such as a stainless-steel

* Corresponding author.

SSDI 0021-9673(94)00350-I

passivated canister) for subsequent laboratory analysis by gas chromatographic (GC) methods. However, analysis of any waste headspace samples containing high concentrations of VOCs cannot be accomplished by standard techniques. Environmental laboratories equipped for air analysis are geared toward trace-level work using method TO-14 [1] (or a related method), which is appropriate for ppbv and sub-ppbv concentrations. The potentially high VOC levels in the waste headspace pose difficulty in sample transfer and processing due to adsorption in the complex gas inlet system and overloading of the analytical column and detector.

To address this issue, various laboratories have made modifications to standard environmental trace-level methods to accommodate high-level samples. The simplest method uses a small syringe aliquot drawn from the sample that is injected into a split-flow GC injection port. Another approach employs a sample loop injection valve to shunt a fixed volume of sample into the analytical system. Some laboratories opt to dilute the high-level samples to concentrations for which their existing instrumentation is suited. These (and possibly other) adaptations to existing techniques have been implemented at various degrees of success. There are some drawbacks to these methods.

The methods involving syringe gas injection of 10 to 100 μl are very operator dependent and tend to suffer from poor precision. The high surface-to-volume ratio of the syringe and the deformable materials in the plunger may affect the sample integrity of the polar constituents in the sample through adsorption and absorption. Sample loop injections through an automated valve are very precise; however, the additional gas flow plumbing and valve surfaces are subject to adsorption of analytes and run-to-run carryover when very-high-level samples are followed by samples with lower concentrations. Finally, though dilution of the sample is very effective in allowing accurate and precise analyses with standard air techniques, this requires additional sample handling by the laboratory personnel, precise pressure or flow gauges, and additional quality assurance and quality control to verify the integrity of the procedure. Each step in the procedure can introduce errors in the final dilution factor calculation.

This paper presents an automated analysis method and sample injection hardware for GC–mass spectrometry (MS) specifically for high-VOC-concentration samples. It is based upon the injection of a low-volume aliquot from a flowing sample stream through a differential pressure switch, which is functionally similar to work described by Deans [2]. The injection volume is adjustable for sensitivity via computer control without any processing (dilution) or other handling of the sample. The sample stream does not contact any surface other than deactivated fused silica between the sample container and the interior of the analytical column. The method was applied to pressurized gas samples containing compounds including methanol, ethanol, acetone, methyl ethyl ketone, *n*-butanol, carbon tetrachloride, tetrachloroethylene, benzene and toluene, as well as gasoline vapors. Tests were performed at levels ranging from low ppmv per analyte up to saturation vapor pressure concentrations. This work is a collaborative effort performed under a Cooperative Research and Development Agreement between the Atmospheric Research and Exposure Assessment Laboratory (AREAL) of the US Environmental Protection Agency (EPA) and Graseby/Nutech Corporation.

2. Experimental

Two separate systems were used for this work. The first is an EPA laboratory prototype assembled from available materials with only minor machining of standard fittings and injection port parts, and this is referred to as system 1. The second system is a manufacturer's prototype built by Graseby/Nutech and based upon experience gained from testing of the laboratory prototype. This is referred to as system 2 in the ensuing text.

2.1. System 1

The injection hardware is composed of standard 1/16-in. and 1/8-in. (1 in. = 2.54 cm)

Swagelok fittings and stainless-steel tubing mounted onto a standard split/splitless injection port on a Varian 3400 GC system as configured as part of a Finnigan MAT (San Jose, CA, USA) ITS40 GC–MS ion trap system. The injection port nut was remachined and internally threaded to accept an O-ring fitting that provides a seal as well as mechanical stability. The injection port plumbing of the GC system was bypassed, and the helium purge flow valve was rerouted to provide control of the on/off switching of the helium gas column flow through computer control. A standard Graseby/Nutech 320-01 controller was modified to provide two feedback-regulated temperature zones, one to heat the injection and gas switching assembly, the other to maintain a constant elevated helium temperature. To accommodate the relatively large switching volume, an additional "sweep" flow was used to rapidly remove residual gas. Helium and sample flows are adjusted so that there is always a positive flow at the vent to keep room air from infiltrating into the system. Fig. 1 shows a simple diagram of this injection scheme. Sample is introduced into the analytical column during the time that the helium flow is off. This time was empirically chosen (0.01 min) so that saturated pressure VOCs presented well-resolved and well-formed chromatographic peaks.

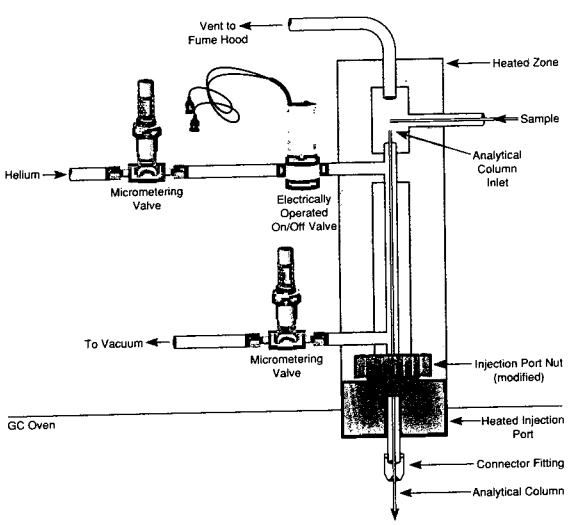

Fig. 1. Diagram of system 1 (laboratory prototype) sample injection hardware. Sample flow is briefly shunted onto the analytical column when the helium valve is placed in the off state. The injection volume of the "switch" is always swept through the coaxial flow around the outside of the analytical column. Helium and sample flows are set to always provide positive flow at the vent.

2.2. System 2

The large, complex configuration of system 1 was redesigned into a small solid steel block drilled with appropriate channels to provide the switching body. Connection tubes were welded into place, and the whole assembly was passivated with a deactivated fused-silica layer, a proprietary process (Silcosteel) from Restek (Bellefonte, PA, USA). Helium pressure and flow were controlled with a dedicated single-stage regulator and fine metering valve. The injector was imbedded in a temperature-controlled zone and installed on top of a Hewlett-Packard (HP; Palo Alto, CA, USA) HP-5890 gas chromatograph with an HP-5971 mass spectrometer as the detector. An external Graseby/Nutech Series 2000 controller was interfaced directly into the Windows-based (Microsoft) HP Chemstation software so that the GC–MS system and the injection system could be operated directly from the GC–MS system computer. Fig. 2 shows a diagram of the simplified system. The injection volume was set by adjusting the helium "time off" parameter empirically to achieve good chromatography.

2.3. Performance tests

All performance tests were based on compressed gas samples in humidified zero grade air or in nitrogen. These were prepared in 6-l-volume Summa-polished canisters from SIS (Moscow, ID, USA). Each sample was fitted with a dedicated fused-silica transfer line and reducing union fitting. All analyses were performed by using full-scan MS data acquisition. For quantitation, the characteristic ion (typically the base peak ion) was extracted from the total ion chromatogram, and the resulting trace was integrated.

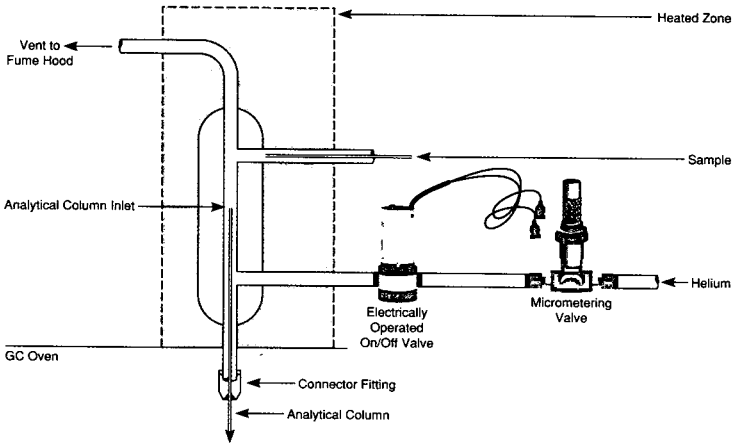

Fig. 2. Diagram of system 2 (commercial prototype) sample injection hardware. This simplified system is a single machined piece internally coated with deactivated fused silica. Sample flow is briefly shunted onto the analytical column when the helium flow is interrupted by the helium on/off valve. The extremely low dead volume does not require an additional sweeping flow as in system 1.

Initial tests

The first developmental tests were performed by using high-level samples prepared in the laboratory by injecting 100 or 200 μl (each) of a variety of liquid analytes (and water) into evacuated 6-l canisters and pressurizing to 3 atm absolute pressure (30 p.s.i.g.; 1 atm = 101 325 Pa, 1 p.s.i. = 6894.76 Pa) with zero-grade air. Depending upon the compound, these samples were at or near saturation vapor pressure for the analytes. Some typical analyte mixtures are given in Table 1. Lower level samples (at 10 or 20 ppmv), composed of primary working standards from method TO-14 [1] calibration mixtures available in the laboratory, were used to test the sensitivity range and to optimize analytical pa-

Table 1
Analyte mixtures used to optimize analytical parameters

High level 1	High level 2	High level 3
Methanol	Methanol	Methanol
Ethanol	Ethanol	Ethanol
2-Propanone (acetone)	2-Propanone (acetone)	1,1′-Oxybisethane (diethyl ether)
2-Butanone (methyl ethyl ketone)	Dichloromethane	2-Propanone (acetone)
2-Propanol	*n*-Hexane	Dichloromethane
n-Butanol	Methylbenzene (toluene)	Cyclohexane
	Tetrachloroethene	Tetrachloromethane (carbon tetrachloride)
	Nitrobenzene	Benzene
	Naphthalene	Fluorobenzene
		n-Butanol
		Methylbenzene (toluene)
		Tetrachloroethene
		Ethylbenzene
		1,2-Dimethylbenzene (*o*-xylene)
		Benzene methanol (benzyl alcohol)
		Nitrobenzene

*Common names of the chemicals are in parentheses.

rameters. The method TO-14 list of compounds is composed of 40 specific "non-polar" VOCs ranging in volatility from the very volatile Freons up to the marginally volatile aromatic hydrocarbons and halogenated aromatic hydrocarbons.

Quantitative precision tests

For system 1, replicate precision tests were performed using high-level samples prepared in the laboratory (as listed in Table 1, columns 1 and 2); for system 2, moderately-high-level standards that were obtained through the AREAL Quality Assurance Division were used. The compounds and concentrations used for system 2 precision tests are listed in Table 3. The area of the integrated extracted ion profile of an analyte's characteristic ion was used for quantitation. All quantitation was based on external standards from various available sources.

Sample contamination and carryover tests

Once system 2 was tested and optimized, the efficacy of the methodology in a complex matrix was demonstrated by using a very challenging mixture —raw gasoline headspace. Various samples were prepared by injecting 5 ml of gasoline into evacuated canisters and pressurizing to 2 atm gauge. Sample blanks were prepared by injecting organic-free deionized water in place of the gasoline. For these tests, three different formulations of gasoline were obtained from the AREAL Mobile Source Emissions Research Branch: unleaded 87 octane with no oxygenates, with methanol additive, and with methyl *tert.*-butyl ether (MTBE) additive. For these tests, the gasoline headspace samples were analyzed with interspersed blank samples to test for sample cross-contamination and to determine if the oxygenated additives could be detected in the very complex hydrocarbon matrix.

2.4. Sample introduction

For all analytical tests, the sample mixture was released from the canister through a 50 cm × 0.25 mm I.D. deactivated fused-silica tube into the analytical system inlet. The resulting transfer flow was in the range of 100 to 250 ml/min, depending upon canister pressure. Only a small aliquot of this constant flow was introduced onto the analytical column through the valveless switch, as the helium flow was briefly interrupted by the helium control valve. (See Figs. 1 and 2 for system diagrams). Injection of sample in this fashion is very precise, and the sample amount can be adjusted through a software parameter that determines the time interval that the helium control valve is off. This time interval was chosen empirically to achieve optimal chromatography for each system and then left unchanged for all tests. An exact injection volume could not be accurately determined because of gas turbulence during the switching pulses, dead volume mixing within the switch volume, and the unknown valve response time. Calculated injection volumes were 12.5 μl for system 1 and 100 μl for system 2.

3. Results and discussion

The major part of the initial development work was performed on system 1 with a wide variety of compound mixtures and other real-world matrices. Once the specific technique was

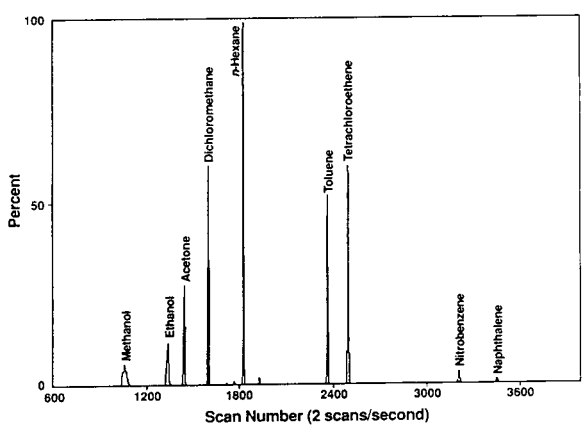

Fig. 3. Example chromatogram of mixed waste headspace precision test of system 1. Compounds are at (or near) saturation vapor pressure in a humid air matrix in a 6-l-volume canister. Column: J & W DB-5 (30 m × 0.25 mm I.D., 1-μm phase). GC oven: 2-min hold at −50°C, ramp 8°C/min to 200°C.

Table 2
System 1 precision test results for high-level mixture 2

Compound	R.S.D. (%) ($n = 7$)
Methanol	6.92
Ethanol	6.19
2-Propanone (acetone)	6.99
Dichloromethane	5.15
n-Hexane	5.75
Methylbenzene (toluene)	5.39
Tetrachloroethene	6.44
Nitrobenzene	7.94
Naphthalene	9.35

Seven replicate runs, statistics based on single ion extracted profile areas. Common names of the chemicals are in parentheses.

developed, high-level headspace samples were more rigorously tested. An example chromatogram of a precision test is given in Fig. 3, and the results for a seven-repeat-analysis sequence are shown in Table 2. In this demonstration, the sample concentrations were near or at saturation vapor pressure. Note that the chromatography is clean and that the precision data indicate a typical run-to-run scatter of 5 to 7% relative standard deviation (R.S.D.). Nitrobenzene's and naphthalene's greater errors at about 8 and 9% R.S.D. are most likely due to the low vapor pressure and marginal suitability for storage in canisters for these compounds. For this particular test, a J & W (Folsom, CA, USA) DB-5, 30 m × 0.25 mm I.D. capillary column with 1-μm stationary phase was used with a GC oven temperature profile consisting of a 2-min hold at −50°C with a ramp to +200°C at 8°C/min. The calculated injection volume was about 12.5 μl. In other tests, J & W DB-1701, Restek Rtx-5 and Restek Rtx-1301 columns (each with appropriate oven temperature programs) were used with good results.

The optimized system 2 was similarly tested for precision by using a nominal 100-ppmv-per-compound mixture and a prepared mixture with a variety of concentrations for each compound. Results for these two tests are given in Table 3. For this particular series of tests, a Restek Rtx1301 30 m × 0.25 mm I.D. column with 1-μm stationary phase was used. The oven tempera-

Table 3
System 2 precision test results for two mixtures

Compound	Test 1		Test 2	
	ppmv	R.S.D. (%)	ppmv	R.S.D. (%)
Methanol	86.5	4.95	725	6.28
1,1,2-Trichloro-1,2,2-trifluoroethane (Freon 113)	86.1	4.16	787	2.24
2-Propanone (acetone)	119	3.83	769	2.49
Dichloromethane	105	4.31	793	2.28
1,1-Dichloroethane	103	4.34	836	2.93
2-Butanone (methyl ethyl ketone)	106	2.78	117	2.83
Trichloromethane (chloroform)	92.6	3.32	731	1.80
1,1,1-Trichloroethane (methylchloroform)	91.1	3.47	325	1.47
Tetrachloromethane (carbon tetrachloride)	89.4	4.11	181	2.45
Trichloroethene	79.1	5.47	104	2.89
4-Methyl-2-pentanone	96.1	4.62	72.0	2.79
Methylbenzene (toluene)	91.1	3.28	172	2.32
Tetrachloroethene	79.9	5.04	19.8	2.10
1,4-Dimethylbenzene (*p*-xylene)	94.6	3.52	31.8	2.26
1,1,2,2-Tetrachloroethane	96.2	3.68	25.9	2.20

Seven replicate runs for each mixture. Statistics based upon single ion extracted profile areas. Common names of the chemicals are in parentheses.

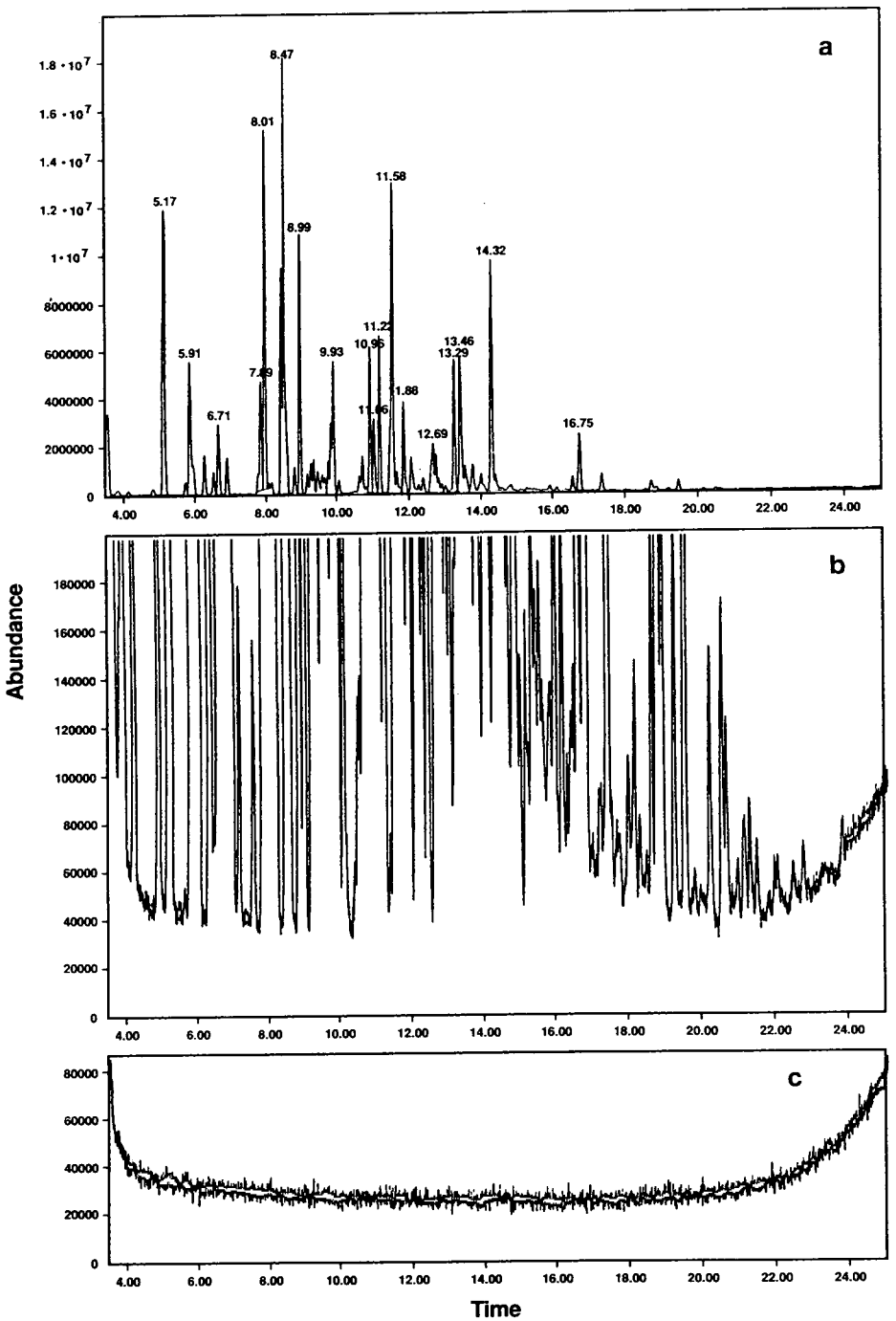

Fig. 4. Example chromatograms demonstrating sample integrity of system 2: (a) headspace of gasoline saturation vapor pressure, full scale; (b) headspace of same sample, chromatogram expanded vertically; (c) humid zero air sample run immediately after gasoline headspace, same scale as (b). Column: Restek Rtx-1301 (30 m × 0.25 mm I.D., 1-μm phase). GC oven: 2-min hold at 5°C, ramp 10°C/min to 200°C. Time in min.

ture program consisted of a 2-min hold at 5°C with a 10°C/min ramp to 200°C. The injection volume was calculated to be 100 μl.

These results are excellent considering the very-high-level concentrations and the associated potential for contamination within the system.

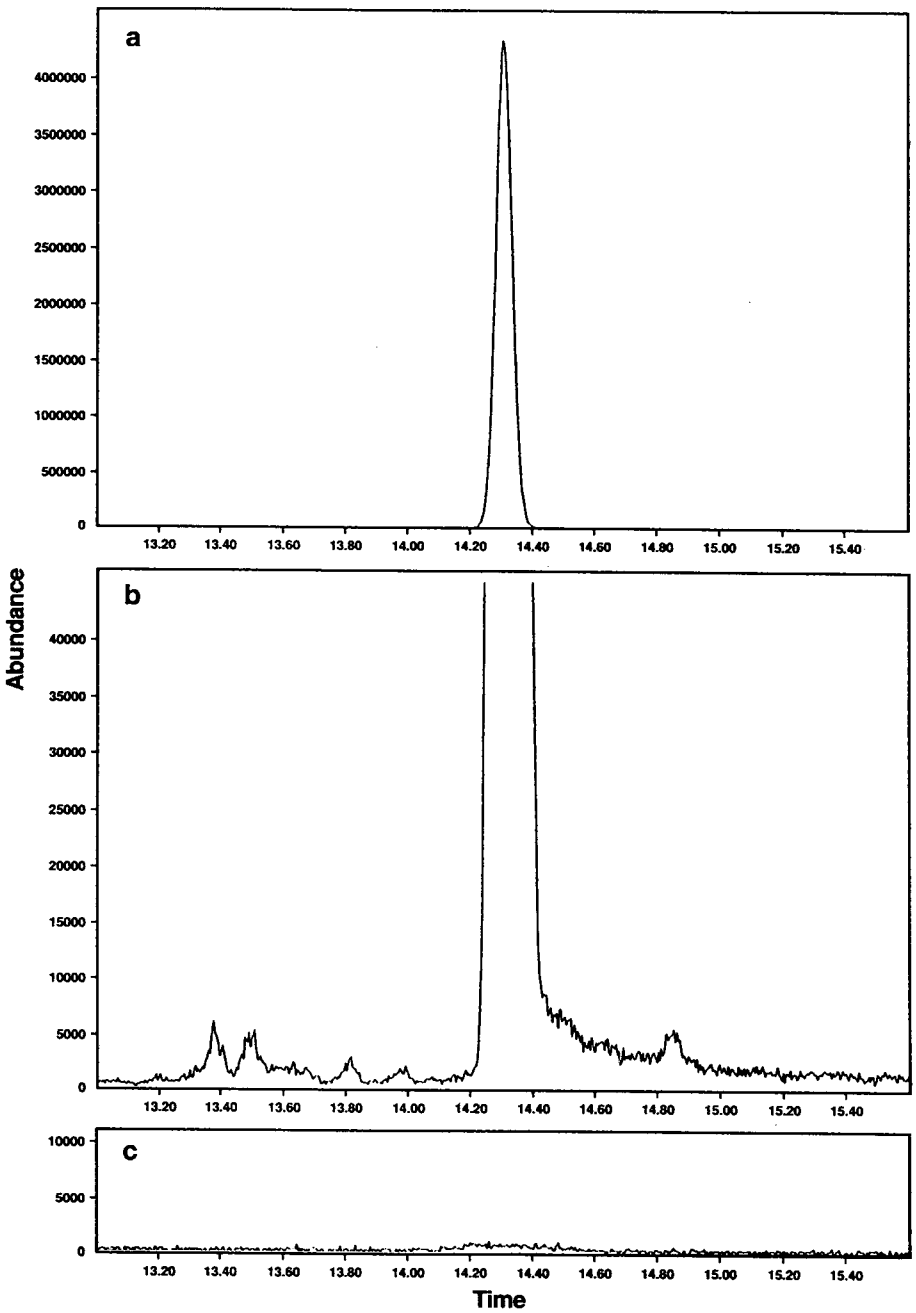

Fig. 5. (a), (b), (c) Example extracted ion 91 chromatograms corresponding to Fig. 4a, b and c, respectively, for the toluene constituent of gasoline headspace demonstrating run-to-run sample integrity. Time in min.

Upon detailed analysis of individual chromatograms, we noticed a slight systematic decline in the overall HP-5971 MS response throughout the day, which contributed to the aggregate error. It was estimated that only about half of the R.S.D. should be attributed to the injection system.

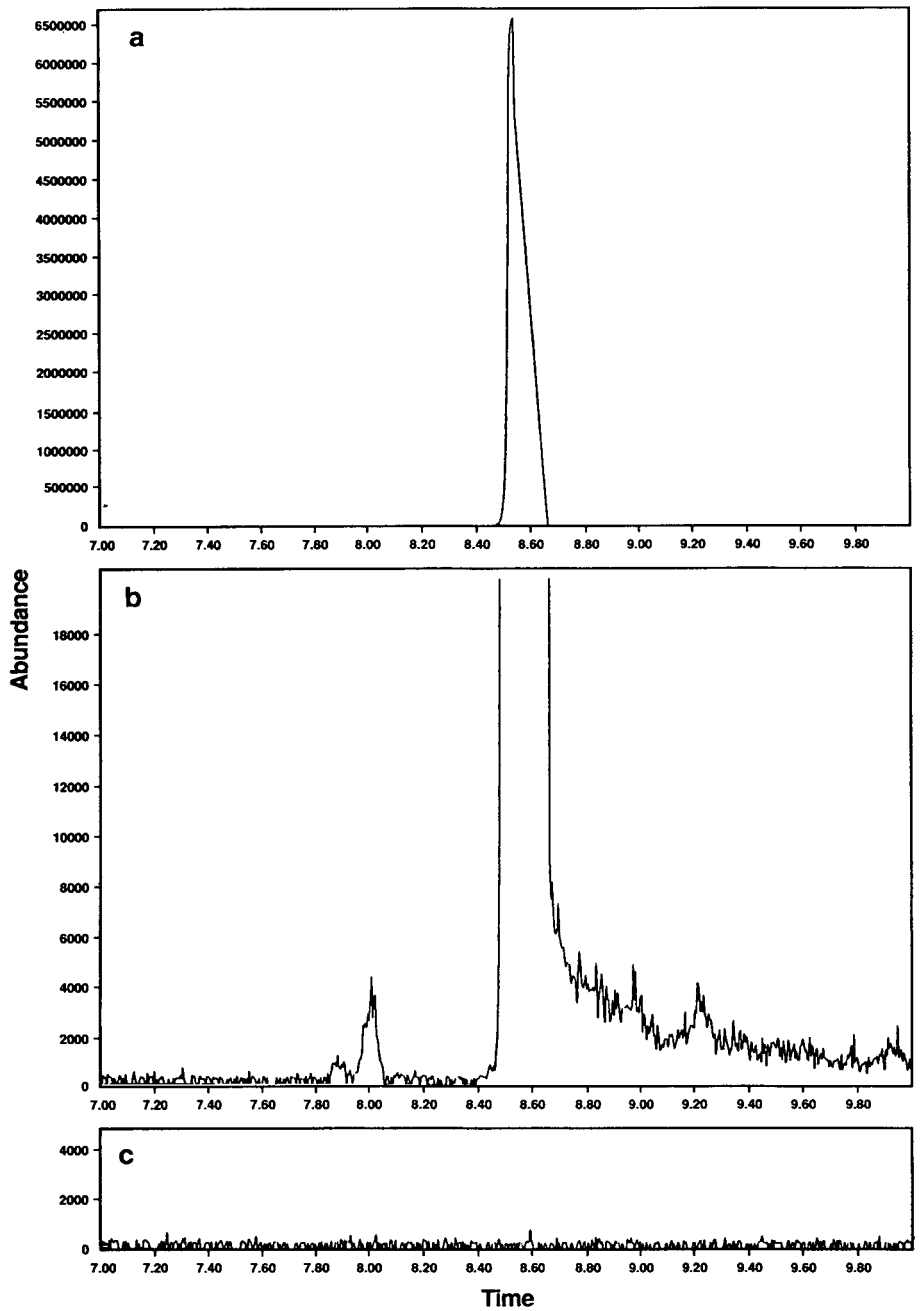

Fig. 6. (a), (b), (c) Example extracted ion 73 chromatograms corresponding to Fig. 4a, b and c, respectively, for the MBTE constituent of gasoline headspace demonstrating run-to-run sample integrity. Time in min.

Numerous tests with blanks on both system 1 and system 2 showed no measurable cross-contamination or carryover from a previous high-concentration sample. A worst-case example, as run with system 2, is presented in the total ion chromatograms in Fig. 4; here, the analysis of the headspace of raw gasoline with MTBE as an additive was followed immediately by the analysis of a humidified zero air sample. The comparison between the expanded vertical scale of the gasoline headspace chromatogram and the blank chromatogram shows this graphically.

For further investigation of possible cross-contamination, Figs. 5 and 6 show detailed sets of extracted ion chromatograms in which toluene and MTBE are used as examples. Here, the full-scale peak, an expanded peak (scale factor of 100), and the correspondingly scaled blank sample chromatogram are shown. Note that there is no measurable carryover into the blank sample.

4. Conclusions

The presented methods and hardware configurations are effective at determining the high-level VOC concentrations in a gas matrix. Even a simple configuration (system 1), as constructed in the research laboratory, was capable of precise headspace analysis (5 to 9% R.S.D.) of high-level VOCs. The optimized system 2 switching device, constructed from a single machined and welded part and then internally coated with fused silica, performed with about a factor of 2 better precision (1.5 to 6% R.S.D.). This type of injection switching performs well within the typical requirement of 20% R.S.D., and it is relatively simple because it requires no syringes, sampling valves, or high-level multiple dilution steps, which require additional laboratory preparation time. Both polar and non-polar VOCs can be analyzed in a single chromatographic run with excellent precision. The absence of run-to-run sample cross-contamination reduces the need for frequent blank checks, thus reducing the overall quality control overhead. With a single parameter setting, the system has a dynamic range of analysis from 10 ppmv up to saturation vapor pressure of a variety of VOCs. Finally, the system is suitable for any type of modern capillary column GC–MS system employing a direct column GC–MS interface.

5. Disclaimer

The research described in this article has been performed under a Cooperative Research and Development Agreement between the US Environmental Protection Agency and Graseby/Nutech Corporation. It has been subjected to Agency review and approved for publication. Mention of trade names or commercial products does not constitute endorsement or recommendation for use.

References

[1] W.T. Winberry, Jr., N.T. Murphy and R.M. Riggan (Editors), *Compendium of Methods for the Determination of Toxic Organic Compounds in Ambient Air, EPA-600/4-89/017*, US Environmental Protection Agency, Research Triangle Park, NC, 1989.

[2] D.R. Deans, *J. Chromatogr.*, 289 (1984) 43–51.

ELSEVIER

Journal of Chromatography A, 676 (1994) 409–420

JOURNAL OF CHROMATOGRAPHY A

New approaches to concentration on a microliter scale of dilute samples, particularly biopolymers with special reference to analysis of peptides and proteins by capillary electrophoresis I☆. Theory

Stellan Hjertén*, Jia-Li Liao, Rong Zhang

Department of Biochemistry, University of Uppsala, Biomedical Center, P.O. Box 576, S-751 23 Uppsala, Sweden

First received 20 December 1993; revised manuscript received 21 March 1994

Abstract

New methods are described for the concentration of ionic analytes, particularly ampholytes, such as peptides and proteins. In most of these methods the sample is depleted (partially) of strong electrolytes concomitantly with the concentration. The methods are based on the fact that electrophoretic migration velocities decrease upon decreasing the absolute value of the zeta potential of a solute and the pore size of the electrophoresis medium and upon increasing the cross section of the electrophoresis chamber, the viscosity and the electrical conductivity of the electrophoresis medium. We have also utilized the zone-sharpening properties of displacement electrophoresis in combination with a hydrodynamic counter flow to create a stationary zone where the sample solutes can be collected continuously.

In practice, the whole electrophoresis tube is filled with the sample solution to be concentrated. When a voltage is applied the solutes begin to migrate, but finally cease to move as they approach the end of the tube, provided that the above-mentioned parameters in that section of the tube have been given appropriate values. By means of this technique the sample can be concentrated into a zone of a width of 0.2–0.5 mm. Accordingly, a 400–1000 fold concentration is obtained when a 200 mm long tube is filled completely with the sample and still more if also an electrode vessel (or a vessel connected to this electrode vessel) is loaded with sample. The narrow sample zone can be withdrawn from the tube and subjected to further studies or used as a starting zone for an in-tube zone electrophoresis. The tendency for broadening of the very narrow starting zone during the initial phase of this electrophoresis step can be counteracted by a short mobilization step involving displacement electrophoresis, electrophoresis in a steep pH gradient, or on-tube dialysis against a (diluted) buffer. This step can be omitted when the concentration is accomplished by a combination of displacement electrophoresis and a counter flow.

In Part II we show how the theory developed in this paper can be utilized practically.

* Corresponding author.

☆ For Part II see ref 1.

0021-9673/94/$07.00
SSDI 0021-9673(94)00316-2

1. Introduction

Every analysis method has a lower detection limit under which one cannot obtain accurate analysis data. Therefore, one must sometimes perform a preconcentration step which usually entails large losses when the sample volume is 1–10 μl or less. The most common methods for the concentration of solutes of biochemical interest (lyophilization [2], ultrafiltration [3,4], partition between two polymer aqueous phases [5], osmotic removal of water [6] and chromatographic adsorption–desorption of the solute) are not applicable on such a small scale.

There is, accordingly, a need for efficient preconcentration techniques applicable for minute-volume samples. Five such methods, based on electrophoretic zone sharpening, have recently been presented [7,8]. They are described in detail in this paper (references to related methods are found in Discussion). A requirement is that the solutes to be concentrated are ionic polymers or weak electrolytes, preferably ampholytes, such as proteins, or can be converted to such by complex formation. When the concentrated zone is to be used as the starting zone for a subsequent electrophoresis the concentration can take place in the electrophoresis chamber, for instance, a capillary.

2. The theory of the concentration (step I), the mobilization of the concentrated zones (step II) and the electrophoretic analysis (step III)

The discussion below refers to an analysis by high-performance capillary electrophoresis (HPCE). However, following the concentration step the sample can be withdrawn from the fused silica tubing and processed by other techniques than HPCE.

2.1. Sample treatment

When the sample is in the form of a solution, for instance a biological sample, it can often with advantage be applied directly into the electrophoresis tube, provided that pH is such that the solutes migrate electrophoretically in the desired direction and not excessively slowly. A pH adjustment may be necessary. If displacement electrophoresis is utilized for the concentration the sample has to contain an appropriate leading (terminating) ion. One must then add to the sample a small volume of a highly concentrated solution of the leading (terminating) buffer. In cases when it is uncertain whether the pH and the background electrolyte of the sample might disturb the concentration and electrophoresis steps the sample should be dialyzed (desalted) by micro methods, as will be described elsewhere [9]. These methods can be used for larger peptides and macromolecules and are based on dialysis in small-pore polyacrylamide tubes [8,9]. For determination of the pH and electrical conductivity in minute (sample) volumes, see Discussion.

2.2. Step I: concentration of the dilute sample

The electrophoretic velocity v of a solute is determined by the expression

$$v = u \frac{I}{q \kappa} \tag{1}$$

where the mobility u can be calculated from the equation

$$u = \frac{\epsilon \zeta}{4 \pi \eta} \tag{2}$$

(I = current, q = cross-sectional area of the electrophoresis chamber, κ = electrical conductivity, ϵ = dielectric constant, ζ = zeta potential of the solute and η = viscosity.)

An electrophoretically migrating zone can be concentrated if its front can be forced to move slower than its rear. According to Eqs. 1 and 2, this requirement will be fulfilled if the zone is permitted to migrate toward a section of the electrophoresis chamber where u decreases or/and q, κ, or η increase. Different approaches to manipulating these parameters to attain a narrow starting zone, *i.e.*, a concentration, are described below, along with an approach based on a combination of displacement electrophoresis and a hydrodynamic counter flow. Unless otherwise

stated, the discussion refers to anions in the sample. Cations are treated in an analogous way.

Alternative a

Concentration by electrophoresis toward a steep, non-buffering pH gradient (isoelectric focusing). The whole capillary is filled with the sample solution and the cathode vessel with buffer BC (for instance, 0.01 *M* Tris–HCl, pH 8.5) and the anode vessel with buffer Ba (for instance, 0.5 *M* tris–HCl, pH 2.5). A steep, non-buffering pH gradient at the anodic end of the capillary is created immediately when the voltage is switched on (see Fig. 1a and Fig. 2a, step I). At the same time the anions in the sample begin migrating toward the anode. The strong anions pass through the pH gradient, *i.e.*, the sample is freed of strong electrolytes, whereas ampholytes will concentrate into very narrow zones. Weak electrolytes, such as carboxylic acids, will also concentrate in the pH gradient. However, they are non-charged at low pH (pH < pK ± 1.5), where ampholytes become positively charged. The diffusional broadening of weak electrolytes is therefore not counteracted by the zone sharpening that is characteristic of ampholytes in a pH gradient (isoelectric focusing). Examples of appropriate experimental conditions (pH, buffers, etc.) given in this and other sections are taken from our subsequent paper [1].

Alternative b

Concentration by electrophoresis toward a small-pore polyacrylamide gel. The whole capillary is filled with the sample and a short plug of the gel is introduced into one end of the capillary as described in ref. 1. The solutes migrate toward the gel plug when a voltage is applied but stop migrating when they come into contact with the gel because it is impermeable to large molecules, *i.e.*, a concentration takes place at the gel surface (see Fig. 1b and Fig. 2b, step I).

Alternative c

Concentration by electrophoresis toward a piece of dialysis tubing that permits the passage of current but not of the analytes. A short dialysis tubing is prepared and attached to one end of the fused silica tubing as described in ref. 1 in section 3.4. This concentration technique is depicted in Fig. 1c and Fig. 2c, step I. When the solutes leave the fused-silica tubing the field strength decreases abruptly (q in Eq. 1 increases) and their migration velocities become

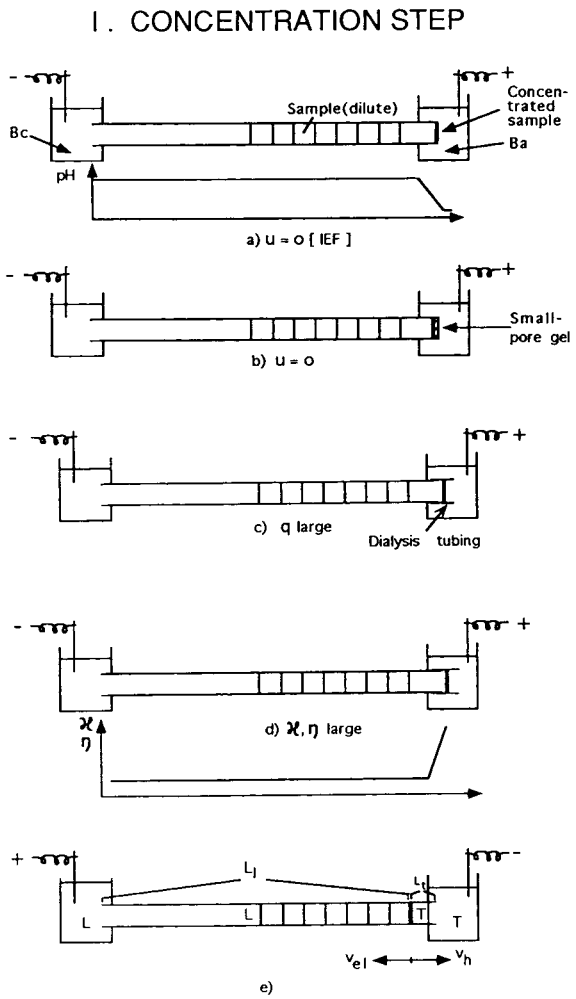

Fig. 1. Different approaches to concentrate a dilute sample solution (step I). (a) By isoelectric focusing in a pH gradient; (b) by zone electrophoresis toward a small-pore gel; (c) toward a gradient in effective cross-section (q); (d) toward a gradient in electrical conductivity (κ) or viscosity (η); (e) by a combination of displacement electrophoresis and a counterflow. In the mobilization (step II) and the electrophoretic analysis (step III) the polarity of the electrodes is reversed [except in (e)], *i.e.*, the anode is to the left (see Fig. 2, a–d).

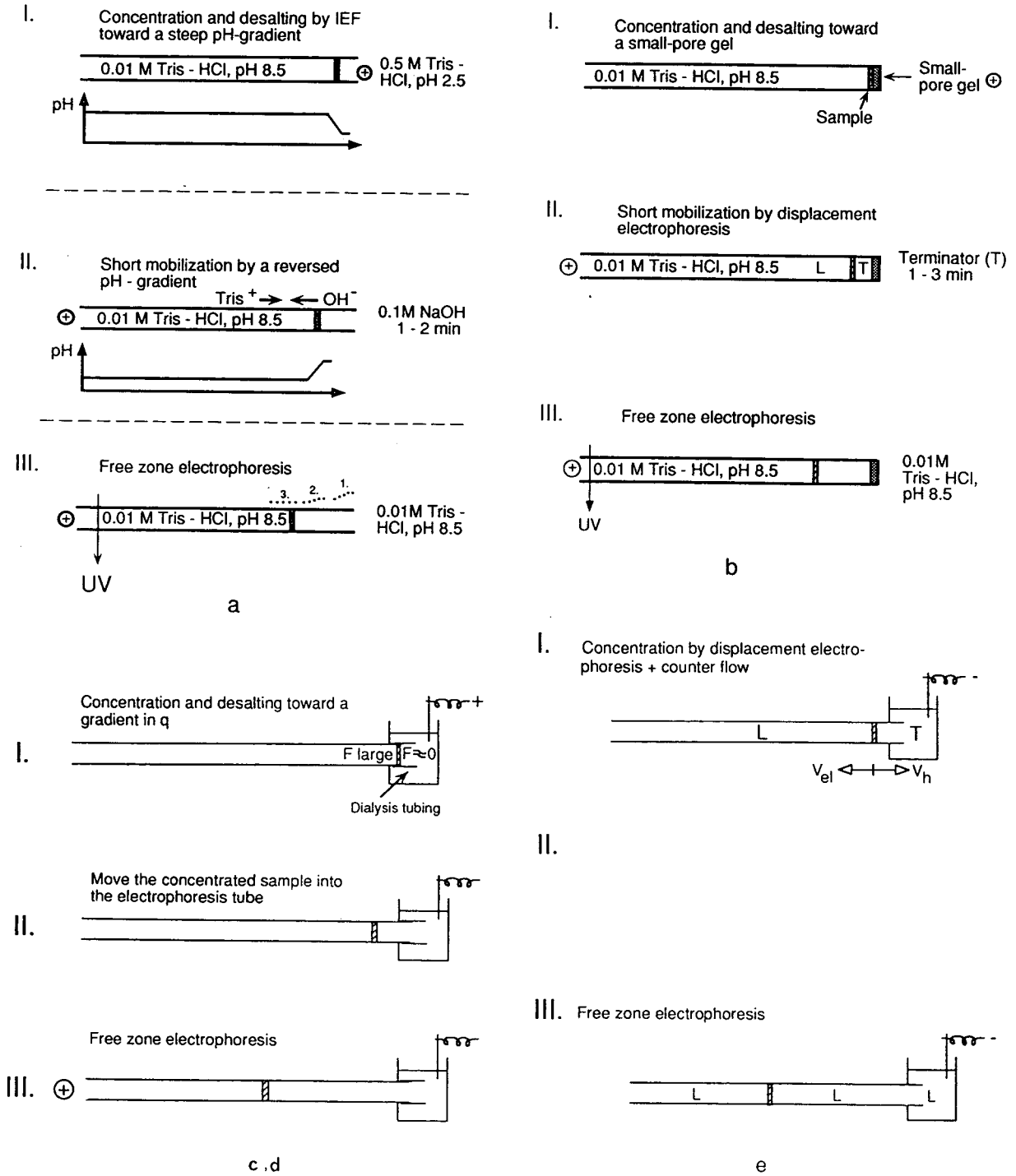

Fig. 2. Different approaches to mobilize (step II) samples concentrated as outlined in Fig. 1 (step I). Step III: analysis of the sample by free zone electrophoresis. All notations are the same as in Fig. 1.

virtually zero. The solutes will, accordingly, become concentrated into a narrow zone. In this step low-molecular weight ions in the sample are removed by diffusion through the pores in the dialysis tubing.

Alternative d

Concentration by electrophoresis toward a gradient in conductivity. If the right-hand electrode vessel in Fig. 1d or Fig. 2d, step I, is filled with a buffer of high ionic strength the sample in the capillary will become concentrated in the conductivity (concentration) gradient formed at the tube end. A similar concentration can be obtained by means of a viscosity gradient.

Alternative e

Concentration by a combination of displacement electrophoresis and a counter flow. The electrophoresis tube is filled with the sample dissolved in the leading buffer or transferred to that buffer as described in ref. 2 (see Fig. 1e and Fig. 2e, step I). A hydrodynamic flow is generated in the electrophoresis tube in a direction opposite to the migration direction of the boundary between the leading and the terminating ions. The magnitude of the counter flow is adjusted such that the boundary becomes stationary. If the sample ions have mobilities between those of the leading and the terminating ions, they will become concentrated at the boundary, because a sample ion which by diffusion or convection enters the terminating (leading) buffer will move back into the concentrated sample zone, since the field strength —and thereby the velocity of the sample ion— is higher (lower) in the terminating (leading) buffer than in the sample zone.

In the initial phase of the displacement electrophoresis step a fast-moving solute can have an electrophoretic velocity which is higher than the velocity of the counter flow. A population of this solute located close to the end of the capillary may, therefore, leave it. As the width of the terminating zone increases the field strength in the leading buffer zone decreases (see below). The velocity of the solute therefore decreases successively until no further solute molecules migrate out of the capillary. To eliminate or suppress this loss of fast-moving solutes one should decrease the concentration of the sample-containing leading buffer in the capillary (but not that of the leading buffer in the anode vessel). The field strength then decreases at this end of the capillary and thereby also the electrophoretic velocities of the proteins as they approach the anolyte. Another alternative is to mix the sample with the terminator instead of with the leading buffer. Part of the very slowly migrating sample ions may then, however, leave the capillary at its cathodic end. The loss can be minimized by decreasing the concentration of the terminator in the cathode vessel (but not that in the capillary).

The hydrodynamic flow should be adjusted so that the boundary layer (the concentrated sample) between the leading and terminating buffers is located about 1–2 cm from one end of the capillary (the right end in Fig. 1e). At a cursory glance, one might expect a small decrease in the hydrodynamic flow to move the boundary layer with the sample in Fig. 1e significantly toward the left, and an increase in the flow to displace the sample out of the capillary. However, moderate changes in the flow will affect the position of the sample only slightly, as shown below.

Assume that the distance from the left end of the capillary in Fig. 1e to the stationary, concentrated, narrow sample zone is L_l cm (= the length of the leading buffer zone) and the distance from the right end to the sample zone is L_t (= the length of the terminating zone). Since the leading ion and the terminating ions migrate with the same velocity

$$u_l \frac{V_l}{L_l} = u_t \frac{V_t}{L_t} \tag{3}$$

where u_l and u_t are the mobilities of the leading and terminating ions, respectively, and V_l and V_t are the voltages over the leading and terminating zones, respectively.

Rearrangement of the factors in Eq. 3 and substitution of V_t for $V - V_l$, where V is the voltage applied over the capillary, gives

$$\frac{L_l}{L_t} = \frac{u_l}{u_t} \frac{V_l}{V - V_l} \tag{4}$$

From the relation $v_l = u_l V_l / L_l$, where v_l = the electrophoretic velocity of the leading ion (= the electrophoretic velocity of the concentrated zone = velocity of the hydrodynamic counter flow when this zone is stationary with respect to the capillary wall) one obtains an expression for V_l which can be introduced into Eq. 4. Solving for L_t following substitution of L_l with $L - L_t$, gives

$$L_t = \frac{u_t}{u_l - u_t}\left(V\frac{u_l}{v_l} - L\right) = \frac{u_t L}{u_l - u_t}\left(\frac{V}{L}\frac{u_l}{v_l} - 1\right) \quad (5)$$

Putting $V/L = F$ (F is the field strength obtained when the capillary is filled completely with terminating or leading buffer) Eq. 5 can be transformed to

$$L_t = \frac{u_t L}{u_l - u_t}\left(F\frac{u_l}{v_l} - 1\right) = \frac{u_t L}{u_l - u_t}\left(\frac{F}{F_l} - 1\right) \quad (6)$$

Insertion of appropriate values in Eqs. 5 or 6 shows that L_t is roughly inversely proportional to v_l. For instance, when the differences between the buffer levels in the electrode vessels in two experiments are 25 and 20 mm, the decrease in the hydrodynamic flow rate is 20%. If the width of the terminating zone is 12 mm in the first experiment it is, accordingly, about 14 mm in the second experiment, *i.e.*, the change in the position of the solute zone is only 2 mm, or in other words, the adjustment of the buffer levels is not critical. It is easy to explain this finding in qualitative terms. If the flow decreases the sample zone moves to the left in Fig. 1e. The terminator zone becomes longer and the leading buffer zone shorter. The current will then decrease, since the former zone has a higher ohmic resistance per cm than has the latter zone. A decrease in current means that the field strength F_l in the leading buffer zone decreases and therefore also the migration velocity of the boundary layer v_l ($= u_l F_l$), which counteracts the above displacement of the sample zone toward the left. Analogously, an increase in hydrodynamic flow (which displaces the sample zone toward the right) gives rise to an increase in the current and thereby an increase in the velocity of the sample zone. It will, accordingly, be displaced electrophoretically to the left. The net movement of the sample zone is, therefore, nearly negligible.

2.3. Step II: short mobilization of the concentrated sample zone

For an electrophoretic analysis of the concentrated sample zone the polarity of the electrodes must be reversed (except in alternative e). However, this very narrow zone will broaden considerably if the polarity is changed immediately after the concentration is finished. To counteract this broadening, a short mobilization step should be introduced between the concentration step and the final electrophoretic step. Some different approaches to accomplish the mobilization are described below.

Alternative a

Mobilization by displacement electrophoresis. Following concentration of the sample, buffer Ba in the right electrode vessel in Fig. 1 is replaced by a terminating buffer, for instance, 0.03 *M* glycine–NaOH, pH 10 (Fig. 2b, step II).

Upon reversing the polarity of the electrodes the anion in the terminating buffer (glycine in our example) forms a migrating boundary with the anion in the buffer in the electrophoresis tube (for instance, chloride). The requirements for displacement electrophoresis become fulfilled if the anions in the sample have a mobility lower than those of the anions in the buffer in the electrophoresis tube and higher than those of the anions in the terminating buffer. In this displacement step the very narrow concentrated zone will move without zone spreading toward the left (the anode is at the left in the mobilization and analysis steps; see Fig. 2b, step II). When the subsequent analysis is based on zone electrophoresis (rather than displacement electrophoresis) the displacement step should be interrupted as soon as the concentrated zone begins to move toward the left (or preferably somewhat earlier). Otherwise, the onset of the zone electrophoresis step (Fig. 2b, step III; see also step

III, alternative b, below) will be delayed, which gives rise to an unnecessarily long analysis time.

Alternative b

Mobilization by a reversed, non-buffering pH gradient. The buffer in the right-hand electrode vessel used for the concentration is exchanged for a solution of high pH (for instance 0.1 *M* NaOH) to make the acidic solutes migrate toward the positive pole in the mobilization step (see Fig. 2a, step II); for basic solutes which migrate toward the negative pole a solution of low pH is chosen (for instance, 1 *M* HCl).

Alternative c

Mobilization by zone electrophoresis following concentration by electrophoresis toward a dialysis tubing. Prior to the subsequent electrophoresis step the concentrated sample in the dialysis tubing is moved hydrodynamically one or two mm into the electrophoresis tube (see Fig. 2c, step II), for instance, by raising the right-hand electrode vessel. Due to the low field strength in the dialysis tubing the sample zone will otherwise broaden when it migrates into the electrophoresis tube upon reversal of the direction of the current. Alternatively, one can move the electrophoresis tube toward the left so that the section of the dialysis tubing that contains the concentrated sample zone will be in contact with air rather than buffer.

Alternative d

Mobilization following concentration toward a gradient in conductivity. Following this concentration (Fig. 1d) the sample should be moved into the dialysis tubing for removal of salt by dialysis against a dilute buffer in the electrode vessel and then back into the capillary (upon reversing the polarity of the electrodes a zone sharpening occurs when the voltage is switched on if the buffer in the sample has a conductivity lower than that of the buffer in the electrophoresis tube). A similar approach can be employed for concentration toward a viscosity gradient when the added viscosity-increasing agent is dialyzable.

One should note that most electrode vessels used in HPCE have an effective cross-sectional area much larger than that of the capillary (see alternative c above). Accordingly, in almost all apparatus, the field strength in the dialysis tubing is sufficiently low without an increase of the ionic strength (or the viscosity) in the electrode vessel. In fact, one can even have a lower ionic strength in the electrode vessel than in the capillary, and thereby omit the above dialysis step aimed at giving a narrow starting zone in the subsequent zone electrophoresis.

2.4. Step III: electrophoretic analysis

Alternative a

Analysis by displacement electrophoresis. In this case the mobilization according to alternative a is not interrupted, but is allowed to proceed until all of the solutes have passed the detector.

Alternative b

Analysis by zone electrophoresis following mobilization by displacement electrophoresis or electrophoresis in a reversed pH gradient (step II, alternatives a or b). When the concentrated starting zone, mobilized as in step II, alternatives a or b, is to be subjected to zone electrophoresis the solution in the right-hand electrode solution is exchanged for a buffer of the same composition as that in the capillary and in the left electrode vessel (see Fig. 2b, step III and Fig. 2a, step III).

Alternative c

Analysis by zone electrophoresis following concentration by a combination of displacement electrophoresis and a counter flow. In this approach the separate mobilization step can be omitted: one can proceed directly from the concentration step to the zone electrophoresis step without reversing the direction of the current following substitution of the terminating buffer in the cathode vessel with the leading buffer (see Fig. 2e, step III).

3. Discussion

A comparison among some concentration methods. On-line electrophoretic concentration of ionic substances by transferring the sample to a buffer with a conductivity lower than that of the electrophoresis buffer was first described by Haglund and Tiselius [10]. The effect can be reinforced by proper choice of the pH of the sample [11]. A concentration based on such manipulations can be performed as a one-step procedure by using two or more buffers, the first step being a concentrating displacement electrophoresis which in a second stage is transformed automatically into an analytical zone electrophoresis. This elegant approach was introduced by Ornstein for concentration of a protein sample in polyacrylamide gel electrophoresis [12]. The same degree of concentration can, however, often be achieved in a simpler way by lowering the conductivity of the sample [13].

The design of Ornstein's discontinuous buffer system is partly based on the fact that a protein migrates more slowly in a sieving gel of polyacrylamide than in free solution. Accordingly, this buffer system cannot be used in carrier-free electrophoresis of high-mobility proteins or peptides. For free electrophoresis of this class of substances we have, therefore, introduced new buffer systems based on the use of terminators, the mobilities of which span over a wide range when the pH is varied [11]. An example of an appropriate terminator is diaminopimelic acid, used in the experiment shown in Fig. 2b in ref. 1 (for similar methods based on displacement electrophoresis, see refs. 14–20). An advantage of the concentration methods described herein over those based on discontinuous buffer systems is that the whole electrophoresis tube, rather than only a fraction of it, can be filled with the sample solution and, if so desired, also an electrode vessel. The degree of concentration is, accordingly, higher.

A counter flow has been used in electrophoresis for several purposes; for instance, in order to compensate for the hydrodynamic flow which attends the electroendosmotic flow in a closed electrophoresis tube or/and to increase the effective length of the electrophoresis tube [21–26].

A method based on displacement electrophoresis, electroendosmotic flow and a counter flow is described in ref. 27. The degree of concentration accomplished by this technique was limited, since only (part of) the capillary, but not the electrode vessel was filled with sample. The authors reversed the polarity of the electrodes when the displacement electrophoresis was replaced by a zone electrophoresis. It was emphasized that "correct timing of the voltage switching is important" to avoid that "the sample zones will migrate out of the capillary" or broaden. In the method presented herein the polarity is the same throughout the experiment and any change in the hydrodynamic flow rate is counteracted by an automatic adjustment of the electrophoretic migration velocity of the concentrated solute zone, *i.e.*, there is no risk that it will leave the capillary (see the discussion of Eqn. 5). For an interesting concentration method based on zone electrophoresis and a hydrodynamic counter flow, see ref. 28.

A sharpening of the starting zone upon decreasing the field strength by increasing the effective cross-section of the electrophoresis medium has been utilized in paper electrophoresis of proteins [29]. The method is very efficient [30]. The same principle was used in the approach presented in Fig. 1c.

The use of a gradient in viscosity and conductivity for concentration purposes has been described earlier [31]. This method differs from that in Fig. 1d, in that the gradient was created inside the electrophoresis tube rather than at the boundary between the electrophoresis tube and an electrode vessel. Stabilization against convection in the tube was accomplished by a sucrose gradient. In a method for recovery of proteins following polyacrylamide gel electrophoresis the protein zone of interest was cut out, the protein eluted eletrophoretically and then concentrated in a conductivity gradient [32]; compare Fig. 1d.

The following considerations are important for the design of the buffer systems used for the concentration of solutes.

(1) *Concentration toward a non-buffering, steep pH gradient (step I, alternative a; Fig. 1a).* When the concentration is performed by means of an anolyte of low pH the number of protons,

N_{H^+}, entering the capillary per time unit from the anode vessel is of interest, since it determines the position and the progress of the pH gradient in the capillary. This number is governed by the expression

$$N_{H^+} = v_{H^+}\, q\, n_{H^+} \tag{7}$$

where v_{H^+} = the migration velocity of the protons in the anolyte, q = the cross-sectional area of the capillary and n_{H^+} = the number of protons per volume unit in the anolyte.

Since $v_{H^+} = F\, u_{H^+} = I\, u_{H^+}/q\, \kappa$ (F = the field strength in the capillary, u_{H^+} = the mobility of the proton in the anolyte, I = the current and κ = the electrical conductivity)

$$N_{H^+} = \frac{I\, u_{H^+}\, n_{H^+}}{\kappa} \tag{8}$$

The conductivity κ is determined by the expression

$$\kappa = \sum c_i \cdot u_i \tag{9}$$

where c_i is the concentration of ion i (in coulomb/ml). For the 0.5 *M* Tris–HCl solution of pH 2.5 (the stop solution) used in the experiment outlined in Fig. 2a we get

$$\kappa = c_{H^+} \cdot u_{H^+} + c_{Tris^+} \cdot u_{Tris^+} + c_{OH^-} \cdot u_{OH^-} + c_{Cl^-} \cdot u_{Cl^-} \tag{10}$$

To obtain an efficient concentration (isoelectric focusing) the pH of the stop solution should be at least one pH unit below the p*I* value of the solute in the sample that has the lowest pI value [c_{H^+}, the first term in Eq. 10, cannot, accordingly, be chosen arbitrarily]. The third term in this equation can be neglected, since c_{OH^-} is very small at low pH values. The remaining second and fourth terms in Eq. 10 can, accordingly, be used to manipulate the conductivity, *i.e.*, the Tris–HCl solution (pH 2.5) in Fig. 2a should be adjusted to a molarity that gives the solution a proper conductivity. When the molarity decreases the number of protons entering the capillary increases, according to Eqs. 8 and 10. At excessively low molarity the pH gradient in the capillary will, therefore, migrate toward the cathode during the concentration, and at very high molarity little or no change in pH will occur in the capillary (*i.e.*, the solutes migrate out of the capillary). Experiments have shown that the molarity of the stop solution should be such that a virtually stationary pH gradient is created at a distance of 0.5–3 mm from the end of the capillary. The suitable molarity can be established experimentally by the use of coloured solutes and transparent glass capillaries.

(2) *Mobilization by a reversed, non-buffering pH gradient (step II, alternative b; Fig. 2a, step II).* Following the concentration of solutes by isoelectric focusing in a steep pH gradient or by zone electrophoresis toward a small-pore gel one can mobilize the solute zone by a solution of high pH, for instance, 0.1 *M* NaOH (Fig. 2a, step II). This solution should contain no other negatively charged ions than hydroxyl ions. Sodium, potassium or ammonium hydroxides are, therefore, recommended. The only ions entering the capillary are then hydroxyl ions, which have a very high mobility and, accordingly, change the pH very rapidly at the cathodic end of the capillary. This is important when the concentration is achieved by isoelectric focusing in a pH gradient, since the focused solute zone will broaden upon reversal of the polarity of the electrodes until the initial pH gradient is abolished (a pH gradient gives a zone sharpening only when the pH increases in the direction of the current). When a sufficiently large number of hydroxyl ions have entered the capillary a reversed pH gradient has been created which gives rise to a zone-sharpening. This pH gradient migrates toward the anode with the proteins gathered in a very narrow zone (about 0.2 mm wide); see Fig. 2a, step II. At this stage, which takes only 1–2 min to attain, the mobilizing high-pH solution should be replaced by the electrophoresis buffer (the same buffer as in the anode vessel and in the capillary). The hydroxyl ions continue to migrate as a plug toward the anode but their concentration decreases as they meet and react with the buffering cations in the capillary as indicated by the broken pH profiles in Fig. 2a, step III (Tris ions, for example, which are fed continuously into the capillary from the anode vessel by electrophoresis). If it is essential to minimize the analysis time one should fill the cathode vessel with the electrophoresis buffer

somewhat before the complete zone-sharpening (stacking) outlined in Fig. 2a, step II, has been achieved, because the large number of hydroxyl ions in the capillary at its cathodic end continue to make the pH gradient still narrower at the same time as the buffer anions (chloride) migrate into the capillary.

Eq. 11, which corresponds to Eq. 8, gives the number of hydroxyl ions, N_{OH^-}, that enter the capillary per time unit during the mobilization (step II in Fig. 2a).

$$N_{OH^-} = \frac{I\, u_{OH^-}\, n_{OH^-}}{\kappa} \qquad (11)$$

Using the same reasoning as for Eq. 8 one can show the importance of choosing an appropriate value of κ, the conductivity, to cause a rapid increase in the pH at the cathodic end of the capillary during the short mobilization step, thereby rapidly replacing the initial zone-broadening pH gradient by a new, reversed, zone-sharpening one. Experiments have shown that 0.1 *M* sodium hydroxide is a suitable mobilizing solution. The pH in the capillary at its cathodic section will not become 13 (that of 0.1 *M* NaOH), since the concentration of hydroxyl ions in the capillary is reduced quickly by the buffering ions in the electrophoresis buffer. Therefore, and also because the solutes start to migrate as soon as the pH rises above their p*I* values, the solutes will not become located in an area of extremely high pH and the risk of denaturation is negligible, particularly since the mobilization and thereby the possible exposure to elevated pH has a duration of only 1–2 min. Mobilization by 0.1 *M* sodium hydroxide is very simple and requires no preexperiments to establish optimum conditions for every new type of electrophoresis buffer. For mobilization at low pH we use 1 *M* HCl.

The concentration of proteins and peptides can be performed also with a pH gradient created with carrier ampholytes in the same way as in isoelectric focusing [25]. However, the high buffering capacity of these ampholytes makes it difficult to abolish the pH gradient quickly. Mobilization, therefore, leads to broadening of the narrow, concentrated zone.

(3) *Mobilization by displacement electrophoresis (step II, alternative a; Fig. 2b, step II).* The mobilizing solution discussed above should contain no anions other than hydroxyl ions. However, buffering anions must be present if mobilization is to be accomplished by a brief displacement electrophoresis step. In the experiment shown in Fig. 1b in the succeeding paper [1] the anion glycine was chosen as terminator. To be useful for displacement of the concentrated zone of sample anions (acidic peptides and proteins) the terminator (in that experiment glycine, p*K* 9.8) should —besides having a mobility lower than that of the leading ion (chloride) and those of the solutes— have a p*K* value 1.0–1.7 units higher than the p*K* value of the leading buffer cation (in that experiment Tris, p$K = 8.1$) and the pH value of the leading buffer (in that experiment Tris–HCl, pH 8.5) should be close to the p*K* value of its cation (Tris) to give optimum buffer capacity. If these requirements are fulfilled a short plug of terminating ions (glycine) will quickly enter the capillary during the brief mobilization step (Fig. 2b, step II). These ions will be rapidly titrated to the pH of the electrophoresis buffer, since upon their migration toward the anode they continuously meet new protons and new buffer cations (Tris) migrating in the opposite direction. The terminating ion (glycine) will thus quickly acquire a low net charge and will, therefore, migrate more slowly than all or most of the sample zones, *i.e.*, the requirements for displacement electrophoresis are fulfilled. A very narrow sample zone is, accordingly, created. The terminating buffer (glycine–NaOH) can then be exchanged for the electrophoresis buffer (Tris–HCl), the anion of which (Cl^-) should have a high mobility to overrun very quickly the sharp protein zones and destack them. The transition from displacement to zone electrophoresis is, accordingly, very rapid. In the experiment shown in Fig. 2b in ref. 1 diaminopimelic acid was used as terminator instead of glycine.

For the concentration of basic ampholytes an

appropriate buffer system has been described in ref. 1 in section 3.1. The theoretical considerations are analogous to those presented above for acidic peptides and proteins. For instance, the different buffers should be designed such that the terminator (for instance Bis–Tris, pK = 6.7), introduced as a short plug in the displacement step, rapidly loses most of its positive charge as it meets the leading buffer (= the zone-electrophoresis buffer = 0.05 M EPPS–NaOH, pH 7.5, in the above buffer system) in the final analytical zone electrophoresis step.

(4) *Estimation of conductivity (ionic strength) and pH of minute-volume samples*. Some of the described concentration methods work only within limited conductivity and pH ranges. Direct measurements of these parameters by means of conductivity and pH probes is not possible owing to the small sample volumes. An indirect estimation can, however, be done as follows. The conductivity (κ) can be determined by filling a capillary with the sample solution and measuring the current I and voltage V as in a conventional HPCE experiment [11]:

$$\kappa = \frac{I\,L'}{V\,\pi\,R^2} \tag{12}$$

where L' is the length of the capillary and R its radius.

For the determination of pH one can utilize (1) the equilibrium between two easily detectable ions (for instance two species of vanadate ions) the concentrations of which are pH dependent [33], or (2) the fact that the spectra of pH indicators change with pH [34]. With such ionic compounds as analytes one can rapidly determine the pH of the sample solution. The conductivity and pH may be estimated conveniently in the same run.

Acknowledgements

The work was financially supported by the Swedish Natural Science Research Council and the Knut and Alice Wallenberg and Carl Trygger Foundations.

References

[1] J.-L. Liao, R. Zhang and S. Hjertén, *J. Chromatogr. A*, 676 (1994) 421.
[2] T.W.G. Rowe, *Ann. N.Y. Acad Sci.*, 85 (1960) 641–681.
[3] H. Laurell, *Studies on Preparative Vertical Zone Electrophoresis (Dissertation)*, Almqvist and Wiksell, Uppsala, 1958.
[4] B. v. Hofsten and S.-O. Falkbring, *Anal. Biochem.*, 1 (1960) 436 .
[5] E.C.J. Norrby and P.Å. Albertsson, *Nature*, 188 (1960) 1047 .
[6] P.Flodin, B. Gelotte and J. Porath, *Nature*, 188 (1960) 493 .
[7] J.-L. Liao and S. Hjertén, *Concentration of Biological Samples on a Microliter Scale and Analysis by Capillary Electrophoresis*, US Patent Application, filed January 26, 1993.
[8] S. Hjertén, J.-L. Liao, A. Palm, L. Valtcheva and R. Zhang, *5th Int. Symp. on High-Performance Capillary Electrophoresis, Orlando, FL, January 25–28, 1993*, Abstracts, p. 56.
[9] S. Hjertén, L. Valtcheva and Y.-M. Li, *J. Cap. Electroph.*, submitted for publication.
[10] H. Haglund and A. Tiselius, *Acta Chem. Scand.*, 4 (1950) 957–962.
[11] S. Hjertén, *Electrophoresis*, 11 (1990) 665–690.
[12] L. Ornstein, *Ann. N.Y. Acad. Sci.*, 121 (1964) 321–349.
[13] S. Hjertén, S. Jerstedt and A. Tiselius, *Anal. Biochem.*, 11 (1965) 219–233.
[14] S. Hjertén, K. Elenbring, K. Kilár, J.-L. Liao, A. Chen, C. Siebert and M.-D. Zhu, *J. Chromatogr.*, 403 (1987) 471.
[15] C. Schwer and F. Lottspeich, *J. Chromatogr.*, 623 (1992) 345.
[16] F. Foret, E. Szoko and B.L. Karger, *J. Chromatogr.*, 608 (1992) 3.
[17] D. Kaniansky, J. Marák, V. Madajková and E. Simunicová, *J. Chromatogr.*, 638 (1993) 137.
[18] T. Hirokawa, A. Ohmori and Y. Kiso, *J. Chromatogr.*, 634 (1993) 101.
[19] J.L. Beckers and M.T. Ackermans, *J. Chromatogr.*, 629 (1993) 371.
[20] F. Foret, E. Szökö and B.L. Karger, *Electrophoresis*, 14 (1993) 417.
[21] S. Hjertén, *Arkiv för Kemi*, Band 13, Nr 16 (1958) 151–152.
[22] S. Hjertén, *Prot. Biol. Fluids (Proceedings of the 7th Colloquium, Bruges, 1959)*, Elsevier, Amsterdam, 1960, pp. 28–30.
[23] B.P. Konstantinov and O.V. Oshurkova, *Zh. Tekhn. Fiz.*, 36 (1966) 942 .
[24] W. Preetz, *Talanta*, 13 (1966) 1649 .
[25] S. Hjertén, *Chromatogr. Rev.*, 9 (1967) 122–219.
[26] F.M. Everaerts, *J. Chromatogr.*, 49 (1970) 262 .

[27] N.J. Reinhoud, U.R. Tjaden and J. van der Greef, *J. Chromatogr.*, 641 (1993) 155–162.
[28] A. Hori, T. Matsumoto, Y. Nimura, M. Ikedo, H. Okada and T. Tsuda, *Anal. Chem.*, 65 (1993) 2882–2886.
[29] S. Hjertén, *Biochim. Biophys. Acta*, 32 (1959) 531–534.
[30] C.J.O.R. Morris and P. Morris (Editors), *Separation Methods in Biochemistry*, Pitman and Sons Ltd., London, 1963, p. 748.
[31] S. Hjertén, *Biochim. Biophys. Acta*, 237 (1971) 395–403.
[32] S. Hjertén, Z.-Q. Liu and S.-L. Zhao, *J. Biochem. Biophys. Meth.*, 7 (1983) 101–113.
[33] T. Groh and K. Bächmann, *J. Chromatogr.*, 646 (1993) 405–410.
[34] S. Hjertén and K. Elenbring, in preparation.

ELSEVIER

Journal of Chromatography A, 676 (1994) 421–430

JOURNAL OF CHROMATOGRAPHY A

New approaches to concentration on a microliter scale of dilute samples, particularly biopolymers with special reference to analysis of peptides and proteins by capillary electrophoresis II☆. Applications

Jia-Li Liao, Rong Zhang, Stellan Hjertén*

Department of Biochemistry, University of Uppsala, Biomedical Center, P.O. Box 576, S-751 23 Uppsala, Sweden

First received 20 December 1993; revised manuscript received 21 March 1994

Abstract

On theoretical grounds several approaches for the concentration of ionic solutes are suggested in ref. 1. The methods are of general applicability. In this paper we describe how they can be employed in high-performance capillary electrophoresis (HPCE) for 1000-fold manual and automated on-line concentration from microliters down to nanoliters. The risk that the solutes may escape detection —the obvious disadvantage of HPCE— is, accordingly, reduced considerably. Briefly, the whole capillary (and for more than 1000-fold concentration also an electrode vessel or a vessel in contact with an electrode vessel) is filled with the dilute sample solution. The sample becomes concentrated as it migrates toward a pH gradient, a small-pore gel, a dialysis tubing attached to one end of the capillary, or by displacement electrophoresis combined with a hydrodynamic counterflow. These concentration steps (except the last) require a short mobilization step to prevent the narrow, concentrated sample zone from broadening in the initial phase of the final analysis step (free zone electrophoresis).

1. Introduction

For any analytical or preparative separation method to work satisfactorily the solute concentration must be above some threshold value, characteristic of the particular method. The reason is not only (1) detection difficulties at extremely low concentration but also (2) adsorptive losses of solutes on the surfaces of containers, filters, spatulas, plastic columns, etc., and (3) contaminants from these items and from air, hands, gloves, etc. The latter two problems may very well turn out to be more severe than the first one, at least for macromolecules such as proteins, which often are adsorbed by a strong multi-point attachment. Owing to surface adsorption the concentrations of the free solutes may differ from those in the original sample, giving rise to erroneous analysis data, or even fall below the detection limit.

There is, accordingly, a need for efficient concentration methods. In the preceding article [1] we have treated theoretically several new methods which were developed especially for minute-volume sample solutions of peptides and

* Corresponding author.

☆ For Part I see ref. 1.

0021-9673/94/$07.00
SSDI 0021-9673(94)00317-3

proteins to be analyzed by capillary electrophoresis. In this article we present a few applications.

This paper is written in such a way that the reader does not need to be acquainted with the theory discussed in ref. 1 in order to employ the concentration methods described in this paper. However, to those who are interested in the theory behind a particular concentration technique we refer to the section or the figure in ref. 1, where that technique is presented.

2. Materials and methods

Fused-silica tubing from Polymicro Technologies (Phoenix, AZ, USA) and glass tubes from Modulohm (Herlev, Denmark) were coated with polyacrylamide to suppress electroendosmosis and adsorption as described in ref. 2, with the difference that γ-methacryloxypropyltrimethoxysilane was used as a 50% (v/v) solution in acetone. Glycine and chemicals used for the preparation of coating and gel plugs of polyacrylamide were electrophoresis purity reagents from Bio-Rad (Hercules, CA, USA). Diaminopimelic acid (DAPA) and N-2-hydroxyethylpiperazine propane sulfonic acid (EPPS) were from Sigma (St. Louis, MO, USA). All standard proteins used were commercial products except *R*-phycoerythrin, which was prepared as described in ref. 3.

3. Experiments and results

The theoretical background is given in ref. 1.

3.1. Concentration of proteins by electrophoresis toward a steep, non-buffering pH gradient (isoelectric focusing: step I, alternative a in ref. 1) and mobilization by displacement electrophoresis (step II, alternative a in ref. 1) followed by zone electrophoresis (step III, alternative b in ref. 1).

The sample consisted of 20 μg of each of the proteins phycoerythrin (Pe), ovalbumin (Ova), human transferrin (Tf), human hemoglobin (Hb) and carbonic anhydrase (CA) dissolved in 1 ml of 0.01 *M* Tris–HCl, pH 8.5. For rapid generation of the pH gradient this buffer should have a relatively low buffering capacity, *i.e.*, a low molarity or/and a pH 0.5–0.7 pH units lower than the p*K* value of the buffering constituent. The same buffer was also used as catholyte in the concentration step. A 0.5 *M* Tris–HCl solution, pH 2.5, served as anolyte. The fused-silica tubing [130(115) × 0.05 mm I.D., where 115 mm is the length of the capillary from the cathodic end to the detector] was filled with the sample solution. A voltage of 1500 V (0.8 μA) was applied during 12 min in order to concentrate the proteins into a narrow zone in the pH gradient (see Fig. 1a in ref. 1). The polarity of the electrodes was then reversed following an exchange of the 0.5 *M* Tris–HCl solution, pH 2.5, for 0.03 *M* glycine–NaOH, pH 10.0 At a voltage of 1500 V for 2.5 min a sharp zone was obtained by displacement electrophoresis (chloride was the leading ion and glycine the terminating ion; *cf.* Fig. 2b, step II in ref. 1). The glycine buffer was then replaced by 0.01 *M* Tris–HCl, pH 8.5 and an analysis of the sample by zone electrophoresis (see Fig. 2b, step III in ref. 1) was performed at 3000 V, corresponding to 1.6 μA (without the above displacement step the starting zone in the zone electrophoresis step became blurred, as revealed by visual inspection during an experiment done in a transparent glass tube). The electropherogram is presented in Fig. 1b. The detection was done at 220 nm. A control experiment was performed without concentrating the sample and with a starting zone 3–4 mm wide with the hope to detect at least the main peaks (Fig. 1a). A comparison between Figs. 1a and 1b shows the efficiency of the concentration technique. The width of the starting zone in the zone electrophoresis step was about 0.2 mm (visual observation in transparent glass capillaries). From the length of the capillary and this zone width one can conclude that we obtained approximately a 500-fold concentration of the sample. The recovery was difficult to determine quantitatively because of the low protein con-

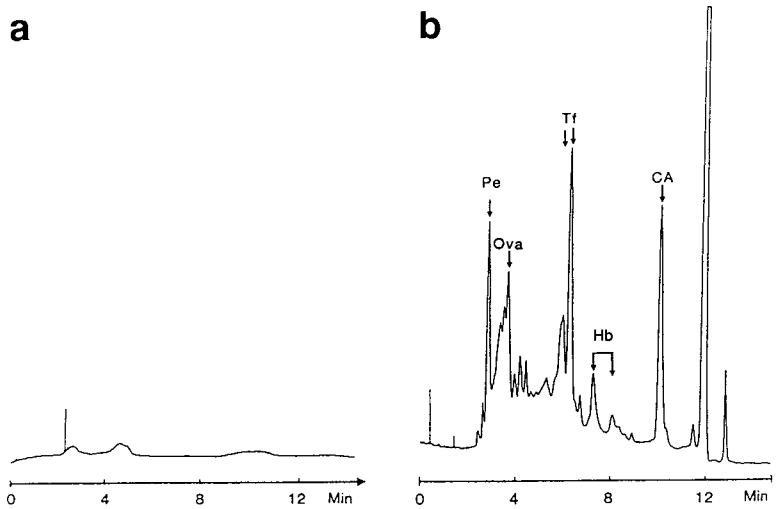

Fig. 1. High-performance capillary zone electrophoresis of model proteins. (a) Prior to concentration (concentration of each protein: 20 μg/ml), (b) following concentration toward a steep, non-buffering pH gradient and a short mobilization by displacement electrophoresis. The large peak at 12 min may correspond to a moving boundary. The width of the applied sample zone was in (a) 3–4 mm and in (b) 130 mm (= the length of the capillary). Following concentration, the zone width in (b) was about 1 mm, but became much narrower in the mobilization step.

tent. However, it should be close to 100% as judged from the fact that no residue of the strongly colored phycoerythrin was observed after completion of a parallel experiment done in a transparent glass tube.

The above buffer system is designed for acidic peptides and proteins and other ampholytes. For basic ampholytes we have used the following buffers.

I. The concentration step (isoelectric focusing): 0.05 *M* N-hydroxyethyl-piperazine propane sulfonic acid (EPPS), pH 7.5, in the left electrode vessel (anolyte) and in the capillary; 0.25 *M* EPPS, pH 11.0, in the right electrode vessel. EPPS was titrated to the desired pH with sodium hydroxide.

II. The mobilization (displacement) step: 0.05 *M* EPPS, pH 7.5, in the left electrode vessel (now catholyte) and in the capillary; 0.1 *M* Bis–Tris (titrated to pH 2.0 with HCl) in the right electrode vessel.

III. The free zone electrophoresis step: 0.05 *M* EPPS, pH 7.5, in both electrode vessels and in the capillary (the polarity the same as in step II).

3.2. Concentration of proteins by electrophoresis toward a small-pore polyacrylamide gel (step I, alternative b in ref. 1) and mobilization by displacement electrophoresis (step II, alternative a in ref. 1) followed by zone electrophoresis (step III, alternative b in ref. 1).

The gel is prepared in a glass tube with an inside diameter of about 1 mm. The pores of the gel must be so small that the solutes cannot penetrate the gel. In our studies we have used crosslinked polyacrylamide gels with the total concentration $T > 20\%$ (v/w) and the crosslinking concentration $C = 3\%$ (w/w); the parameters C and T are defined in ref. 4. Observe that the pores of a polyacrylamide gel decrease when T increases if $C \leq 3\%$ and that these C values give transparent gels, independently of the T values. For C values $> 5\%$ the pore size increases when C increases and the gels become white and non-transparent [5]. A short plug of the gel is introduced into one end of the fused-silica tubing (filled with sample solution) by pressing the tubing into the gel in the glass tube. The tubing should be drawn up slowly to avoid

detachment of the gel plug from the tubing wall. Upon electrophoresis the analytes cease to migrate for steric reasons when they come into contact with the gel plug (see Fig. 1b in ref. 1).

The capillary [140 (125) × 0.05 mm I.D.] was filled with a solution of the same proteins as were used in the experiment presented in Fig. 1. They were dissolved in the same buffer (0.01 *M* Tris–HCl, pH 8.5) at the same concentrations (20 μg/ml). This buffer was also employed as catholyte in step I (the concentration) and step III (the free zone electrophoresis). The catholyte in step II (the terminating solution in the displacement electrophoresis) was 0.03 *M* diaminopimelic acid, titrated to pH 9.2 with Tris [6]. The experiment is outlined in Fig. 2b in ref. 1.

With a polyacrylamide gel of the composition $T = 60\%$ (v/w) and $C = 3\%$ (w/w) at the anodic end of the capillary the concentration of the proteins toward the gel plug was completed in 10 min at 2000 V (anolyte: 0.01 *M* Tris–HCl, pH 8.5). The mobilization by displacement electrophoresis of the very narrow, concentrated protein zone took place at 2000 V for 1.5 min following reversal of the polarity of the electrodes (see Fig. 2b, step II, in ref. 1). This displacement electrophoresis step was introduced to avoid a broad starting zone in the subsequent zone electrophoresis, which was performed at 3000 V after replacing the diaminopimelic acid–Tris buffer in the cathode vessel by 0.01 *M* Tris–HCl, pH 8.5 (Fig. 2b).

The experiment was repeated, with the difference that the analysis was performed without concentration of the sample. The width of the starting zone was 3–4 mm. The 0.01 *M* Tris–HCl buffer (pH 8.5) was used both in the capillary and in the anode and cathode vessels. The striking difference between the electropherogram obtained (Fig. 2a) and that in Fig. 2b shows the importance of having access to a method for in-tube concentration of dilute protein solutions. For a discussion of the degree of concentration obtained, see 3.1.

An analysis similar to that in Fig. 2b was performed with a urine sample from a diabetic patient. The essential differences in the experimental conditions were that (1) the gel plug had the composition $T = 40\%$ (w/v), $C = 3\%$ (w/w), (2) the capillary was 130 (120) mm long and made of glass, and the terminator was a 0.03 *M* glycine–NaOH solution, pH 10. The urine was diluted 10-fold with 0.01 *M* Tris–HCl, pH

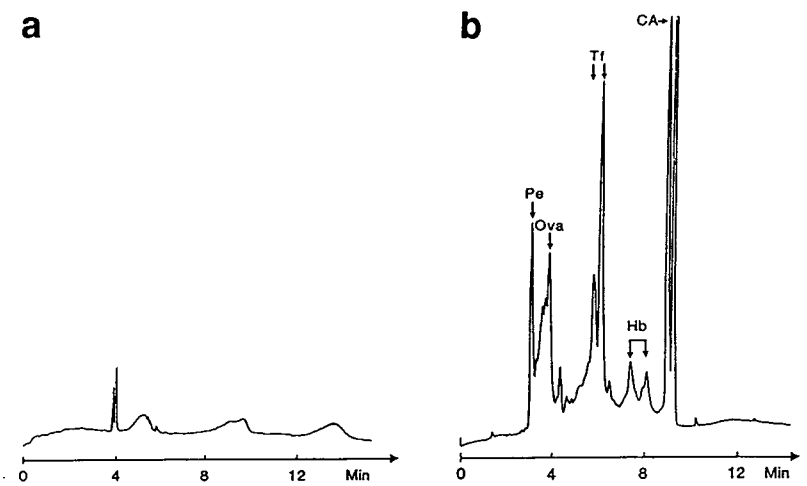

Fig. 2. High-performance capillary zone electrophoresis of model proteins. (a) Prior to concentration (concentration of each protein: 20 μg/ml), (b) following concentration toward a small-pore polyacrylamide gel and a short mobilization by displacement electrophoresis. The width of the applied sample zone was in (a) 3–4 mm and in (b) 140 mm (= the length of the capillary). Following concentration the zone width in (b) was about 0.2 mm.

8.0, before it was sucked into the capillary. The concentration required 15 min at about 1200 V, the mobilization 50 s at about 3000 V with 0.03 *M* glycine NaOH, pH 10, as terminator and the zone electrophoresis in 0.01 *M* Tris–HCl, pH 8.5, 25 min at 3000 V. The detection was done at 280 nm, where proteins have an absorption maximum, albeit with an absorption coefficient much smaller than that at 220 nm. In spite of this, the protein zones were easily detected (Fig. 3). No peaks were recorded with the non-concentrated 10-fold diluted urine sample.

3.3. Concentration of proteins and peptides by a combination of displacement electrophoresis and a hydrodynamic counterflow (step I, alternative e in ref. 1) followed by zone electrophoresis (step III, alternative c in ref. 1).

The concentration method is outlined in Fig. 2e in ref. 1.

As leading buffer (anolyte) we chose 0.015 *M* HCl, titrated to pH 8.5 with Tris, and as terminator (catholyte) 0.1 *M* glycine titrated to pH 8.5 with NaOH. The electrophoresis tube [155 (145) × 0.05 mm I.D.] was filled with the sample solution (about 20 μg/ml of each of the proteins phycoerythrin (Pe), human serum albumin (Alb), human transferrin (Tf), human hemoglobin (Hb) and carbonic anhydrase (CA)) dissolved in the leading buffer. The liquid level in the anode vessel was 2 cm higher than that in the cathode vessel. The buffer flow thus created in the capillary gave a virtually stationary boundary between the leading chloride ions and the terminating glycine ions 1–2 cm from the cathodic end of the capillary at a voltage of 500 V. The proteins gathered between these ion species in a very narrow zone. Following a 15-min concentration, the glycine–NaOH solution was replaced by the HCl–Tris buffer, and a zone electrophoretic analysis was performed at 3000 V for 18 min with no difference in the liquid levels (see Fig. 4b). The experiment was then repeated with the difference that not only the capillary was filled with the sample solution but also the anode vessel and that the duration of the concentration step was 22 min (Fig. 4c). A blank experiment was also performed (Fig. 4a), *i.e.*, a zone electrophoresis in the HCl–Tris buffer with a 5 mm wide starting zone (without concentration). A comparison between Fig. 4b and Fig. 4c shows that a continuous concentration with the sample solution in the anode vessel (in addition to the capillary) is the method of choice for very dilute samples.

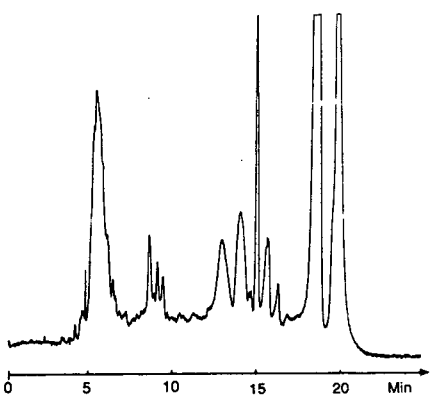

Fig. 3. High-performance capillary zone electrophoresis of urine following concentration toward a small-pore polyacrylamide gel and a short mobilization by displacement electrophoresis. The experimental conditions were similar, but not identical, to those used in the experiment presented in Fig. 2b. For details, see text.

The following two experiments illustrate that precautions should be taken in order to avoid some loss of the most rapidly and most slowly migrating proteins during the concentration procedure.

A commercial HPCE apparatus, BioFocus 3000, from Bio-Rad (Hercules, CA, USA) was employed in these experiments. Eppendorf 0.7-ml plastic vials served as electrode vessels. The leading buffer was the same as that used in the experiment presented in Fig. 4. The anode vessel contained 600 μl of this buffer. A 200-μl volume of 0.01 *M* glycine, titrated with NaOH to pH 9.0, was employed as terminator (catholyte). The resulting difference in buffer levels (1–2 cm) provided the counterflow required to give a stationary boundary between the leading chloride ions and the terminating glycinate ions in the concentration step. About 1.5 μg of each of the proteins β-lactoglobulin A (β), α-lactal-

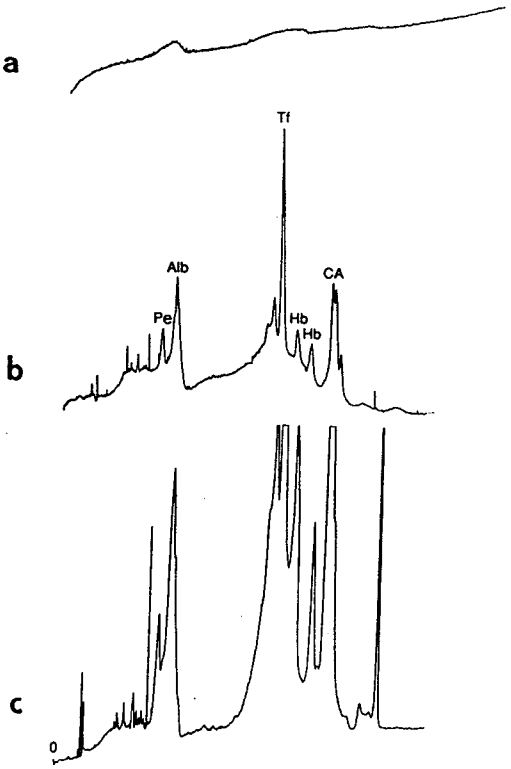

Fig. 4. High-performance capillary zone electrophoresis of model proteins. (a) Prior to concentration (concentration of each protein: 20 μg/ml). The width of the applied sample zone was 5 mm. (b) Following concentration by a combination of displacement electrophoresis and a hydrodynamic counterflow. The whole capillary was filled with the sample solution. (c) = (b) with the difference that not only the capillary was filled with sample solution but also the anode vessel.

bumin (α), and hemoglobin A (Hb A) was dissolved in the terminator diluted 5-fold with water. The capillary [250 (203) × 0.1 mm I.D. mm] was filled with this sample solution. The concentration took place at 3000 V for 12 min (see Figs. 1e and 2e in ref. 1). The distance from the cathodic end of the capillary to the stationary boundary was 1–2 cm. Prior to the final zone electrophoresis step the inlet carousel moved to a position where the vial contained 600 μl of 0.015 *M* HCl, titrated with Tris to pH 8.5. Without counterflow, the zone electrophoresis was conducted at 8000 V for 9 min. The temperature of the carousel was 15°C and that of the coolant 20°C. All operations were performed automatically and gave the electropherogram in Fig. 5a upon detection at 220 nm. Part of the slowly migrating proteins moved out of the capillary when the sample was dissolved in the non-diluted terminator, resulting in a reduced peak of hemoglobin A (not shown herein).

The run shown in Fig. 5b was performed as that presented in Fig. 5a, although the experimental conditions were as follows. Dimensions of the coated capillary: 260 (213) × 0.1 mm I.D.; leading buffer: 0.015 *M* HCl, titrated to pH 8.8 with Tris; terminating buffer: 0.1 *M* alanine, titrated to pH 8.8 with Tris. The sample (1.5 μg/ml of each protein) was dissolved in the leading buffer. Buffer level difference: 19 mm. Concentration step: 2000 V, 20 min; zone electrophoresis step: 10 000 V, 17 min. Detection wavelength: 220 nm. Temperature of the carousel: 15°C; temperature of the coolant: 20°C. Observe that the first two peaks are smaller than in Fig. 5a because the sample was dissolved in the leading, rather than the terminating buffer. This loss of protein can be avoided by diluting the leading buffer in the capillary (but not that in the anodic vessel) 10-fold.

The above automated experiment was repeated, although with basic proteins (cytochrome *c* (Cyt C), ribonuclease A (Rib A) and α-chymotrypsinogen A (α-chy)) which required other experimental conditions. Each of the proteins was dissolved in 700 μl of the leading solution (0.02 *M* ammonium acetate, titrated to pH 4.5 with acetic acid) to a concentration as low as 50 ng/ml. The main purpose of this experiment was to demonstrate that the concentration technique permits detection of proteins even at this very low concentration. The capillary [260 (213) × 0.1 mm I.D.] was filled with this sample solution. A 0.01 *M* solution of acetic acid (100 μl) was chosen as terminator (anolyte). The buffer level in the cathode vessel was 2 cm higher than that in the anode vessel. Following concentration at 2000 V for 20 min with the stationary boundary

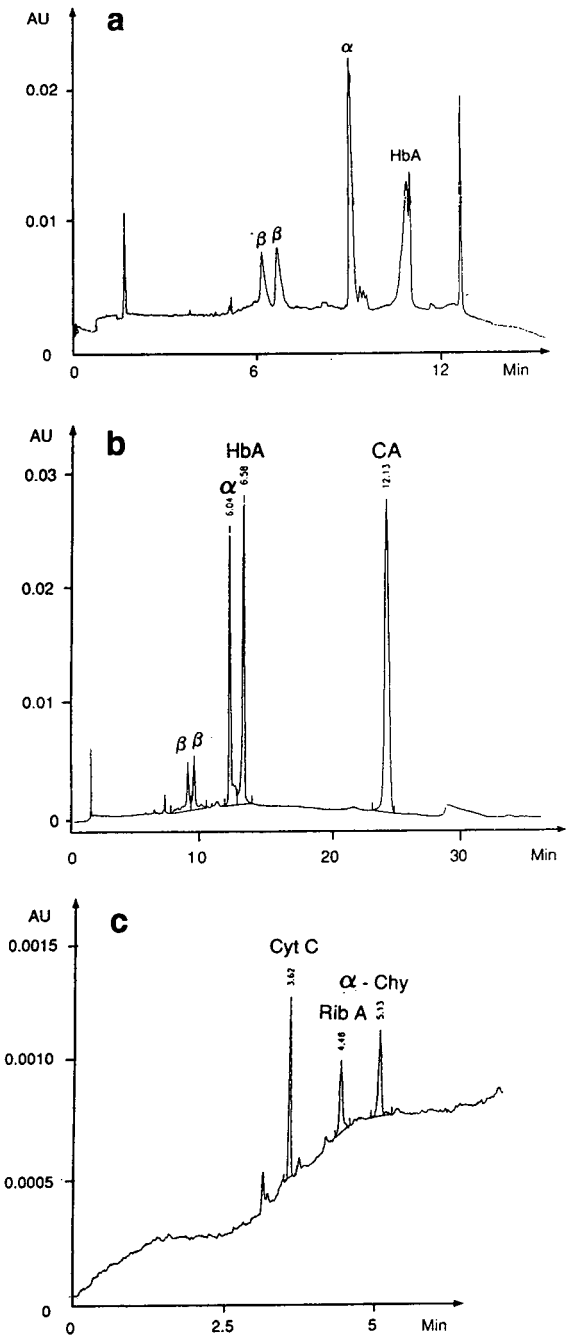

Fig. 5. Automated high-performance capillary zone electrophoresis of model proteins following concentration by a combination of displacement electrophoresis and a hydrodynamic counter flow. (a, b) acidic proteins, (c) basic proteins.

about 1–2 cm from the anodic end of the capillary the acetic acid in the anode vessel was replaced by the ammonium acetate solution. The subsequent zone electrophoresis at 10 000 V gave the electropherogram shown in Fig. 5c. The monitoring was done at 220 nm at a sensitivity of 0.002 AUFS to get relatively large peaks in spite of the extremely low concentrations of the proteins in the applied sample. Variations in the composition of the buffer and in its concentration in different sections of the capillary are detectable at this high sensitivity and account for the stepped form of the base line. In experiments where the protein concentration was lower than 50 ng/ml the adsorption of the proteins to the sample vial was significant. Several approaches to decrease this adsorption are mentioned in Discussion.

A tryptic digest of bovine albumin was concentrated in-tube and subjected to electrophoretic analysis essentially as described for the experiment presented in Fig. 4b. The electropherogram in Fig. 6 shows that the concentration method is applicable also in the concentration of peptides, *i.e.* substances of relatively low molecular weight.

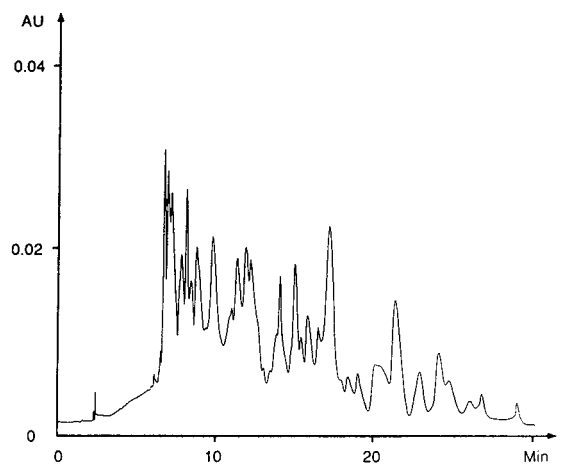

Fig. 6. Automated high-performance capillary electrophoresis of trypsin-digested bovine albumin following concentration by a combination of displacement electrophoresis and a hydrodynamic counterflow.

3.4. Concentration of proteins by electrophoresis toward a piece of dialysis tubing (= gradient in cross sectional area) (step I, alternative c in ref. 1) followed by zone electrophoresis (see Fig. 2c in ref. 1).

The fused-silica tubing [150 (135) × 0.1 mm I.D.] was coated with polyacrylamide to suppress adsorption of solutes and electroendosmosis [2].

The dialysis tubing was prepared as follows. A single hair with a diameter only slightly smaller than that of the inside diameter of the fused-silica tubing was inserted into the tubing, which was then placed in the mold shown in Fig. 7. The groove G was filled with a deaerated aqueous solution of acrylamide (276 mg/ml), N,N'-methylenebisacrylamide (24 mg/ml) and ammonium persulfate (2 mg/ml). Accordingly, the total concentration of the monomer (T) was 30% (w/v) and the crosslinking concentration (C) was 8% (w/w). Upon heating at 60°C a gel formed which was transparent and had very small pores. The single hair was then cautiously removed.

The silica tubing was filled with 0.1 M Tris–HCl, pH 8.5 containing the sample (15 μg/ml of each of the proteins β-lactoglobulin A, β-lactoglobulin B and α-lactalbumin). The cathode vessel (at the left) was filled with the same buffer and the anode vessel with 0.01 M Tris–HCl, pH 8.5, *i.e.*, a buffer of low conductivity to create a sharp starting zone for the subsequent electrophoretic analysis. Upon electrophoresis for 16 min at 2000 V all proteins became concentrated into a sharp band in the dialysis tubing (see Fig. 1c in ref. 1). The concentrated zone was moved into the capillary by a hydrodynamic flow to a position 3 mm from the end of the capillary (*cf.* Fig. 2c, step II in ref. 1). A free zone electrophoresis was then performed at 3000 V (cf. Fig. 2c, step III in ref. 1) following exchange of the 0.01 M Tris buffer in the cathode vessel with the 0.1 M buffer to avoid the pH and concentration changes which may occur in dilute buffers by electrolysis (Fig. 8b). This step can be omitted when the volume of the cathode vessel is relatively large, particularly when only a few analy-

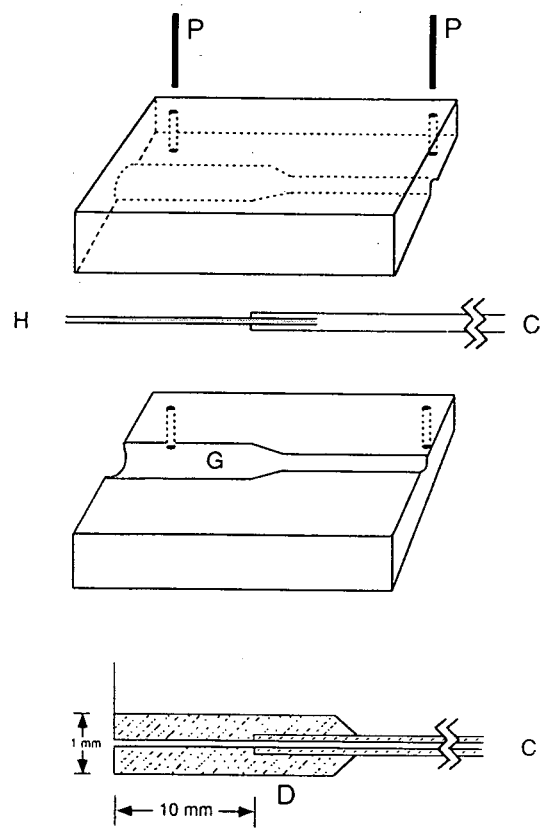

Fig. 7. Preparation of dialysis tubing (D) attached to the capillary (C). G, groove; H, single hair; P, guide pins.

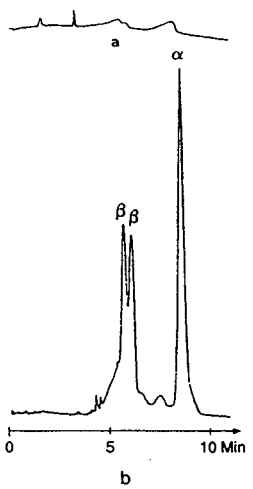

Fig. 8. Automated high-performance capillary zone electrophoresis of model proteins following concentration by electrophoresis toward a dialysis tubing.

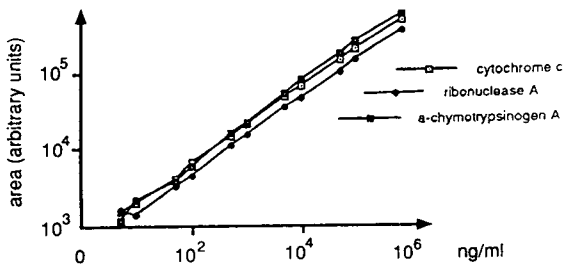

Fig. 9. A plot of peak area against sample concentration. Data from experiments similar to that presented in Fig. 5c.

ses are performed. The monitoring was done at 220 nm. A blank experiment was also performed (Fig. 8a), i.e. a zone electrophoresis without concentration of the sample.

3.5. The influence of sample concentration on peak area

The areas of the three main peaks in the electropherogram shown in Fig. 5c and similar electropherograms for other sample concentrations were used for the plot in Fig. 9. Obviously, a linear relationship between peak area and protein concentration was obtained over the whole concentration area 5 ng/ml–1 mg/ml.

4. Discussion

To better understand the design of the experiments described herein consult the theoretical treatment in ref. 1. Readers who do not study the theory in detail may find it difficult to tailor-make buffers for their own experiments. Therefore we have compiled in Table 1 several buffer systems from which one can easily select the appropriate one for any particular protein sample.

In this investigation we have generated a hydrodynamic counter flow in the capillary with the aid of different buffer levels in the two electrode vessels, although also other techniques, including the electroendosmotic pump [6], can be used to create a small pressure difference. Colored proteins and transparent glass tubes were used to establish experimentally the correct combination of flow rate and voltage to obtain a stationary boundary. Although one can, with the aid of an optical sensor, automatically and continuously adjust one of these parameters to a value that will keep the boundary stationary, we must point out that a moderate change in the flow rate affects the position of the boundary very little [1].

When the sample is dissolved in the leading buffer for concentration by displacement electrophoresis and a counterflow there is a risk that some part of the fastest migrating protein may migrate out of the capillary (Fig. 5b). To avoid this the concentration of the leading buffer in the electrode vessel should be higher than in the sample solution (see Table 1) or the sample should be dissolved in the terminator (Fig. 5a). Analogously, some part of the slowest protein can be lost when the sample is dissolved in the terminator. The loss can be eliminated if the terminator in the electrode vessel has a lower concentration than has the terminator in the sample solution.

As mentioned in ref. 1, high salt concentrations in the sample may eliminate the possibility to concentrate a sample by displacement electrophoresis. Different approaches to circumvent the problem were discussed therein.

The fact that the measuring points in the plot in Fig. 9 do fall on a straight line and are not scattered around it indicate that the concentration method described is highly reproducible.

Most solutes adsorb to some extent to most surfaces they come in contact with. This surface adsorption is very disturbing when the solute concentrations are extremely low, particularly when the sample consists of proteins with their tendency for multi-point attachment. It may very well happen that all of the sample molecules become adsorbed to pipette tips, the vial, the capillary, etc. and thereby escape detection. This surface adsorption combined with contamination from the surrounding milieu might be a greater hindrance to analysis of minute quantities of material than is the performance of the detectors. We have found that glass vials coated with methyl cellulose [7] exhibit less adsorption than

Table 1
Appropriate buffers for different concentration methods

Concentration method	Buffer system	I. Concentration	II. Mobilization	III. Free Zone Electrophoresis
Steep pH gradient (see Fig. 2a in ref. 1)	1 (P^-)	(+): 0.5 *M* Tris–HCl (pH 2.5) (S): 0.01 *M* Tris–HCl (pH 8.5) (−): 0.01 *M* Tris–HCl (pH 8.5)	(+): 0.01 *M* Tris–HCl (pH 8.5) (−): 0.01 *M* glycine–NaOH (pH 10.0) or 0.1 *M* NaOH	(+): 0.01 *M* Tris–HCl (pH 8.5) (−): 0.01 *M* Tris–HCl (pH 8.5)
	2 (P^+)	(+): 0.05 *M* EPPS–NaOH (pH 7.5) (S): 0.05 *M* EPPS–NaOH (pH 7.5) (−): 0.25 *M* EPPS–NaOH (pH 11.0)	(+): 0.1 *M* Bis–Tris–HCl (pH 2.0) or 1 *M* HCl (−): 0.05 EPPS–NaOH (pH 7.5)	(+): 0.05 *M* EPPS–NaOH (pH 7.5) (−): 0.05 *M* EPPS–NaOH (pH 7.5)
Small-pore gel ($T > 20\%$, $C = 3\%$) (see Fig. 2b in ref. 1)	(P^-)	(+): 0.01 *M* Tris–HCl (pH 8.5) or 0.03 *M* DAPA–Tris (pH 9.2) (S): 0.01 *M* Tris–HCl (pH 8.5) (−): 0.01 *M* Tris–HCl (pH 8.5)	(+): 0.01 *M* Tris–HCl (pH 8.5) (−): 0.03 *M* DAPA–Tris (pH 9.2) or 0.01 *M* glycine–NaOH (pH 10.0)	(+): 0.01 *M* Tris–HCl (pH 8.5) (−): 0.01 *M* Tris–HCl (pH 8.5)
Dialysis tubing (gradient in *q*) (see Fig. 2c in ref. 1)	P^-	(+): 0.01 *M* Tris–HCl (pH 8.5) (S): 0.1 *M* Tris–HCl (pH 8.5) (−): 0.1 *M* Tris–HCl (pH 8.5)		(+): 0.1 *M* Tris–HCl (pH 8.5) (−): 0.1 *M* Tris–HCl (pH 8.5)
Displacement electrophoresis + hydrodynamic counterflow (see Fig. 2e in ref. 1)	1 (P^-)	(+): 0.015 *M* HCl–Tris (pH 8.5) (S): 0.015 *M* HCl–Tris (pH 8.5) or 0.0015 *M* HCl–Tris (pH 8.5) or 0.002 *M* glycine–NaOH (pH 8.5) (−): 0.01 *M* glycine–NaOH (pH 8.5)		(+): 0.015 *M* HCl–Tris (pH 8.5) (−): 0.015 *M* HCl–Tris (pH 8.5)
	2 (P^-)	(+): 0.015 *M* HCl–Tris (pH 8.8) (S): 0.015 *M* HCl–Tris (pH 8.8) (−): 0.01 *M* alanine–Tris (pH 8.8)		(+): 0.015 *M* HCl–Tris (pH 8.8) (−): 0.015 *M* HCl–Tris (pH 8.8)
	3 (P^+)	(+): 0.01 *M* HAc (S): 0.02 *M* NH_4Ac–HAc (pH 4.5) (−): 0.02 *M* NH_4Ac–HAc (pH 4.5)		(+): 0.02 NH_4Ac–HAc (pH 4.5) (−): 0.02 NH_4Ac–HAc (pH 4.5)

(+), (S) and (−) refer to anolyte, sample buffer and catholyte, respectively. P^- and P^+ stand for buffer systems designed for acidic and basic solutes, respectively. EPPS = N-2-hydroxyethylpiperazine propane sulfonic acid. DAPA = diaminopimelic acid. The molarity of the buffers refers to the first mentioned constituent.

do plastic vials. Another alternative is to pretreat all contact surfaces with an aliquot of the sample prior to the analysis which, however, requires access to relatively large amounts of the sample. A variant of this coating method is to saturate all surfaces with solutes having a structure similar to that of the sample molecules and which are available in larger quantities.

Acknowledgements

The work was supported by the Swedish National Science Research Council and the Knut and Alice Wallenberg and Carl Trygger Foundations.

References

[1] S. Hjertén, J.-L. Liao and R. Zhang, *J. Chromatogr. A*, 676 (1994) 409.
[2] S. Hjertén, *J. Chromatogr.*, 347 (1985) 191–198.
[3] H. Kylin, *Z. Physiol. Chem.*, 69 (1910) 169–239.
[4] S. Hjertén, *Arch. Biochem. Biophys. Suppl.*, 1 (1962) 147–151.
[5] S. Hjertén, S. Jerstedt and A. Tiselius, *Anal. Biochem.*, 11 (1965) 219–223.
[6] S. Hjertén, *Electrophoresis*, 11 (1990) 665–690.
[7] S. Hjertén and K. Kubo, *Electrophoresis*, 14 (1993) 390–395.

ELSEVIER

Journal of Chromatography A, 676 (1994) 431–436

JOURNAL OF CHROMATOGRAPHY A

Enantiomeric separation of diniconazole and uniconazole by cyclodextrin-modified micellar electrokinetic chromatography

Ritsuko Furuta*, Tadashi Doi

Environmental Health Science Laboratory, Sumitomo Chemical Co., Ltd., 3-1-98, Kasugade Naka, Konohana-ku, Osaka 554, Japan

First received 30 December 1993; revised manuscript received 11 March 1994

Abstract

Enantiomeric separation of the structural analogues diniconazole and uniconazole by cyclodextrin (CD)-modified micellar electrokinetic chromatography was studied. The effects of the type of CDs, CD concentration and other operating parameters on the resolution of the enantiomers were clarified and the addition of an organic modifier to the separation solution was demonstrated to improve significantly the enantiomeric separation of both compounds. Enantiomeric separation of uniconazole was, in fact, achieved only with the addition of organic modifiers.

1. Introduction

Diniconazole and uniconazole (Fig. 1), which are vinyl triazoles, have fungicidal and plant growth-regulating activities. They each have an asymmetric carbon, and their enantiomers are known to differ significantly in their biological properties. In both instances, the *R*-enantiomer demonstrates stronger fungicidal activity than the *S*-enantiomer, whereas the *S*-enantiomer is more active than the *R*-enantiomer with regard to plant growth-regulating activity. In addition, uniconazole has a higher plant growth-regulating activity than diniconazole but is less active as a fungicide. Consequently, diniconazole-M, containing a high proportion of the *R*-enantiomer, and uniconazole-P, containing a high proportion of the *S*-enantiomer, have been developed as a high-activity fungicide and an effective plant growth regulator, respectively [1,2]. Reliable and efficient methods for separating the enantiomers are therefore necessary and we reported previously a reversed-phase liquid chromatographic approach using cyclodextrin (CD)-bonded columns and discussed the possible mechanisms of chiral recognition [3,4].

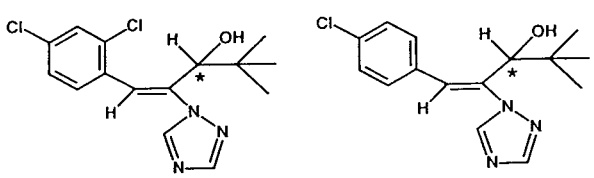

Diniconazole Uniconazole

Fig. 1. Structures of diniconazole and uniconazole.

Micellar electrokinetic chromatography (MEKC) is a high-resolution separation method [5–7] that is somewhat similar to reversed-phase chromatography. Solutes are separated due to differences in their hydrophobic interaction with

* Corresponding author.

0021-9673/94/$07.00
SSDI 0021-9673(94)00257-A

the stationary phase bonded to the surfaces of packing materials. Separation in MEKC results from the distribution of solutes between micelles, which act as a pseudo-stationary phase, and the aqueous phase in the presence of electroosmotic flow [8–10]. For enantiomeric separation in MEKC, CDs have been successfully used as chiral additives [11,12], as well as for HPLC.

We also found that the enantiomers of diniconazole and uniconazole can be separated by CD-modified MEKC (CD-MEKC) and, further, that organic modifiers offer an effective approach to improving the resolution.

2. Experimental

2.1. Apparatus

The MEKC experiments were performed with a P/ACE 2100 capillary electrophoresis system (Beckman, Palo Alto, CA, USA). The capillary cartridge (Beckman) contained a 75-μm I.D. capillary with a total length of 57 cm and 50 cm to the detector.

2.2. Chemicals

Diniconazole-M (S:R = 16:84) and uniconazole-P (S:R = 79:21) were synthesized by Sumitomo Chemical (Osaka, Japan) and used in all experiments as diniconazole and uniconazole, respectively. The α- and β-CDs were purchased from Kanto (Tokyo, Japan), γ-CD from Wako (Osaka, Japan), heptakis (2,6-di-O-methyl)-β-CD (DM-β-CD) from Aldrich (Milwaukee, WI, USA) and heptakis (2,3,6-tri-O-methyl)-β-CD from Sigma (St. Louis, MO, USA). Sudan IV, organic solvents and other reagents were of analytical-reagent grade from Kanto or Wako. Water was processed through an RO/NANOpureII system (Barnstead, Dubuque, IA, USA).

2.3. Procedures

Standard operating conditions, unless stated otherwise in the text or figure legends, were as follows: applied voltage, 15 kV; temperature, 25°C; detection, UV at 254 nm; and sample introduction, 1-s pressure. The separation solution was 100 mM sodium dodecyl sulphate (SDS) and 2 M urea in 100 mM borate buffer (pH 9.0) containing 50 mM γ-CD. Organic modifiers were added to the separation solution, where appropriate. Sample solutions (0.2 mg/ml) were prepared by dissolving each compound in methanol followed by mixing with the separation solution (Sudan IV was added to the aqueous solution in order to measure the migration time of the micelle, where appropriate) in the ratio of 1:4.

3. Results and discussion

3.1. Chiral recognition of CDs

The effect of the type of CDs on the chiral recognition of diniconazole and uniconazole was investigated by using α-, β-, γ-, DM-β- and TM-β-CDs as chiral additives.

Chiral recognition was dependent on the type of CDs, that is, the cavity diameter and lipophilic nature of the external portion of the CD molecule. The enantiomers of diniconazole were separated when γ-CD or DM-β-CD were used and the S-enantiomer eluted first in both instances. Because γ-CD is not solubilized by the micelle and migrates with the same velocity as the electroosmotic flow, the stable inclusion complex formation of the solute with the CD provides a faster migration under experimental conditions where the electroosmotic flow is stronger than the electrophoretic mobility of the micelle [12]. This is also the case for DM-β-CD, although this latter may be somewhat solubilized by the micelle. The findings indicate that the S-enantiomer forms a more stable inclusion complex than the R-enantiomer with γ-CD or DM-β-CD. With uniconazole, separation occurred only with γ-CD and the R-enantiomer was followed by the S-enantiomer (see Table 1). With HPLC using CD-bonded columns (α-, β- and γ-types were used), the enantiomers of diniconazole were separated completely on the β-CD column (retention order R, S) and partly

Table 1
Enantiomeric separation of uniconazole and diniconazole with CDs.

CD	Uniconazole			Diniconazole		
	t_R [a] (min)	t_S [b] (min)	R_s	t_S (min)	t_R (min)	R_s
α	61.72	61.72	0.00	68.45	68.45	0.00
β	43.84	43.84	0.00	54.11	54.11	0.00
γ	30.47	30.70	0.63	38.49	39.33	1.91
DM-β	23.79	23.79	0.00	27.14	27.59	2.21
TM-β	21.00	21.00	0.00	22.42	22.42	0.00

Separation solution, 100 m*M* SDS and 2 *M* urea in 100 m*M* borate buffer (pH 9.0) containing 50 m*M* CD–acetonitrile (95:5, v/v).
[a] t_R = Migration time of the *R*-enantiomer.
[b] t_S = Migration time of the *S*-enantiomer.

separated on the γ-CD column (retention order *S*, *R*), and those of uniconazole were partly separated on the γ-CD column (retention order *S*, *R*) as reported in previous papers [3,4]. The observed differences in enantioselectivity between the two methods could be explained by the presence of an SDS monomer, which can be included in the CD and can influence inclusion complex formation in MEKC [12]. An investigation to clarify these differences is in progress.

γ-CD was used in all subsequent experiments as it was the only form with which all enantiomers were separated.

3.2. Effect of CD concentration

The effects of γ-CD concentration on retention and resolution were examined by varying the concentration in steps from 20 to 70 m*M*. Organic modifiers were not added in this experiment. Fig. 2 shows plots of the capacity factor for the *R*-enantiomers, calculated according to the equation derived by Terabe *et al.* [5], the separation factor and the resolution, against the CD concentrations for diniconazole. The capacity factor decreased with increase in the CD concentration, because a more stable inclusion complex of the solute with the CD is formed at higher CD concentration and it therefore migrates faster, as described in the above section. The separation factor and resolution increased with increase in the CD concentration up to 50 or 60 m*M*. The peaks obtained with 60 and 70 m*M* CD were not symmetrical and 50 m*M* CD was the optimum concentration for the enantiomeric separation of diniconazole. Enantiomeric separation of uniconazole was not achieved at any concentration.

3.3. Effects of other operating parameters

The effects of operating parameters, other than the CD concentration described above, on retention and resolution were investigated to establish the optimum conditions without organic modifiers. The parameters investigated were

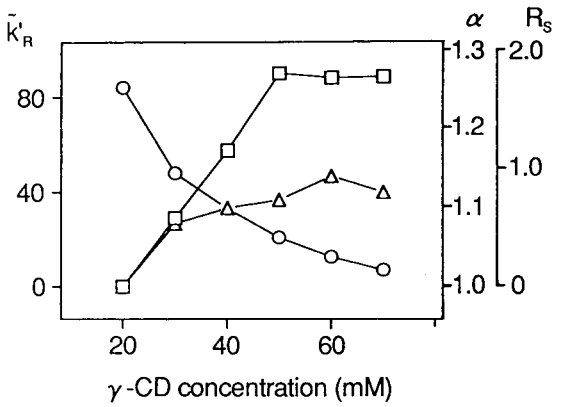

Fig. 2. Effect of γ-CD concentration in the separation solution on the (○) capacity factor, $\tilde{k}'_R$ (capacity factor of the *R*-enantiomers), (△) the separation factor, α, and (□) the resolution, R_s. Separation solution, 100 m*M* SDS and 2 *M* urea in 100 m*M* borate buffer (pH 9.0) containing γ-CD; for other analytical conditions, see the text.

concentration of SDS, urea or borate buffer in the separation solution, pH, temperature and applied voltage.

Data on the capacity factor, separation factor and resolution for diniconazole are summarized in Table 2. None of the parameters significantly influenced the chiral recognition at a constant CD concentration, as shown by the fact that the separation factors hardly changed. The resolutions obtained under the same operating conditions, that is, 100 m*M* SDS, 2 *M* urea, 100 m*M* borate buffer, pH 9.0, 15 kV at 25°C, decreased gradually with time (from 1.71 to 1.42). This is probably due to change in the capillary surface condition caused by, *e.g.*, corrosion by alkaline solution, because it is accompanied by a decrease in the migration time of methanol, which shows electroosmotic flow. A different capillary was used when the effect of the applied voltage was studied and less resolution was obtained. These phenomena represent problems which require further investigation to improve reproducibility.

As optimum conditions, 100 m*M* SDS, 2 *M* urea, 100 m*M* borate buffer and pH 9.0 were chosen because these gave the best resolution. With regard to temperature and voltage, 25°C and 15 kV were used in further experiments because of the appropriate analysis time and ease of control, although they did not provide the best resolution. Uniconazole could not be optically resolved under any of the conditions.

3.4. *Effects of organic modifiers*

It has been reported that adding an organic solvent to the separation solution is effective for

Table 2
Effects of operating parameters on the enantiomeric separation of diniconazole

Separation solution[a]				Applied voltage (kV)	Temperature (°C)	$\tilde{k}'_R$[b]	α	R_s
SDS (m*M*)	Urea (*M*)	Buffer (m*M*)	pH					
70	2	100	9.0	15	25	4.7	1.08	1.40
100	2	100	9.0	15	25	20.1	1.12	1.70
100	0	100	9.0	15	25	32.0	1.14	1.29
100	2	100	9.0	15	25	20.9	1.12	1.71
100	4	100	9.0	15	25	17.0	1.09	1.70
100	2	50	9.0	15	25	25.1	1.11	1.08
100	2	100	9.0	15	25	20.8	1.11	1.49
100	2	100	8.0	15	25	24.0	1.11	1.25
100	2	100	8.5	15	25	24.4	1.11	1.20
100	2	100	9.0	15	25	20.8	1.11	1.49
100	2	100	9.0	15	22	21.7	1.12	1.60
100	2	100	9.0	15	25	20.9	1.11	1.42
100	2	100	9.0	15	30	19.1	1.10	1.20
100	2	100	9.0	10	25	24.2	1.12	1.13[c]
100	2	100	9.0	15	25	22.7	1.11	1.00[c]
100	2	100	9.0	20	25	21.5	1.10	0.95[c]

[a] Concentration of γ-CD was 50 m*M*.
[b] $\tilde{k}'_R$ = Capacity factor of the *R*-enantiomer.
[c] A different capillary was used in these three experiments.

improving the enantioselectivity for some compounds in MEKC [13–15]. The effects of addition of organic solvents on the enantiomeric separation were therefore investigated under the optimum conditions determined as described above. The organic solvents added were acetonitrile, methanol, ethanol, 1-propanol, 2-propanol, 1-butanol, 2-butanol, 2-methyl-1-propanol and 2-methyl-2-propanol. The concentrations of each organic modifier tested were 2% and 5%, if miscible.

Table 3 shows the resulting data for migration times and resolutions of the enantiomers of diniconazole and uniconazole. The migration times are given instead of capacity factor values, which may be unreliable when an organic solvent is present because the marker for the micelle, Sudan IV, can distribute between the micelle and the aqueous phase containing the organic solvent [9]. Organic modifiers effectively improved the resolution of both compounds, and in fact the enantiomers of uniconazole were only resolved with separation solutions containing an organic modifier. The higher the content of the organic modifier, the better was the resolution, except with 2-butanol and 2-methyl-2-propanol for diniconazole. Hence there might be an optimum content of organic modifiers for each compound.

The organic modifier added to the separation solution not only increases the hydrophobicity of the solution and influences the distribution of the solute among the micelle, the aqueous phase and the CD, but can also compete with the solute in forming an inclusion complex with the CD. This indicates that the enantioselectivity by CD would decrease when bulkier and more hydrophobic

Table 3
Effects of organic modifiers on the enantiomeric separation of uniconazole and diniconazole

Organic modifier	Content (%)	Uniconazole			Diniconazole		
		t_R [a] (min)	t_S [b] (min)	R_s	t_S (min)	t_R (min)	R_s
None		27.35	27.35	0.00	31.17	31.56	1.24
Acetonitrile	2	27.60	27.60	0.00	32.22	32.69	1.54
	5	30.47	30.70	0.63	38.49	39.33	1.91
Methanol	2	29.23	29.23	0.00	34.50	35.08	1.42
	5	32.54	32.54	0.00	40.06	40.97	1.97
Ethanol	2	31.16	31.16	0.00	36.82	37.47	2.08
	5	34.58	34.87	0.75	43.77	44.73	2.25
1-Propanol	2	29.42	29.51	[c]	35.06	35.78	2.53
	5	31.99	32.47	1.40	41.70	42.96	3.10
2-Propanol	2	29.98	30.07	[c]	35.61	36.28	2.34
	5	32.33	32.78	1.38	41.63	42.68	2.64
1-Butanol	2	26.88	27.22	1.22	32.81	33.62	3.00
2-Butanol	2	28.21	28.43	0.73	33.91	34.69	2.62
	5	27.67	28.23	2.16	36.01	37.07	2.09
2-Methyl-1-propanol	2	28.62	29.03	1.32	35.50	36.57	3.59
2-Methyl-2-propanol	2	28.33	28.53	0.69	33.82	34.51	2.52
	5	29.28	29.99	2.52	38.61	39.62	2.13

[a] t_R = Migration time of the *R*-enantiomer.
[b] t_S = Migration time of the *S*-enantiomer.
[c] First peak eluted as a shoulder.

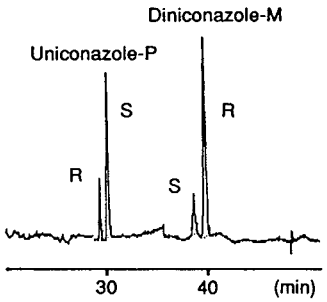

Fig. 3. Enantiomeric separation of diniconazole-M and uniconazole-P. Separation solution, 100 m*M* SDS and 2 *M* urea in 100 m*M* borate buffer (pH 9.0) containing 50 m*M* γ-CD–2-methyl-2-propanol (95:5, v/v); for other analytical conditions, see the text.

organic modifiers are used, because their molecules would be expected to form stable inclusion complexes. However, bulkier and more hydrophobic modifiers in the present experiments gave a better resolution. From this, we can hypothesize that the modifier molecule might be included together with the solute in the CD cavity and play a positive role in filling the space. It has been reported that tight fitting of a molecule to be complexed to a CD cavity is one of the important factors for chiral recognition by CD [16]. A typical chromatogram of uniconazole and diniconazole is shown in Fig. 3.

4. Conclusions

The pairs of enantiomers of both diniconazole and uniconazole can be successfully separated by CD-MEKC. Chiral recognition is dependent on the type of CDs and the CD concentration is the most important operating parameter determining the capacity factor and the enantiomeric separation. Addition of an organic modifier to the separation solution can significantly improve the enantiomeric separation, as shown for both compounds, even in cases where no resolution is observed in their absence.

5. References

[1] H. Takano, Y. Oguri and T. Kato, *Nippon Noyaku Gakkaishi*, 11 (1986) 373.
[2] H. Oshio, S. Tanaka and K. Izumi, *Shokubutsu no Kagakuchosetsu*, 25 (1990) 8.
[3] R. Furuta and H. Nakazawa, *J. Chromatogr.*, 625 (1992) 231.
[4] R. Furuta and H. Nakazawa, *Chromatographia*, 35 (1993) 555.
[5] S. Terabe, K. Otsuka, K. Ichikawa, A. Tsuchiya and T. Ando, *Anal. Chem.*, 56 (1984) 111.
[6] A.T. Balchunas and M.J. Sepaniak, *Anal. Chem.*, 59 (1987) 1466.
[7] M.M. Bushey and J.W. Jorgenson, *J. Microcol. Sep.*, 1 (1989) 125.
[8] S. Terabe, K. Otsuka and T. Ando, *Anal. Chem.*, 57 (1985) 834.
[9] K. Otsuka, S. Terabe and T. Ando, *Nippon Kagakukaishi*, 7 (1986) 950.
[10] S. Terabe, *Trends Anal. Chem.*, 8 (1989) 129.
[11] T. Ueda, F. Kitamura, R. Mitchell, T. Metcalf, T. Kuwana and A. Nakamoto, *Anal. Chem.*, 63 (1991) 2979.
[12] H. Nishi, T. Fukuyama and S. Terabe, *J. Chromatogr.*, 553 (1991) 503.
[13] J. Gorse, A.T. Balchunas, D.F. Swaile and M.J. Sepaniak, *J. High Resolut. Chromatogr. Chromatogr. Commun.*, 11 (1988) 554.
[14] K. Otsuka and S. Terabe, *Electrophoresis*, 11 (1990) 982.
[15] I.S. Lurie, *J. Chromatogr.*, 605 (1992) 269.
[16] A.M. Krstulović (Editor), *Chiral Separations by HPLC*, Ellis Horwood, Chichester, 1989, Ch. 10, pp. 213–214.

ELSEVIER

Journal of Chromatography A, 676 (1994) 437–442

JOURNAL OF CHROMATOGRAPHY A

Potentiometric detection of anions separated by capillary electrophoresis using an ion-selective microelectrode

André Nann, Ernö Pretsch*

Department of Organic Chemistry, Swiss Federal Institute of Technology (ETH), Universitätstrasse 16, CH-8092 Zurich, Switzerland

Received 28 February 1994

Abstract

Capillary electrophoresis in fused-silica capillaries of 10 μm I.D. coupled to an anion-selective microelectrode as on-column detector allows inorganic and organic anions, especially lipophilic ones, to be separated with high resolution and sensitivity of detection. For perchlorate, plate numbers of up to 10^7/h and a detection limit of $5 \cdot 10^{-8}$ M have been achieved. After delogarithmizing the response function of the microelectrode, quantitative results are obtained as described previously.

1. Introduction

Capillary electrophoresis (CE) has two major advantages as compared with conventional ion chromatography. On the one hand, there are almost no limits to the miniaturization of electrophoretic separation systems [1], allowing the injection of sample volumes down to the 100-fl range [2]. On the other hand, CE methods yield a flat elution profile providing much higher separation efficiency. To fully take advantage of these two facts, the detector must meet the following requirements: the detection must take place on-column since the elution profile outside the electric field changes to a parabola (as in conventional ion chromatography), which causes a drastic drop in the maximum resolution to be reached [3]. Furthermore, the detection device must be so sensitive as to respond to even a few ions only. For a CE analysis performed on an analyte solution of 10^{-10} M with a total run time of 200 s in a capillary of 50 cm × 10 μm I.D., the detector must respond to 20 zmol (ca. 10 000 ions)/s. Up to now, on-column detection of such low quantities was only possible with fluorescence spectroscopy. As an example, the detection of rhodamine 6G with axial-beam laser-excited fluorescence in a capillary of 75 μm I.D. has been reported with a limit of detection (LOD) in the 10^{-11} M region [4]. However, the sample, apparently prepared with distilled water, was injected electrokinetically which entails an enormous on-column analyte concentration [5] and makes it difficult to compare the result with others. Wu and Dovichi [6] detected amino acids labelled with fluoresceine isothiocyanate, obtaining a LOD in the pM region but give no details about the specific resistance or total ionic strength of the sample solutions. The major drawback of fluorescence detection is its limita-

* Corresponding author.

0021-9673/94/$07.00
SSDI 0021-9673(94)00340-F

tion to fluorescent ions, although this is of minor importance when dealing with organic and easily derivatizable analytes. In the case of small organic and of inorganic ions, derivatization is not possible. Nevertheless, Milofsky and Yeung [7] separated non-derivatized, i.e. unlabelled, amino acids and performed native fluorescence detection achieving a LOD up to four orders of magnitude higher than for the corresponding derivatized compounds. Jones and Jandik [8] succeeded in separating 36 inorganic and organic anions with excellent resolution in a total analysis time of only 3 min, using indirect UV absorption as detection method and a chromate buffer as background electrolyte. The analyte solutions were prepared with distilled water to obtain samples of high specific resistance. On-column analyte enrichment was obtained by electrokinetic injection and for certain ions, LODs in the sub-ppt region were achieved. This means that the specific LOD of the detection system may be up to some orders of magnitude higher than the concentrations of the samples injected. Recently, CE systems with suppressed conductivity detection were described [9,10] for which detection limits in the range of 1–10 ppb were found with buffered sample solutions.

In view of achieving as low a LOD as possible, it seems more promising to concentrate on the development of direct detection methods. Indirect procedures have the disadvantage of implying the subtraction of two high values to give a very small difference thus limiting the LOD. For example, with indirect fluorescence detection [11,12], no significant improvement in sensitivity is to be expected over indirect UV.

In previous work, the use of ion-selective microelectrodes (ISMEs) as on-column detectors for cations in a CZE separation system has been reported [13,14]. The present paper describes the application of this technique to the separation of anions, using ISMEs based on anion-exchanger liquid membranes [15]. Their selectivity coefficients depend on the free enthalpy of hydration of the analyte anions [16], i.e. the more lipophilic the anion, the higher is the sensitivity of the ISME. Several inorganic anions plus an organic one have been separated in a total analysis time of 4 min. For perchlorate, a plate number of 300 000 and a LOD $< 10^{-7}$ M have been achieved. In analogy to the procedure described for the separation of cations [14], a calibration plot allows quantitative determinations of perchlorate.

2. Experimental

2.1. Reagents

Chemicals of the highest purity available (Fluka, Buchs, Switzerland) and doubly quartz-distilled water were used.

2.2. CZE–ISME system with data acquisition

Except for minor modifications, the CZE apparatus with fused-silica capillary of conical aperture and an ISME as potentiometric on-column detector is similar to that described earlier [13,14]. The electrophoretic field was generated by a high-voltage power supply, Model 225-50 R (Bertan Associates, Hicksville, NY, USA). Fused-silica capillaries of 10 μm I.D. were purchased from Scientific Glass Engineering (Ringwood, Australia) and cut to a length of 50 cm. Poly(N,N,N′,N′-tetramethyl-N-trimethylenehexamethylenediammonium dibromide) (Polybrene)-coated capillaries were prepared by purging them with a 0.01% aqueous polybrene solution for 30 min. Afterwards, they were rinsed under pressure (50 bar) with buffer solution passed through a microfilter (0.2-μm Nalgene syringe filter; Nalge Company, NY, USA). The conically shaped aperture at the detection end was then obtained by immersing the buffer-filled capillary over a length of 3 mm in 40% hydrofluoric acid for 20 min. Potentials were measured differentially, i.e., the potential difference between ISME and reference electrode (Ag|AgCl| electrophoretic buffer solution saturated with AgCl; 1 mm tip diameter) was determined with a platinum wire serving at the same time as common electrode and electrophoretic ground (anode). The reference and anion-selective electrodes were directly con-

nected to operational amplifiers (type AD 515 KH, Analog Devices, Norwood, MA, USA) wired as voltage followers. Potentials were monitored with a laboratory-made electrode amplifier. The ISME, reference electrode, platinum anode and conically etched capillary end were placed in a small Plexiglass vessel filled with buffer solution. On-column positioning of the ISME was achieved with the aid of micromanipulators and an inverse microscope (Narishige and Diaphot; Nikon, Tokyo, Japan).

For data acquisition, an Apple Macintosh IIfx computer (Cupertino, CA, USA) equipped with a 16-bit NuBus A/D converter card (MacAdios II; GW Instruments, Somerville, MA, USA) was used. Electropherograms were displayed using the program LabView (National Instruments, Austin, TX, USA) and hard copies of the acquired data were generated with the graphic program DeltaGraph (Delta Point, Monterey, CA, USA).

2.3. Anion-selective microelectrodes

Glass micropipettes were pulled from clean borosilicate glass tubes (GC 150T-15, Clark Electromedical Instruments, Pangbourne, Reading, UK) with the help of a vertical pipette puller (Model 700C, David Kopf Instruments, Tujunga, CA, USA). Under a microscope, their tips were broken to a diameter of ca. 1 μm against a polished glass rod. The micropipettes were put vertically in a glass desiccator (without drying agent), flushed with nitrogen, placed in an oven with the desiccator valve left open and predried at 180°C for 1 h. After reflushing the desiccator with nitrogen and increasing the temperature to 200°C, N,N-dimethyltrimethylsilylamine (0.1 ml) was injected into it and allowed to react in the vapour phase with the micropipettes for 30 min. The hot silanized micropipettes were then transferred to another desiccator. They can be stored over silica gel for some weeks. Back-filling of the micropipette with electrophoretic buffer solution (saturated with silver chloride) was performed by applying a slight overpressure (ca. 5 bar) with a syringe. The tip was then front-filled to a height of ca. 100 μm by dipping it into the anion-selective membrane phase which consisted of 10% tridodecylmethylammonium chloride in 2-nitrophenyl octyl ether. After inserting a chloridized silver wire (prepared by immersing a 1 mm silver wire in 10% iron trichloride dissolved in 0.1 *M* hydrochloric acid for 24 h), the microelectrode was completed by fixing the silver chloride electrode at the top with insulating tape.

3. Results and discussion

Generally, the electrolyte solution in a fused-silica capillary is driven by the electroosmotic force from the anode towards the cathode. This can have an adverse influence on the separation, particularly when the absolute mobilities of the analyte anions are smaller than the electroosmotic mobility. It must be attempted, therefore, to reverse, stop or at least slow down the electroosmotic flow (EOF). This can be achieved by different techniques, e.g. by applying an external electric field to the outer capillary wall [17], adding a surfactant [18–20] or a viscosity modifier to the running buffer [21] or coating the inner capillary wall with a polymer [22]. With ISMEs as detectors in CE, surfactants (especially lipophilic additives, e.g. cetyltrimethylammonium salts, CTMA) proved to be useless. Although the addition of $5 \cdot 10^{-4}$ *M* CTMA to the background buffer causes a reversal of the EOF, the anion-selective liquid membrane phase was spontaneously washed out of the microelectrode. A further disadvantage of CTMA and similar quaternary ammonium salts is their affinity to lipophilic anions (as perchlorate, salicylate and others), causing precipitates or bulky agglomerates. Polybrene has proved to be a good surfactant, covering the glass surface with a positively charged layer [23], and specially useful when employing ISMEs as CE detectors. There is no need to add it to the background buffer. To obtain a robust film providing a stable EOF in the reverse direction, it is sufficient to rinse the capillary with a 0.01% aqueous Polybrene solution. From run to run, an average slowing down in EOF of only 0.02% has been observed (n =

500). This is significantly lower than the statistic variation in EOF for a single measurement, even without reversal.

Another possibility to decrease the EOF or bring it to a halt consists in lowering the pH of the background buffer to 2–3 [24]. This method can only be used if the pK values of the anionic analytes are smaller, or at least not significantly higher than the pH of the buffer. Otherwise, the elution times will become unacceptably long due to a drastic drop in effective charge number of the analyte ions.

To ensure that the results, particularly the LODs, can be compared with those obtained with other detection methods, on-column enrichment (as a consequence of electrokinetic injection) was avoided by preparing the analyte samples from 10^{-2} M stock solutions diluted with background buffer.

Fig. 1 shows a CZE–ISME analysis at pH 7.0 of six anions (each 10^{-4} M) in a Polybrene-coated capillary. Evidently, the peak heights are a function of the lipophilicity of the analyte anions. While the signal for ClO_4^- has a height of ca. 110 mV, that for Br^- reaches only ca. 7 mV. In the delogarithmized form (B), i.e. for $\mathcal{D}$ vs. t (where $\mathcal{D} = 10^{E/s} - 1$, with E as the potential measured and $s = -2.303\ RT/F$, the slope of the ISME response function for monovalent anions [14], R is the universal gas constant and F the Faraday constant), the effect of these differences in selectivity is even more obvious. The delogarithmized response allows to compare the CZE–ISME system with other ones, e.g. CE with UV, fluorescence or amperometric [2] detection or with ion chromatography. As in the last-mentioned method, the resolution of the CZE separation can be evaluated directly from the delogarithmized form. For the ClO_4^- peak, a plate number of 300 000 has been achieved. With regard to routine analysis, this means almost 10^7 theoretical plates/h. Besides, it is noteworthy that the resolution of peaks 4 (ClO_4^-) and 5 (SCN^-) is better, with less tailing, than the logarithmic form (A) of the electropherogram might suggest.

Similar electropherograms (Fig. 2) are obtained with an uncoated capillary when the EOF is greatly reduced or even brought to a standstill by lowering the pH to 2.5. Even at this low pH, the ISME shows the same characteristics as in neutral background buffer.

Fig. 3 shows the detection of 0.1 μM ClO_4^-. The peak height is of the same order of magnitude as the amplitude of the long-term noise [13], so that proper peak identification becomes difficult, whereas a signal/short-term noise ratio of 10 was obtained. Considering these results, the LOD was established at $5 \cdot 10^{-8}$ M.

A ClO_4^- concentration as low as 10^{-8} M in tap

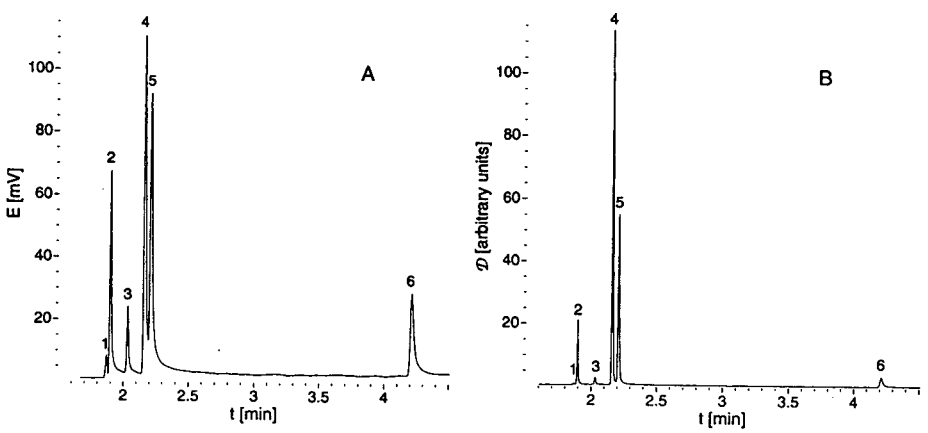

Fig. 1. CZE–ISME analysis of the Na^+ salts of (1) Br^-, (2) I^-, (3) NO_3^-, (4) ClO_4^-, (5) SCN^- and (6) salicylate, each 10^{-4} M in background buffer. Buffer: 20 mM Tris–formate, pH 7.0; separation voltage: 25 kV; electrokinetic injection: 3 kV for 3 s. Polybrene-coated capillary. (A) As recorded by ISME detector, (B) delogarithmized form (see text and [14]).

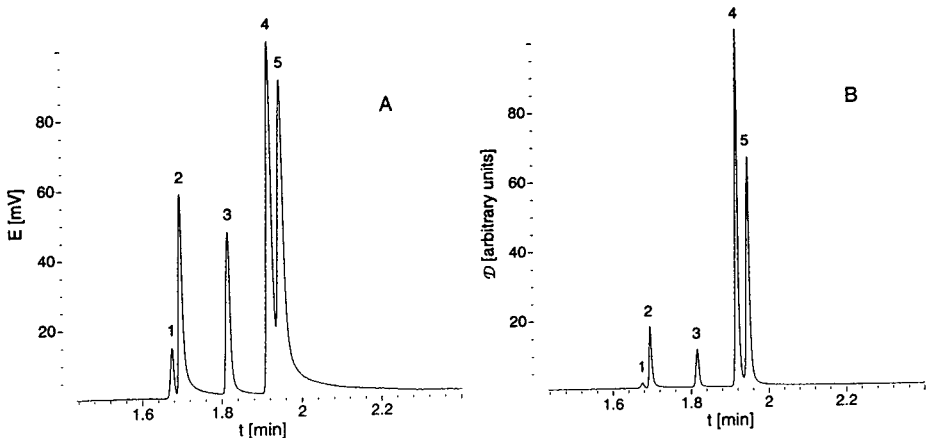

Fig. 2. CZE–ISME analysis of the Na^+ salts of (1) $5 \cdot 10^{-4}$ *M* Br^-, (2) 10^{-4} *M* I^-, (3) $5 \cdot 10^{-4}$ *M* NO_3^-, (4) 10^{-4} *M* ClO_4^- and (5) 10^{-4} *M* SCN^- in background buffer. Buffer: 20 m*M* Na_2SO_4, adjusted to pH 2.5 with H_2SO_4; separation voltage: 30 kV; electrokinetic injection: 2 kV for 2 s. Uncoated capillary. (A) As recorded by ISME detector, (B) delogarithmized form (see text and [14]).

water can be detected owing to the on-column concentration effect achieved by electrokinetically injecting a sample of high specific resistance (Fig. 4). If the total ionic strength of the sample is adjusted with running buffer salt, no enrichment occurs and only NO_3^- gives an appreciable signal.

From Fig. 5, it can be gathered that quantitative CZE–ISME analysis of anions can be carried out in the same way as that of cations, using the integrals $\mathcal{J} = \int \mathcal{D}\, dt$ [14]. In the case of ClO_4^-, a mean error (residual S.D. divided by

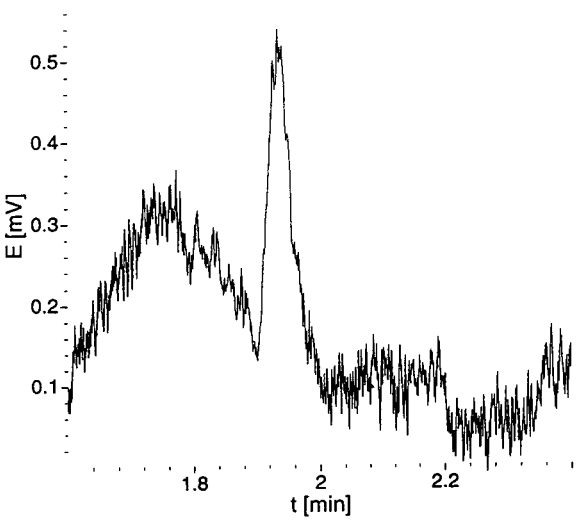

Fig. 3. CZE–ISME analysis of ClO_4^- (10^{-7} *M*) near the detection limit. Buffer: 20 m*M* Na_2SO_4, adjusted to pH 2.5 with H_2SO_4; separation voltage: 30 kV; electrokinetic injection: 5 kV for 10 s. Uncoated capillary.

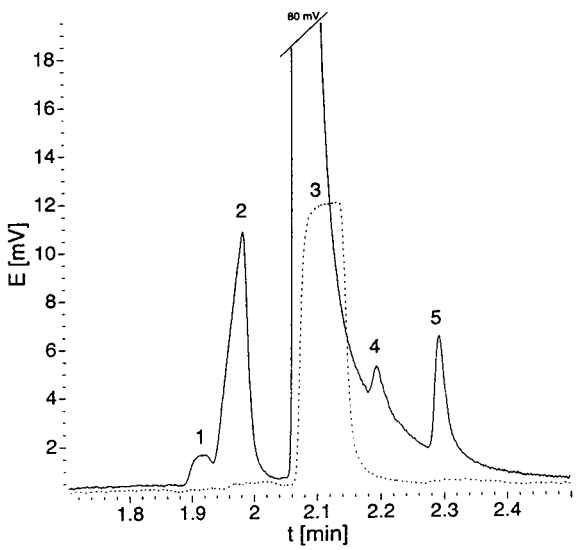

Fig. 4. Determination of 10^{-8} *M* (ca. 1 ppb, w/w) ClO_4^- in tap water as recorded by IMSE. Buffer: 20 m*M* Na_2SO_4, adjusted to pH 2.5 with H_2SO_4; separation voltage: 30 kV; electrokinetic injection: 10 kV for 10 s. Uncoated capillary. Solid line = 10^{-8} *M* $NaClO_4$ in tap water; broken line = 10^{-8} *M* ClO_4^- + 20 m*M* Na_2SO_4 in tap water. Peaks: 1 = Br^-; 2 = Cl^-; 3 = NO_3^-; 4 = ClO_4^-; 5 = unknown.

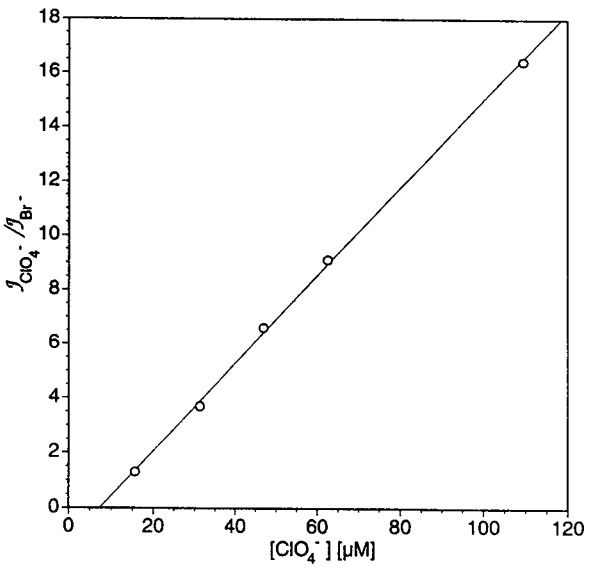

Fig. 5. Linear calibration plot (see text and [14]) for (1.5 to 11)·10^{-5} *M* ClO_4^- ($n = 5$) with 10^{-3} *M* Br^- as internal standard (Na^+ as counter ion). Buffer: 20 m*M* Tris–formate, pH 7.0; separation voltage: 25 kV; electrokinetic injection: 2 kV for 2 s. Polybrene-coated capillary.

the mean ordinate value) of 3% was obtained from the calibration plot.

4. Conclusions

It is shown that anion-selective microelectrodes can be used as powerful detectors in CE. Considering the detection limits and the possibility of miniaturizing the separation systems, even better results are achievable than with conventional detection methods [25].

Acknowledgements

Part of this work was supported by the Swiss National Science Foundation and by Ciba-Corning Diagnostic Corp.

References

[1] Z.H. Fan and D.J. Harrison, *Anal. Chem.*, 66 (1994) 177–184.
[2] T.M. Olefirowicz and A.G. Ewing, *Anal. Chem.*, 62 (1990) 1872–1876.
[3] E. Grushka, *J. Chromatogr.*, 559 (1991) 81–93.
[4] J.A. Taylor and E.S. Yeung, *Anal. Chem.*, 64 (1992) 1741–1744.
[5] D.S. Burgi and R.L. Chien, *Anal. Chem.*, 64 (1992) 489A–496A.
[6] S. Wu and N.J. Dovichi, *J. Chromatogr.*, 480 (1989) 141–155.
[7] R.E. Milofsky and E.S. Yeung, *Anal. Chem.*, 65 (1993) 153–157.
[8] W.R. Jones and P. Jandik, *J. Chromatogr.*, 608 (1992) 385–393.
[9] P.K. Dasgupta and L. Bao, *Anal. Chem.*, 65 (1993) 1003–1011.
[10] N. Avdalovic, C.A. Pohl, R.D. Rocklin and J.R. Stillian, *Anal. Chem.*, 65 (1993) 1470–1475.
[11] L. Gross and E.S. Yeung, *J. Chromatogr.*, 480 (1989) 169–178.
[12] K. Bachmann, I. Haumann and T. Groh, *Fresenius' J. Anal. Chem.*, 343 (1992) 901–902.
[13] A. Nann and W. Simon, *J. Chromatogr.*, 633 (1993) 207–211.
[14] A. Nann, I. Silvestri and W. Simon, *Anal. Chem.*, 65 (1993) 1662–1667.
[15] B.P. Nikolskii, E.A. Materova and A.L. Grekovich, *Elektrokhimiya*, 13 (1977) 740–744.
[16] D. Wegmann, H. Weiss, E. Pretsch, W. Simon, K. Sugahara, D. Ammann and W.E. Morf, *Mikrochim. Acta*, III (1984) 1–16.
[17] M.A. Hayes, I. Kheterpal and A.G. Ewing, *Anal. Chem.*, 65 (1993) 2010–2013.
[18] T. Tsuda, *J. High Resolut. Chromatogr. Chromatogr. Commun.*, 10 (1987) 622–624.
[19] M.P. Harrold, M.J. Wojtusik, J. Riviello and P. Henson, *J. Chromatogr.*, 640 (1993) 463–471.
[20] X.W. Yao, D. Wu and F.E. Regnier, *J. Chromatogr.*, 636 (1993) 21–29.
[21] W. Buchberger and P.R. Haddad, *J. Chromatogr.*, 608 (1992) 59–64.
[22] G.J.M. Bruin, J.P. Chang, R.H. Kuhlman, K. Zegers, J.C. Kraak and H. Poppe, *J. Chromatogr.*, 471 (1989) 429–436.
[23] J. Vandekerckhove, G. Baue, M. Puype, J. Damme and M. Montagu, *Eur. J. Biochem.*, 152 (1985) 9–19.
[24] M.B. Amran, M.D. Lakkis, F. Lagarde, M.J.F. Leroy, J.F. Lopez-Sanchez and G. Rauret, *Fresenius' J. Anal. Chem.*, 345 (1993) 420–423.
[25] I. Isildak and A.K. Covington, *Electroanalysis*, 5 (1993) 815–824.

ELSEVIER

Journal of Chromatography A, 676 (1994) 443–450

JOURNAL OF CHROMATOGRAPHY A

Determination of chromate ion in chromium plating baths using capillary zone electrophoresis with micellar solution

Maria Martínez*, Manuel Aguilar

Department of Chemical Engineering (ETSEIB-UPC), Diagonal 647, 08028 Barcelona, Spain

First received 7 October 1993; revised manuscript received 14 February 1994

Abstract

Chromate anion (CrO_4^{2-}) has been determined by capillary zone electrophoresis with on-column UV detection at 273 nm by using a negative power supply. A fused-silica capillary (53 cm × 0.05 mm I.D.) was employed and a high voltage of 20 kV was applied.

The addition of a cationic surfactant, tetradecyltrimethylammonium bromide (TTAB) in the buffer solution reverses the direction of the electroosmotic flow (EOF) in the capillary, so that EOF augments the mobility of the anion. This results in an exceedingly short analysis time of under 2 min.

From migration time data, the electroosmotic mobility, the electrophoretic mobility of the micelle and apparent electrophoretic mobility of the chromate ion in the micellar solution were determined as a function of the concentration of TTAB.

Linear calibration for chromate ion was established over the concentration range 25–300 pg with a detection limit of 1.2 pg/nl by using a 0.01 *M* carbonate buffer and 5 m*M* TTAB solution (pH 10).

The method was applied to the determination of the chromate anion in a rinse water from chromium plating baths.

1. Introduction

There is a rapidly increasing demand for fast and reliable analytical methods for the determination of chemical forms of elements in environmental samples. The interest in chromium is motivated by the fact that its toxicity depends critically on its oxidation state. It has long been known that Cr(III) and Cr(VI) have very different biological and toxicological properties. Whereas Cr(III) is essential for mammals, Cr (VI) is considered to be a moderate to severe toxic agent [1]. Cr(III) and Cr(VI) enter the environment as a result of effluent discharge from steel works, electroplating, tanning industries, oxidative dyeing, chemical industries and cooling water towers.

In view of the difference between the oxidation states, and in order to follow the reaction pathways in the environment, it is increasingly important to monitor the concentration of the individual chemical species as well as the total concentration of chromium in the environment.

Of the numerous methods developed for chromium speciation, those which physically separate the individual species followed by direct quantification are preferred because they are relatively fast and require only minimal sample

* Corresponding author.

0021-9673/94/$07.00
SSDI 0021-9673(94)00334-6

pretreatment. In this context, methods such as HPLC or flow injection analysis, coupled with photometric or spectrometric detection, have been employed most for the determination of chromium species [2–5] and the use of capillary zone electrophoresis (CZE) is emerging as an alternative technique.

In recent years CZE has been shown to be a highly efficient in the separation of small inorganic and organic cations and anions [6,7]. On the other hand, the use of CZE for the separation of metal species with good resolution has also been shown to be feasible [8–10].

Under a conventional CZE system, anions with an electrophoretic mobility higher than the electroosmotic mobility of the bulk electrolyte escape detection and it is necessary to reverse the polarity of the applied electric field. Therefore, the separation of highly mobile inorganic and organic anions usually requires longer times than the separation of cations and it is not possible to perform both analyses together in a single run. However, it has been shown that the addition of a cationic surfactant to the electrolyte significantly reduces the migration times for anionic species by reducing or reversing the electroosmotic flow (EOF).

Previously, some authors have reported a reversed EOF direction when a long-chain cationic surfactant, such as: cetyltrimethylammonium bromide [11,12], dodecyltrimethylammonium bromide [13] or tetradecyltrimethylammonium bromide (TTAB) [14], was added to the electrolyte. A cationic surfactant with a longer alkyl chain is preferred because the EOF can be suppressed or reversed at lower concentration. In this way, the influence on the constitution of the background electrolyte can be reduced [15].

In our experiments, TTAB was the cationic surfactant chosen; it is electrostatically attracted to the silanol groups on the inner wall of the capillary. It effectively shields these negative charges from the bulk of the electrolyte and creates a net positive wall charge.

In this paper, the determination of chromate anion by CZE with a micellar solution containing TTAB is described. The effect of the cationic surfactant concentration on electroosmotic and electrophoretic mobilities is also studied. The results were applied to the determination of the chromate ion in rinse waters from chromium plating baths.

2. Experimental

2.1. Instrumentation

An integrated capillary electrophoresis system ISCO (Lincoln, NE, USA) Model 3850, equipped with high-voltage power supply (0–30 kV) with a reversible polarity and vacuum injection control was used.

A 53 cm × 50 μm I.D. unmodified fused-silica capillary tube with a 33 cm distance from the injection point to the detector cell was employed. Detection was carried out by on-column measurements of UV absorption at 273 nm. All experiments were performed with an applied voltage of 20 kV.

Electropherograms were recorded using a Spectra-Physics (San Jose, CA, USA) SP-4270 integrator.

Samples were introduced hydrodynamically at the cathode (negative polarity) by vacuum for a constant period of time (5–10 s) depending on the desired volume of injection.

A Perkin-Elmer Model 2380 atomic absorption spectrometer was used to determine the total concentration of chromium in rinse water by atomic absorption spectrometry (AAS).

2.2. Reagents and solutions

Buffer solutions were prepared from sodium hydrogencarbonate, disodium tetraborate or disodium hydrogenphosphate dihydrate, from Merck (Darmstadt, Germany) by adding 0.1 *M* NaOH solution to adjust its pH to 10.

HPLC-grade TTAB, obtained from Scharlau, was used without further purification. TTAB solution was added to buffer solution to reverse of the direction of the EOF.

HPLC-grade methanol from Romil Chemicals and analytical-grade anthracene from Merck were used without further purification.

Stock standard solutions of sodium chromate were prepared by dissolution of an accurately weighed amount of the analytical-grade reagent supplied by Merck in a 0.01 *M* solution of the appropriate buffer, followed by dilution as required.

The pH of solutions was adjusted at 10 to obtain only the chromate anion in the solution, in absence of the rest of the chromium complexes, which can be at lower pH.

The acidic rinsewater sample was provided by Inoxcrom (Barcelona, Spain). No sample pretreatment other than dilution in buffer solution was required.

Purified (18 MΩ) water using a Millipore Milli-Q water purification system was used for all solutions.

The buffer and sample solutions were filtered through a 0.45 μm membrane filter from Lida (Kenosha, WI, USA) and were degassed by ultrasonication.

2.3. Procedure

Before sample injection, the capillary was washed with 0.1 *M* NaOH solution for 30 min, followed by rinsing with the buffer solution for 30 min. Between each injection the capillary was filled with the buffer solution using a syringe purge that flushed the entire capillary in a few seconds, and both ends of the tube were dipped into two separate beakers filled with the same buffer solution.

Vacuum injection sample is carried out by placing the inlet of the capillary into a vial of sample (75 μl). After a constant period of time (5–10 s), the inlet of the tube was returned to the beaker and a high voltage (20 kV) was applied.

3. Results and discussion

3.1. Control of electroosmotic flow

In a conventional CZE system, the detector is located near the cathode and the EOF direction is toward the cathode, hence the chromate anion moves toward the anode and is not detected because its electrophoretic mobility is higher than the electroosmotic mobility (μ_{eo}), whose directions are opposed. It might be imagined that this problem could be solved simply by reversing the polarity of the applied electric field. Fig. 1A shows the resulting electropherogram indicating that its peak is badly broadened, probably caused by the great difference in mobility values between the chromate and buffer [16].

However, this problem can be overcome by simultaneously reversing both the polarity of the applied electric field and the intrinsic direction of the EOF. Under these conditions, and in order

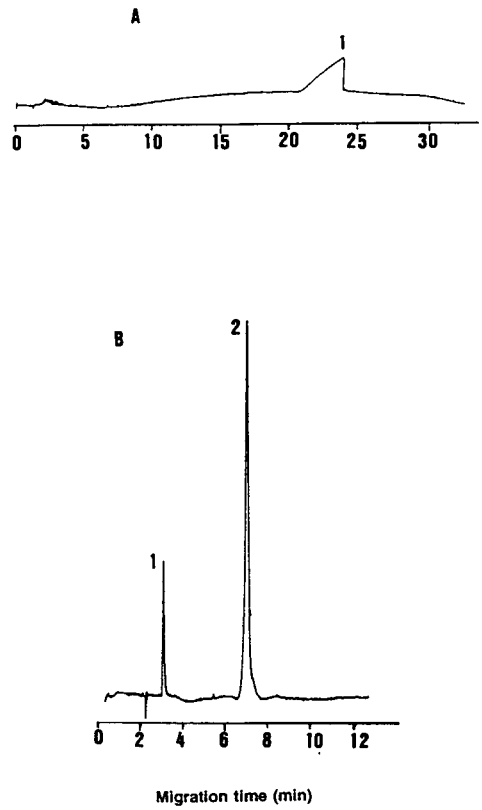

Fig. 1. Electropherograms of standard chromate solutions. Detection wavelength: 273 nm; fused-silica capillary (53 cm × 50 μm I.D.); negative power supply; 0.01 *M* borate buffer (pH 10); applied voltage: 20 kV. (A) No TTAB, 320 pg CrO_4^{2-}; (B) 20 m*M* of TTAB, 64 pg CrO_4^{2-}. Peaks: 1 = CrO_4^{2-}; 2 = anthracene.

Table 1
Effect of TTAB concentration on electroosmotic mobility and electrophoretic mobility of the micelle, using different buffer solutions at a constant concentration of 0.01 *M* at pH 10

TTAB (m*M*)	Phosphate				Carbonate				Borate			
	t_0	μ_{eo}	t_m	$\mu_{ep(m)}$	t_0	μ_{eo}	t_m	$\mu_{ep(m)}$	t_0	μ_{eo}	t_m	$\mu_{ep(m)}$
0	2.1	6.9			2.1	6.9			2.2	6.6		
0.5	9.5	−1.5	9.5	0	3.3	−4.4	3.3	0	3.4	−4.3	3.4	0
1.0	4.9	−3.0	4.9	0	3.3	−4.4	3.3	0	3.4	−5.2	2.8	0
5.0	3.6	−4.0	9.0	2.4	2.8	−5.2	7.9	3.4	2.8	−6.3	8.0	4.5
10.0	3.6	−4.0	8.3	2.2	2.8	−5.2	6.9	3.1	2.3	−6.3	8.0	4.5
20.0	2.9	−5.0	5.2	2.2	2.9	−5.0	7.4	3.0	2.3	−6.6	7.3	4.6
90.0	2.8	−5.2	6.1	2.8								

Applied voltage 20 kV. Negative power supply. t_0 and t_m in min; μ_{eo} and $\mu_{ep(m)}$ in 10^{-4} cm^2 V^{-1} s^{-1}.

to reduce the migration time of chromate ion, the cationic surfactant TTAB was added to the buffer solution. Table 1 shows the results obtained when different TTAB concentrations are added to the different buffer solutions. Reversed EOF (the negative sign of μ_{eo} means that the migration is toward the anode) was observed at less than the critical micelle concentration (CMC) of TTAB (its value is 3.4 m*M* [17]). As Table 1 shows, for the three buffers the EOF direction is reversed at 0.5 m*M* of TTAB.

3.2. Measurement of electroosmotic and micelle mobilities

The electroosmotic mobility is readily determined by measuring the migration time of methanol (t_0) and can be obtained from the equation [18]

$$\mu_{eo} = LL_D/Vt_0 \quad (1)$$

where L is the capillary length, L_D is the length of capillary to the detector cell and V is the applied voltage.

Methanol has been used to mark t_0 because is not associated with the micelles. Methanol is not detected by absorption of UV light but absorbs here due to the slight change of the refractive index [19].

The micelle mobility (μ_m) is determined by measuring the migration time of a fully solubilized solute, which is completely distributed in the micellar interior and moves with the same velocity of ionic micelles for time t_m. Anthracene has been used to mark t_m [20].

The micelle and electroosmotic mobilities are related by the relation:

$$\mu_m = \mu_{eo} - \mu_{ep(m)} \quad (2)$$

where $\mu_{ep(m)}$ is the electrophoretic mobility of the micelle.

By taking into account the sign of the migration direction, we can calculate $\mu_{ep(m)}$ from

$$\mu_{ep(m)} = [LL_D(1/t_m - 1/t_0)]/V \quad (3)$$

It should be noted that the directions of EOF and electrophoretic migration of micelles are opposite (Fig. 2).

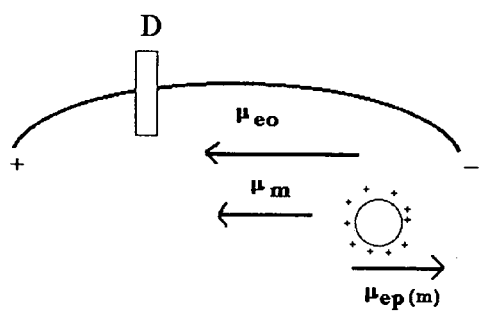

Fig. 2. Schematic illustration of mechanism with TTAB micelle in the buffer solution. Negative power supply. D = Detector; circle shows the cationic micelle.

In a series of experiments, the influence of the TTAB concentration in the buffer was investigated. As can be seen in Table 1, the electroosmotic mobility obtained is always lower than in absence of cationic surfactant, but it slightly increases as the TTAB concentration increases. On the other hand, the micelles begin to form in the solution at a TTAB concentration between 1.0 and 5.0 m*M*. This value is in accordance with the CMC value of TTAB (3.4 m*M*). Moreover, when the micelles are formed no appreciable change in the magnitude of the $\mu_{ep(m)}$ is noted.

Table 1 also shows that μ_{eo} is greater than $\mu_{ep(m)}$. This means that the micelles are transported toward the anode but exhibit a slower net mobility than the bulk aqueous phase.

3.3. Measurement of electrophoretic mobilities

In the absence of cationic surfactant, and taking into account the electropherogram of Fig. 1A, the electrophoretic mobility of the chromate anion in the buffer solution, $\mu_{ep}(CrO_4^{2-})$, can be calculated as the sum of the observed mobility of the anion and the electroosmotic mobility (Fig. 3A). By taking into account the sign of the migration direction, $\mu_{ep}(CrO_4^{2-})$ may be calculated from the following equation

$$\mu_{ep}(CrO_4^{2-}) = (LL_D(1/t_R + 1/t_0))/V \quad (4)$$

where t_R is the migration time of chromate anion.

It should be noted that the direction of electrophoretic mobility of the anion is the reverse of that of EOF.

Table 2 shows for the three buffers that $\mu_{ep}(CrO_4^{2-})$ is greater than μ_{eo} (Table 1). For this reason the chromate ion escapes detection with a positive-polarity power supply.

When the cationic surfactant is added (Fig. 3B) the difference between the observed mobility of chromate ion and the electroosmotic mobility can be considered to be the apparent electrophoretic mobility of the chromate in the micellar solution ($\mu^*_{ep}(CrO_4^{2-})$) and can be calculated from the equation

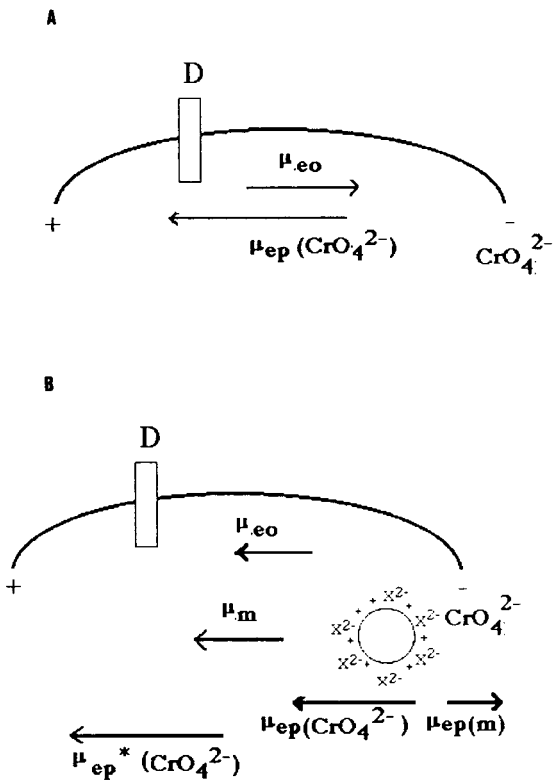

Fig. 3. Schematic illustration of mechanism. Negative power supply. (A) Chromate anion in the capillary without TTAB in the buffer solution; (B) chromate anion and TTAB micelle in the capillary. $X^{2-} = CrO_4^{2-}$.

$$\mu^*_{ep}(CrO_4^{2-}) = [LL_D(1/t_R - 1/t_0)]/V \quad (5)$$

In this case the electrophoretic and electroosmotic mobilities are in the same direction: toward the anode.

Fig. 1B shows a good symmetrical peak obtained under these conditions, and the migration time of the chromate is much less than in absence of TTAB.

Apparent electrophoretic mobilities of the chromate, $\mu^*_{ep}(CrO_4^{2-})$, as function of TTAB concentration are shown in Table 2. It can be seen that the addition of TTAB reduces considerably the migration time of the chromate anion (t_R) for the three buffers, which allows the chromate ion to be determined in under 2 min.

When micelles are formed, the anion is electrostatically adsorbed on the surface of the

Table 2
Effect of TTAB concentration on migration time and electrophoretic mobilities of chromate

TTAB (m*M*)	Phosphate			Carbonate			Borate		
	t_R	μ^*_{ep}	μ_{ep}	t_R	μ^*_{ep}	μ_{ep}	t_R	μ^*_{ep}	μ_{ep}
0	19		−7.7	22		−7.6	24		−7.2
0.5	1.6	7.6		1.2	7.7		1.3	6.9	
1.0	1.5	6.7		1.2	7.7		1.3	6.0	
5.0	1.9	3.6		1.7	3.4		1.7	2.3	
10.0	2.3	2.3		2.3	1.1		2.4	−0.2	
20.0	2.4	1.1		2.9	0.0		3.1	−1.9	
90.0	2.8	0.0							

Conditions as in Table 1. t_R in min; μ^*_{ep} and μ_{ep} in 10^{-4} cm^2 V^{-1} s^{-1}.

cationic micelle, reducing the migration velocity of the anion. This can be observed in Table 2, where $\mu^*_{ep}(CrO_4^{2-})$ decreases when the TTAB concentration increases. When the TTAB concentration reaches certain values (90 m*M* for phosphate, 20 m*M* for carbonate and slightly higher than 10 m*M* for borate buffer), $\mu^*_{ep}(CrO_4^{2-})$ is zero.

Table 2 also shows that, for carbonate and phosphate buffers, the observed mobility of the chromate is greater than electroosmotic mobility. However, for borate buffer (10 m*M* and 20 m*M* of TTAB) the inverse phenomenon is observed, so $\mu^*_{ep}(CrO_4^{2-}) > 0$.

3.4. Choice of experimental conditions

By comparing of the results with the different buffers, it seems that μ_{eo} and $\mu_{ep(m)}$ values follow the order: borate > carbonate > phosphate, which is the inverse of that found for $\mu^*_{ep}(CrO_4^{2-})$.

The different behaviour observed for the tree buffers can be understood in terms of the electrostatic adsorption of the corresponding anion of the buffer on the surface of the micelle, which competes for the chromate anion.

Borate, a Lewis acid [21], is found in mild alkaline solutions as a mixture of $B(OH)_4^-$ and $B(OH)_3$. At pH 10, the predominant form is $B(OH)_4^-$, while the carbonate anion is in transition between 50% HCO_3^- and 50% CO_3^{2-} and the phosphate is in the solution as HPO_4^{2-}. When the borate anion is in the solution, since it is a Lewis acid, it forms a polar bond with the hydroxide ions, acquiring a greater mobility than the other buffers. This fact means that the electroosmotic mobility will be greater than for carbonate and phosphate (Table 1), and as a consequence the absorption of chromate anion on the micelle is favoured over that of borate. This fact is reflected in a lower apparent electrophoretic mobility of the chromate in the micellar solution, $\mu^*_{ep}(CrO_4^{2-})$, than in the other buffers (Table 2).

On the other hand, additional data on the influence of TTAB concentration on the electric current (I) in the capillary for the different buffers are shown in Table 3. Electric current

Table 3
Comparison of current among three buffer solutions at different TTAB concentrations

TTAB (m*M*)	I (μA)		
	Phosphate	Carbonate	Borate
0	14	10	14
0.5	15	11	15
1.0	17	17	20
5.0	20	19	26
10.0	20	20	27
20.0	20	25	31
90.0	37		

Conditions as in Table 1.

increases as the TTAB concentration increases. Moreover, the results indicate that the lowest electric current was for carbonate buffer at the same concentration of surfactant. This fact contributes to minimize the rise in temperature of the liquid in the capillary [22].

From all these reasons, carbonate was chosen as best buffer to determine chromate anion in aqueous solutions. A TTAB concentration value of 5 m*M* was used because the migration time (t_R) of chromate was short enough (1.7 min) and micelles had already been formed. Fig. 4 shows a good symmetrical peak obtained under these conditions.

3.5. Quantification

From the experimental conditions chosen (0.01 *M* carbonate and 5 m*M* TTAB), detection limits were calculated as the amount of sample equivalent to a signal due to the analyte equal to three times the standard deviation of a series of ten replicate measurements of a reagent blank signal [23]. The detection limit obtained was 1.2 pg of CrO_4^{2-}/nl.

The relative standard deviation (R.S.D) for peak areas and migration times, calculated from injections of 150 pg of standard chromate, was 3.5%.

Peak areas change with the chromate ion concentration, indicating a linear relationship in the range 25 to 300 pg of chromate. The regression equation obtained was $A = -18.0 + 34.4C$, where A is the peak area and C the chromate amount in pg, and the correlation coefficient (r) was 0.997 ($n = 7$). Therefore this method can be employed for the quantitative analysis of the chromate anion.

3.6. Application to rinse waters from chromium plating baths

On the basis of the results obtained for chromate standard solutions, the application of the CZE method to determine chromate anion concentrations in rinsewater samples was attempted.

A sample from chromium plating baths (Inoxcrom) was analyzed. This sample is an acidic (pH 2.6) solution containing Cr(VI) as chromic acid.

After the appropriate dilution (1:10) in 0.01 *M* carbonate buffer solution at pH 10, the pe (= Eh159.16) value of the solution was measured, and was found to be 7.0. Under these experimental conditions of pe and pH and in order to know the predominant species in this aqueous solution, distribution species–pH and pe–pH diagrams for chromium were performed using equilibrium constants given in ref. 24. From the diagrams we can assure that only the chromate anion is present in the solution.

The sample was injected directly into the CZE system and the electropherogram in Fig. 5 was obtained. It can be seen that only one peak was obtained; no other peaks were observed. From the electropherogram, the chromate concentration in the sample was determined.

Fig. 4. Electropherogram of standard chromate solution. Micellar solution 5 m*M* TTAB in 0.01 *M* carbonate buffer (pH 10); sample amount 150 pg CrO_4^{2-}, injection volume 5 nl. Other conditions as in Fig. 1.

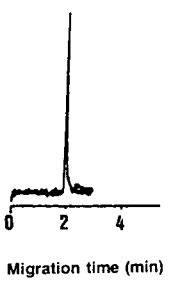

Fig. 5. Electropherogram of commercial sample. Micellar solution 5 m*M* TTAB in 0.01 *M* carbonate buffer (pH 10); dilution (1:10); injection volume 10 nl. Other conditions as in Fig. 1.

The same sample was also analyzed by AAS. The results are 283 and 271 mg of CrO_4^{2-}/l, using CZE and AAS, respectively. Good agreement between the two methods was observed. As AAS gives the total metal concentration, this agreement corroborates that all chromium metal present in the sample is in the form of chromate anion and no other species of this metal are formed under the experimental conditions used.

Finally, we want to point out that the CZE technique, using micellar solution, allows a rapid determination (less than 2 min) of the chromate anion in real samples.

Furthermore, the addition of TTAB to the buffer solution reverses the direction of the EOF and opens up new possibilities for the determination of highly mobile inorganic anions; it may be carried out in a single run with short analysis times in the most diverse matrices and with no sample pretreatment other than a dilution procedure.

Acknowledgement

Financial support provided by CICYT (Project No. NAT-1089), Ministry of Science and Education of Spain, is gratefully acknowledged.

References

[1] J.O. Nriagu and E. Nieboer, *Chromium in the Natural and Human Environment*, Wiley, New York, 1988.
[2] J.C. de Andrade, J.C. Rocha and N. Baccan, *Analyst*, 110 (1985) 197–199.
[3] I.S. Krull, K.W. Panaro and L.L. Gershman, *J. Chromatogr. Sci.*, 21 (1983) 460–472.
[4] I.T. Urasa and S.H. Nam, *J. Chromatogr. Sci.*, 27 (1989) 30–37.
[5] M. Sperling, S. Xu and B. Welz, *Anal. Chem.*, 64 (1992) 3101–3108.
[6] A. Weston, P.R. Brown, P. Jandik, W.K. Jones and A.L. Heckenberg, *J. Chromatogr.*, 593 (1992) 289–295.
[7] J. Romano, P. Jandik, W.R. Jones and P.E. Jackson, *J. Chromatogr.*, 546 (1991) 411–421.
[8] M. Aguilar, X. Huang and R.N. Zare, *J. Chromatogr.*, 480 (1989) 427–431.
[9] M. Aguilar, A. Farran and M. Martıńez, *J. Chromatogr.*, 635 (1993) 127–131.
[10] N. Wu, W.J. Horvath, P. Sun and C.W. Huie, *J. Chromatogr.*, 635 (1993) 307–312.
[11] D. Altria and C.F. Simpson, *Chromatographia*, 24 (1987) 527–532.
[12] T. Tsuda, *J. High Resolut. Chromatogr. Chromatogr. Commun.*, 10 (1987) 622–624.
[13] K. Otsuka, S. Terabe and T. Ando, *J. Chromatogr.*, 332 (1985) 219–226.
[14] X. Huang, J.A. Luckey, M.J. Gordon and R.N. Zare, *Anal. Chem.*, 61 (1989) 766–770.
[15] T. Kaneta, S. Tanaka and H. Yoshida, *J. Chromatogr.*, 538 (1991) 385–391.
[16] F.E.P Mikkers, F.M. Everaerts and Th.P.E.M. Verheggen, *J. Chromatogr.*, 169 (1979) 11–20.
[17] I.V. Rao and E. Ruckenstein, *J. Colloid Interface Sci.*, 113 (1986) 375–387.
[18] A.S. Cohen, S. Terabe, J.A. Smith and B.L. Karger, *Anal. Chem.*, 59 (1987) 1021–1027.
[19] S. Terabe, K. Otsuka and T. Ando, *Anal. Chem.*, 57 (1985) 834–841.
[20] J. Gorse, A.T. Balchunas, D.F. Swaile and M.J. Sepaniak, *J. High Resolut. Chromatogr. Chromatogr. Commun.*, 11 (1988) 554–559.
[21] F.A. Cotton and G. Wilkinson, *Advanced Inorganic Chemistry*, Wiley, New York, 1980, p. 289.
[22] K. Kleparnik and P. Boček, *J. Chromatogr.*, 569 (1991) 3–42.
[23] Analytical Methods Committee, *Analyst*, 112 (1987) 199–204.
[24] F.C. Richard and A.C.M. Bourg, *Wat. Res.*, 25 (1991) 807–816.

ELSEVIER

Journal of Chromatography A, 676 (1994) 451–454

JOURNAL OF CHROMATOGRAPHY A

Short communication

Normal-phase high-performance liquid chromatographic separation of halocyclophosphazenes

Pavel Janoš[a,*], Miroslav Broul[b], Vlastimil Novobilský[b], Václav Kolský[b]

[a]*Research Institute of Inorganic Chemistry, Revoluční 86, 400 60 Ústí nad Labem, Czech Republic*

[b]*J.E. Purkyně University, České Mládeže 8, 400 96 Ústí nad Labem, Czech Republic*

First received 15 February 1994; revised manuscript received 2 May 1994

Abstract

Lower members of the chlorocyclophosphazene homologous series $(NPCl_2)_n$, $n = 3–6$, were separated using normal-phase HPLC. Very good separation was achieved using Separon SGX (7 μm) silica gel column (250 × 4 mm I.D.) and *n*-heptane as the mobile phase. An addition of a more polar solvent (2-propanol) depressed the retention dramatically. The separated substances can be detected by spectrophotometry at a wavelength of *ca.* 220 nm, the detection limits varying the range *ca.* 30–1500 ng. The bromo derivative $(NPBr_2)_3$ exhibits a similar behaviour to the chloro derivatives.

1. Introduction

Cyclophosphazenes are inorganic cyclic compounds with staggered atoms of phosphorus and nitrogen. Their chloro derivatives, chlorocyclophosphazenes, having the general formula $(NPCl_2)_n$, were discovered about 160 years ago [1]. The greatest contributions to the chemistry of cyclophosphazenes were made by Stokes [2]. The chemistry of cyclophosphazenes is now a relatively widely developed field (see, e.g., reviews and monographs [3–7]) and the derivatives of cyclophosphazenes have been used in various branches of industry, agriculture and medicine (fertilizers, herbicides, fungicides, antioxidants, stabilizers for polymers, flame retardants, etc.) [8–11].

The separation of individual members of the homologous series of cyclophosphazenes is comparatively difficult. As far as chromatographic methods are concerned, gas chromatography [12–14], paper chromatography [15] and, most successfully, thin-layer chromatography (TLC) [16–18] have been applied. The objective of this work was to verify the viability of separating halocyclophosphazenes by liquid chromatography. The separation of the lower oligomers of cyclophosphazenes ($n = 3–6$) and the chromatographic behaviour of hexabromocyclotriphosphazene $(NPBr_2)_3$ were examined.

2. Experimental

The liquid chromatograph consisted of an HPP 5001 high-pressure pump, an LCI 30 injection valve with a 20-μl sampling loop, a TZ 4261 strip-chart recorder (all from Laboratorní

* Corresponding author.

0021-9673/94/$07.00
SSDI 0021-9673(94)00426-A

přístroje, Prague, Czech Republic) and a Model 732780 UV–Vis spectrophotometric detector (Knauer, Berlin, Germany). Separation was effected on a 250 × 4 mm I.D. column packed with Separon SGX (7 μm) unmodified silica (Tessek, Prague, Czech Republic). *n*-Heptane (UV grade), alone or mixed with 2-propanol (analytical-reagent grade) (both supplied by Lachema, Brno, Czech Republic), served as the mobile phase. Prior to measurements the mobile phase was deaerated in an ultrasonic bath. The mobile phase flow-rate was 0.5 ml min^{-1}.

The chlorocyclophosphazenes were prepared by reaction of phosphorus pentachloride with ammonium chloride in tetrahydrofuran. Extraction, fractional distillation and fractional crystallization were applied for isolation and purification of the individual derivatives [19]. The purity of the preparations was checked by TLC [16,18].

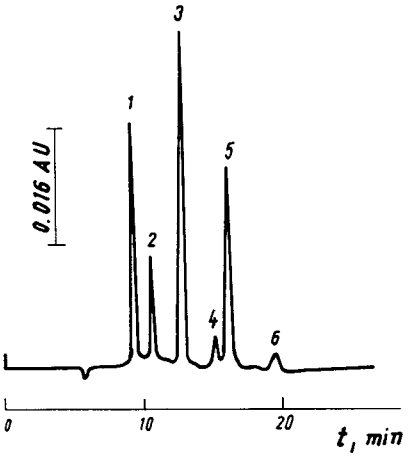

Fig. 1. Separation of a mixture of chlorocyclophosphazenes Column, 250 × 4 mm I.D. Separon SGX (7 μm); mobile phase, *n*-heptane; UV detection at 220 nm. Peaks: 1 = $(NPCl_2)_4$; 2 = $(NPCl_2)_5$; 3 = $(NPCl_2)_6$; 5 = $(NPCl_2)_3$; 4, 6 = unidentified (presumably higher derivatives).

3. Results and discussion

Halo derivatives of cyclophosphazenes are soluble in non-polar and low-polarity solvents and insoluble in water [19–22]. Consequently, chromatographic systems employing non-polar organic solvents as the mobile phases appear to be most convenient for their separation. It has been ascertained that the lower derivatives of chlorocyclophosphazenes (n = 3–6) can be readily separated on a silica column with *n*-heptane as the mobile phase (Fig. 1). The retention of analytes in a homologous series increases with increasing number of atoms in the ring, the exception being the lowest member, hexachlorocyclotriphosphazene, which is retained more strongly than the other derivatives examined. It was not possible to explain such a behaviour, but a similar anomaly was noticed during separation by TLC [16,17].

The retention of halocyclophosphazenes may be influenced by adding polar solvents to the mobile phase. The retention of analytes decreased steeply with increasing content of 2-propanol in *n*-heptane, the dependences of the capacity factors on 2-propanol concentration being almost linear (Fig. 2), which is inconsistent with both the common theoretical and empirical relationships for adsorption chromatography [23]. The limited number of experimental data,

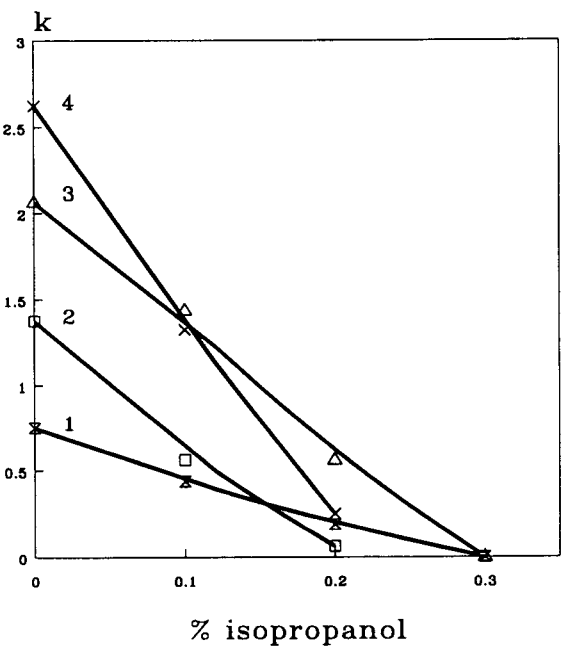

Fig. 2. Dependence of capacity factor on the content of 2-propanol in the mobile phase. 1 = $(NPCl_2)_4$; 2 = $(NPCl_2)_5$; 3 = $(NPCl_2)_3$; 4 = $(NPBr_2)_3$.

Table 1
Detection limits and parameters of calibration lines for the determination of halocyclophosphazenes

Substance	Detection limit (ng)	Slope (absorbance ng^{-1})	Intercept on the ordinate (absorbance)	Correlation coefficient ($n = 7$)
$(NPCl_2)_3$	86	$1.83 \cdot 10^{-6}$	$2.15 \cdot 10^{-2}$	0.9955
$(NPCl_2)_4$	31	$6.26 \cdot 10^{-6}$	$7.32 \cdot 10^{-2}$	0.9991
$(NPCl_2)_5$	54	$2.04 \cdot 10^{-6}$	$4.67 \cdot 10^{-2}$	0.9983
$(NPCl_2)_6$	72	$2.68 \cdot 10^{-6}$	$6.36 \cdot 10^{-2}$	0.9991
$(NPBr_2)_3$	1500	N.D.[a]	N.D.[a]	

[a] Not determined.

however, make it impossible to draw any more definite conclusions concerning the retention mechanism.

Direct spectrophotometric detection in the UV region was adopted for studying the separation of halocyclophosphazenes. Inconsistent data relating to the character of the spectra of halocyclophosphazenes in that region have been reported [24,25] and, therefore, the spectra of halocyclophosphazenes were measured in the mobile phase (Fig. 3). The shape of the spectrum is similar to that measured by Krause [24]. The highest sensitivity of detection was found at *ca.* 220 nm; at lower wavelengths the sensitivity was lower and additionally the baseline noise was higher. With increasing wavelength the sensitivity also decreased sharply, so that the most common UV detectors operating at 254 nm cannot be used for the detection of halocyclophosphazenes. Parameters of the calibration straight lines and the detection limits were measured at 220 nm (Table 1). It is obvious that for the chloro derivatives the detection limit is related to their retention (broadening of more strongly retained peaks).

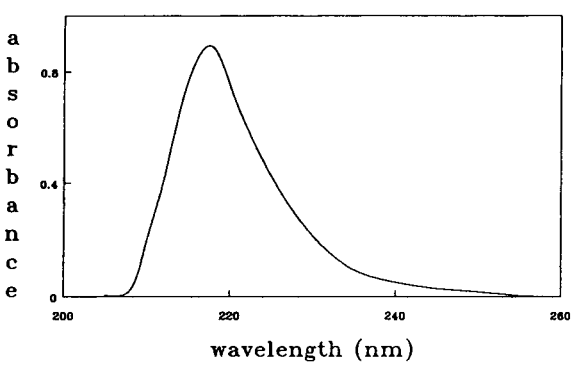

Fig. 3. UV spectrum of hexachlorocyclotriphosphazene in *n*-heptane. Spectra of other chlorocyclophosphazenes were very similar.

References

[1] J. Liebig and W. Woehler, *Justus Liebigs Ann. Chem.*, 11 (1834) 139.
[2] H.N. Stokes, *Am. Chem. J.*, 17 (1895) 275.
[3] I. Haiduc, *The Chemistry of Inorganic Ring Systems*, Part II, Wiley-Interscience, London, 1970.
[4] V.S. Matveev, *Khim. Volokna*, No. 4 (1992) 3.
[5] C.W. Allen, *Organophosphorus Chem.*, 24 (1993) 359.
[6] V. Chandrasekhar and K.R. Thomas, *Struct. Bonding (Berlin)*, 81 (1993) 41.
[7] C.W. Allen, *Coord. Chem. Rev.*, 130 (1994) 137.
[8] S.M. Zhivukhin and V.S. Tolstoguzov, *Plast. Massy*, 5 (1963) 24.
[9] C.W. Allen, *J. Fire Sci.*, 11 (1993) 320.
[10] H.R. Allock and M.L. Turner, *Macromolecules*, 26 (1993) 3.
[11] D. Kumar, A.D. Gupta and M. Khullar, *J. Polym. Sci., Part A*, 31 (1993) 707.
[12] L.G.R. Gimblett, *Chem. Ind. (London)*, (1958) 365.
[13] H. Rotzsche, R. Stahlberg and E. Steger, *J. Inorg. Nucl. Chem.*, 28 (1966) 687.
[14] K.S. Brenner, *J. Chromatogr.*, 57 (1971) 191.
[15] E. Uhlig and H. Eckert, *Z. Anorg. Allg. Chem.*, 204 (1969) 322.
[16] V. Novobilský, V. Kolský and W. Waněk, *Z. Anorg. Allg. Chem.*, 416 (1975) 187.
[17] V. Novobilský, V. Kolský and W. Waněk, *Z. Anorg. Allg. Chem.*, 423 (1976) 273.
[18] V. Novobilský, *Z. Anorg. Allg. Chem.*, 427 (1976) 189.
[19] J. Novák, *Ph.D. Thesis*, Purkyné University, Brno, 1970.

[20] M. Yokoyama and F. Yamada, *Kogakuin Daigaku Kenkyn Hokoku*, 6 (1958) 94; *Ref. Zh. Khim.*, 81 (1959) 507.
[21] N.L. Paddock and H.T. Searle, *Adv. Inorg. Chem. Radiochem.*, 1 (1959) 347.
[22] K. John and T. Moeller, *J. Inorg. Nucl. Chem.*, 22 (1961) 199.
[23] P. Jandera and J. Churáček, *J. Chromatogr.*, 91 (1974) 207.
[24] H.J. Krause, *Z. Elektrochem.*, 59 (1955) 1034.
[25] N.B. Jurinski, C.C. Thompson and P.A.D. DeMaine, *J. Inorg. Nucl. Chem.*, 27 (1965) 1571.

ELSEVIER

Journal of Chromatography A, 676 (1994) 455–460

JOURNAL OF CHROMATOGRAPHY A

Short communication

High-performance liquid chromatographic determination of betamethasone and dexamethasone☆

Keh-Ren Liu, Su-Hwei Chen, Shou-Mei Wu, Hwang-Shang Kou, Hsin-Lung Wu*

Graduate Institute of Pharmaceutical Sciences, Kaohsiung Medical College, Kaohsiung 807, Taiwan

First received 22 November 1993; revised manuscript received 6 April 1994

Abstract

A simple method was developed for the determination of glucocorticoid epimers of betamethasone (BTM) and dexamethasone (DXM) by high-performance liquid chromatography with UV detection, using silica as the stationary phase and dichloromethane–ethanol (34:1, v/v) as the mobile phase. The linear range of the method for the determination of BTM and DXM in 1.0 ml of sample solution was over 5–50 nmol. The detection limits (signal-to-noise ratio = 5) of BTM and DXM with an injection volume of 25 μl were 80 and 60 pmol, respectively. The method was satisfactorily applied to the individual determination of BTM and DXM in commercial tablets.

1. Introduction

Betamethasone (9α - fluoro - 16β - methyl - 11β,17α,21 - trihydroxypregna - 1,4 - diene - 3,20 - dione) and dexamethasone (9α - fluoro - 16α - methyl - 11β,17α,21 - trihydroxypregna - 1,4 - diene - 3,20 - dione) (Fig. 1) are potent synthetic glucocorticoids that are widely used for the treatment of inflammation, allergies and other diseases related to glucocorticoid deficiency [1]. The official methods of the United States Pharmacopeia [2] for the individual assay of BTM or DXM in bulk powder and tablet formulations are based on reversed-phase high-performance liquid chromatography (HPLC) with a C_{18} or C_8 column; because of very similar structures of BTM and DXM epimers, no HPLC methods have been reported for the direct separation and determination of BTM and DXM except those of HPLC coupled with analytical derivatization [3,4] and thin-layer chromatography followed by off-line UV absorption spectrophotometry [5] with multiple steps for determination.

In this paper, a simple, specific and rapid HPLC method is described for the determination of BTM and DXM without derivatization. It provides a possible approach for the simultaneous recognition of the epimeric BTM and

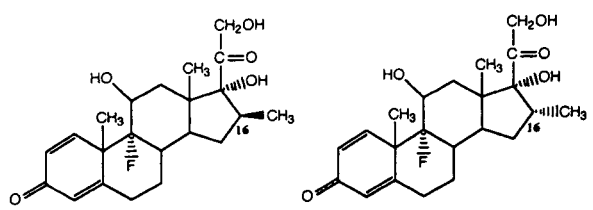

Betamethasone **Dexamethasone**

Fig. 1. Structures of betamethasone and dexamethasone.

* Corresponding author.

☆ This work was presented at the *1993 Taipei International Chemical Conference, October 13–16th, 1993.*

0021-9673/94/$07.00
SSDI 0021-9673(94)00379-N

DXM, which could be useful in cases of illegal use of DXM as a substitute for BTM, because BTM is more expensive than DXM. The method with the same analytical column was applied to the individual determination of BTM and DXM in bulk samples and formulations.

2. Experimental

2.1. Reagents and chemicals

BTM, DXM, hydrocortisone, 6α-methylprednisolone, prednisolone, prednisone and cortisone (internal standard; I.S.) (Sigma, St. Louis, MO, USA), dichloromethane, chloroform and *n*-butanol (Fisher, Fair Lawn, NJ, USA) and ethanol (Merck, Damstadt, Germany) were used without further purification. All other chemicals were of analytical-reagent grade.

2.2. HPLC conditions

A Waters–Millipore LC system with a U6K injector, a Model 510 pump and a Model 484 UV–Vis detector was used. A Nova-Pak silica (4 μm) column (75 × 3.9 mm I.D.) with a Guard-Pak of Resolve Si column (dead volume 60–75 μl; particle size 5 μm) (Waters–Millipore) and dichloromethane–ethanol (34:1, v/v) as the mobile phase at a flow-rate of 0.7 ml/min were used. The column eluate was monitored at 240 nm. The mobile phase solvents were pretreated with a vacuum filter for degassing.

2.3. Reference standard solution

Approximately 7.85 mg of BTM or DXM was accurately weighed and transferred into a 100-ml volumetric flask with the aid of a suitable amount of the mobile phase, and dissolved in and diluted to volume with the same solvent. The concentration was 200 μ*M*. Appropriate dilutions were made for analytical calibration at various levels.

2.4. Internal standard solution

Approximately 7.22 mg of cortisone was accurately weighed and transferred into a 100-ml volumetric flask with the mobile phase, and dissolved in and diluted to volume with the same solvent. The concentration was 200 μ*M*. Appropriate dilutions were made for analytical calibration.

2.5. Analytical calibration

Five samples each containing 1.0 ml of the reference standard solution over the concentration range 5.0–50.0 μM of BTM or DXM were pipetted in to a series of 10-ml glass-stoppered test-tubes and 0.5 ml of the internal standard solution (40.0 μ*M*) was added and mixed. A 5-μl aliquot of each solution was subjected to HPLC analysis (for the individual determination of the epimer).

Five samples each containing 0.5 ml of BTM and 0.5 ml of DXM reference standard solutions over the concentration range 10.0–100.0 μ*M* were pipetted into a series of 10-ml glass-stoppered test-tubes and 0.5 ml of the internal standard solution (40.0 μ*M*) was added and mixed. A 5-μl aliquot of each solution was subjected to HPLC analysis (for the determination of both epimers).

2.6. Sample preparation

Twenty tablets of BTM or DXM were weighed and finely pulverized. A suitable amount of the resulting powder equivalent to about 0.5 mg of BTM or DXM (synthetic mixtures of BTM and DXM with various proportions of powdered tablet were used for simultaneous determination) was accurately weighed and transferred into a 30-ml test-tube, then 10 ml of water were added for maceration of the powder. After sonication for 15 min, the suspension was transferred into a 125-ml separator and extracted with three 15-ml portions of chloroform–*n*-butanol (95:5, v/v). The combined extracts were filtered through anhydrous sodium sulphate (1 g, moistened with the solvent). The filtrates were collected in a

50-ml volumetric flask and diluted to the volume with the solvent. To 1.0 ml of the resulting solution, 0.5 ml of I.S. solution (40.0 μM) was added and mixed. A 5-μl aliquot of the solution was subjected to HPLC analysis.

3. Results and discussion

Our previous study [3] on the reversed-phase HPLC of BTM and DXM indicated no separation of the epimers, leading to an overlapping single peak. Basically, reversed-phase HPLC is less suitable than normal-phase HPLC (NP-HPLC) for positional isomers. Therefore, simultaneous separation of BTM and DXM by NP-HPLC with a silica column was studied in this work. NP-HPLC of BTM and DXM without derivatization on a silica column with a conventional mobile phase of n-hexane or dichloromethane led to extremely tailing peaks unsuitable for quantification. This can be partially explained by the structures of BTM and DXM in Fig. 1. Each of the epimers has three polar hydroxyl groups in addition to the carbonyl and unsaturated functions that result in a strong interaction between the epimers and the silanol function of the silica. Therefore, an NP-HPLC-compatible mobile phase with an appropriate solvent strength will be essential for the elution of BTM and DXM with good chromatographic properties, and a mobile phase consisting of dichloromethane and ethanol was optimized for the resolution of BTM and DXM.

The response of BTM and DXM was evaluated by measuring the peak-area ratios of the epimer to the I.S. The I.S. was added after the extraction of the epimer in tablet assay simply to keep the I.S. as a relatively constant factor. It would better be added before extraction if evidence for its constant recovery can be proved.

3.1. Mobile phase for NP-HPLC

In the HPLC of BTM and DXM on a silica (4 μm) column (75 × 3.9 mm I.D.), the mobile phase used for the elution of the epimers was studied including various ratios of dichloromethane to ethanol over the range 26:1 to 34:1 (v/v) in order of decreasing elution strength. The results found that the baseline resolution of BTM and DXM can be achieved using dichloromethane–ethanol (34:1, v/v), leading to capacity factors of 4.99 and 3.87, respectively, and a resolution of 1.7.

A typical chromatogram of BTM and DXM is illustrated in Fig. 2, indicating good chromatographic properties of symmetrical peaks and fast separation in less than 7 min. The greater retention of the epimers of BTM in the NP-HPLC system is probably due to the β-orientation of the methyl group at C_{16} that hinders less the α-hydroxyl group at C_{17} from forming hydrogen bonds with the silanol function of the silica stationary phase. The α-orientations of both the methyl group at C_{16} and the hydroxyl group at C_{17} in DXM result in unfavourable hydrogen bonding between the solute and the stationary

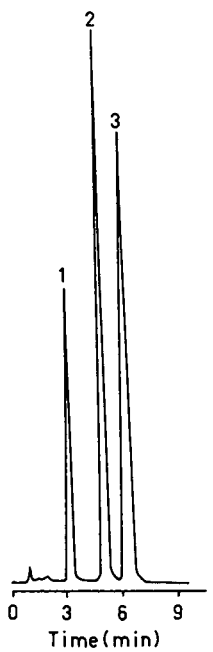

Fig. 2. HPLC of DXM (33 μM)–BTM (33 μM) mixture. Peaks: 1 = cortisone (I.S.); 2 = DXM; 3 = BTM. Conditions: Nova-Pak silica (4 μm) column (75 × 3.9 mm I.D.); mobile phase, dichloromethane–ethanol (34:1, v/v); flow-rate, 0.7 ml/min; UV detection at 240 nm; sample size, 5 μl.

phase, leading to less adsorption and faster elution.

3.2. Analytical calibration

To evaluate the quantitative applicability of the method, five different amounts of BTM and DXM in the range 5–50 nmol were analysed and the linearity between the peak-area ratios (y) and the epimer mass (x, nmol) was examined. The linear regression equations obtained for individual determination ($n = 5$) were $y = (0.05650 \pm 0.00033)x - (0.02797 \pm 0.00443)$ ($r = 0.999$) and $y = (0.05826 \pm 0.00084)x - (0.01801 \pm 0.01010)$ ($r = 0.999$) for BTM and DXM, respectively. The detection limits (signal-to-noise ratio = 5) of BTM and DXM per injection (25 μl) were 80 ± 20 and 60 ± 20 pmol, respectively.

In parallel, analytical calibration for both BTM and DXM based on five different amounts of the epimers each over the range 5–50 nmol resulted in the linear regression equations $y = (0.05678 \pm 0.00096)x - (0.02999 \pm 0.01796)$ ($r = 0.9999$) and $y = (0.05811 \pm 0.00113)x - (0.01329 \pm 0.01721)$ ($r = 0.9999$) for BTM and DXM, respectively. The results for the calibration of the epimers indicated good linearity of the method for the amounts of the epimers *versus* peak-area ratio studied. Because standard BTM and DXM were eluted with different retention times, as shown in Fig. 2, the method can identify which is being analysed when DXM is used as a partial or total substitute for the more expensive BTM in formulations for economic purposes. Demonstration of the application of the method to the analysis of synthetic mixtures of BTM and DXM was shown in Table 1.

3.3. Reproducibility and selectivity

The precision (relative standard deviation, R.S.D.) of the method based on the peak-area ratios for replicate determinations of BTM and DXM each at 40- and 8-nmol levels was studied. The results indicated that the intra-day precisions ($n = 9$) for BTM and DXM at 40 nmol were <0.8% and those at 8 nmol were <2.4%; the inter-day precisions ($n = 9$) for BTM and DXM were <1.0% at 40 nmol and <3.4% at 8 nmol.

The selectivity of the method was examined by spiking samples of BTM and DXM with other glucocorticoids including cortisone, hydrocortisone, prednisone, prednisolone and 6α-methylprednisolone. The results in Fig. 3 indicate that BTM and DXM can be well resolved from other glucocorticoids of oral use, revealing the favourable specificity of the method and its potential use for the direct HPLC of other glucocorticoids after suitable modification.

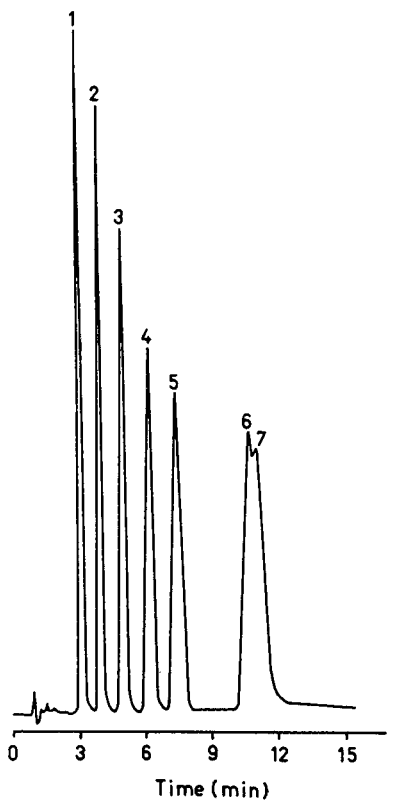

Fig. 3. HPLC of a mixture of standard glucocorticoids. Peaks: 1 = cortisone; 2 = prednisone; 3 = DXM; 4 = BTM; 5 = hydrocortisone; 6 = 6α-methylprednisolone; 7 = prednisone (each at 25 μM). HPLC conditions as in Fig. 2.

3.4. Application

Prior to application of the method to the determination of BTM or DXM in tablets, the solvent system for the extraction of BTM or DXM from tablet was investigated. A finely pulverized tablet of mass equivalent to about 0.5 mg of BTM or DXM was transferred into a 30-ml test-tube and macerated with 10 ml of water and further treated by sonication as indicated in Section 2.6. The resulting suspension was extracted with various proportions (0–15%, v/v) of *n*-butanol in chloroform (3 × 15 ml), leading to the selection of *n*-butanol–chloroform (5:95, v/v) as the optimum. The extraction of BTM or DXM from the water-macerated tablet suspension is facilitated by using water-immiscible chloroform with a suitable amount of *n*-butanol (≥5%, v/v). Because the common excipients such as lactose and starch used for tablet formulations are also polar, containing hydroxyl groups, these result in interaction of the excipient with DXM and BTM and an extraction solvent system with a hydroxyl function is therefore useful for BTM and DXM. This is in accordance with the behaviour of the polar epimers interacting with the silica stationary phase and needs a mobile phase containing ethanol for better elution in NP-HPLC.

The extraction of a known amount of BTM or DXM added to its powdered tablet with *n*-butanol–chloroform (5:95, v/v) resulted in satisfactory recoveries, *e.g.*, 98.7 ± 2.1 and 99.3 ± 1.8% ($n = 3$) for BTM at spiking levels of 0.1 and 0.3 mg, respectively, and 97.7 ± 1.5 and 99.4 ± 1.0% ($n = 3$) for DXM at spiking levels of 0.1 and 0.3 mg, respectively. This reveals the good extraction of BTM and DXM from their tablet diluents with chloroform containing a suitable amount of *n*-butanol. The recoveries were calculated as follows: recovery (%) = (total amount of BTM or DXM found after adding the epimer to its powdered tablet − amount of the epimer found in its powdered tablet before spiking) × 100/amount of the epimer added. The detailed extraction protocol for BTM and DXM is given in Section 2.6.

The method was applied to the determination of BTM and DXM in tablets and synthetic mixtures. The results are given in Table 1; all the analytical values for BTM and DXM tablets fell within the labelled range of 90–110% required by the USP.

In conclusion, an adsorption HPLC method has been developed for the determination of BTM and DXM. The method uses no derivatization reagent in the determination of the epimers; as a consequence, no additional and time-con-

Table 1
Assay results (mean ± S.D.; $n = 3$) for BTM and DXM tablets and their synthetic mixture

Sample	Percentage of claimed content[a]	
	BTM	DXM
BTM tablet		
B_1	96.2 ± 1.7	
B_2	94.0 ± 0.2	
B_3	94.6 ± 1.2	
B_4	91.2 ± 1.6	
B_5	94.6 ± 0.8	
Mean	94.1	
S.D.	1.8	
DXM tablet		
D_1		100.6 ± 1.0
D_2		99.8 ± 1.1
D_3		100.0 ± 1.5
D_4		101.8 ± 1.4
D_5		103.4 ± 0.7
Mean		101.1
S.D.		1.5
Test mixture[b]		
M_1	94.8 ± 1.2	104.0 ± 1.0
M_2	95.1 ± 1.3	100.9 ± 0.6
M_3	93.4 ± 1.0	100.7 ± 0.6
Mean	94.4	101.9
S.D.	0.9	1.8

[a] The labelled amount of BTM and DXM in each tablet is 0.5 mg.

[b] Synthetic mixtures were formulated with various proportions of pulverized tablets of BTM and DXM in mg of labelled amount: M_1 (0.40 mg BTM + 0.10 mg DXM), M_2 (0.25 mg BTM + 0.25 mg DXM) and M_3 (0.10 mg BTM + 0.40 mg DXM).

suming step for analytical derivatization is required. Hence this direct HPLC method is simple, rapid and selective for the determination of BTM and DXM. It seems to be practical and economical for the quality control of BTM and DXM in bulk and pharmaceutical products.

Acknowledgement

The authors are grateful to the National Science Council, Taiwan, for financial support of part of this work.

References

[1] H. Kalant and W.H.E. Roschlau, *Principles of Medical Pharmacology*, B.C. Decker, Philadelphia, PA, 1989.
[2] *The United States Pharmacopeia, 22nd Revision*, US Pharmacopeial Convection, Rockville, MD, 1990, pp. 158–160.
[3] S.H. Chen, S.M. Wu and H.L. Wu, *J. Chromatogr.*, 595 (1992) 203.
[4] S.M. Wu, S.H. Chen and H.L. Wu, *Anal. Chim. Acta*, 268 (1992) 255.
[5] B. Das, K. Datta and S.K. Das, *J. Liq. Chromatogr.*, 8 (1985) 3009.

ELSEVIER

Journal of Chromatography A, 676 (1994) 461–468

JOURNAL OF CHROMATOGRAPHY A

Short communication

Optimization of the simultaneous determination of acids and sugars as their trimethylsilyl(oxime) derivatives by gas chromatography–mass spectrometry and determination of the composition of six apple varieties

Sándor Tisza[a], Pál Sass[b], Ibolya Molnár-Perl*[,a]

[a]*Institute of Inorganic and Analytical Chemistry, L. Eötvös University, P.O. Box 32, H-1518 Budapest 112, Hungary*
[b]*Faculty of Horticulture, University of Horticulture and Food Industry, 6001 Kecskemét, Hungary*

First received 20 December 1993; revised manuscript received 25 March 1994

Abstract

A GC–MS method is reported for establishing the reproducibility of the determination of widely different amounts of sugars and acids as their trimethylsilyl derivatives simultaneously, from one solution with one injection. Optimum conditions were achieved on a 30-m DB-5 column. The determination of the components was based on their TIC and on selected ion monitoring. Data furnished by a Varian Saturn II GC–MS system equipped with a Varian Model 8200 AutoSampler showed that 4–20 ng of the minor constituents, in the presence of 50–250 ng of the main components, could be determined with a relative standard deviation of 10.6% or less. The utility of the procedure was demonstrated by the analysis of the composition of six different apple varieties, gathered at three different time of ripeness, in two consecutive years (1991, 1992), and stored for various periods of time. The separated carboxylic acids and sugars were phosphoric, succinic, pyruvic, 5-hydroxy-N-valeric and malic acid, butanal, 3-methyl-2-hydroxy-2-butenoic acid, 1,2-hydroxycyclohexene, pimelic acid, 2-deoxy-D-erythrose, tartaric acid, xylitol, arabinose, caffeic acid, D-ribose, citric acid, rhamnose, quinic acid, D-*erythro*-tetrafuranose, talose, 2-ketogluconic acid, mannitol, sorbitol, fructose, galactose, glucose, fructose (open form), glucaric and galacturonic acid, lactose, *meso*-inositol, gluconic, linoleic, glucuronic, stearic and arachidic acid, sucrose, turanose, maltose, chlorogenic acid, β-sitosterol, raffinose and maltotriose.

1. Introduction

The importance of knowing the qualitative and quantitative distribution of organic acids and sugars present in fruits and vegetables and in their different products is well known. The concentrations of these compounds in fruits and vegetables are characteristic, and are influenced by a number of factors, such as variety, maturity, ripeness and storage conditions.

Optimum possibilities for the simultaneous derivatization and gas chromatographic (GC) determination of more than 30 components present in several fruits and vegetables, (on both packed and capillary columns) have been reported recently [1–8].

In studies of the simultaneous determination of sugars and acids (monitored by GC–MS as

* Corresponding author.

0021-9673/94/$07.00
SSDI 0021-9673(94)00380-R

their TMS derivatives), Chapman and Horváth [9] determined four acids and eight sugars in extracts of apple, peach, pear and sweet potatoes, and Maciejewicz *et al.* [10] found four phenolic acids, six sugars and glucitol in the extract of propolis.

The aim of this paper is to show the extended possibilities of the simultaneous determination of sugars and acids as their trimethylsilyl derivatives, present in widely different concentrations, in one solution, by one injection, performing mass spectrometric detection with six apple varieties.

2. Experimental

2.1. Materials, reagents and samples

Chemicals and reagents were of analytical-reagent grade. Pyridine and hydroxylamine hydrochloride and model sugars and acids were obtained from Reanal (Budapest, Hungary), hexamethyldisilazane from Fluka (Buchs, Switzerland) and trifluoroacetic acid from Serva (Heidelberg, Germany).

Authentic apple varieties (Jonnee, Jonagold, Jonathan, Redspur, Gloster and Mutsu) were obtained from the Research Garden of the University of Horticulture and Food Industry (Péterimajor, Hungary). All six varieties were gathered at three different stages ($Jonnee_{1-3}$–$Mutsu_{1-3}$) of ripeness, in two consecutive years (1991, 1992), in order of listing at 03.09.91 and 03.09.92 ($Jonnee_1$–$Mutsu_1$), at 13.09.91 and 13.09.92 ($Jonnee_2$–$Mutsu_2$) and at 23.09.91 and 23.09.92 ($Jonnee_3$–$Mutsu_3$). Analyses were performed immediately after gathering (O tests), and every succeeding month, three times (A, B and C tests). Peeled apples were homogenized in a mixer and the sieved pulps were used for derivatization.

2.2. Preparation of the TMS-oxime and TMS derivatives

Model solutions containing various amounts of minor components ($5 \cdot 10^{-5}$–$2.5 \cdot 10^{-4}$ g) and main constituents ($0.5 \cdot 10^{-3}$–$5 \cdot 10^{-3}$ g of malic acid, glucose, fructose and sucrose), and stock solutions of apple pulps (containing approximately the corresponding amounts of acids and sugars, *i.e.*, 0.2–0.5 g wet samples) were evaporated to dryness in a rotary evaporator at 50–60°C using 2- or 4-ml reaction vials. The dehydrated residues were then derivatized in the same reaction vials. First they were treated with 0.5 ml of pyridine (containing 1.25 g of hydroxylamine hydrochloride per 100 ml) and were heated for 30 min at 75°C. The cooled samples were then trimethylsilylated with a mixture of 0.9 ml of hexamethyldisilazane (HMDS) and 0.1 ml of trifluoroacetic acid (TFAA), in the same vials for 60 min at 100°C.

Thereafter the solutions were ready for the analysis and could be kept at ambient temperature for at least 3 months in their initial condition. The amounts of stock solutions injected for GC–MS were the variously (10–50-fold) diluted aliquots of the derivatized stock solutions.

Table 1
Optimum parameters for GC–MS measurements

Column temperature programme

Start (°C)	End (°C)	Rate (°C/min)	Time (min)
60	120	16.0	3.75
120	155	4.0	8.75
155	155	0.0	12.00
155	210	4.0	13.75
210	320	16.0	6.87
320	320	0.0	18.00

Injector temperature programme

Start (°C)	End (°C)	Rate (°C/min)	Time (min)
60	60	0.0	2.00
60	320	180.0	1.44
320	320	0.0	10.00

Actual atomatic set-up conditions

Mass range, 40–650 u; Time per scan, 0.55; acquisition time, 60 min; Fil/Mul delay (time at the beginning of the elution, that data acquisition does not work) 420 s; peak threshold, 0 count; mass defect, 100 mu per 100 u; background mass, 50 u

2.3. Separation of the TMS-oxime and TMS derivatives

The apparatus was a Saturn II GC–MS system from Varian (Walnut Creek, CA, USA), equipped with a Varian 8200 AutoSampler and a septum-equipped programmable injector (SPI). A DB-5 (0.25 mm) column (30 m × 0.248 mm I.D.) was obtained from J & W Scientific (Folsom, CA, USA). Four other columns were obtained from Chrompack (Middelburg, Netherlands): CPF-Sil 5 CB (0.12 μm) (10 m × 0.25 mm I.D. and 25 m × 0.25 mm, I.D.) and CP-Sil 19 CB (0.2 mm) (10 m × 0.32 mm I.D. and 25 m × 0.32 mm I.D.). The temperature programmes for the columns and for the SPI are given in Table 1. The temperature of the transfer line was 300°C. The actual parameters of the ion-trap detector (ITD) were defined by the automatic set-up mode (Table 1).

3. Results and discussion

In order to utilize the possibilities offered by the mass detector (*i.e.*, to separate and determine more than 40 components, in widely different concentrations, in the presence of each

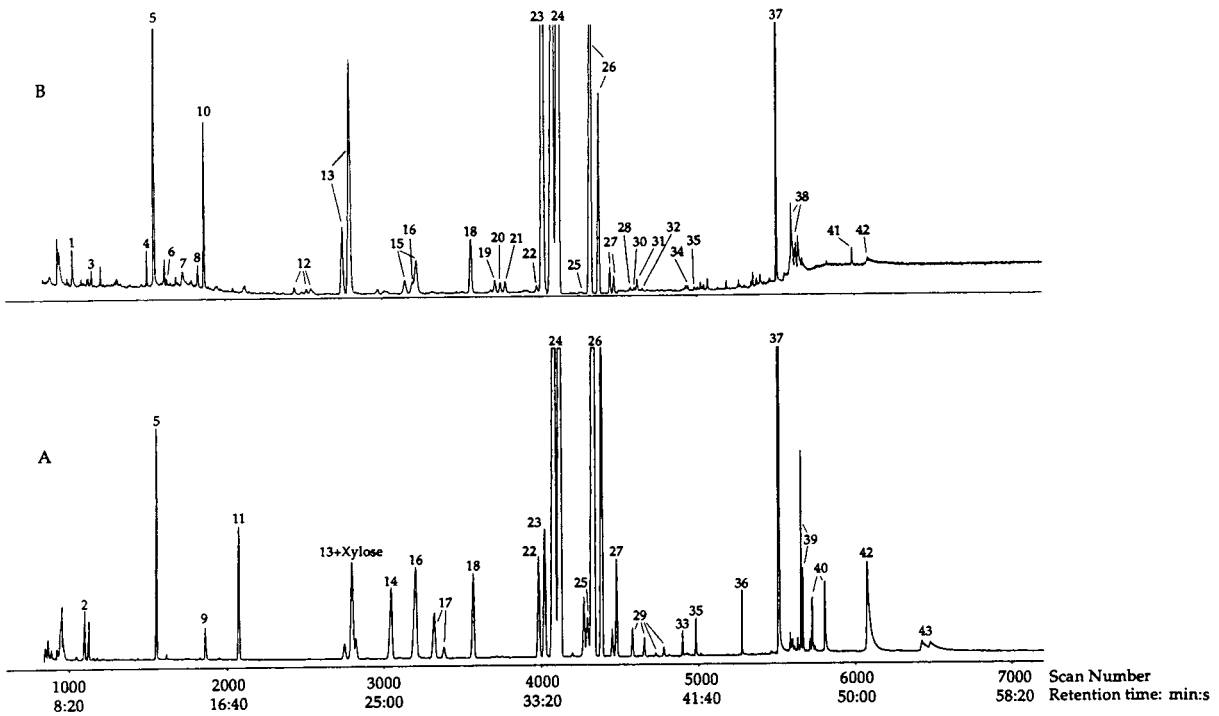

Fig. 1. Total ion chromatograms (TIC) of a (A) calibration solution and (B) an apple (Jonnee$_2$) sample. Peaks in order of retention times (min:s, in parentheses), 1 (8:35) = Phosphoric acid; 2 (9:07) = succinic acid; 3 (9:36) = pyruvic acid; 4 (12:32) = 5-hydroxy-N-valeric acid; 5 (12:55) = malic acid; 6 (13:36) = butanal; 7 (14:26) = 3-methyl-2-hydroxy-2-butenoic acid; 8 (15:13) = 1,2-hydroxycyclohexene; 9 (15:29) = pimelic acid; 10 (15:33) = 2-deoxy-D-erythrose; 11 (17:16) = tartaric acid; 12 (20:22, 20:59, 21:13) = xylitol; 13 (22:54, 23:16) = arabinose; 14 (25:22) = caffeic acid; 15 (26:13, 26:47) = D-ribose; 16 (26:36) = citric acid; 17 (27:37, 28:08) = rhamnose; 18 (29:41) = quinic acid; 19 (30:58) = D-*erythro*-tetrafuranose; 20 (31:14) = talose; 21 (31:29) = 2-ketogluconic acid; 22 (33:10) = mannitol; 23 (33:30) = sorbitol; 24 (34:03, 34:22) = fructose; 25 (35:35) = galactose; 26 (36:11, 36:33) = glucose; 27 (37:04, 37:19) = fructose (open form); 28 (38:09) = glucaric acid; 29 (38:10, 38:46, 39:22, 39:47) = galacturonic acid; 30 (38:30) = lactose; 31 (83:30) = *meso*-inositol; 32 (38:47) = gluconic acid; 33 (38:48) = linoleic acid; 34 (40:48) = glucuronic acid; 35 (41:31) = stearic acid; 36 (43:56) = arachidic acid; 37 (45:53) = sucrose; 38 (46:29, 46:36) = turanose; 39 (47:05, 47:11) = maltose; 40 (47:41, 48:21) = chlorogenic acid; 41 (49:53) = β-sitosterol; 42 (50:42) = raffinose; 43 (53:29, 53:59) = maltotriose.

Table 2
Reproducibility of the simultaneous determination of organic acids and sugars as TMS or TMS-oxime derivatives

No.	Compound	Integrator units equivalent to 1 ng of substance ($n = 3$)					
		A		B		C	
		Mean ± S.D.	R.S.D. (%)	Mean ± S.D.	R.S.D. (%)	Mean ± S.D.	R.S.D. (%)
2	Succinic acid	809 ± 19.1	2.3	862 ± 20.4	2.3	795 ± 49.0	6.1
5	Malic acid	2280 ± 40.7	1.8	2931 ± 44.5	1.5	3273 ± 133.7	4.1
9	Pimelic acid	1375 ± 26.6	1.9	1419 ± 35.6	2.5	1083 ± 115.0	11
11	Tartaric acid	4381 ± 55.7	1.3	5262 ± 109.8	2.1	3976 ± 225.3	5.7
13	Arabinose + xylose	5667 ± 102.8	1.8	6760 ± 129.9	1.9	6074[a]	
14	Caffeic acid	2204 ± 133.3	6.0	2504 ± 176.6	7.1	2641 ± 60.1	2.2
16	Citric acid	4691 ± 266.3	5.7	5051[a]		3831 ± 277.5	7.2
17	Rhamnose	2827 ± 27.7	1.0	5709 ± 40.4	0.7	5850 ± 94.1	1.6
18	Quinic acid	6898 ± 352.3	5.1	7844 ± 453.0	5.8	7736 ± 309.7	4.0
22	Mannitol	7883 ± 404.0	5.1	9545[a]		9536 ± 236.8	2.5
23	Sorbitol	7711 ± 184.6	2.4	8717 ± 340.4	3.9	8962 ± 534.7	6.0
24	Fructose	7656 ± 153.6	2.0	8592 ± 398.6	4.6	9036 ± 528.9	5.9
26	Glucose	6946 ± 191.9	2.8	7863 ± 193.1	2.4	8426 ± 171.1	2.0
29	Galacturonic acid	1998 ± 56.5	2.8	1303 ± 35.0	2.7	1278 ± 53.4	4.2
33	Linoleic acid	349 ± 7.6	2.2	323 ± 10.4	3.2	223 ± 14.5	6.5
35	Stearic acid	825 ± 21.5	2.6	898 ± 10.8	1.2	784 ± 47.6	6.0
36	Arachidic acid	760 ± 9.5	1.3	746 ± 18.1	2.4	506 ± 31.0	6.1
37	Sucrose	6439 ± 235.7	3.7	7284 ± 173.4	2.4	7443 ± 247.4	3.3
39	Maltose	4754 ± 166.8	3.5	5309 ± 166.9	3.1	5263 ± 186.4	3.5
40	Chlorogenic acid	857 ± 15.5	1.8	997 ± 30.0	3.0	–	–
42	Raffinose	1863 ± 58.9	3.2	2007 ± 46.1	2.3	–	–

Amounts injected: (A) 20 ng of the minor constituents and 250 ng of the main constituents (fructose, glucose, sucrose); (B) 8 ng of the minor constituents and 100 ng of the main constituents; (C) 4 ng of the minor constituents and 50 ng of the main constituents. S.D. = standard deviation; R.S.D. = relative standard deviation. Numbers in the first column refer to the peaks in Fig. 1A.
[a] $n = 2$.

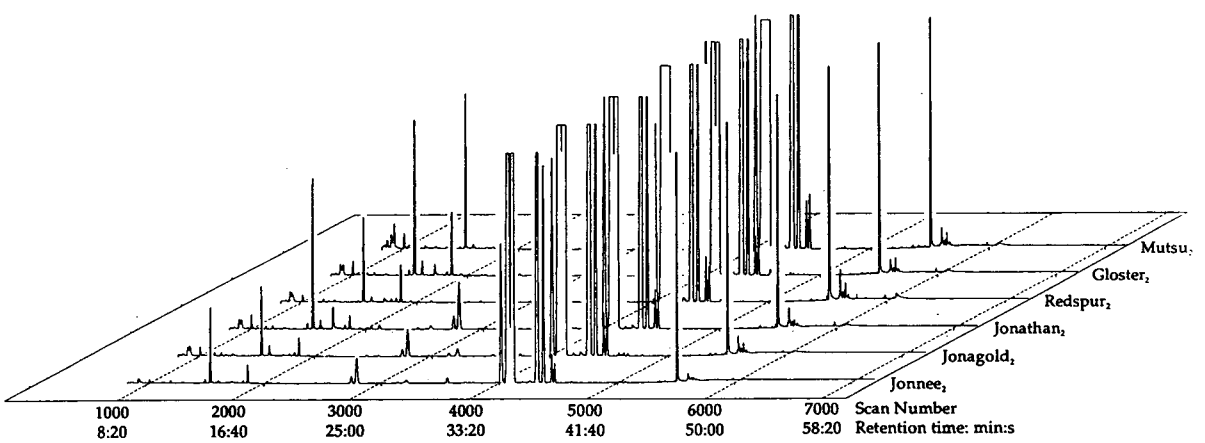

Fig. 2. TIC of the six apple varieties (Jonnee$_2$, Jonagold$_2$, Jonathan$_2$, Redspur$_2$, Gloster$_2$, Mutsu$_2$) presented in three dimensions. For further details, see Table 3).

other), the main task was to find the optimum conditions. In our earlier studies [2–7], a CP-Sil 5CB column, coated with methylsilicone, showed an excellent performance in the separation of more than 30 TMS derivatives (including members of various series of carboxylic acids and sugars of different degrees of polymerization, but excluding similar components, such as aldonic, uronic or sugar dicarboxylic acids). A 30-m DB-5 column, coated with 5% phenyl- and 95% methylsilicone, proved to be a good solution of the determination of all characteristic components of apples, similarly to the separation of citric acid from isocitric acid present in lemon and grapefruit samples [8].

The quantitative evaluation of the components were performed on the basis of the total ion count (TIC) data applying external standards (Table 2, Fig. 1A). As can be seen (Table 2) the concentration proportionality of the compounds (expressed in integration units per 1 ng of substance injected), provided by the ITD, was good, but not completely linear. This experience is in accordance with literature data [11]. Therefore,

Table 3
Compositions of six different apple varieties, expressed as percentages (w/w) of their dry matter contents (1992, B tests)

No.[a]	Component	$Jonnee_2$	$Jonagold_2$	$Jonathan_2$	$Redspur_2$	$Gloster_2$	$Mutsu_2$
	Dry matter content (%)	12.14	11.51	12.27	13.04	12.76	11.19
1	Phosphoric acid	0.10	0.21	0.29	0.16	0.30	0.35
3	Pyruvic acid × 10^2	3.6	7.5	6.2	6.7	6.5	4.1
4	5-Hydroxy-N-valeric acid × 10^2	8.2	–	–	–	–	3.3
5	Malic acid	1.8	1.4	3.2	1.6	3.3	3.8
6	Butanal × 10^2	1.5	2.2	2.9	–	–	2.8
7	3-Methyl-2-hydroxy-2-butenoic acid × 10^2	7.3	4.1	57.0	–	2.7	1.4
8	1,2-Hydroxy-cyclohexene × 10^2	6.7	11.0	11.0	11.0	10.0	6.5
10	2-Deoxy-D-erythrose	0.19	0.19	0.13	0.36	0.59	0.18
12	Xylitol × 10^2	3.6	5.5	14.0	4.4	6.1	9.5
13	Arabinose	0.79	0.67	1.29	1.31	0.47	1.50
15	D-Ribose × 10^2	7.2	30.0	20.0	36.0	14.0	–
16	Citric acid × 10^3	9.4	–	–	9.3	9.4	120.0
18	Quinic acid	0.11	0.22	0.19	0.15	0.35	0.29
19	D-*erythro*-Tetrafuranose × 10^2	5.2	10.0	11.0	8.9	12.0	3.8
20	Talose × 10^2	3.9	9.3	8.4	9.4	7.4	1.4
21	2-Ketogluconic acid × 10^2	1.9	1.1	1.5	9.7	7.8	9.1
22	Mannitol × 10^3	8.0	17.7	16.4	12.0	1.16	33.2
23	Sorbitol	2.0	3.0	3.5	2.7	4.0	4.0
24	Fructose	33.7	54.1	47.1	51.0	44.8	47.3
25	Galactose × 10^3	20.8	17.1	15.8	35.1	6.79	97.5
26	Glucose	12.8	22.4	19.4	15.6	20.6	27.9
27	Fructose (open form)	0.50	0.82	0.62	0.76	0.77	1.13
28	Glucaric acid × 10^2	1.2	12.0	2.1	8.9	19.0	27.0
30	Lactose × 10^3	10.2	32.3	6.2	15.5	16.7	41.5
31	*meso*-Inositol × 10^2	4.6	12.0	7.0	87.0	16.0	54.0
32	Gluconic acid × 10^2	1.1	9.6	–	6.8	14.0	19.0
34	Glucuronic acid × 10^2	1.7	4.9	–	1.6	3.5	0.6
35	Stearic acid × 10^2	3.3	2.2	–	2.8	3.5	3.9
37	Sucrose	6.2	11.0	9.1	15.4	10.4	9.6
38	Turanose × 10^2	17.0	25.0	18.0	31.0	18.0	2.4
41	β-Sitosterol × 10^2	4.3	4.6	6.8	8.1	7.5	1.4
42	Raffinose × 10^2	3.0	7.5	19.0	45.0	24.0	17.0
	Identified in total w/w%	59.1	95.7	86.7	91.9	87.3	98.0

[a] Numbers refer to the peaks in Fig. 1.

Table 4
Variations in the amounts of the main components of six apple varieties as a function of the times of their gathering ($Jonnee_{1-3}$, $Mutsu_{1-3}$) and of their storage (O, A, B, C), expressed as percentages (w/w) of their dry matter contents

Component		$Jonnee_1$	$Jonnee_2$	$Jonnee_3$	$Jonagold_1$	$Jonagold_2$	$Jonagold_3$	$Jonathan_1$	$Jonathan_2$	$Jonathan_3$	$Redspur_1$	$Redspur_2$	$Redspur_3$	$Gloster_1$	$Gloster_2$	$Gloster_3$	$Mutsu_1$	$Mutsu_2$	$Mustu_3$
Malic acid	O	5.1	4.6	3.9	4.2	5.7	4.3	6.4	6.2	4.8	3.4	1.8	2.1	6.2	5.2	5.4	6.6	5.6	5.3
	A	1.7	2.2	2.6	2.7	2.2	1.5	2.8	3.0	3.9	2.0	1.0	0.8	2.7	2.6	2.3	2.7	2.0	2.0
	B	2.1	1.6	1.6	1.7	1.7	1.6	2.2	2.3	2.3	0.9	1.2	1.3	2.6	2.5	2.6	1.9	2.0	1.9
	C	2.7	1.4	1.6	2.4	1.8	1.4	2.7	2.5	2.5	1.3	1.1	1.0	2.4	2.6	3.0	1.8	2.1	2.1
Arabinose	O	0.5	0.4	0.4	0.4	0.5	0.5	0.4	0.6	0.5	0.6	0.7	0.6	0.3	0.3	0.3	0.5	0.4	0.4
	A	0.5	0.5	0.4	0.2	0.2	0.2	0.4	0.4	0.4	0.7	0.5	0.1	0.3	0.2	0.2	0.4	0.4	0.4
	B	0.5	0.2	0.2	0.3	0.3	0.3	0.4	0.3	0.3	0.3	0.3	0.3	0.3	0.2	0.3	0.4	0.5	0.4
	C	0.5	0.2	0.2	0.3	0.3	0.2	0.3	0.3	0.3	0.4	0.3	0.3	0.2	0.2	0.2	0.3	0.2	0.3
Sorbit	O	2.0	2.3	2.4	2.1	1.9	2.1	1.7	1.1	1.1	1.7	1.0	1.1	2.8	2.1	2.7	2.3	1.9	2.2
	A	1.3	1.3	1.4	1.6	1.9	1.4	1.3	2.0	2.0	1.2	0.7	1.0	2.2	1.4	1.2	1.6	1.5	1.3
	B	1.9	1.3	1.3	1.5	1.3	1.8	1.6	1.5	1.7	0.5	0.5	1.0	1.3	1.2	1.5	1.6	1.9	1.2
	C	1.7	1.1	1.5	1.2	1.3	1.3	1.4	2.1	2.2	0.9	0.9	1.2	3.0	1.3	1.3	1.3	1.3	1.3
Fructose	O	42.9	39.3	41.5	42.2	41.0	51.0	42.2	40.4	52.6	44.8	44.7	48.0	36.9	37.3	39.3	43.4	36.3	43.5
	A	24.9	24.8	24.8	29.2	35.8	26.2	25.1	28.0	32.1	31.3	26.8	26.2	24.3	25.4	26.4	31.0	31.1	28.9
	B	29.5	29.2	28.8	24.7	23.0	22.2	24.6	25.5	22.7	18.4	27.0	19.6	20.7	22.3	22.7	25.6	27.0	28.4
	C	27.7	24.8	24.0	22.9	23.2	20.6	23.7	25.2	11.9	18.6	18.5	19.7	22.8	17.5	18.2	16.5	16.8	23.0
Glucose	O	8.1	7.6	11.0	12.3	7.7	17.7	7.7	8.2	15.8	18.1	17.7	19.1	9.9	16.6	13.8	8.2	6.0	9.8
	A	6.9	7.3	6.2	6.7	8.6	4.4	6.9	8.7	10.3	13.0	10.2	12.5	9.1	9.7	9.8	6.0	6.9	7.0
	B	8.2	8.3	7.4	7.0	4.3	5.9	7.0	7.6	6.8	7.9	9.9	7.4	9.9	9.6	9.5	8.2	8.2	7.2
	C	8.0	7.1	6.9	5.9	4.8	5.4	6.9	6.3	4.0	7.3	7.6	8.2	7.8	7.2	7.9	4.4	6.0	8.1
Sucrose	O	22.2	22.1	24.1	25.8	34.2	22.6	26.0	26.7	35.6	12.4	13.4	11.1	23.2	24.2	3.10	23.8	28.9	31.5
	A	5.9	6.5	9.5	15.9	16.3	14.0	8.1	14.7	10.9	1.9	2.4	2.6	15.7	8.4	4.5	17.8	9.6	10.3
	B	8.9	8.9	9.8	8.5	13.2	13.0	10.0	7.6	7.8	1.8	3.0	2.2	4.9	7.7	8.9	3.8	6.1	4.1
	C	5.0	5.4	6.3	9.9	13.3	9.5	5.3	8.5	10.8	1.6	1.5	1.5	11.8	6.0	5.7	5.4	2.3	1.6

to obtain acceptable and reliable analytical values for the calculation of the composition of apple samples (Tables 3 and 4), the corresponding responses (Table 2) were taken into account.

In the determination of those components that were not present in the external standard solution, the closest eluting member of standard solution, *i.e.*, the corresponding carboxylic acid or sugar (depending on the compound to be determined), served as the basis of calculation.

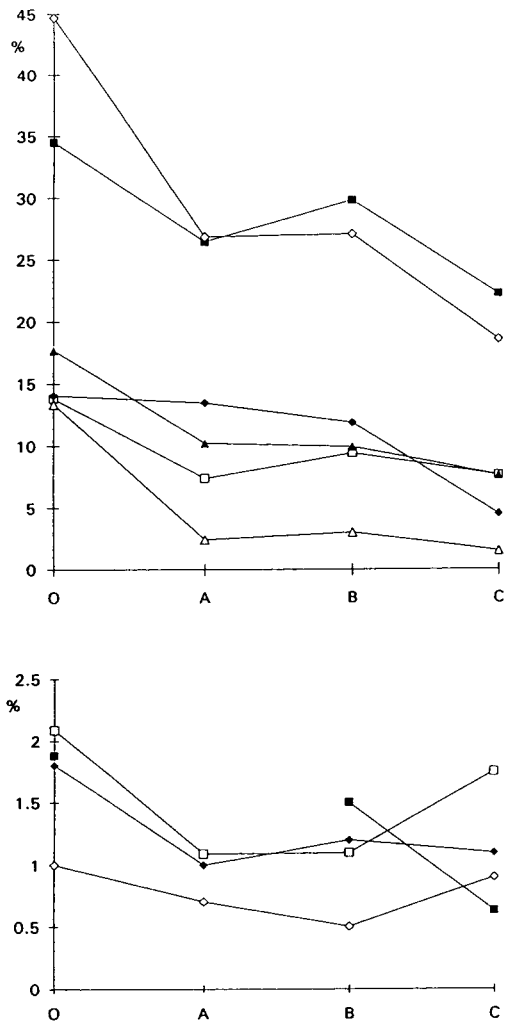

Fig. 3. Changes in the amounts of the main components, measured in varieties Redspur$_2$ (B tests), obtained in two consecutive years. The ordinates represent the percentages of components expressed as the corresponding dry matter content of the samples. For O, A, B and C, see Experimental) Top: ■ = fructose (1992); □ = glucose (1992); ◆ = sucrose (1992); ◇ = fructose (1991); ▲ = glucose (1991); △ = sucrose (1991). Bottom: ■ = malic acid (1992); □ = sorbitol (1992); ◆ = malic acid (1991); ◇ = sorbitol (1991).

For the identification of those apple constituents which were not available in our standard solution, selected ion monitoring was applied, utilizing the mass selectivity of the fragments of silylated compounds, provided by the characteristic electron impact (EI) mass spectra, present in the NIST or Wiley libraries, mostly in both (Fig. 1B, Table 3).

Evaluating the composition of various apple varieties, gathered and stored under the same conditions (Fig. 2, Table 3), it is obvious that considerable differences were measured (Fig. 2), mainly in the concentrations of the minor constituents (Table 3). High levels of 3-methyl-2-hydroxy-2-butenoic acid and xylitol (Jonathan), citric acid, mannitol, galactose, glucaric acid, lactose and gluconic acid (Mutsu) and D-ribose, *meso*-inositol, turanose and raffinose (Redspur) were found. The distribution also of the main constituents proved to be characteristic of the variety.

Variations in the amounts of the main constituents, due to the date of gathering and storage times, are compiled in Table 4 and Fig. 3.

It can be stated, both on the basis of values obtained from samples collected in 1991 (data in Table 3) and in 1992 (data in Fig. 3) and in comparison with each other, that the amounts of the main constituents decrease with increasing storage time. Large losses on storage were found in the fructose and sucrose contents of all varieties, independently of their date of gathering.

4. Conclusions

A CS–MS method was developed for the simultaneous determination of sugars and acids, including aldonic-, uronic- and sugar dicarboxylic acids, as their TMS oxime and TMS derivatives, present in six different apple varieties. The determination of the components was based on

the evaluation of their TIC. The identification and determination of those compounds which were not available was based on their EI mass spectra provided by the NIST and/or Wiley libraries.

Acknowledgement

This work was supported by the Hungarian Academy of Sciences (Project Numbers OTKA I/3 2284 and I/4, T5053).

References

[1] I. Molnár-Perl, M. Morvai, M. Pintér-Szakács and M. Petro-Turza, in *Agric. Food Chem. Consum. Proc. Eur. Conf. Food Chem.*, Vol. 2, INRA, Versailles, 1989, p. 649.

[2] I. Molnár-Perl, M. Morvai and M. Pintér-Szakács, *Anal. Chim. Acta*, 239 (1990) 165.

[3] M. Morvai and I. Molnár-Perl, *J. Chromatogr.*, 520 (1990) 201.

[4] I. Molnár-Perl, M. Morvai and M. Pintér-Szakács, *Anal. Chim. Acta*, 239 (1990) 165.

[5] I. Molnár-Perl and M. Morvai, *Food Addit. Contam.*, 9 (1992) 505.

[6] M. Morvai, I. Molnár-Perl and D. Knausz, *J. Chromatogr.*, 552 (1991) 337.

[7] M. Morvai and I. Molnár-Perl, *Chromatographia*, 34 (1992) 502.

[8] M. Morvai-Vitányi, I. Molnár-Perl, D. Knausz and P. Sass, *Chromatographia*, 36 (1993) 204.

[9] G.W. Chapman and R.J. Horváth, *J. Agric. Food Chem.*, 37 (1989) 947.

[10] W. Maciejewicz, M. Daniewski and Z. Mielniczuk, *Chem. Anal. (Warsaw)*, 29 (1984) 421.

[11] M. Linscheid, *Fresenius' J. Anal. Chem.*, 337 (1990) 648.

ELSEVIER

Journal of Chromatography A, 676 (1994) 469–473

JOURNAL OF CHROMATOGRAPHY A

Short communication

Enantiomer separation of amino acids by capillary gas chromatography using cyclodextrin derivatives as chiral stationary phases

Iwao Abe*, Noriteru Fujimoto, Taketoshi Nakahara

Department of Applied Chemistry, College of Engineering, University of Osaka Prefecture, Gakuen-Cho, Sakai, Osaka 593, Japan

Received 4 March 1994

Abstract

Amino acids were derivatized to N(O)-trifluoroacetyl methyl and isopropyl esters and studied with respect to the gas chromatographic separation of their enantiomers by using capillary columns coated with four types of cyclodextrin derivatives of 6-O-*tert.*-butyldimethylsilyl-2,3-di-O-acetyl or *n*-butyryl-β- and -γ-cyclodextrin. All amino acids could be separated into enantiomeric pairs except Trp. Methyl ester derivative showed the best separation on octakis(2,3-di-O-*n*-butyryl-6-O-*tert.*-butyldimethylsilyl)-γ-cyclodextrin and isopropyl esters on heptakis(2,3-di-O-acetyl-6-O-*tert.*-butyldimethylsilyl)-β-cyclodextrin. Pro showed complete separation as its N(O)-trifluoroacetyl isopropyl ester derivative, and the same derivative of Ala showed a very high separation factor of 1.808 at 100°C.

1. Introduction

Open-tubular capillary columns coated with chiral stationary phases are a powerful tool for the gas chromatographic (GC) determination of enantiomeric composition [1,2]. For amino acid enantiomers, Chirasil-Val is the most thoroughly studied capillary column and is capable of separating all protein amino acid enantiomeric mixtures almost completely in the form of N(O)-perfluoroacyl alkyl esters in a single run within 30 min [3]. This column has been applied to the determination of the optical purity of amino acids. However, it gives an unsatisfactory separation of the Pro enantiomeric pair, which is important in biomedical research [4,5]. Chiral recognition with Chirasil-Val can be attributed to diastereomeric associations formed mainly by hydrogen bonding between chiral solutes and the phase. Therefore, with Pro, the only amino acid with a pyrrolidine ring, and which possesses no amide hydrogen in its N-perfluoroacyl alkyl ester derivative, it is difficult to carry out an adequate interaction enantioselectively with this phase.

Recently, modified cyclodextrins have been introduced as chiral stationary phases in capillary GC and proved to be powerful tools in the enantioselective determination of volatile chiral compounds with different functional groups, including amino acids [6–10]. In this work, we

* Corresponding author.

0021-9673/94/$07.00
SSDI 0021-9673(94)00331-3

investigated the GC separation of amino acid enantiomers as their N(O)-trifluoroacetyl (TFA) methyl and isopropyl ester derivatives on four types of cyclodextrin derivatives coated on capillaries.

2. Experimental

2.1. Synthesis of cyclodextrin derivatives

Four cyclodextrin derivatives were prepared: heptakis(2,3-di-O-acetyl-6-O-*tert.*-butyldimethylsilyl)-β-cyclodextrin (CD-1), octakis(2,3-di-O-acetyl-6-O-*tert.*-butyldimethylsilyl)-γ-cyclodextrin (CD-2), heptakis(2,3-di-O-*n*-butyryl-6-O-*tert.*-butyldimethylsilyl)-β-cyclodextrin (CD-3) and octakis(2,3-di-O-*n*-butyryl-6-O-*tert.*-butyldimethylsilyl)-γ-cyclodextrin (CD-4). Samples of β- and γ-cyclodextrins were obtained form Wako (Osaka, Japan).

6-O-*tert.*-Butyldimethylsilyl-β- and γ-cyclodextrins were prepared according to the literature [11,12]. The raw products were purified by silica gel column chromatography using chloroform–methanol (3:1, v/v) as the eluent. The purified products were diacetylated with acetic anhydride in pyridine according to the cited references. The products were purified by chromatography on a silica gel column with toluene–ethanol (10:1, v/v) as the eluent. 2,3-Di-*n*-butyrylation was carried out in analogy with the procedure described in ref. [10]. The raw products were purified by silica gel column chromatography with toluene–ethyl acetate (5:1, v/v) as the eluent.

2.2. Preparation of glass capillary columns

Glass capillaries (0.8 mm O.D., 0.25 mm I.D.) were drawn from borosilicate glass tubing (Pyrex, 8 mm O.D., 2.5 mm I.D.) on a Shimadzu GDM-1B glass-drawing machine. The capillaries were leached with 6 *M* HCl, dehydrated and silylated with diphenyltetramethyldisilazane according to Grob [13]. The capillaries were coated with 10% of the cyclodextrin derivative dissolved in SE-30 (CD-1, CD-3, CD-4) or OV-1701 (CD-2) by a static method using a 0.3% solution of the stationary phases in CH_2Cl_2–*n*-C_5H_{12} (1:1, v/v).

2.3. Instrumentation

A Shimadzu Model 7AG gas chromatograph equipped with a flame ionization detector was used throughout. The carrier gas was helium and split-mode injection was used. The output signal was processed by a Shimadzu C-R1A digital integrator.

3. Results and discussion

Table 1 gives the separation factors of N(O)-TFA methyl esters of fifteen amino acid enantiomers on four different types of cyclodextrin derivatives. Similarly, Table 2 gives the separation factors of N(O)-TFA isopropyl esters of amino acid enantiomers. The highest separation factor for each amino acid is given in italics. The differences in the enantioselectivities of these four cyclodextrin derivatives towards amino acid derivatives can be easily established from these results.

With N(O)-TFA methyl esters, CD-4 showed the best enantioselectivity. High values of the separation factor could be obtained from Pro (1.563, 100°C) and Asp (1.406, 120°C); however, Thr, Phe, and Trp could not be separated. The highest values of the separation factor were observed for Thr on CD-3 (1.348, 120°C) and Phe on CD-1 (1.084, 130°C). None of these four phases could separate Trp enantiomers.

For N(O)-TFA isopropyl esters, CD-1 was the most efficient. Ala showed a very high separation factor of 1.808 at 100°C. The separation factors of Thr and Ser were 1.694 (110°C) and 1.292 (120°C), respectively. However, the other amino acids showed lower values of the separation factor than with the N(O)-TFA methyl ester derivatives. Especially Pro and Asp showed very low values, and there was no separation from Trp on the four phases. Notwithstanding, Pro could be separated completely on CD-4 with separation factor of 1.236 (100°C).

Table 1
Separation factors for N(O)-TFA methyl esters of amino acid enantiomers

Amino acid	Separation factor[a]				Column temperature (°C)
	CD-1	CD-2	CD-3	CD-4	
Ala	1.128	1.125	1.102	1.124	100
Val	1.102	1.146	1.042	1.243	100
Ile	1.112	1.131	1.013	1.288	100
Leu	1.137	1.109	1.000	1.229	100
Pro	1.198	1.398	1.315	1.563	100
Thr	1.290	1.168	1.348	1.000	120
Asp	1.310	1.300	1.000	1.406	120
Ser	1.347	1.369	1.108	1.158	130
Glu	1.103	1.169	1.000	1.262	130
Phe	1.084	1.009	1.017	1.000	130
Met	1.017	1.049	1.040	1.138	140
Tyr	1.021	1.022	1.070	1.029	160
Orn	1.088	1.026	1.077	1.098	170
Lys	1.054	1.020	1.021	1.071	170
Trp	1.000	1.000	1.000	1.000	170

The highest separation factor for each amino acid is underlined.
[a] Stationary phases: CD-1 = heptakis(2,3-di-O-acetyl-6-O-*tert.*-butyldimethylsilyl)-β-cyclodextrin; CD-2 = octakis(2,3-di-O-acetyl-6-O-*tert.*-butyldimethylsilyl)-γ-cyclodextrin; CD-3 = heptakis(2,3-di-O-*n*-butyryl-6-O-*tert.*-butyldimethylsilyl)-β-cyclodextrin; CD-4 = octakis(2,3-di-O-*n*-butyryl-6-O-*tert.*-butyldimethylsilyl)-γ-cyclodextrin.

Table 2
Separation factors for N(O)-TFA isopropyl esters of amino acid enantiomers

Amino acid	Separation factor[a]				Column temperature (°C)
	CD-1	CD-2	CD-3	CD-4	
Ala	1.808	1.156	1.117	1.233	100
Val	1.078	1.012	1.039	1.000	100
Ile	1.020	1.011	1.000	1.000	100
Leu	1.061	1.021	1.025	1.000	100
Pro	1.016	1.034	1.017	1.236	100
Thr	1.694	1.114	1.453	1.042	110
Ser	1.292	1.075	1.000	1.000	120
Asp	1.016	1.000	1.000	1.000	130
Glu	1.029	1.000	1.000	1.000	130
Met	1.048	1.018	1.030	1.000	140
Phe	1.052	1.013	1.000	1.000	140
Tyr	1.047	1.049	1.000	1.000	160
Orn	1.137	1.069	1.069	1.000	180
Lys	1.073	1.022	1.025	1.000	180
Trp	1.000	1.000	1.000	1.000	180

The highest separation factor for each amino acid is underlined.
[a] See Table 1.

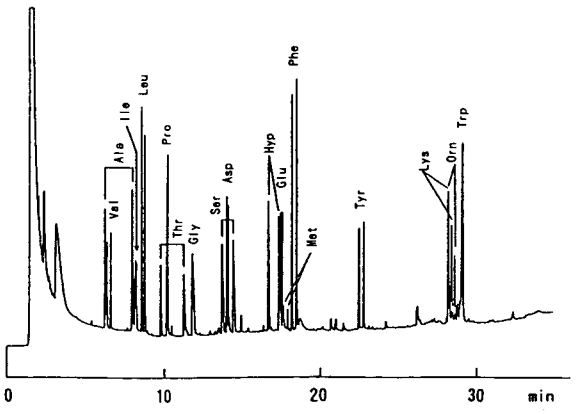

Fig. 1. Gas chromatogram of N(O)-TFA isopropyl esters of amino acid enantiomeric mixture. Column, glass capillary (20 m × 0.25 mm I.D.) coated with heptakis(2,3-di-O-acetyl-6-O-*tert.*-butyldimethylsilyl)-β-cyclodextrin–SE-30 (1:9, w/w). Column temperature, 100°C, held for 4 min, then programmed at 4°C/min to 220°C. For each amino acid enantiomeric pair, the D-enantiomer eluted faster.

From the data in Tables 1 and 2, the cyclodextrin derivative with the largest cavity and with a large substituent (*n*-butyryl) at the 2- and 3-positions (CD-4) gave the best results for the separation of N(O)-TFA methyl esters of amino acid enantiomers. On the other hand, the amino acid derivatives esterified with larger-sized alcohol of N(O)-TFA isopropyl esters could be separated best on the cyclodextrin derivative with smallest cavity size acylated with a smaller substituent (acetyl) at the 2- and 3-positions. The reasons for these unexpected results are not yet understood. Konig *et al.* [10] reported that N(O)-TFA methyl esters of amino acid enantiomers can be separated almost completely on octakis(3-O-*n*-butyryl-2,6-di-O-pentyl)-γ-cyclodextrin. Taking into account the simultaneous use with Chirasil-Val in practical applications, the choice of the N(O)-TFA isopropyl ester derivatives is considered to be more versatile. Fig. 1 shows a representative gas chromatogram of N(O)-TFA isopropyl esters of an amino acid enantiomeric mixture on CD-1. Pro enantiomers can hardly be separated. Nevertheless, the same derivative of Pro enantiomers could be separated completely on CD-4 without interference from other amino acid peaks (Fig. 2).

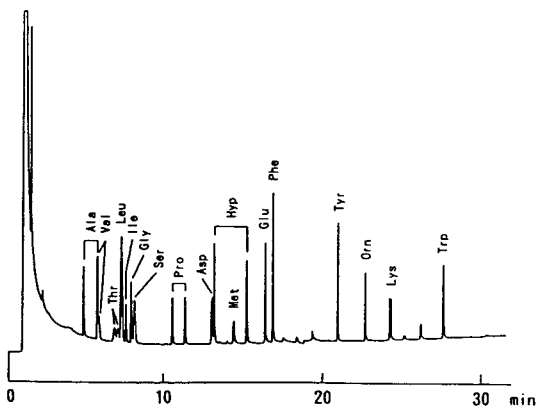

Fig. 2. Gas chromatogram of N(O)-TFA isopropyl esters of amino acid enantiomeric mixture. Column, glass capillary coated with octakis(2,3-di-O-*n*-butyryl-6-O-*tert.*-butyldimethylsilyl)-γ-cyclodextrin–SE-30 (1:9, w/w). Column temperature, 90°C, held for 4 min, then programmed at 4°C/min to 200°C. For other conditions, see Fig. 1 and text.

Acknowledgement

This work was supported partially by the Ministry of Education of Japan, Science and Culture, Project No. 05835009.

References

[1] S.G. Allenmark, *Chromatographic Enantioseparation*, Ellis Horwood, Chichester, 1988.
[2] W.A. Konig, *The Practice of Enantiomer Separation by Capillary Gas Chromatography*, Hüthig, Heidelberg, 1987.
[3] H. Frank, G.J. Nicholson and E. Bayer, *Angew. Chem.*, 90 (1978) 396.
[4] H. Bruckner and M. Hausch, *J. Chromatogr.*, 614 (1993) 7.
[5] M. Dixon and E.C. Webb, *Enzymes*, Longman, London, 1977.
[6] T. Koscielski, D. Sybilska and J. Jurczak, *J. Chromatogr.*, 280 (1983) 1.
[7] W.A. Konig, S. Lutz and G. Wenz, *Angew. Chem., Int. Ed. Engl.*, 27 (1988) 979.
[8] V. Schurig and H.-P. Nowotny, *Angew. Chem., Int. Ed. Engl.*, 29 (1990) 939.

[9] D.W. Armstrong, W. Li, C.-D. Chang and J. Pitha, *Anal. Chem.*, 62 (1990) 914.
[10] W.A. Konig, R. Krebber and P. Mischnick, *J. High Resolut. Chromatogr.*, 12 (1989) 732.
[11] K. Takeo, K. Uemura and H. Mitoh, *J. Carbohydr. Chem.*, 7 (1988) 293.
[12] A. Dietrich, B. Maas, V. Karl, P. Kreis, D. Lehmann, B. Weber and A. Mosandl, *J. High Resolut. Chromatogr.*, 15 (1992) 176.
[13] K. Grob, *Making and Manupulating Capillary Columns for Gas Chromatography*, Hüthig, Heidelberg, 1986.

Author Index

Experimental Design: A Chemometric Approach

Second, Revised and Expanded Edition

By **S.N. Deming** and **S.L. Morgan**

Data Handling in Science and Technology Volume 11

Now available is the second edition of a book which has been described as
"...an exceptionally lucid, easy-to-read presentation... would be an excellent addition to the collection of every analytical chemist. I recommend it with great enthusiasm."
(Analytical Chemistry).
N.R. Draper reviewed the first edition in Publication of the International Statistical Institute
"...discussion is careful, sensible, amicable, and modern and can be recommended for the intended readership."

The scope of the first edition has been revised, enlarged and expanded. Approximately 30% of the text is new. The book first introduces the reader to the fundamentals of experimental design. Systems theory, response surface concepts, and basic statistics serve as a basis for the further development of matrix least squares and hypothesis testing. The effects of different experimental designs and different models on the variance-covariance matrix and on the analysis of variance (ANOVA) are extensively discussed. Applications and advanced topics (such as confidence bands, rotatability, and confounding) complete the text. Numerous worked examples are presented.

The clear and practical approach adopted by the authors makes the book applicable to a wide audience. It will appeal particularly to those with a practical need (scientists, engineers, managers, research workers) who have completed their formal education but who still need to know efficient ways of carrying out experiments. It will also be an ideal text for advanced undergraduate and graduate students following courses in chemometrics, data acquisition and treatment, and design of experiments.

Contents:

© 1993 454 pages Hardbound
Price: Dfl. 310.00 (US$ 177.25)
ISBN 0-444-89111-0

ELSEVIER SCIENCE

ORDER INFORMATION
ELSEVIER SCIENCE B.V.
P.O. Box 330
1000 AH Amsterdam
The Netherlands
Fax: (+31-20) 5862 845
For USA and Canada
P.O. Box 945
Madison Square Station
New York, NY 10159-0945
Fax: (212) 633 3680

US$ prices are valid only for the USA & Canada and are subject to exchange rate fluctuations; in all other countries the Dutch guilder price (Dfl.) is definitive. Customers in the European Union should add the appropriate VAT rate applicable in their country to the price(s). Books are sent postfree if prepaid.

Hyphenated Techniques in Supercritical Fluid Chromatography and Extraction

Edited by **K. Jinno**

Journal of Chromatography Library Volume 53

This is the first book to focus on the latest developments in hyphenated techniques using supercritical fluids. The advantages of SFC in hyphenation with various detection modes, such as FTIR, MS, MPD and ICP and others are clearly featured throughout the book. Special attention is paid to coupling of SFE with GC or SFC.
In this edited volume, chapters are written by leading experts in the field. The book will be of interest to professionals in academia, as well as to those researchers working in an industrial environment, such as analytical instrumentation, pharmaceuticals, agriculture, food, petrochemicals and environmental.

Contents:

ELSEVIER SCIENCE B.V.

© 1992 x + 334 pages Hardbound
Price: Dfl. 275.00 (US$ 157.25)
ISBNN0-444-88794-6

"...will be a good guide to the scope of successful applications of supercritical fluids and clearly demonstrates the ability of SFC to provide a wealth of information about analytes."
Chromatographia

"...a valuable new source of information describing the latest developments in SFC and SFE hyphenated techniques. The book is highly recommended for advanced undergraduate students and chromatographers."
LC-GC International

ORDER INFORMATION

For USA and Canada
ELSEVIER SCIENCE INC.
P.O. Box 945
Madison Square Station
New York, NY 10160-0757
Fax: (212) 633 3880

In all other countries
ELSEVIER SCIENCE B.V.
P.O. Box 330
1000 AH Amsterdam
The Netherlands
Fax: (+31-20) 5862 845

US$ prices are valid only for the USA & Canada and are subject to exchange rate fluctuations; in all other countries the Dutch guilder price (Dfl.) is definitive. Customers in the European Union should add the appropriate VAT rate applicable in their country to the price(s). Books are sent postfree if prepaid.

PUBLICATION SCHEDULE FOR THE 1994 SUBSCRIPTION

Journal of Chromatography A and *Journal of Chromatography B: Biomedical Applications*

MONTH	1993	J–M	J	J	A	
Journal of Chromatography A	652–657	658–669	670/1 + 2 671/1 + 2 672/1 + 2	673/1 673/2 674/1 + 2 675/1 + 2 676/1	676/2 677/1 677/2 678/1	The publication schedule for further issues will be published later.
Bibliography Section		681/1	681/2			
Journal of Chromatography B: Biomedical Applications		652–655	656/1 656/2	657/1 657/2	658/1 658/2	

INFORMATION FOR AUTHORS

(Detailed *Instructions to Authors* were published in *J. Chromatogr. A*, Vol. 657, pp. 463–469. A free reprint can be obtained by application to the publisher, Elsevier Science B.V., P.O. Box 330, 1000 AH Amsterdam, Netherlands.)

Types of Contributions. The following types of papers are published: Regular research papers (full-length papers), Review articles, Short Communications and Discussions. Short Communications are usually descriptions of short investigations, or they can report minor technical improvements of previously published procedures; they reflect the same quality of research as full-length papers, but should preferably not exceed five printed pages. Discussions (one or two pages) should explain, amplify, correct or otherwise comment substantively upon an article recently published in the journal. For Review articles, see inside front cover under Submission of Papers.

Submission. Every paper must be accompanied by a letter from the senior author, stating that he/she is submitting the paper for publication in the *Journal of Chromatography A* or *B*.

Manuscripts. Manuscripts should be typed in **double spacing** on consecutively numbered pages of uniform size. The manuscript should be preceded by a sheet of manuscript paper carrying the title of the paper and the name and full postal address of the person to whom the proofs are to be sent. As a rule, papers should be divided into sections, headed by a caption (*e.g.*, Abstract, Introduction, Experimental, Results, Discussion, etc.). All illustrations, photographs, tables, etc., should be on separate sheets.

Abstract. All articles should have an abstract of 50–100 words which clearly and briefly indicates what is new, different and significant. No references should be given.

Introduction. Every paper must have a concise introduction mentioning what has been done before on the topic described, and stating clearly what is new in the paper now submitted.

Experimental conditions should preferably be given on a *separate* sheet, headed "Conditions". These conditions will, if appropriate, be printed in a block, directly following the heading "Experimental".

Illustrations. The figures should be submitted in a form suitable for reproduction, drawn in Indian ink on drawing or tracing paper. Each illustration should have a caption, all the *captions* being typed (with double spacing) together on a *separate sheet*. If structures are given in the text, the original drawings should be provided. Coloured illustrations are reproduced at the author's expense, the cost being determined by the number of pages and by the number of colours needed. The written permission of the author and publisher must be obtained for the use of any figure already published. Its source must be indicated in the legend.

References. References should be numbered in the order in which they are cited in the text, and listed in numerical sequence on a separate sheet at the end of the article. Please check a recent issue for the layout of the reference list. Abbreviations for the titles of journals should follow the system used by *Chemical Abstracts*. Articles not yet published should be given as "in press" (journal should be specified), "submitted for publication" (journal should be specified), "in preparation" or "personal communication".

Vols. 1–651 of the *Journal of Chromatography*; *Journal of Chromatography, Biomedical Applications* and *Journal of Chromatography, Symposium Volumes* should be cited as *J. Chromatogr.* From Vol. 652 on, *Journal of Chromatography A* (incl. Symposium Volumes) should be cited as *J. Chromatogr. A* and *Journal of Chromatography B: Biomedical Applications* as *J. Chromatogr. B.*

Dispatch. Before sending the manuscript to the Editor please check that the envelope contains four copies of the paper complete with references, captions and figures. One of the sets of figures must be the originals suitable for direct reproduction. Please also ensure that permission to publish has been obtained from your institute.

Proofs. One set of proofs will be sent to the author to be carefully checked for printer's errors. Corrections must be restricted to instances in which the proof is at variance with the manuscript.

Reprints. Fifty reprints will be supplied free of charge. Additional reprints can be ordered by the authors. An order form containing price quotations will be sent to the authors together with the proofs of their article.

Advertisements. The Editors of the journal accept no responsibility for the contents of the advertisements. Advertisement rates are available on request. Advertising orders and enquiries can be sent to the Advertising Manager, Elsevier Science B.V., Advertising Department, P.O. Box 211, 1000 AE Amsterdam, Netherlands; courier shipments to: Van de Sande Bakhuyzenstraat 4, 1061 AG Amsterdam, Netherlands; Tel. (+31-20) 515 3220/515 3222, Telefax (+31-20) 6833 041, Telex 16479 els vi nl. *UK*: T.G. Scott & Son Ltd., Tim Blake, Portland House, 21 Narborough Road, Cosby, Leics. LE9 5TA, UK; Tel. (+44-533) 753 333, Telefax (+44-533) 750 522. *USA and Canada*: Weston Media Associates, Daniel S. Lipner, P.O. Box 1110, Greens Farms, CT 06436-1110, USA; Tel. (+1-203) 261 2500, Telefax (+1-203) 261 0101.

FOR ADVERTISING INFORMATION PLEASE CONTACT OUR ADVERTISING REPRESENTATIVES